سمپوزیوم منطقه‌ای نوآوری در علم و فناوری
الندوة الثاني الإقليمية حول الابتكار في العلوم و التكنولوجيا
Regional Symposium on Innovation in Science and Technology

ReSIST 2025

دانشگاه فردوسی مشهد

2nd Regional Symposium on Innovation in Science and Technology

2-4 January 2025

Symposium Proceedings

دومین سمپوزیوم منطقه ای نوآوری در علم و فناوری

الندوة الثاني الإقليمية حول الابتكار في العلوم و التكنولوجيا

05138804188

resist@um.ac.ir

http://www.resist.um.ac.ir

Mashhad, Iran

ReSIST 2025

2nd Regional Symposium On Innovation In Science And Technology

Symposium Proceeding

دومین سمپوزیوم منطقه‌ای نوآوری در علم و فناوری

الندوة الثانية حول الابتكار في العلوم والتكنولوجيا

2-4 January 2025

+985138804188
resist@um.ac.ir
https://resist.um.ac.ir/2025
Mashhad, Iran

SPONSORS AND COLLEAGUES

We extend our sincere gratitude to the organizations and universities that are supporting this symposium.

PREFACE

It is with great pleasure that we present the **Proceedings of the RESIST Symposium – 2nd Regional Symposium on Innovation in Science & Technology**, held from **January 2–4, 2025 (Dey 12–14, 1403)** at **Ferdowsi University of Mashhad, Iran**. This symposium brought together a distinguished group of researchers, academicians, industry professionals, and policymakers from across the region to discuss **emerging trends, innovations, and challenges** in science and technology.

The symposium was **organized as part of the university's strategic initiative in scientific diplomacy**, fostering collaboration among scholars from Iran and other regional countries. In total, **over 120 participants, including faculty members, graduate students, and experts**, contributed to this event, engaging in **keynote speeches, panel discussions, and research presentations**.

This proceeding contains **extended abstracts (2 to 4 pages)** covering key themes of the symposium, including:

- **Nano Technology**
- **Airbase Studies**
- **Water and Environmental Sciences**
- **Biotechnologies**
- **Quantum Technology**
- **Medical Engineering**
- **Clean and Renewable Energies**
- **Artificial Intelligence and Cloud Computing**
- **Cognitive Sciences and Technologies**
- **Oil, Gas, and Petrochemical Processes**
- **Minerals and Ore Deposits**

One of the **highlights** of the symposium was the presence of **keynote speakers from leading universities and research institutions** worldwide, sharing their **cutting-edge insights** on critical scientific advancements. The discussions and collaborations initiated here have laid the groundwork for **future joint research projects, international partnerships, and academic exchanges**.

Additionally, the symposium facilitated **interdisciplinary dialogue**, fostering an environment where researchers from diverse fields explored how science and technology can **drive innovation, sustainability, and resilience** in the face of global challenges.

We extend our deepest appreciation to **all authors, reviewers, and organizing committee members** whose dedication and hard work made this symposium a success. Special thanks go to **Ferdowsi University of Mashhad, the International Scientific Cooperation Office, and all sponsors and institutional partners** for their invaluable support.

As we look ahead, we are excited to announce that the **next edition of the RESIST Symposium (RESIST 2026)** will be held at **the University of Kufa, Iraq, in January 2026**, further strengthening regional scientific cooperation.

We hope that this proceeding serves as a **valuable academic reference**, inspiring future research and collaboration among scholars and professionals.

On behalf of the Organizing Committee
[Seyed Alireza Seyedin]
Chairperson, RESIST Symposium
Ferdowsi University of Mashhad

ACKNOWLAGEMENT

We are honored to acknowledge the esteemed individuals whose contributions were instrumental to the success of this event.

SCIENTIFIC COMMITTEE

Dr. Mohammad Hassan Djavareshkian
Dr. Sayyed Keivan Hosseini
Dr. Hossein Sadeghi
Dr. Mohamad Hosein Mahmudy Gharaie
Dr. Zeinab Neshati
Dr. Zahra Alaminia
Dr. Hadi Rastegar Moghaddam Rezaion
Dr. Hossein Ali Akhlaghi Amiri
Dr. Hossein Mohammadzadeh
Dr. Hadi Sadoghi Yazdi
Dr. Ali Ahmadpour
Dr. Rouzbeh Shad
Dr. Abdorreza Savadi
Dr. Abbas Ghaemi Bafghi
Dr. Mahdi Saadatmand
Dr. Mahmoud Pasandidehfard
Dr. Javad Sepahi-Younsi
Dr. Hossein Vahidi
Dr. Gholamreza Arab Markadeh
Dr. Amir Reza Attari
Dr. Mohammad Ali AmirAbadi
Dr. Haider Toosian Shandiz
Dr. Harith Alsaad
Dr. Ammar R. Algburi
Dr. Syed Jamil Kazmi
Dr. Adnan Al-Badran
Dr. Ali-Wadi Al-fatlawi
Dr. Hasan Mahdi M. Al-Khateeb
Dr. Faouzi Chokri
Dr. Ramzy S. Ali Al-Waily

ORGANIZING COMMITTEE

Dr. Masoud Mirzaei Sharabi
Dr. Seyed Alireza Seyedin
Dr. Hossein Sadeghi
Dr. Mohamad Hosein Mahmudy Gharaie
Dr. Hadi Rastegar Moghaddam Rezaion
Dr. Ali Esmaeili
Dr. Zeinab Neshati
Dr. Mahmoud Shariati
Dr. Mir Mohammad Ayubi
Dr. Syed Ali Raza Naqvi
Dr. Abdul-Sattar Jaber Ali
Dr. Taki AlAbduwani
Dr. Seyyed Hashem Miri Hakimabad
Dr. Mohammad Vahidinia
Dr. Hossein Ali Akhlaghi Amiri
Dr. Sayyed Keivan Hosseini
Dr. Mohammad Hassan Djavareshkian
Dr. Mohammad Ali Amirabadi
Dr. Ammar R. Algburi
Dr.Abdulzahir Shakib

CONTENTS

1. KEYNOTE SPEAKERS

The RESIST Symposium was honored to feature a series of distinguished keynote speakers, each contributing their expertise and cutting-edge research to the diverse thematic areas of the symposium. Their presentations provided profound insights into emerging scientific challenges and innovative solutions across multiple disciplines. Below are the highlights from their keynote addresses:

Application of Phase Change Materials for Environmental and Green Technologies
Speaker: Seyed Mojtaba Sadrameli
Affiliation: Department of Engineering, German University of Technology in Oman, Muscat, Oman
Summary:
Phase Change Materials (PCMs) are crucial in energy storage and thermal management, with applications spanning from solar panels to biomedical devices. This keynote explored the classification of PCMs, their use in enhancing energy efficiency, and case studies demonstrating significant energy savings in thermal management systems over the past two decades.

Biotechnology and Modulation of Immune Response
Speaker: Prof. Dr. Walaa Najm Abood
Affiliation: Department of Microbiology, College of Veterinary Medicine, University of Diyala, Iraq
Summary:
This presentation delved into the role of nanoparticles in immunotherapy, highlighting their potential and risks. Prof. Abood discussed the immunotoxicity of various nanoparticles and stressed the importance of establishing their safety profiles for biomedical applications as their use expands.

Hybrid Supercapacitor Based on Nanostructured Materials: Current Research and Outlook
Speaker: Ahmed S. Al-Asadi
Affiliation: Department of Physics, College of Education for Pure Science, University of Basrah, Iraq
Summary:
Al-Asadi's keynote highlighted the advancements in hybrid supercapacitors (HSCs), particularly through the use of nanostructured materials like graphene and metal oxides. He addressed the challenges of optimizing energy-power balances and the role of computational modeling in enhancing material performance.

Artificial Intelligence: Revolutionizing Activities, Industries, and Everyday Experiences
Speaker: Dr. Mohammed F. Al-Mudhaffer
Affiliation: Department of Physics, College of Education for Pure Sciences, University of

Basrah, Iraq

Summary:

Dr. Al-Mudhaffer discussed AI's transformative impact across sectors such as healthcare, manufacturing, and education. The keynote underscored AI's role in driving operational efficiency, personalizing experiences, and the ethical considerations associated with its widespread adoption.

Genotypic Characterization of Plasmids Elements from Multiple-Drug Resistant Escherichia coli Using Next-Generation Sequencing Technique

Speaker: Halah M.H. Al-Hasani

Affiliation: Department of Molecular Biology, Iraqi Center for Cancer and Medical Genetics Research, Mustansiriyah University, Baghdad, Iraq

Summary:

This presentation focused on the critical issue of antimicrobial resistance (AMR), exploring the genetic mechanisms behind E. coli's resistance patterns through Next-Generation Sequencing. Al-Hasani emphasized the need for understanding plasmid behavior to combat AMR effectively.

Cognitive Science and Technologies: Bridging Innovation with Soft Skills in Academia

Speaker: Prof. Dr. Taqi Bin Abdul Redha Bin Ali Al Abdwani

Affiliation: Gulf College, Oman

Summary:

Prof. Dr. Al Abdwani explored the intersection of cognitive science and technology, emphasizing how insights into human cognition can drive innovation. His talk highlighted the importance of integrating cognitive empathy and strategic thinking into academic curricula to foster versatile professionals.

2. THEMATIC SECTIONS

2.1. NANO TECHNOLOGY

Investigation Of The Effect Of Electrolyte Type In The Anodizing Process Of Titanium

N. Yazdanparast[1], F. Darvishian Haghiggi[1], M. Hadada Sabzevar[1*], S. Mollazadeh Beidokhti [1]

[1] *Department of Materials and Metallurgical Engineering, Faculty of Engineering, Ferdowsi University of mashhad, mashhad, Iran*

**Corresponding author: haddadm@um.ac.ir*

Abstract— The leading project aims to form a TiO_2 oxide layer on a Ti (grade 2) substrate by electrochemical anodization and investigate the morphology of titanium dioxide. TiO_2 has attractive properties such as increased ion exchange capacity, non-toxicity, environmental safety, photocatalytic properties, and a high surface area to volume ratio. In this project, we investigate the morphology of TiO_2 formed in two types of organic and aqueous electrolytes. The titanium metal present in the substrate acts as a titanium source and, by creating a closed interface, fulfills the need for the presence of one of these electrodes. This titanium process allows TiO_2 with different morphologies to be formed in situ on the surface of the titanium metal. Ultimately, a porous structure with very strong adhesion to the substrate and a regular crystalline structure is formed. Titanium dioxide formation was performed by anodizing pure titanium in a standard two-electrode bath consisting of an organic electrolyte containing fluoride ions and an acidic aqueous electrolyte bath to investigate the effect of electrolyte on titania morphology. The results showed that acidic electrolytes cause the formation of titania with dense hardness. In the sample anodized with fluoride-containing electrolyte, we see the formation of titanium dioxide nanotubes due to the mechanism of action of fluoride ions.

Keyword: Nanotube -Titanium Dioxide -Electrochemical Anodization – electrolyte type

INTRODUCTION

Nanoscale structures have attracted much attention in recent years due to their unique properties, including high corrosion resistance, good magnetic properties, low specific gravity, high strength, and good biocompatibility. Among these nanostructures, titania nanotubes

(TiO_2) are of interest due to their unique properties. Titanium dioxide (TiO_2) can be Synthesis in the form of a variety of nanostructures, including nanorods, nanoparticles, nanotubes, and nanowires [1].

Titania is a versatile material and is widely used in scientific and commercial fields such as biomedicine, photocatalysis, and photovoltaic cells. By coating the titanium surface with TiO_2 nanotubes, bioactive implants can be prepared. Therefore, coating the surface of Ti implants with TiO_2 nanotubes is very promising in clinical investigation, and the fabrication of nanoporous/nanotube arrays of titanium dioxide on titanium is essential to increase its clinical efficacy [1].

The electrochemical anodizing process can be an efficient and cost-effective method to prepare nanostructured TiO_2 layers on titanium substrates with precise dimensional control (length, diameter, and morphology of nanotubes) [2].

METHODS &MATERIALS

The surface of the titanium samples is sanded with silicon carbide paper up to grade 3000. Samples are washed, degreased with acetone, and thoroughly rinsed with distilled water. Before anodizing, each sample will be treated with an etchant solution containing HNO3, H2O, and HF in a ratio of 3:5:1 to reduce the surface resistance. Anodizing experiments at room temperature and with various electrolytes are performed using a two-electrode electrochemical anodizing cell consisting of Ti with specified dimensions as the anode and platinum as the cathode. The distance between the cathode and anode electrodes will be considered to be 20 mm. Both electrodes are connected to a direct current (DC) voltage source, and the anodizing process is performed at different voltages. As shown in Table 1 the organic electrolyte bath contains 98cc of ethylene glycol (C2H6O2), 0.37g of NH4F, and 2cc of H2O. Also, anodizing in a fluoride ionfree aqueous electrolyte solution with a

composition of 150 cc DW water and 14 g H_2SO_4 was also performed potentiostatically. XRD analysis was performed to examine pure titanium, and imaging was performed by FESEM scanning electron microscope, and EDX analysis was performed to examine the morphology of the coating.

RESULTS AND DISCUSSION

Comparing the results of FESEM and EDS images, fluoride ion (F^-) is an essential factor for the formation of the tubular structure. The electric field applied between the cathode and anode drives Ti^{4+} ions from the Ti surface towards the electrolyte; then these ions combine with oxygen decomposed from H_2O in the electrolyte due to the oxidation reaction form TiO_2. After that, when the field dissolution reaction starts by F ions, a stable complex of titanium hexafluoride, TiF_6, is formed. Anions such as O_2 and OH, which are obtained from the separation of electrolyte components, migrate towards the anode and are formed as hydrogen bubbles in the cathode, and, depending on the conditions, there is also the possibility of oxygen evolution on the anode surface. Excess ions from the electrolyte also move towards or away from the anode in proportion to their electrostatic charge. The following equations represent the reactions carried out during the anodizing process, Eq. (1), (2), (3) [3].

$$Ti \rightarrow Ti^{4+} + 4e \quad (1)$$

$$Ti^{4+} + 2H_2O \rightarrow TiO_2 + 4H^+ \quad (2)$$

$$TiO_2 + 6F^- + 4H^+ \rightarrow [TiF_6]^{2-} + 2H_2O \quad (3)$$

In summary, the TNT formation mechanism includes the following steps: (a) formation of an oxide layer, (b) formation of pores on the oxide surface by F ions and their deepening, (c) merging of adjacent small pores and becoming larger pores, (d) formation of primary nanotubes, and (e) evolution of titanium dioxide nanotubes formed during the electrochemical anodizing process. In the absence of fluoride ions, the field dissolution reaction does not occur during the anodizing process. Therefore, the formation of the TiF_6 complex and the initiation of pore formation on the non-porous TiO_2 surface will not be possible. For this reason, the TiO_2 formed in the electrolyte containing H_2SO_4 is a non-porous oxide layer [3].

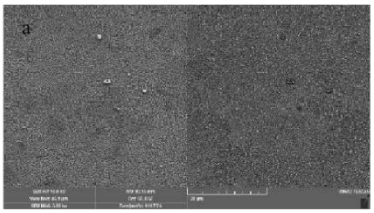

Fig. 1 FESEM images of samples before anodizing (a)Ti

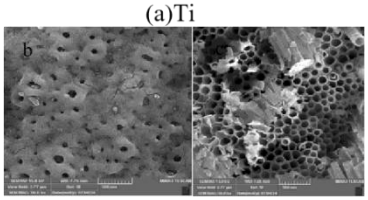

Fig. 2 FESEM images of samples after anodizing in (b) H_2SO_4 (c) NH_4F electrolyte solution

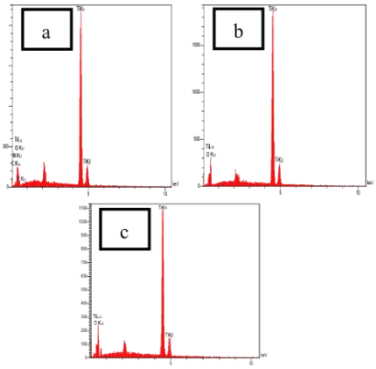

Fig. 3 EDS spectrum of (a) Ti (b) samples after anodizing in H_2SO_4 (c) NH_4F electrolyte solution

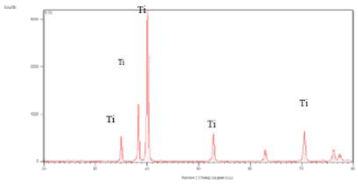

Fig. 4 XRD patterns of (a)Ti

Table 1. Anodizing parameters

Anodizing parameters	b	c
Thickness	0.5 mm	0.5mm
Electrolyte	150cc DW	2cc DW+98cc EG

	14gr H_2SO4	0.37 gr NH4F
Voltage	100	60
Time	120	120

REFERENCES

D. Khudhaira, A. Bhatti. (2016). Anodization parameters influencing the morphology and electrical properties of TiO2 nanotubes for living cell interfacing and investigations. Materials Science and Engineering C 59 (2016) 1125–1142. https://doi.org/10.1016/j.msec.2015.10.042

V. Galstyan, A. Vomiero. (2011). TiO2 nanotubular and nanoporous arrays by electrochemical anodization on different substrates. RSC Advances,2011,1,1038–1044.10.1039/c1ra00077b

D. Regoninia, C.R. Bowen. (2013). A review of growth mechanism, structure and crystallinity of anodized TiO2nanotubes. Materials Science and Engineering R 74 (2013) 377–406. https://doi.org/10.1016/j.mser.2013.10.001

Design of DNA Origami-Heparin Nanostructures for the Development of Viral Therapies

Sadegh Dastorani[1*], Mahmoud Shariati[2], Reza Hasanzadeh Ghasemi[3]

[1]*PhD Candidate, Ferdowsi University of Mashhad, Department of Mechanical Engineering, Mashhad, Iran.*

[2]*Full Professor, Ferdowsi University of Mashhad, Department of Mechanical Engineering, Mashhad, Iran.*

[3]*Associate Professor, Hakim Sabzevari University, Department of Mechanical Engineering, Sabzevar, Iran.*

**Corresponding author: S.dastorani1994@gmail.com*

Abstract — Given the increasing prevalence of viral diseases and limitations of current treatments, the development of a new generation of highly effective antiviral drugs with fewer side effects is imperative. This research introduces novel nanostructures based on DNA origami, heparin, and a spermidine-containing linker, which show great potential for targeted drug delivery and the treatment of viral diseases. These nanostructures form stable complexes, enabling efficient transport of antiviral drugs to infected cells. Additionally, the unique properties of these nanostructures make them a promising platform for the development of new antiviral drugs. The results of this study present a promising outlook for the development of a new generation of nanotechnology-based antiviral therapies.

Keyword: Virus, DNA origami, heparin, linker

INTRODUCTION

Recent advancements in nanotechnology and pharmaceutical sciences, particularly in the field of targeted drug delivery, have brought about significant transformations. One notable achievement is the utilization of precise engineering to produce highly efficient and effective drug compounds. In this context, biomolecules and engineered nanostructures play a pivotal role in the development of therapeutic technologies. Heparin, as a biological polyanion [1-3] and anticoagulant, is widely used in the treatment of cardiovascular diseases [4-6], prevention of blood clots [7, 8], and reduction of inflammation and infection [9-12]. Additionally, it holds great potential for the development of novel methods to combat viral diseases [13-16]. The unique properties of heparin in interacting with biological systems and nanostructures make it an ideal platform for designing innovative structures capable of inhibiting viruses with high precision and efficacy. The presence of protein spikes on viruses, which are the primary agents of replication and infectivity, allows heparin to bind to these spikes, such as the spike protein in the coronavirus, thereby preventing viral replication and infection [17, 18].

In recent decades, DNA origami has emerged as one of the most advanced tools in nanotechnology, revolutionizing the design and construction of complex nanostructures [19-20]. By leveraging DNA's ability to form precise and controlled three-dimensional structures, this technique enables the creation of a wide range of nanostructures with diverse applications in scientific and medical fields [21]. Notable features of DNA origami include the ability to design intricate structures, high stability, and the capacity to carry molecular payloads [22-25].

The combination of heparin with DNA origami structures, given the unique properties of both molecules, represents an innovative approach to designing antiviral nanostructures [26]. Recent studies have demonstrated promising results in viral inhibition using large-scale DNA origami structures combined with heparin or heparan sulfate derivatives [27-26]. However, this approach faces challenges such as time-consuming design and fabrication processes, high costs of materials and equipment, limitations in accurately studying molecular interactions in complex biological environments, and the need for extensive studies to evaluate the efficacy and side effects of these structures. Therefore, this paper proposes a novel method that focuses on smaller, simpler DNA origami structures

to overcome the challenges associated with designing large-scale DNA origami structures. This approach not only significantly reduces design time and costs but also enables more accurate investigation of molecular interactions and optimization of structure performance.

Given the similar negative charges of heparin and DNA, direct and effective interactions between these two molecules alone are not observed. Therefore, to establish a linkage between DNA and heparin, intermediaries such as linkers, multivalent ligands, or polycationic dendrimers are employed. These intermediaries act as bridges between the two molecules, enabling their connection through non-covalent interactions [28-30].

Therefore, this study, focusing on the design of new complexes comprising heparin, linker, and DNA origami, can be considered as an initial step towards the development of innovative nanostructures for combating viruses. The primary objective of this research is to design hybrid nanostructures based on DNA origami, linker, and heparin with potential applications in various fields, especially medicine. By conducting this research, a significant step will be taken towards the development of intelligent nanostructures with diverse applications in the medical field. Ultimately, it will pave the way for the more precise design of molecular structures with various applications, including viral inhibition.

2.3. METHODS & MATERIALS

The Materials and Methods section is divided into four main parts. In the first part, a suitable DNA origami structure will be modeled. The second part will focus on the design and modeling of the linker as a bridge connecting the different components. The third part will describe the method for modeling the heparin molecule. Finally, the fourth part will detail the assembly and modeling of the final complex comprising DNA origami, linker, and heparin.

2.1. DNA ORIGAMI MODELING

We first designed an arbitrary double-stranded DNA structure in the caDNAno software, as shown in Fig. 1. To create a complex, we needed the structure in PDB format. We used the oxViewe and tacoxdna websites to convert the structure to PDB format.

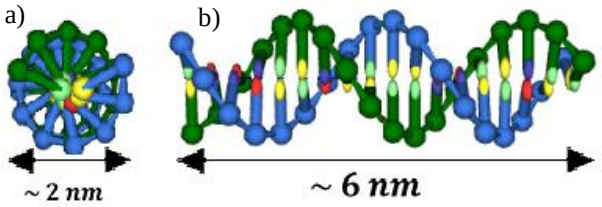

Fig. 1. Custom-sized double-stranded DNA origami. a) Front view. b) Side view.

2.2. LINKER MODELING

Cationic linkers, renowned for their strong affinity to anionic biomolecules like DNA and proteins, have emerged as indispensable tools in molecular engineering. By acting as molecular bridges, they enable the construction of complex molecular architectures. Building upon the foundational principles established in earlier studies [30-28], researchers can rationally design cationic linkers with tailored properties. The structural diversity of reported cationic linkers attests to their versatility in a myriad of biological and chemical applications.

Therefore, in this research, a linker based on a six spermidine branches and a palmitic acid core was designed and optimized (Fig. 2). Avogadro software was employed as a powerful tool for modeling and structural optimization of this linker. The objective of this design was to achieve a stable and efficient structure capable of effectively binding to DNA molecules and heparin. The optimizations performed in Avogadro enabled the selection of optimal conformations that were energetically stable

and capable of interacting with biological molecules.

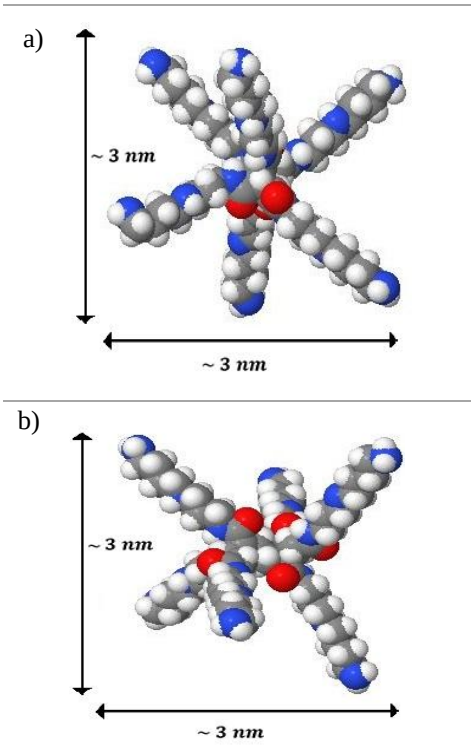

Fig. 2. Design of linker with six spermidine branches in Avogadro software. a) Front view. b) Side view.

2.3. HEPARIN MOLECULE

In this study, the structure of heparin molecule with the PDB code 1HPN was downloaded from the Protein Data Bank [31]. Heparins are known as linear polysaccharides composed of repeating disaccharide units. For a more detailed investigation of the molecular interactions between the linker and DNA, a heparin fragment with an approximate length of 4.5 nanometers, consisting of ten saccharide rings, was selected for modeling (Fig. 3).

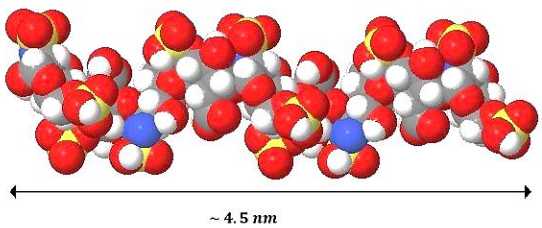

Fig. 3. Heparin structure [31] in MATLAB Molviewer software.

2.4. COMPLEXES

In this study, three different types of complexes were created by combining a custom DNA origami structure, a connecting linker, and heparin. Specifically, Complex 1 was formed by combining the linker structure and heparin (Fig. 4-a). Complex 2 was formed by combining the linker with DNA (Fig. 4-b). Complex 3 was formed by combining DNA, linker, and heparin (Fig. 4-c).

Given the unique properties of heparin and the cationic linker, each of the three designed complexes has the potential for wide-ranging applications in the fields of pharmacy and drug delivery.

Complex 1: The simultaneous presence of heparin and the cationic linker in this complex makes it a suitable candidate for targeting and binding to negatively charged biological structures, such as certain cellular receptors or pathogenic molecules. This feature makes this complex highly useful for designing targeted drugs and reducing their side effects.

Complex 2: The use of DNA origami technology in the construction of this complex allows for the design of nanoscale structures with diverse shapes and sizes. These structures can be used as nanocarriers for drug delivery to target cells. Additionally, the ability to engineer the surface of these nanocarriers with cationic linkers improves their interaction with the biological environment and enhances their application potential.

Complex 3: This complex has the most complex structure and is a combination of the advantages of the previous two complexes. By combining DNA origami, heparin, and a cationic linker, it is possible to design nanocarriers with highly accurate detection and targeting capabilities. These nanocarriers can be used for the diagnosis and treatment of infectious diseases, especially viral infections.

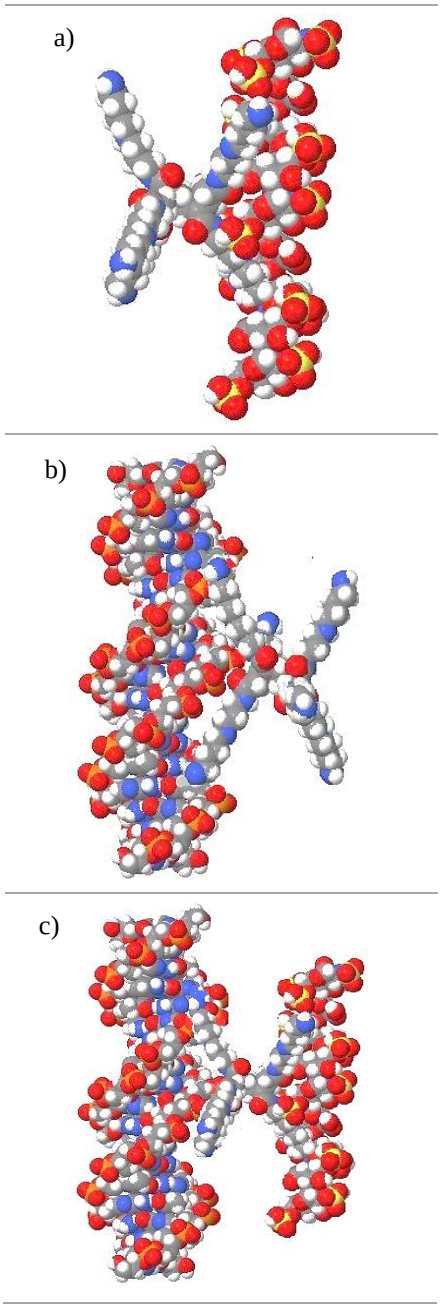

Fig. 4. Nanostructures of three complexes including DNA, linker and heparin in MATLAB Molviewer software. a) Complex 1. b) Complex 2. c) Complex 3.

Considering the challenges associated with designing large DNA origami structures, this research proposes a novel approach that focuses on smaller and simpler structures. This approach not only significantly reduces design time and cost but also allows for a more detailed investigation of molecular interactions and optimization of structure performance. The combination of DNA origami, heparin, and a linker creates a powerful platform for designing antiviral nanostructures with high efficiency and customizable features.

CONCLUSION

This paper, through the intelligent combination of DNA origami, heparin, and a cationic linker, has successfully designed nanostructures with high potential for targeted drug delivery and the treatment of viral diseases. These nanostructures, by creating different complexes, enable the efficient delivery of antiviral drugs to infected cells. Additionally, the unique properties of these nanostructures introduce them as a foundation for the development of a new generation of antiviral drugs. The results of this study paint a promising picture for the development of a new generation of nanotechnology-based antiviral therapies.

REFERENCES

Oduah, E., Linhardt, R., and Sharfstein, S. "Heparin: Past, Present, and Future," Pharmaceuticals, Vol. 9, No. 3, 2016, p. 38.

Marson, D., Laurini, E., Aulic, S., et al. "Unchain My Blood: Lessons Learned from Self-Assembled Dendrimers as Nanoscale Heparin Binders," Biomolecules, Vol.9, No. 8, 2019, p. 385.

Linhardt, R. J. "Heparin and anticoagulation," Frontiers in Bioscience, Vol.21, No. 7, 2016, pp. 1372–92.

Mukherjee, D., and Topol, E. J. "The role of low-molecular–weight heparin in cardiovascular diseases," Progress in Cardiovascular Diseases, Vol. 45, No. 2, 2002, pp. 139–56.

Aslani, S., Kabiri, M., HosseinZadeh, S., et al. "The applications of heparin in vascular tissue engineering," Microvascular Research, Vol. 131, 2020, p. 104027.

Wang, P., Chi, L., Zhang, Z., et al. "Heparin: An old drug for new clinical applications," Carbohydrate Polymers, Vol. 295, 2022, p. 119818.

Bal dit Sollier, C., Dillinger, J.-G., and Drouet, L. "Anticoagulant activity and pleiotropic effects of heparin," JMV-Journal de Médecine Vasculaire, Vol. 45, No. 3, 2020, pp. 147–57.

Zhou, P., Yin, J.-X., Tao, H.-L., et al. "Pathogenesis and management of heparin-induced thrombocytopenia and thrombosis," Clinica Chimica Acta, Vol. 504, 2020, pp. 73–80.

Litov, L., Petkov, P., Rangelov, M., et al. "Molecular Mechanism of the Anti-Inflammatory Action of Heparin," International Journal of Molecular Sciences, Vol. 22, No. 19, 2021, p. 10730.

1. Vitiello, A., and Ferrara, F. "Low Molecular Weight Heparin, Anti-inflammatory/Immunoregulatory and Antiviral Effects, a Short Update," Cardiovascular Drugs and Therapy, Vol. 37, No. 2, 2021, pp. 277–81.

Seffer, M.-T., Cottam, D., Forni, L. G., et al. "Heparin 2.0: A New Approach to the Infection Crisis," Blood Purification, Vol. 50, No. 1, 2020, pp. 28–34.

Li, L., Tian, X., Feng, G., et al. "The predictive value of heparin-binding protein for bacterial infections in patients with severe multiple trauma," 2024.

Thachil, J. "The versatile heparin in COVID-19," Journal of Thrombosis and Haemostasis,Vol. 18, No. 5, 2020, pp. 1020–2.

Mazilu, L., Katsiki, N., Nikolouzakis, T. K., et al. "Thrombosis and Haemostasis challenges in COVID-19 – Therapeutic perspectives of heparin and tissue-type plasminogen activator and potential toxicological reactions-a mini review," Food and Chemical Toxicology, Vol. 148, 2021, p. 111974.

Magnani, H. N. "Rationale for the Role of Heparin and Related GAG Antithrombotics in COVID-19 Infection," Clinical and Applied Thrombosis/Hemostasis, Vol. 27, 2021, p. 107602962097770.

Hogwood, J., Gray, E., and Mulloy, B. "Heparin, Heparan Sulphate and Sepsis: Potential New Options for Treatment," Pharmaceuticals, Vol. 16, No. 2, 2023, p. 271.

Shi, D., Bu, C., He, P., et al. "Structural Characteristics of Heparin Binding to SARS-CoV-2 Spike Protein RBD of Omicron Sub-Lineages BA.2.12.1, BA.4 and BA.5," Viruses, Vol. 14, No. 12, 2022, p. 2696.

Lippi, G., Henry, B. M., and Favaloro, E. J. "The Benefits of Heparin Use in COVID-19: Pleiotropic Antiviral Activity beyond Anticoagulant and Anti-Inflammatory Properties," Seminars in Thrombosis and Hemostasis, Vol. 49, No. 01, 2022, pp. 073–5.

Dey, S., Fan, C., Gothelf, K. V., et al. "DNA origami," Nature Reviews Methods Primers, Vol. 1, No. 1, 2021.

Dastorani, S., Hasanzadeh Ghasemi, R. "Modeling and investigating the behavior of triangular origami DNA under the influence of laboratory temperature", Science and Technology in Mechanical Engineering, 2023; 1(1): 58-69. doi: 10.22034/stme.2022.162701.

Mogheiseh, M., Hasanzadeh Ghasemi, R., and Soheilifard, R. "The effect of crossovers on the stability of DNA origami type nanocarriers," Multidiscipline Modeling in Materials and Structures, Vol. 17, No. 2, 2020, pp. 426–36.

Dastorani, S., Ghasemi, R. H., and Soheilifard, R. "A Study on the Bending Stiffness of a New DNA Origami Nano-Joint," Molecular Biotechnology, Vol. 63, No. 11, 2021, pp. 1057–67.

Mogheiseh, M., Etemadi, E., and Hasanzadeh

Ghasemi, R. "Design, molecular dynamics simulation, and investigation of the mechanical behavior of DNA origami nanotubes with auxetic and honeycomb structures," Journal of Biomolecular Structure and Dynamics, Vol. 41, No. 24, 2023, pp. 14822–31.

Dastorani, S., Mogheiseh, M., Ghasemi, R. H., et al. "Modelling and structural investigation of a new DNA Origami based flexible bio-nano joint," Molecular Simulation, Vol. 46, No. 13, 2020, pp. 994–1003.

Dastorani, S., Shariati, M., Hasanzadeh Ghasemi, R. "Comparison of the bending behavior of DNA origami Nano beam using the nonlinear theory method and steered molecular dynamics simulation", Nano World, 2024; 19(73): 54-45.

Monferrer, A., Kohler, F., Sigl, C., et al. "DNA origami traps for large viruses," Cell Reports Physical Science, Vol. 4, No. 1, 2023, p. 101237.

Monferrer, A., Kretzmann, J. A., Sigl, C., et al. "Broad-Spectrum Virus Trapping with Heparan Sulfate-Modified DNA Origami Shells," ACS Nano, Vol. 16, No. 12, 2022, pp. 20002–9.

Albanyan, B., Laurini, E., Posocco, P., Pricl, S., & Smith, D. K. (2017). Self-Assembled Multivalent (SAMul) Polyanion Binding—Impact of Hydrophobic Modifications in the Micellar Core on DNA and Heparin Binding at the Peripheral Cationic Ligands. In Chemistry – A European Journal (Vol. 23, Issue 26, pp. 6391–6397). Wiley. https://doi.org/10.1002/chem.201700177.

Fechner, L. E., Albanyan, B., Vieira, V. M. P., Laurini, E., Posocco, P., Pricl, S., & Smith, D. K. (2016). Electrostatic binding of polyanions using self-assembled multivalent (SAMul) ligand displays – structure–activity effects on DNA/heparin binding. In Chemical Science (Vol. 7, Issue 7, pp. 4653–4659). Royal Society of Chemistry (RSC). https://doi.org/10.1039/c5sc04801j.

Marson, D., Laurini, E., Aulic, S., Fermeglia, M., & Pricl, S. (2020). Perceptions and Misconceptions in Molecular Recognition: Key Factors in Self-Assembling Multivalent (SAMul) Ligands/Polyanions Selectivity. In Molecules (Vol. 25, Issue 4, p. 1003). MDPI AG.https://doi.org/10.3390/molecules25041003.

Mulloy, B., & Forster, M. J. (1995). N.M.R. AND MOLECULAR-MODELLING STUDIES OF THE SOLUTION CONFORMATION OF HEPARIN. Worldwide Protein Data Bank. https://doi.org/10.2210/pdb1hpn/pdb.

Tuning Surface Structure of BiOI Photocatalysts Using Magnetized Methanol: Applied Magnetic Field

Sara Abolhasani[2], Ali Ahmadpour[1,2*], Mostafa Gholizadeh[3]

[1]*Department of Chemical Engineering, Faculty of Engineering, Ferdowsi University of Mashhad, Mashhad, Iran*

[2]*Industrial Catalysts, Adsorbents, and Environment Lab., Oil and Gas Research Institute, Ferdowsi University of Mashhad, Mashhad, Iran*

[3]*Department of Chemistry, Faculty of Science, Ferdowsi University of Mashhad, Mashhad*

**Corresponding author: ahmadpour@um.ac.ir*

Abstract— Magnetic fields have been extensively used for the synthesis of nanostructures. In this study, a magnetic field was applied to methanol, named magnetized methanol, to be utilized as a solvent in the solvothermal synthesis of bismuth oxyiodide (BiOI) photocatalysts. The primary goal of this research is to present a novel technology for modifying nanostructures to enhance their applications.

Keywords: Magnetized methanol, Nanostructures, BiOI, Morphology control

INTRODUCTION

Among bismuth oxyhalides, BiOI has been recognized as semiconductors with a two-dimensional layered structure, featuring a narrow band gap and activation under visible light [1]. Modifying synthesis conditions can alter the crystal structures and morphologies leading to the utilization of their anisotropic properties in different plane orientations [2]. Arumugam et al. identified different BiOI morphologies, such as 2D square-like nanosheets and 3D hierarchical flower-like structures, which are obtained by altering the solvents (water, ethanol, methanol, and ethylene glycol) during solvothermal synthesis [3].

The effect of magnetic fields on solvent molecule clusters has always been a serious challenge in industry and academia [4]. The physical and chemical properties of the solvent, such as viscosity, zeta potential, and hydrogen bonding, were changed under this modification [5]. Rashidi et al. used ordinary and magnetized ethanol as a solvent to synthesize various zinc oxide (ZnO) structures under the solvothermal method [6].

The main purpose of this research is to create tunable bismuth oxyiodide structures by varying the duration of magnetic field exposure on methanol as a novel solvent to control morphology.

METHODOLOGY

A solvent-magnetizing device was applied to magnetize methanol [7]. The magnetic field exposure time was controlled in a closed cycle from 1 pass to 60 min (Fig. 1).

The primary synthesis of BiOI photocatalysts followed the solvothermal method from the literature [3]. The synthesized BiOI photocatalysts were labeled as Bi-X (x: 0, 1 pass, 15, 30, and 60), corresponding to the magnetization time of methanol.

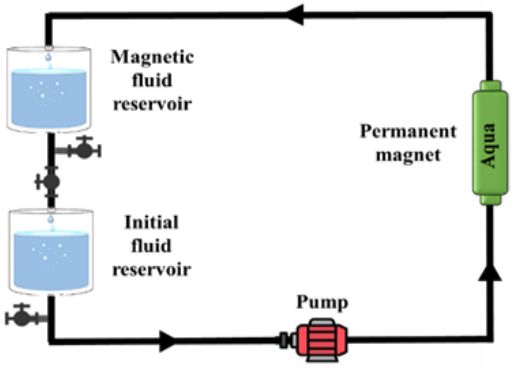

Fig.1 Schematic of Solvent Magnetizing Apparatus (SMA)

RESULTS AND DISCUSSION

Fig. 2 illustrates the morphological structure of the synthesized BiOI photocatalysts. The pristine BiOI and Bi- 1 pass displayed numerous irregular 2D nanosheets assembled into 3D flower-like

structures (Fig. 2 (a, b) to (c, d)). In contrast, Fig. 2 (e, f) depicted Bi-15 formed regular 3D flower-like microsphere structures [3]. The development of the nanoflower structure from Bi-0 to Bi-30 highlights the impact of magnetic field exposure time on the morphology of methanol-treated BiOI (Fig. 2 (a, b) to (g, h)). Finally, the nanoflake structures of Bi-60 are shown in Fig. 2 (i, j). This indicates that magnetized methanol significantly influences the synthesis process and structural arrangement.

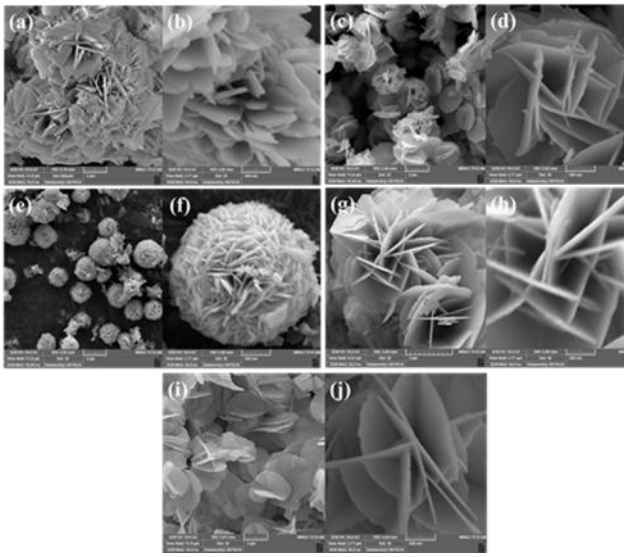

Fig.2 FESEM images of (a, b) Bi-0, (c, d) Bi-1 pass, (e, f) Bi-15, (g, h) Bi-30, and (i, j) Bi-60 in the 2 µm and 500 nm scales.

CONCLUSION

In conclusion, a novel approach utilizing magnetized solvent for the synthesis of bismuth oxyiodide semiconductors was introduced. It was found that adjusting the magnetic field exposure time could yield the desired bismuth oxyiodide structure.

This study has shown that magnetized methanol can affect the crystallinity and morphology of BiOI. Overall, this method provides a sustainable and efficient way for the synthesis of nanostructures, consistent with environmentally friendly practices.

ACKNOWLEDGMENT

The authors have appreciated the financial support of Ferdowsi University of Mashhad Research Council, Mashhad, Iran (Grant No. 61392) for this work.

REFERENCES

[1] X. Wei, M. U. Akbar, A. Raza, and G. Li, “A review on bismuth oxyhalide based materials for photocatalysis,” Nanoscale Adv., vol. 3, no. 12, p. 3353, 2021, doi: 10.1039/d1na00223f.

[2] R. A. Jagt, T. N. Huq, and K. M, Borsig, “Controlling the preferred orientation of layered BiOI solar absorbers,” J. Mater. Chem. C, vol. 8, no. 31, p. 10791, 2020, doi: 10.1039/d0tc02076a.

[3] M. Arumugam, Y. Yu, and H. J. Jung, “Solvent-mediated synthesis of BiOI with a tunable surface structure for effective visible light active photocatalytic removal of Cr(VI) from wastewater,” Environ. Res., vol. 197, no. February, p. 111080, 2021, doi: 10.1016/j.envres.2021.111080.

[4] Y. Absalan, M. Gholizadeh, and H. J. Choi, “Magnetized solvents: Characteristics and various applications,” J. Mol. Liq., vol. 335, p. 116167, 2021, doi: 10.1016/j.molliq.2021.116167.

[5] E. Esmaeilnezhad, H. J. Choi, M. Schaffie, M. Gholizadeh, and M. Ranjbar, “Characteristics and applications of magnetized water as a green technology,” J. Clean. Prod., vol. 161, p. 908, 2017, doi: 10.1016/j.jclepro.2017.05.166.

[6] H. Rashidi, A. Ahmadpour, M. Gholizadeh, F. F. Bamoharram, and F. Moosavi, “Effect of Magnetized Ethanol on the Shape Evolution of Zinc Oxide from Nanoparticles to Microrods: Experimental and Molecular Dynamic Simulation

Study," Adv. Powder Technol., vol. 29, no. 2, p. 349, 2018, doi: 10.1016/j.apt.2017.11.022.

[7] M. Gholizadeh, "Process of chemical reaction in magnetized solvents," U.S. patent (US10507450B2), 2019.

Nanobiosensors: Novel Tools for Accurate Detection of Zoonotic Pathogenic Bacteria and Improving Global Health

Marziyeh Tavakolizadeh[1], Soheil Sadr[2], Abbas Rahdar[3], Sadanand Pandey[4]

[1]*Department of Food Hygiene and Aquaculture, Faculty of Veterinary Medicine, Ferdowsi University of Mashhad, Mashhad, Iran.*

[2]*Department of Pathobiology, Faculty of Veterinary Medicine, Ferdowsi University of Mashhad, Mashhad, Iran.*

[3]*Department of Physics, University of Zabol, Zabol, Iran.*

[4]*Department of Chemistry, College of Natural Science, Yeungnam University, 280 Daehak-Ro, Gyeongsan 38541, Korea*

**Corresponding author: a.rahdar@uoz.ac.ir*

Abstract- A new generation of advanced diagnostic tools has been developed based on nanobiosensors that have revolutionized the method of detecting bacterial zoonotic diseases more quickly and accurately. In addition to being a major threat to public health, bacteria, and zoonotic diseases, which may be transmitted from humans to animals, can negatively affect the global economy. Nanobiosensors combine biological components with nanotechnology to detect biological targets, such as antigens, DNA, or bacterial cells, compassionately and accurately. This review article provides an overview of nanobiosensors, including their structure and function. In addition to their advantages of having short response times and high accuracy, these new tools can also detect complex samples quickly. A rapid and more efficient method of detecting microorganisms than that employed by molecular methods such as PCR or microbial culture. Despite this, their widespread use in clinical settings has yet to be extended due to challenges such as production costs and a need for standardization.

Keywords: Nanotechnology, Nanobiosensors, Bacterial infection, Zoonotic diseases, Diagnosis

INTRODUCTION

Public health and food security are seriously threatened by zoonotic diseases transmitted by bacteria to humans [1]. It is vital to detect these bacteria early and accurately, even at the initial stages of infection, to control disease outbreaks, reduce treatment costs, and prevent epidemics from spreading.

Traditional means of diagnosing diseases, such as microbial cultures and polymerase chain reactions (PCR), have made considerable advances in recent decades; however, they still have some limitations, such as being time-consuming, requiring sophisticated equipment, and being relatively expensive [2]. While nanobiosensors have been shown to have great potential in providing new, accurate, and efficient tools to overcome these challenges, they still have a long way to go [3].

Nanobiosensors are nanotechnology-based diagnostic devices that detect a specific target using biological components such as enzymes, antibodies, or DNA [4]. Due to their high sensitivity, fast response time, and multiplex detection capabilities, these devices rapidly expand in the biomedical, environmental, and food industries [5]. The current review aims to investigate the application of nanobiosensors to detect zoonotic bacteria.

NANOBIOSENSORS

Nanoniosensors usually comprise three main parts: the biocomponent, the transducer component, and the signal processing system. The biocomponent, which often includes antibodies, aptamers, or enzymes, recognizes the specific target [6]. As a result of the transducer, the biological signal produced by the biocomponent is converted into an electrical, optical, or electromagnetic signal to process it. After the signals are collected, the processing system analyzes them to determine whether there is an actual presence or concentration of the target [7]. This provides qualitative and quantitative analysis of the signals.

Because of their unique optical and electrical properties, these nanoparticles can be used to produce high sensor sensitivity and accuracy [8]. An example of using gold nanoparticles to enhance optical signals is using plasmonic nanobiosensors, which can detect targets with low concentrations of pollutants using plasmonic nanoparticles to amplify optical signals. Furthermore, nanobiosensors can perform faster and more accurate measurements because they are constructed using carbon nanotubes and quantum dots. In recent years, nanobiosensors have been widely used in various fields, including medicine and disease diagnosis [9].

APPLICATION

Nanobiosensors have become increasingly widespread in recent years in diagnosing zoonotic diseases caused by bacterial species, and positive results have been reported in this field. *Brucella* spp. has been detected successfully by antibody-based nanobiosensors, one of the most successful examples of this type of detection in serum and milk samples [10]. These nanobiosensors, utilizing gold nanoparticles and monoclonal antibodies, have detected bacteria rapidly and accurately with higher sensitivity than conventional methods [1]. Such technologies are particularly useful in remote areas with limited access to advanced laboratories. Moreover, leptospirosis can also be detected via aptamer-based nanobiosensors [11]. Nanobiosensors use synthetic aptamers that bind to specific antigens of Leptospira species, enabling early disease detection.

Gold nanoparticle-based plasmonic nanobiosensors have been developed to detect campylobacteriosis DNA in food [12]. This technology reduces detection time to less than an hour, making food safety and disease prevention essential.

CONCLUSION

Since nanobiosensors are sensitive, have a short response time, and are applicable in a wide range of conditions, they are considered practical tools for detecting bacterial zoonotic diseases. However, several challenges still need to be addressed, such as production costs, stability under real-world conditions, and standardization.

ACKNOWLEDGMENT

We thank the Ferdowsi University of Mashhad Research Deputy for their support.

REFERENCES

1. Rios TB, Maximiano MR, Feitosa GC, Malmsten M, Franco OL. Nanosensors for animal infectious disease detection. Sensing and Bio-Sensing Research. 2024:100622.
2. Arshad R, Sargazi S, Fatima I, Mobashar A, Rahdar A, Ajalli N, et al. Nanotechnology for therapy of zoonotic diseases: A comprehensive overview. ChemistrySelect. 2022;7(21):e202201271.
3. Kerry RG, Ukhurebor KE, Kumari S, Maurya GK, Patra S, Panigrahi B, et al. A comprehensive review on the applications of nano-biosensor-based approaches for non-communicable and communicable disease detection. Biomaterials Science. 2021;9(10):3576-602.
4. Hajjafari A, Sadr S, Rahdar A, Bayat M, Lotfalizadeh N, Dianaty S, et al. Exploring the integration of nanotechnology in the development and application of biosensors for enhanced detection and monitoring of colorectal cancer. Inorganic Chemistry Communications. 2024:112409.
5. Sadr S, Lotfalizadeh N, Ghafouri SA, Delrobaei M, Komeili N, Hajjafari A. Nanotechnology innovations for

increasing the productivity of poultry and the prospective of nanobiosensors. Veterinary Medicine and Science. 2023;9(5):2118-31.
6. Sadr S, Lotfalizadeh N, Abbasi AM, Soleymani N, Hajjafari A, Roohbaksh Amooli Moghadam E, et al. Challenges and prospective of enhancing hydatid cyst chemotherapy by nanotechnology and the future of nanobiosensors for diagnosis. Tropical medicine and infectious disease. 2023;8(11):494.
7. Hajjafari A, Sadr S, Santucciu C, Masala G, Bayat M, Lotfalizadeh N, et al. Advances in Detecting Cystic Echinococcosis in Intermediate Hosts and New Diagnostic Tools: A Literature Review. Veterinary Sciences. 2024;11(6):227.
8. Castillo-Henríquez L, Brenes-Acuña M, Castro-Rojas A, Cordero-Salmerón R, Lopretti-Correa M, Vega-Baudrit JR. Biosensors for the detection of bacterial and viral clinical pathogens. Sensors. 2020;20(23):6926.
9. Ahangari A, Mahmoodi P, Mohammadzadeh A. Advanced nano biosensors for rapid detection of zoonotic bacteria. Biotechnology and Bioengineering. 2023;120(1):41-56.
10. Ahangari A, Mahmoodi P, Mohammadzadeh A. Biosensors functionalized with nanoparticles for rapid detection of Brucella. Microchemical Journal. 2022;181:107697.
11. Vishwakarma A, Meganathan Y, Ramya M. Aptamer-based assay for rapid detection, surveillance, and screening of pathogenic Leptospira in water samples. Scientific Reports. 2023;13(1):13379.
12. Ghazy A, Nyarku R, Faraj R, Bentum K, Woube Y, Williams M, et al. Gold Nanoparticle-Based Plasmonic Detection of Escherichia coli, Salmonella enterica, Campylobacter jejuni, and Listeria monocytogenes from Bovine Fecal Samples. Microorganisms. 2024;12(6):1069.

Novel Applications of Nanoparticles in Food Packaging: Improving Food Safety, Stability, and Shelf Life

Marziyeh Tavakolizadeh[1], Soheil Sadr[2], Abbas Rahdar[3], Sadanand Pandey[4]

[1]*Department of Food Hygiene and Aquaculture, Faculty of Veterinary Medicine, Ferdowsi University of Mashhad, Mashhad, Iran.*

[2]*Department of Pathobiology, Faculty of Veterinary Medicine, Ferdowsi University of Mashhad, Mashhad, Iran.*

[3]*Department of Physics, University of Zabol, Zabol, Iran.*

[4]*Department of Chemistry, College of Natural Science, Yeungnam University, 280 Daehak-Ro, Gyeongsan 38541, Korea*

**Corresponding author: a.rahdar@uoz.ac.ir*

Abstract- Nanoparticles and nanotechnology have attracted much attention in various fields, especially in the food packaging industry, in recent decades. Food packaging, which plays a fundamental role in maintaining food products' quality, safety, and sustainability, can reach a new efficiency level using nanotechnology. Nanoparticles such as metal nanoparticles and nanocomposites have unique properties, including antibacterial properties, preventing gas and moisture penetration, improving mechanical strength, increasing the shelf life of food, and reducing waste. In addition, using nanosensors in active and intelligent packaging makes it possible to detect food spoilage and provide accurate information to the consumer. Hence, the current review aims to explore nanotechnology, nanoparticles' critical properties, and their application in food packaging. Moreover, the current review examines the various applications of nanotechnology in food packaging, including active, innovative, and biodegradable packaging, with practical examples.

Keywords: Nanoparticles, Nanotechnology, Active packaging, Food safety, Waste reduction

INTRODUCTION

Food packaging is one of the most important components in the food supply chain due to its ability to prevent spoilage and contamination as well as maintain the product's quality throughout its lifespan [1]. As the global population continues to grow at an exponential rate, as well as the increasing demand for healthy and safe food at all levels, it has become increasingly evident that advanced and effective packaging is needed today more than ever before [2]. Considering this, nanotechnology has been introduced as a revolutionary method of improving the performance of food packaging.

Nanotechnology has the capability of modifying the properties of materials at the nanometer scale [3]. As a result, nanotechnology can expand the functionality of packaging as a whole. It has been proven that nanotechnology is capable of offering unique properties to packaging designers by supplying nanoparticles and nanostructured materials, which in turn have enabled packaging design with unique properties like excellent gas penetration resistance, antibacterial properties, and the ability to detect gases [4]. In addition to improving the shelf life of the product, these features increase the safety of the product. It has been shown that silver nanoparticle packaging inhibits microorganism growth so that gas and moisture cannot penetrate the package [5].

Hence, the current review explores nanotechnology, nanoparticles' critical properties, and their application in food packaging. It uses practical examples to examine nanotechnology applications in food packaging, including active, innovative, and biodegradable packaging.

NANOTECHNOLOGY

In the field of nanotechnology, there are a variety of material production, application, and design methods that are used to produce materials that are smaller than one nanometer in size, typically between one and a hundred nanometers [6]. Depending on the size and shape of the material, it can possess physical, chemical, and biological properties that may differ from those of its bulk state [7]. A

variety of properties can be observed in this material, including increased surface area, improved reactivity, and changes in optical and mechanical properties [8].

Among the critical components of nanotechnology are nanoparticles, which are small, highly crystalline particles [9]. Nanoparticles can be manufactured from any type of material, such as metals, polymers, natural materials, or combinations of these materials. Nanoparticles are widely used in a wide variety of industrial, biomedical, and environmental applications because of their high surface areas and unusual behavior [9]. The use of nanoparticles, such as silver nanoparticles that have a high level of antibacterial activity, is widespread in food packaging and medical devices [10].

APPLICATION IN FOOD PACKAGING

Nanoparticles in food packaging fall into three categories: active, smart, and biodegradable. Active packaging involves materials that interact directly with food and extend product shelf life by releasing or absorbing specific compounds [11]. For example, packaging containing silver or copper nanoparticles can inhibit microorganism growth and prevent food spoilage [12].

Nanosensors based on gold and silver nanoparticles in food packaging can detect pH changes or spoilage gas production. They provide information about product quality [13].

Biodegradable packaging is another nanotechnology application in the food industry. Added nanoparticles to natural polymers such as chitosan or polylactic acid can improve the strength and durability of these materials while maintaining biodegradability. This approach reduces plastic waste and protects the environment [14].

CONCLUSION

As nanotechnology and nanoparticles are emerging as novel means of enhancing food packaging safety, quality, and sustainability, they provide unique opportunities for improvement. Nevertheless, there are still many challenges that are yet to be overcome, such as high production costs, safety concerns, and environmental impacts.

ACKNOWLEDGMENT

We thank the Ferdowsi University of Mashhad Research Deputy for their support.

REFERENCES

1. Biswas R, Alam M, Sarkar A, Haque MI, Hasan MM, Hoque M. Application of nanotechnology in food: processing, preservation, packaging and safety assessment. Heliyon. 2022;8(11).
2. Duncan TV. Applications of nanotechnology in food packaging and food safety: barrier materials, antimicrobials and sensors. Journal of colloid and interface science. 2011;363(1):1-24.
3. Enescu D, Cerqueira MA, Fucinos P, Pastrana LM. Recent advances and challenges on applications of nanotechnology in food packaging. A literature review. Food and Chemical Toxicology. 2019;134:110814.
4. Wesley SJ, Raja P, Raj AA, Tiroutchelvamae D. Review on-nanotechnology applications in food packaging and safety. International Journal of Engineering Research. 2014;3(11):645-51.
5. Berekaa MM. Nanotechnology in food industry; advances in food processing, packaging and food safety. International Journal of Current Microbiology and Applied Sciences. 2015;4(5):345-57.
6. Sadr S, Poorjafari Jafroodi P, Haratizadeh MJ, Ghasemi Z, Borji H, Hajjafari A. Current status of nano -

vaccinology in veterinary medicine science. Veterinary Medicine and Science. 2023;9(5):2294-308.
7. Hajjafari A, Sadr S, Santucciu C, Masala G, Bayat M, Lotfalizadeh N, et al. Advances in Detecting Cystic Echinococcosis in Intermediate Hosts and New Diagnostic Tools: A Literature Review. Veterinary Sciences. 2024;11(6):227.
8. Soleymani N, Sadr S, Santucciu C, Rahdar A, Masala G, Borji H. Evaluation of the In-Vitro Effects of Albendazole, Mebendazole, and Praziquantel Nanocapsules against Protoscolices of Hydatid Cyst. Pathogens. 2024;13(9):790.
9. Primožič M, Knez Ž, Leitgeb M. (Bio) Nanotechnology in food science—food packaging. Nanomaterials. 2021;11(2):292.
10. Majid I, Nayik GA, Dar SM, Nanda V. Novel food packaging technologies: Innovations and future prospective. Journal of the Saudi Society of Agricultural Sciences. 2018;17(4):454-62.
11. del Rosario Herrera-Rivera M, Torres-Arellanes SP, Cortés-Martínez CI, Navarro-Ibarra DC, Hernández-Sánchez L, Solis-Pomar F, et al. Nanotechnology in food packaging materials: role and application of nanoparticles. RSC advances. 2024;14(30):21832-58.
12. Onyeaka H, Passaretti P, Miri T, Al-Sharify ZT. The safety of nanomaterials in food production and packaging. Current Research in Food Science. 2022;5:763-74.
13. Alfadul S, Elneshwy A. Use of nanotechnology in food processing, packaging and safety–review. African Journal of Food, Agriculture, Nutrition and Development. 2010;10(6).
14. Alfei S, Marengo B, Zuccari G. Nanotechnology application in food packaging: A plethora of opportunities versus pending risks assessment and public concerns. Food Research International. 2020;137:109664.

Optimized Statistical Analysis of Factors Influencing the Growth of Carbon Nanotubes in Chemical Vapor Deposition (CVD) Processes

Elahe Khosravifard[1], Mohammad Taghi Hamed Mosavian[2]*, Morteza Maghrebi [3]

[1,2,3] *Department of Chemical Engineering, Faculty of Engineering, Ferdowsi University of Mashhad, Mashhad, Iran*

**Corresponding author: mosavian@um.ac.ir*

Abstract— Carbon nanotubes (CNTs) have remarkable properties, making them suitable for diverse applications. Chemical Vapor Deposition (CVD) is a widely adopted synthesis technique due to its scalability and flexibility. This study investigates critical factors such as temperature, catalyst type, pressure, growth time, and carbon sources, statistically analyzing data from 400 studies. Results indicate that optimal conditions vary based on CNT type (SWNT or MWNT) and desired properties, such as length and alignment. Understanding these dependencies enables improved control of the CVD process, resulting in higher-quality CNT production.

Keyword: CNTs, CVD, Statistical Analysis, Growth Factors.

INTRODUCTION

Carbon nanotubes (CNTs) possess extraordinary mechanical, electrical, and thermal properties, making them essential in diverse applications, such as sensors, display panels, and lightweight composites [1] [2] [3, 4]. Among the various synthesis methods, Chemical Vapor Deposition (CVD) is particularly effective for producing vertically aligned CNTs (VACNTs). This process involves using a substrate coated with a catalyst, heated above 700°C, to facilitate the interaction between carbon precursors and the catalyst. CVD enables large-scale production, but its success depends on controlling various interrelated factors, such as temperature, pressure, and carbon source. This study analyzes data from approximately 400 studies to identify optimal conditions for CNT growth, aiming to simplify and enhance production while minimizing defects.

METHODS OF GROWING VACNTS A.

CVD techniques are categorized based on chamber pressure, reactor type, carbon source, and heating methods. Thermal CVD (TCVD) and Plasma-Enhanced CVD (PECVD) are prominent techniques:

Thermal CVD (TCVD) Operates at high temperatures and is widely used for large-scale CNT production.

Plasma-Enhanced CVD (PECVD) Allows for lower synthesis temperatures and produces free-standing structures, making it versatile for growing VACNTs and other carbon-based materials [5] .

ROLE OF SUBSTRATE AND BUFFER LAYERS

Buffer layers are crucial in preventing undesired reactions between the catalyst and substrate. For instance:

Silica (SiO2) Acts as a protective barrier, preventing catalyst-substrate reactions and enhancing CNT spinnability into yarns [6, 7].

Alumina (Al2O3) Minimizes catalyst agglomeration and improves gas permeability, ensuring controlled growth [8].

Aluminum (Al) Functions as a buffer layer due to its low melting point, which prevents substrate infiltration [9, 10].

Statistical analyses show that combinations like Si/SiO2 and composite layers (e.g., Al2O3/SiO2/Si) are optimal for consistent CNT growth.

CATALYST SELECTION

Transition metals such as iron (Fe), cobalt (Co), and nickel (Ni) are widely used due to their high carbon solubility and catalytic activity. These catalysts influence CNT structure, diameter, and yield. Key advancements include:

Bimetallic Catalysts (e.g., Fe-Co, Fe-Ni) Improve catalytic efficiency through synergistic effects.

Nanostructured Catalysts (e.g., nanoparticles, nanowires) Provide higher surface area, promoting efficient growth.

Non-metallic Catalysts (e.g., MgO, Al2O3) Reduce poisoning and enhance chirality control.

Statistical data highlights Fe and Ni as the most effective catalysts for producing single-walled (SWNTs) and multi-walled CNTs (MWNTs).

EFFECT OF TEMPERATURE

Temperature is a critical factor in CNT synthesis. Statistical studies reveal that:

Higher Temperatures (900–1200°C) Favor SWNT growth and result in longer CNTs.

Moderate Temperatures (750–850°C) Are optimal for MWNTs.

Low Temperatures (600–900°C) Result in diminished growth and lower quality.

For example, CNT length increases from 8 µm at 800°C to 165 µm at 1100°C, illustrating the importance of precise temperature control [11].

GROWTH TIME

CNT length is strongly influenced by growth time. Optimal durations are:

2400–3600 Seconds: Lead to maximum CNT length due to continuous carbon deposition.

Extended Durations (>3600 Seconds): Result in catalyst deactivation and accumulation of amorphous carbon, reducing CNT length [12].

Statistical data underscores the need for balanced growth times to ensure high-quality production.

PRESSURE

Pressure plays a pivotal role in controlling CNT morphology and yield. Key findings include:

Moderate Pressures (~8000 Pa) Promote longer CNT growth and higher yield.

Low Pressures (<133 Pa) Lead to hollow structures and additional graphene layers [13].

High Pressures (>8000 Pa) Favor bamboo-like structures with denser layering [14].

The results highlight the necessity of pressure optimization to tailor CNT properties for specific applications.

CARBON SOURCE

The choice of carbon source depends on the type of CNT being synthesized:

SWNTs Require high-temperature-stable sources like methane (CH4) and carbon monoxide (CO).

MWNTs Utilize sources like acetylene (C2H2) and ethanol (C2H5OH) at moderate temperatures.

Statistical analysis confirms that selecting the appropriate carbon source is vital for achieving desired CNT quality and structure.

OPTIMAL GROWTH CONDITIONS

Key parameters for SWNT and MWNT synthesis include:

Temperature: SWNTs require 900–1200°C, while MWNTs grow optimally at 600–1000°C.

Catalyst: Precise control of particle size enhances SWNT production, whereas MWNT synthesis tolerates larger particles.

Pressure: Lower pressures reduce defects for SWNTs, while MWNTs are produced under a wider range of conditions.

Carbon Source: Stable hydrocarbons are essential for SWNTs; a broader range of sources is acceptable for MWNTs.

CONCLUTION

The study identifies critical factors—temperature, catalyst, growth time, pressure, and carbon source—that influence CNT synthesis via CVD. These parameters are interdependent, requiring precise control to optimize CNT properties. Future research should focus on understanding these interactions to further improve synthesis efficiency and scalability, enabling CNTs to meet diverse industrial needs.

ACKNOWLEDGMENT

THE AUTHORS GRATEFULLY ACKNOWLEDGE THE PERSONNEL OF CHEMICAL ENGINEERING RESEARCH LAB OF FERDOWSI UNIVERSITY OF MASHHAD

REFERENCES

[1] X. Liang, J. Xia, G. Dong, and B. Tian, "Carbon nanotube thin film transistors for flat panel display application," Single-Walled Carbon Nanotubes, pp. 225-256, 2019.

[2] M. Penza, P. J. Martin, and J. T. Yeow, "Carbon nanotube gas sensors," Gas sensing fundamentals, pp. 109-174, 2014.

[3] S. Zhang et al., "Carbon nanotube/carbon composite fiber with improved strength and electrical conductivity via interface engineering," Carbon, vol. 144, pp. 628-638, 2019.

[4] X. Zhang et al., "Ultrastrong, stiff, and lightweight carbon‐nanotube fibers," Advanced materials, vol. 19, no. 23, pp. 4198-4201, 2007.

[5] R. Liu, Y. Chi, L. Fang, Z. Tang, and X. Yi, "Synthesis of carbon nanowall by plasma-enhanced chemical vapor deposition method," Journal of nanoscience and nanotechnology, vol. 14, no. 2, pp. 1647-1657, 2014.

[6] B. Wei et al., "Organized assembly of carbon nanotubes," Nature, vol. 416, no. 6880, pp. 495-496, 2002.

[7] C. C. Chiu, T. Y. Tsai, N. H. Tai, and C. Y. Lee, "Synthesis of ultra long vertically aligned carbon nanotubes using the rapid heating and cooling system in the thermal chemical vapor deposition process," Surface and Coatings Technology, Article vol. 200, no. 10 SPEC. ISS., pp. 3215-3219, 2006.

[8] S. Chakrabarti, H. Kume, L. Pan, T. Nagasaka, and Y. Nakayama, "Number of walls controlled synthesis of millimeter-long vertically aligned brushlike carbon nanotubes," Journal of Physical Chemistry C, Article vol. 111, no. 5, pp. 1929-1934, 2007.

[9] L. Qu, F. Du, and L. Dai, "Preferential syntheses of semiconducting vertically aligned single-walled carbon nanotubes for direct use in FETs," Nano Letters, Article vol. 8, no. 9, pp. 2682-2687, 2008.

[10] S. Parveen, A. Kumar, S. Husain, M. Zulfequar, and M. Husain, "Synthesis of highly dense and vertically aligned array of SWCNTs using a catalyst barrier layer: High performance field emitters for devices," Physica B: Condensed Matter, vol. 550, pp. 15-20, 2018.

[11] Y. T. Lee, J. Park, Y. S. Choi, H. Ryu, and H. J. Lee, "Temperature-Dependent Growth of Vertically Aligned Carbon Nanotubes in the Range 800−1100 °C," The Journal of Physical Chemistry B, vol. 106, no. 31, pp. 7614-7618, 2002/08/01 2002.

[12] P. L. Redmond, E. C. Walter, and L. E. Brus, "Photoinduced thermal copper reduction onto gold nanocrystals under potentiostatic control," The Journal of Physical Chemistry B, vol. 110, no. 50,

pp. 25158-25162, 2006.

[13] W. Li, J. Wen, and Z. Ren, "Effect of temperature on growth and structure of carbon nanotubes by chemical vapor deposition," Applied Physics A, vol. 74, pp. 397-402, 2002.

[14] W. Li, J. Wen, Y. Tu, and Z. Ren, "Effect of gas pressure on the growth and structure of carbon nanotubes by chemical vapor deposition," Applied Physics A, vol. 73, no. 2, pp. 259-264, 2001.

Synergistic Effects of Silane-Modified Carbon Black and Nano-Silica on Filler Dispersion and Dynamic Properties of Butyl Rubber Nanocomposites

F. Jaberi Mofrad[1], A. Ahmadpour[1*], S. Ostad Movahed[2]

[1] *Department of Chemical Engineering, Faculty of Engineering, Ferdowsi University of Mashhad, Mashhad, Iran.*

[2] *Department of Chemistry, Faculty of Science, Ferdowsi University of Mashhad, Mashhad, Iran*

* *Corresponding author: ahmadpour@um.ac.ir*

Abstract— In this research, the effect of silane-modified carbon black and nano-silica hybrid fillers on the curing and dynamic properties of butyl rubber (IIR) nano compounds was studied. Results revealed that the modification process influenced curing properties. The ΔTorque and Maximum torque (M_h) increased to the value of 3.4 dN.m and 4.3 dN.m after silane modification CB, which led to higher cross-link density (163.1 mol/m^3). Scanning electron microscopy (SEM) analysis indicated better dispersion of the modified CB in IIR nano compounds, which led to better properties and performance. The dynamic-mechanical-thermal analysis (DMTA) showed that modified CB reduced rolling resistance and improved ice grip potential. Overall, selecting modification approaches is crucial for achieving optimal results in the performance and application of IIR.

Keywords: Nano-silica, Carbon black, butyl rubber, Modification, DMTA

INTRODUCTION

Butyl rubber, also known as isobutylene-isoprene rubber (IIR), exhibits a low rate of gas permeability, High long-term thermal stability, ozone and weather resistance, and chemical and moisture resistance. It is used in tire tubes, inner liners for tubeless tires, wire and cable applications, tire curing bladders, and sealants [1]. IIR is reinforced with different types of fillers to improve its properties. Tire inner liners are commonly reinforced with carbon black. Carbon black and nano-silica significantly improve the mechanical and dynamic properties of the rubber compound [2]. Based on our previous work [3], modified CB demonstrates significant potential for application as a filler in rubber compounding. Therefore, silane-modified CB in nano-silica-reinforced IIR nano compounds aiming to enhance tire performance have been studied. Understanding butyl rubber compounds' curing and dynamic properties is essential for realizing their optimal design and applications. The present study aims to investigate the effect of modified CB and nano-silica as hybrid fillers on the performance of IIR-filled rubber nano compounds.

METHODOLOGY

As described in our previous work [3], carbon black was first oxidized by citric acid monohydrate and after that, the obtained material was modified with silane coupling agent (TESPT) and was labeled "Modified-CB". Table 1 presents the composition of the IIR nano compounds prepared in this study. A two-roll mill was used to mix the ingredients, and after that, the rubber nano compounds were cured in a compression mold at a temperature of 160 °C and a pressure of 150 bar.

Table 1. Formulation of butyl rubber nano compounds.

Samples Ingredients*	CB/Nano-Silica/IIR	Modified-CB/Nano-Silica/IIR
IIR (phr)	100	100
CB (phr)	5	0
Modified-CB (phr)	0	5

*Amounts of other components in both nano compounds:Nano-Silica, 5, Nano-ZnO, 6, Stearic acid, 2, S, 3, and TBBS, 4 phr.

RESULTS & DISCUSSION

"Fig. 1" shows the cure curve (torque vs time) of IIR nano compounds obtained by MDR at 160 °C. ΔTorque represents the variation between the maximum and minimum torque observed in the cured samples, indicating alterations in the cross-

link density (CLD) of the vulcanized rubber. According to "Fig. 1", the Modified-CB/nano-silica/IIR compound revealed higher ΔTorque (3.4 dN.m) and, as a result, a higher CLD value (163.1 mol/m^3). The obtained results conformed with the other report [4].

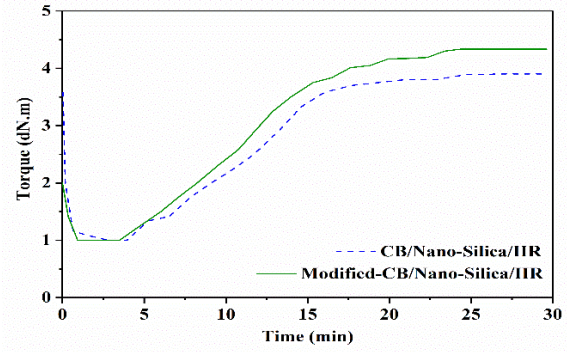

Fig 1. The curing curve of IIR nano compounds obtained by MDR at 160 ℃.

"Fig. 2" presents a comparison of SEM images (at the magnitude of 1 μm) showing the cross-sectional surfaces of cured IIR compounds with CB/nano-silica and Modified-CB/nano-silica nano-fillers. The addition of TESPT agents improves the interaction between the fillers and rubber, reducing their tendency to aggregate. As a result, modified-CB/nano-silica is better dispersed within the IIR matrix, leading to improved dynamic properties. The results of SEM images were consistent with the results of dynamic properties [5].

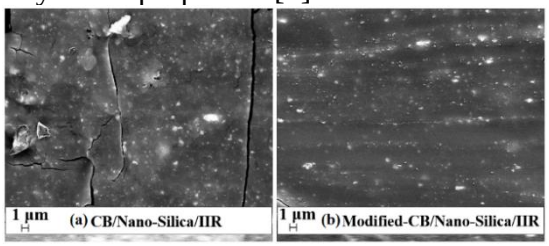

Fig 2. SEM images of CB/Nano-Silica/IIR (a) and Modified-CB/Nano-Silica/IIR (b) nano compounds at the magnitude of 1 μm.

The DMTA test was conducted to investigate the dynamic behavior of the cured nano compounds at a constant frequency of 1 Hz with a temperature sweep between -150 to 80 ℃ at a heating rate of 5 ℃/min. "Fig. 3" illustrates the comparison of damping or loss factor (tan δ) at temperatures of -20 ℃ and 60 ℃ for selected IIR nano compounds. Modified-CB/Nano-Silica/IIR represented a high ice grip (high tan δ at -20 ℃). At the same time, it illustrates low rolling resistance and reduced fuel consumption and pollution (low tan δ at 60 ℃) compared to the CB/Nano-Silica/IIR sample due to the better filler dispersion in IIR nano compounds. Similar observations were reported in another report [4].

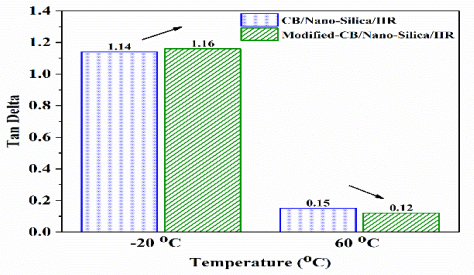

Fig 3. Comparison of damping factor (Tan δ) at temperatures of -20 ℃ and 60 ℃ for CB/Nano-Silica/IIR and Modified-CB/Nano-Silica/IIR compounds at 1 Hz.

CONCLUSIONS

IIR nano compounds were prepared via a two-roll mill with different types of fillers. DMTA and SEM analysis showed that the prepared IIR nano compound with modified-CB/nano-silica hybrid fillers has lower rolling resistance and enhanced ice grip than CB/nano-silica fillers due to better filler dispersion. Moreover, the silane-modified CB increased ΔTorque, which resulted in a higher CLD value.

ACKNOWLEDGMENT

The authors appreciate the support of Ferdowsi University of Mashhad, Iran (Grant No. 56010) for this work.

REFERENCES

Thomas, S., and Maria, H. J. (2016). Progress in rubber nanocomposites. Woodhead Publishing.

Sattayanurak, S., Sahakaro, K., Kaewsakul, W., Dierkes, W. K., Reuvekamp, L. A., Blume, A., and Noordermeer, J. W. (2020). Synergistic effect by high

specific surface area carbon black as secondary filler in silica reinforced natural rubber tire tread compounds. Polymer Testing, 81, 106173.

Jaberi Mofrad F., Ostad Movahed, S., and Ahmadpour, A. (2024). Surface modification of commercial carbon black by silane coupling agents for improving dispersibility in rubber compounds. Journal of Applied Polymer Science, 141(13), e55155. https://doi.org/10.1002/app.55155.

Wang, X., Wu, L., Yu, H., Xiao, T., Li, H., and Yang, J. (2021). Analysis of the effect of modification of silica and carbon black co-filled rubber composite on mechanical properties. e-Polymers, 21(1), 279-288.

Movahed, S. O., Ansarifar, A., and Song, M. (2009). Effect of silanized silica nanofiller on tack and green strength of selected filled rubbers. Polymer International, 58 (4), 424-429.

A Multi-scale Monte Carlo Simulation on Gold Nanoparticle Dose Enhancement for a Lung Tumor Treated with I-125 Brachytherapy

Elahe Movahedizade[1], Zahra Sajjadi[1*]

[1] *Department of Physics, Payame Noor University, PO BOX: 19395-3697, Tehran, Iran*

**Corresponding author: h_sajadi@pnu.ac.ir*

Abstract— It has been shown that the addition of gold nanoparticles in the tumour can improve the treatment gain in radiation therapy. In the present study, the dose enhancement ratio caused by I-125 Brachytherapy seeds with the presence of 3, 5, and 7 mg/g gold nanoparticles has been evaluated. The simulations were carried out on both macroscopic and microscopic scales using Geant4 and Geant4-DNA Monte Carlo toolkits, respectively. In both simulation scales, increasing the concentration of gold nanoparticles resulted in a dose enhancement of up to nearly 75%. Simulation results were similar at both macroscopic and microscopic scales when gold nanoparticles were physically defined, as opposed to when only tumour and cell densities were increased by the presence of nanoparticles. Direct and indirect DNA damage per primary photon also increased by raising the concentration of gold nanoparticles. In conclusion, the combination of gold nanoparticles with I-125 brachytherapy will be a promising approach for the treatment of lung tumours.

Keyword: Brachytherapy, Lung cancer, Nanoparticles, Monte Carlo simulation, Geant4

INTRODUCTION

Brachytherapy is one of the appropriate methods for treating lung cancers [1]. In brachytherapy, very small radioactive sources are placed within the tumour. Therefore, the maximum dose is delivered to the tumour and the nearby tissues are well sparred [1]. The low-energy I-125 seeds with dimensions of less than 5 mm are presented as encapsulated seeds from which only photons with an average energy of about 28 keV are emitted [2]. In the past decades, using gold nanoparticles (NPs) in radiotherapy, particularly in brachytherapy, has been introduced as an interesting idea to enhance the tumour dose [3]. By increasing the atomic number (Z) of the NP, the possibility of photoelectric interaction increases, which will result to the tumour dose enhancement. In related Monte Carlo simulations, some studies have simulated the physical presence of NPs in detail, while others have only investigated the effect of increasing tumour density [4]. That is, NPs were not simulated in a real way and only one of their effects in the tumour, i.e., the increase in density was taken into account. Recently, multi-scale Monte Carlo simulation studies have attracted the attention of researchers in various fields. Numerous studies have been carried out on a cellular scale that examined DNA damage in the nucleus of a mammalian cell with and without the presence of gold NPs [5]. A comparative study of these approaches has not been performed so far for a lung tumour under the treatment of brachytherapy with I-125. Thus, this study aims to examine this dose enhancement ratio (DER) at macroscopic and microscopic scales using the Geant4 Monte Carlo simulation toolkit [7].

METHODS & MATERIALS

We used the Geant4 toolkit (version 11.1) with the "G4EmStandardPhysics_option4" physics constructor for calculating DER at the macroscopic scale. The Geant4-DNA extension with the "G4EmDNAPhysics_option4" physics constructor was used for calculating DER at the microscopic scale. The MIRD human phantom was employed using the "Human_Phantom" example from the Geant4 advanced examples. A cubic tumour with a size of 3 cm was placed in the right lung. The tumour was defined as soft tissue (1.0 g/cm^3). The tumour is divided into a voxelized volume, where each voxel contains a gold NP with a diameter of 50 nm. Four concentrations of 0, 3, 5, and 7 mg/g were

defined for gold NPs. Thirty-five Amersham OncoSeed 6702 LDR seeds [2] were implanted in the tumor in five planes with a center-to-center distance of 1 cm. Each I-125 seed was defined as a cylinder with a radius of 0.4 mm and the total length of 4.5 mm. At microscopic stage, we used the "WholeNuclearDNA" extended example [7] of the Geant4 toolkit to fully simulate the details of DNA structure. The cell model is an ellipsoid of 13.0 × 11.0 × 5.0 μm^3 dimensions. A total of 1544, 3603, and 5662 gold NPs were implanted in the cytoplasm for 3, 5, and 7 mg/g concentrations, respectively. DNA damage is categorized into two general classes: SSB and DSB, which can be direct, indirect, or Mix. Direct and indirect DNA damages are the damages resulting from physical and chemical stages, respectively. At macroscopic and microscopic simulation stages, the DER was calculated by Eq. (1) and Eq. (2), respectively:

DER = (Tumor dose with NPs) / (Tumor dose without NPs)

DER = (Nucleus dose with NPs) / (Nucleus dose without NPs)

In the case that NPs were not physically present, the DER was calculated by Eq. (3):

DER = (Tumor dose with new density) / (Tumor dose with original density)

RESULT & CONCLUSION

In Fig. 1, the DER is compared in two macroscopic (tumor) and microscopic (cell) scales. Two different approaches of physical and non-physical (i.e., based on the tumor density) definition of NPs have been compared. According to Fig. 1, with increasing NP concentration, the dose increases rapidly. The results of two different approaches to implementing the definition of nanoparticle are completely different. At the macroscopic scale, when NPs are physically defined the DER is less than when only tumor density is manipulated. At the microscopic scale, the opposite is true. One of the reasons that in the previous simulation studies, many researchers used the density enhancement method to calculate the DER at the macroscopic scale is that a huge number of NPs must be defined for a typical weight percentage. It required extremely high computing resources. Recently, many researchers have been moving towards microscopic scale simulations in order to simulate higher concentrations of NPs for DER calculations. The correspondence of DER with the physical definition of NPs highlights the importance of the physical definition of NPs in both macroscopic and microscopic scales (see Fig. 1). The advantage of simulation on a microscopic scale is that it is possible to simulate higher concentrations of NPs due to the micrometric dimensions of cells and the relatively low number of NPs.

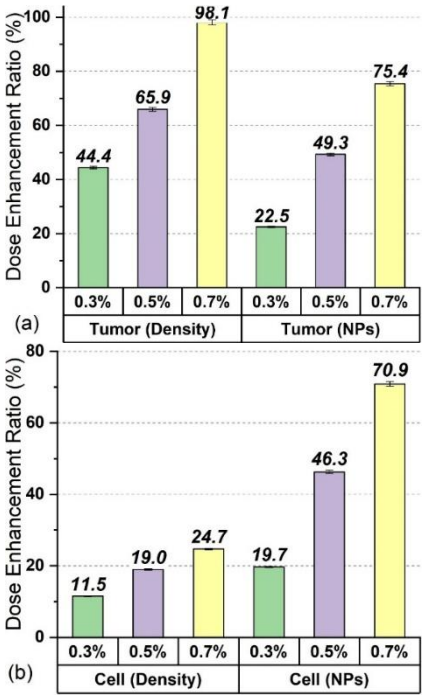

Fig. 1 The DER obtained with the presence of 3, 5, and 7 mg/g gold NPs in macroscopic **(a)** and microscopic **(b)** scales with two simulation approaches.

The induced DNA damage (direct and indirect SSBs as well as direct, indirect, and mix DSBs) per event in a fibroblast cell with and without the presence of gold NPs is presented in Fig. 2.

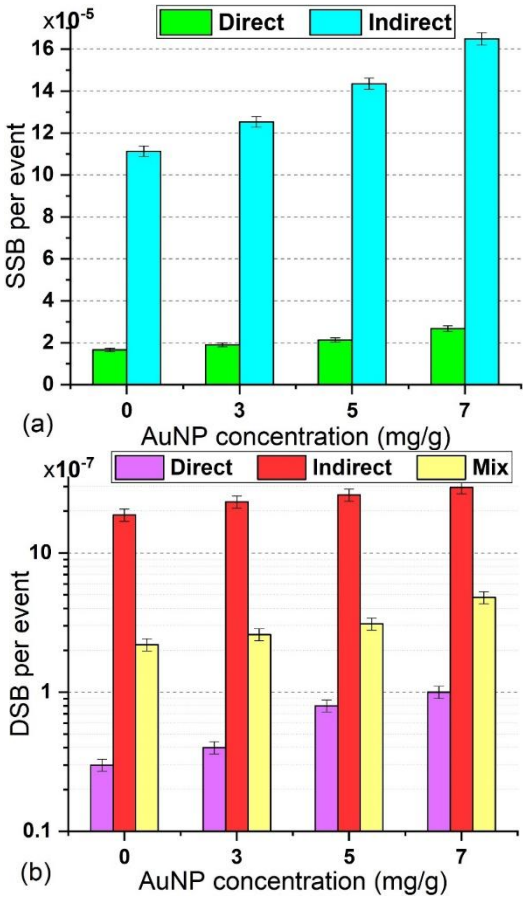

Fig. 2 Single **(a)** and double **(b)** strand break (SSB and DSB) per history induced in a fibroblast cell model with and without the presence of gold NPs in its cytoplasm.

According to Fig. 2, with the increase in the concentration of gold NPs, both SSB and DSB damages (per primary photon) increase because with an increase in the concentration of NPs, the probability of photons hitting them increases. Also, an increase in the production of high-energy secondary electrons will be observed due to the increase in the photoelectric effect as well as auger electrons. These extra secondary electrons are the main cause of DNA damage. The predominance of indirect damages is consistent with previous studies [8]. It is due to the fact that by increasing the energy deposited in the cell, more free radicals are produced in the chemistry stage. In general, simultaneous Monte Carlo simulation studies at both macroscopic and microscopic scales are recommended for a better understanding of dosimetry outputs.

In conclusion, gold NPs are a promising agent for the treatment of lung tumor along with brachytherapy since they can increase the dose to the tumor up to 75%. The resulting DNA damage per primary photon increased with increasing the concentration of gold NPs, which confirms the usefulness of gold NPs with higher concentrations (if possible) in the treatment of lung tumors with I-125 seeds.

REFERENCES

Skowronek, J. (2015). Brachytherapy in the treatment of lung cancer–a valuable solution. Journal of contemporary brachytherapy, 7(4), 297-311.

Rivard, M. J., and et al. (2004). Update of AAPM Task Group No. 43 Report: A revised AAPM protocol for brachytherapy dose calculations. Medical physics, 31(3), 633-674.

Laprise-Pelletier and et al. (2018). Gold Nanoparticles in Radiotherapy and Recent Progress in Nanobrachytherapy. Advanced healthcare materials, 7(16), e1701460.

Dheyab, M. A. and et al. (2023). Monte Carlo simulation of gold nanoparticles for X-ray enhancement application. Biochimica et biophysica acta. General subjects, 1867(4), 130318.

Taheri, A. and et al. (2023). A review of recent advances in the modeling of nanoparticle radiosensitization with the Geant4-DNA toolkit. Radiation Physics and Chemistry, 111146.

Agostinelli S, and et al. (2003). Geant4—a simulation toolkit. Nucl. Instruments Methods Phys. Res. Sect. A Accel. Spectrometers, Detect. Assoc. Equip. 506, 250–303.

Dos Santos, M., Villagrasa, C., Clairand, I., & Incerti, S. (2013). Influence of the DNA density on the number of clustered damages created by protons

of different energies. Nuclear Instruments and Methods in Physics Research Section B: Beam Interactions with Materials and Atoms, 298, 47-54.

Jalalvand, Z., Zobdeh, P., & Sani, V. E. (2024). Assessment of early DNA damage induced in human fibroblasts by four therapeutic radionuclides using Geant4-DNA. Radiation Physics and Chemistry, 219, 111670.

Magneto-impedance and Magnetic Sensitivity of FeCoSiB Nano-crystalline Micro-wires under Applied Longitudinal Stress

A. Dadsetan[1, 2*]

[1]*Farhangian university, Tehran, Iran*
[2] *Institute of Nano science & Nanotechnology of Kashan University, Kashan, Iran*
*Corresponding author: ali.dadsetan@gmail.com

Abstract— The study examined the effect of longitudinal stress on the magneto-impedance (MI) and magnetic sensitivity of FeCoSiB nano-crystalline micro-wires at frequencies from 0.5 to 8 MHz. Results showed that longitudinal stress significantly enhanced MI, with the highest MI response of 189% at 3 MHz and 70 MPa stress. This method is proposed as a cost-effective and efficient approach for designing stress sensors using the giant magneto-impedance effect.

Keyword: Magneto-impedance, Magnetic sensitivity, Nano-crystalline, Micro-wires, Longitudinal stress

INTRODUCTION

The magneto-impedance (MI) effect causes significant impedance changes in magnetic materials under AC current and a DC magnetic field. The MI ratio (MIR) depends on factors like magnetic permeability, sensitivity, and the skin effect. Structural defects in materials like micro-wires and thin films can alter their magnetic properties and domain structure. The MI ratio (MIR) is expressed as follows:

$$MIR(\%) = \frac{\Delta z}{z} = \frac{\{Z(H) - Z(Hmax)\}}{Z(Hmax)} * 100 \quad (1)$$

Magnetic sensitivity, crucial for sensor applications, is measured by the slope of the MIR curve in response to an external magnetic field.

$$S = \frac{d(\frac{\Delta Z}{Z})}{dH} \quad (2)$$

Fe-based nano-crystalline micro-wires are promising sensor materials due to their high permeability and ease of fabrication, though research on the impact of longitudinal stress is limited. Studies show that applying stress can slightly improve magnetic properties, with Fe-rich wires showing a small increase in MIR. This study explores the MI and magnetic sensitivity of FeCoSiB micro-wires under stress, finding significant improvements and identifying optimal annealing conditions and measurement techniques for sensor applications. [1-4].

MATERIALS & METHODS

Nano-crystalline Fe68.15 Co4.35 Si12.5 B15 micro-wires were prepared using rapid quenching from the melt in a vacuum. Pieces measuring 40 mm in length and 20 micrometers in diameter were subjected to longitudinal stress. Initially, the magneto-impedance ratio (MIR) of the as-cast samples was measured at fixed frequencies. The measurements were taken using a Hioki 7581 impedance analyser.

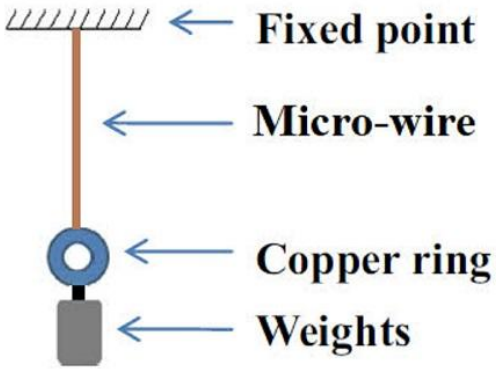

Fig 1: Schematic view of the tensile stress annealing setup

To apply longitudinal stress to the micro-wires, we utilized a homemade setup, as illustrated in Fig. 1. One end of the sample was anchored to a fixed point, while the other end was attached to various weights. The samples were subjected to tension for 30 minutes using weights of 118, 165 and 282 g, corresponding to tensions of 50, 70, and 120 MPa, respectively.

RESULTS & DISCUSSION

Figure 2 presents the Magneto-impedance Response (MIR) of Fe-based nano-crystalline micro-wires under varying longitudinal stresses at frequencies of 1, 3, and 5 MHz, plotted against an external magnetic field. As the DC field increases, the MIR initially rises to a peak before declining.

In detail:

- At 1 MHz (Fig. 2a): With a longitudinal stress of 70 MPa, MIR increases from 122% to 153%, and magnetic sensitivity rises from 3.17 to 6.22 %/Oe.

- At 3 MHz (Fig. 2b): The MIR under the same stress condition improves from 132% to 186%, with sensitivity increasing from 4.90 to 7.73 %/Oe, marking the best results of the study.

- At 5 MHz (Fig. 2c): Here, the MIR increases from 124% to 162% and sensitivity from 4.52 to 5.59 %/Oe.

The application of longitudinal stress enhances the magneto-elastic anisotropy of the micro-wires, increasing wall energy and leading to domain realignment. This reorganization reduces internal area, thereby altering the interaction between external and internal stresses and affecting the domain structure. As a result, the circumferential permeability increases due to the AC-induced circumferential field, raising the switching field and requiring a larger DC magnetic field to achieve saturation in the longitudinal direction as H_{ex} approaches the anisotropy field.

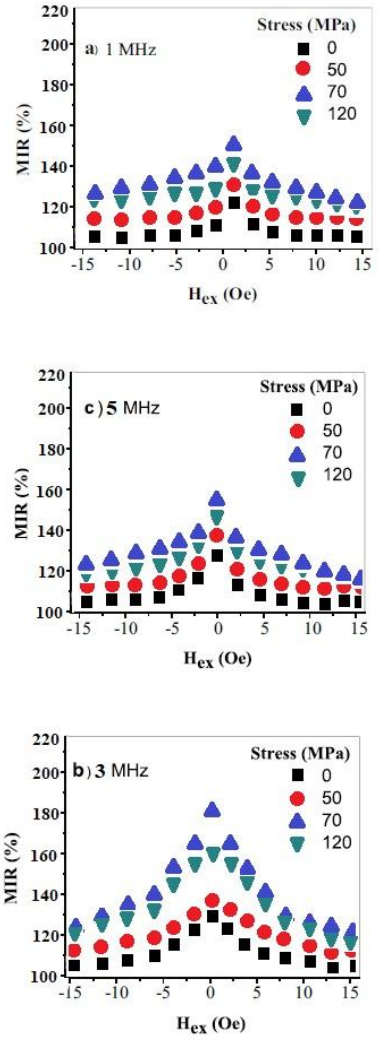

Fig 2: MI curves for frequencies a 1, b 3 and c 5 MHz of Fe-based magnetic micro-wire

The second key factor influencing the MI effect is the magnetic sensitivity of the sample. For a clearer comparison, Fig. 3 presents the magnetic sensitivity as a function of longitudinal stress at frequencies of 1, 3 and 5 MHz The highest magnetic sensitivity observed across all measurements is 7.73 %/Oe, achieved with a longitudinal stress of 70 MPa applied to the sample [5].

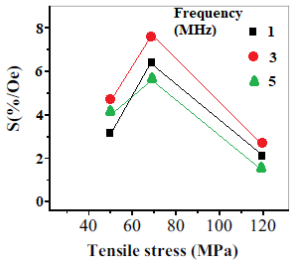

Fig 3. Field sensitivity versus tensile stress at frequencies of 1, 3and 5 MHz

CONCLUSIONS

This study examines the effects of longitudinal stress on the magnetic properties of FeCoSiB nano-crystalline micro-wires. It finds that applying a longitudinal stress significantly enhances the magneto-impedance (MI) and magnetic sensitivity of these micro-wires. The underlying mechanism involves the rearrangement of domain walls due to the applied stress, which increases both circumferential anisotropy and magnetic permeability [6]. Specifically, an optimized stress of 70 MPa can boost the MI ratio by up to 189% and enhance magnetic sensitivity to 7.73%/Oe. These findings suggest that utilizing a longitudinal stress of 70 MPa could effectively improve the impedance response of FeCoSiB micro-wires, paving the way for the development of stress sensors based on the MI effect.

ACKNOWLEDGMENT

I would like to express my sincere gratitude to the Farhangian University for their invaluable support and resources throughout my research. Their commitment to fostering academic excellence has greatly contributed to the completion of this article. Thank you for providing a stimulating environment for learning and growth.

REFERENCES

Corte-Leon, P., Zhukova, V., Chizhik, A., Blanco, J. M., Ipatov, M., Gonzalez-Legarreta, L., & Zhukov, A. (2020). Magnetic microwires with unique combination of magnetic properties suitable for various magnetic sensor applications. Sensors, 20(24), 7203. https://doi.org/10.3390/s20247203

Volchkov, S. O., Pasynkova, A. A., Derevyanko, M. S., Bukreev, D. A., Kozlov, N. V., Svalov, A. V., & Semirov, A. V. (2021). Magnetoimpedance of CoFeCrSiB ribbon-based sensitive element with FeNi covering: Experiment and modeling. Sensors, 21(20), 6728. https://doi.org/10.3390/s21206728

Shuai, S., Lu, S., Xiang, Z., & Lu, W. (2022). Stress-induced giant magneto-impedance effect of amorphous CoFeNiSiPB ribbon with magnetic field annealing. Journal of Magnetism and Magnetic Materials, 551, 169131. https://doi.org/10.1016/j.jmmm.2022.16913

Orelj, J. M., Mitrović, N. S., & Pavlović, V. B. (2023). MI-sensor element features and estimation of penetration depth and magnetic permeability by magnetoresistance and magnetoreactance of CoFeSiB amorphous wires. IEEE Sensors Journal, 23(13), 14017-14024. https://doi.org/10.1109/JSEN.2023.3274598

Deng, Z., Yu, Z., Yuan, Z., Song, X., & Kang, Y. (2022). Mechanism of magnetic permeability perturbation in magnetizing-based eddy current nondestructive testing. Sensors, 22(7), 2503. https://doi.org/10.3390/s22072503

Buznikov, N. A. (2023). Off-Diagonal Magnetoimpedance in Annealed Amorphous Microwires with Positive Magnetostriction: Effect of External Stresses. Magnetism, 3(1), 45-60. https://doi.org/10.3390/magnetism3010000.

Antidiabetic activity of Citrullus Colocynthis Compounds Against Glycogen Phosphorylase Using Molecular Docking

Zahra Shakeri[1*], Reza Shidpour[1]

Department of Materials and Industrial Engineering, Babol Noshirvani University of Technology, Babol, Iran

**Corresponding author: zsh.zahrashakeri@gmail.com*

Abstract— Diabetes is one of the developing diseases in the world that leads to increased blood sugar. Chemical drugs such as metformin, acarbose, etc. are used to treat diabetes, which have side effects. As a result, the desire to replace and use medicinal plants to treat diabetes has increased. Citrullus colocynthis is one of these medicinal plants whose compounds are effective in treating blood sugar. Our approach is to identify the compounds present in this plant and investigate the inhibitory effect of the compounds on the Glycogen phosphorylase protein, one of the proteins involved in diabetes. We use AutoDock Vina software to perform molecular docking and find effective compounds.

Keyword: Diabetes, Citrullus colocynthis, AutoDock Vina, Glycogen-phosphorylase

INTRODUCTION

Diabetes mellitus (DM) is a chronic disease that results from uncontrolled glucose levels and causes an increase in extracellular sugar [1]. According to the latest statistics reported in 2021, about 537 million people have diabetes [2]. The most common type of diabetes is type II diabetes. This type of diabetes is characterized by insulin resistance due to defective and delayed insulin secretion, improper functioning of the glucagon hormone, and impaired binding of insulin to the cell surface, along with relative insulin deficiency. Hereditary history, inactivity, increasing age, and weight are among the factors that contribute to diabetes [3]. Diabetes usually presents with symptoms such as thirst, excessive urination, blurred vision, and frequent infections [4]. There are various oral medications for managing diabetes, but the use of these medications can cause numerous side effects such as hypoglycemic shock, weight gain, loss of appetite, and digestive problems [5]. Medicinal plants can be a good alternative to chemical drugs in the treatment of various diseases such as diabetes due to their availability, good efficacy, and low side effects [1].

Citrullus colocynthis from the Cucurbitaceae family is one of the most effective plants in the treatment of diabetes. The extract of this plant contains effective compounds such as alkaloids, flavonoids, saponins, terpenoids, and glycosides, the consumption of which leads to increased insulin secretion [6, 7].

We intend to use the AutoDock Vina molecular docking simulation software to investigate the interaction and binding of compounds found in Abu Jahl watermelon on the glucagon phosphorylase enzyme, an enzyme effective in diabetes.

METHOD

In this study, after identifying the compounds in Citrullus colocynthis, five compounds were downloaded from the PubChem database at https://pubchem.ncbi.nlm.nih.gov/ and transferred to Chimera 1.15rc.lnk software, and after optimizing the compounds, they were saved in (.pdb) format. Also, the Glycogen-phosphorylase protein (PDB ID: 5IKO), which causes the enzymatic synthesis of glucose from glycogen and consequently increases blood glucose [8], was downloaded from the PDB database at https://www.rcsb.org/ and edited, optimized, and saved in PDB format by Chimera 1.15rc.lnk software.

Using AutoDock Vina software, docking between 5IKO protein and compounds was performed in a grid box with Maximize coordinates and Exhaustiveness: 100; to obtain the strongest interaction with the lowest binding energy, in order to determine the inhibitory effect of the compounds on this

protein. The interaction between the protein and the compound is shown in "Fig. 1".

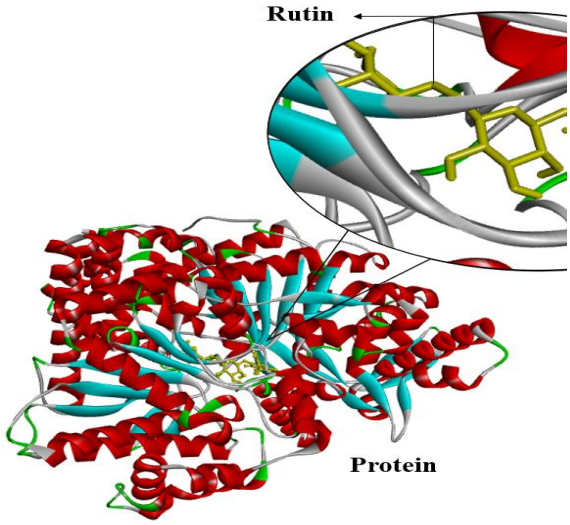

Fig. 1 Interaction of Glycogen phosphorylase with Rutin in Citrullus colocynthis

RESULT

The 5IKO protein was bound to each of these compounds separately, and the results of these interactions are shown in Table 1. The results obtained may differ from the results of other systems due to the randomness of the molecular docking process. We considered the difference between the results of -0.3 to +0.3 to be acceptable. Based on the molecular docking results, rutin, one of the flavonoid compounds with a binding energy of -11.3 kcal/mol, was obtained as the best combination with the lowest energy.

Table 1. Molecular docking of the herbal compounds with Glycogen phosphorylase

Compound	BE[a] (kcal/mol)
Rutin	-11.3
Colocynthin A	-11.1
8-p-Hydroxybenzylisoviexin 4'-glucoside	-10.9
6-p-Hydroxybenzylvitexin	-10.4
Colocynthin B	-10.4

[a]Binding Energy

In order to investigate the effectiveness of the plant compounds, we also bound a number of drugs effective in diabetes, including metformin, acarbose, repaglinide, and sitagliptin, with the 5IKO protein in the same way, and sitagliptin with -9.4 kcal/mol showed the best result. Citrullus colocynthis compounds had lower binding energy and better inhibitory effect than drugs, and this could be a strong point for replacing herbal compounds with chemical compounds. Medicinal plants have long been of interest to the natives of each region due to their easy accessibility, and given the progress of science and technology and the production of chemical drugs, the use of these plants is still popular among people. Diabetes is also one of the diseases that can be controlled with herbal drugs. All compounds that had better results than drugs in molecular docking are suitable options for investigation and study, and after their extraction, they can be used in the synthesis of herbal drugs or as an aid with synthetic inhibitors to reduce the dose of chemical drugs.

REFERENCES

Odeyemi, S. and G. Bradley, Medicinal plants used for the traditional management of diabetes in the Eastern Cape, South Africa: pharmacology and toxicology. Molecules, 2018. 23(11): p. 2759. https://diabetesatlas.org/.

Hurtado, M.D. and A. Vella, What is type 2 diabetes? Medicine, 2019. 47(1): p. 10-15.

Consultation, W., Definition, diagnosis and classification of diabetes mellitus and its complications. 1999, Part.

Modi, P., Diabetes beyond insulin: review of new drugs for treatment of diabetes mellitus. Current drug discovery technologies, 2007. 4(1): p. 39-47.

Abdulridha, M.K., A.-H. Al-Marzoqi, and A. Ghasemian, The anticancer efficiency of Citrullus colocynthis toward the colorectal cancer therapy. Journal of Gastrointestinal Cancer, 2020. 51: p. 439-444.

Marwat, S.K., et al., Useful ethnophytomedicinal recipes of angiosperms used against diabetes in

South East Asian Countries (India, Pakistan & Sri Lanka). Pakistan journal of pharmaceutical sciences, 2014. 27(5).

Sabapathy, I., et al., Molecular docking analysis of tetracyclic triterpenoids from Cassia fistula L. with targets for diabetes mellitus. Bioinformation, 2022. 18(3): p. 200.

2.2. AIRBASE STUDIES

Development of an Innovative Method to Modify Magnetic Lignin by a Green Modifier Agent for Water Treatment

A. Moatamed Sabzevar[1 2], A. Ahmadpour[1 2*], M. Ghahramaninezhad[1 2]

[1] *Chemical Engineering Department, Faculty of Engineering, Ferdowsi University of Mashhad, Mashhad, Iran*

[2] *Industrial Catalysts, Adsorbents, and Environment Lab., Oil and Gas Research Institute, Ferdowsi University of Mashhad, Mashhad, Iran*

**Corresponding author: ahmadpour@um.ac.ir*

Abstract— In the present work, a novel and eco-friendly method was developed to prepare a green multifunctional adsorbent by modifying magnetic lignin via a beta-cyclodextrin agent (β-CD@lignin/Fe_3O_4). The produced β-CD@lignin/Fe_3O_4 were then characterized using Fourier transform infrared spectroscopy (FTIR). The β-CD@lignin/Fe_3O_4 was employed as an adsorbent to remove methylene blue from aqueous solutions. The results showed that methylene blue removal could reach up to approximately 97 % under an initial concentration of 20 mg L^{-1}, pH 7, contact time of 45 min, and adsorbent dosage of 0.6 g L^{-1}.

Keywords: Magnetic lignin, beta-cyclodextrin, Citric acid, Methylene blue

INTRODUCTION

The release of dyes, such as methylene blue (MB), into water can severely damage the ecological environment and threaten human health and safety [1]. Various adsorbents have been employed for adsorption. However, many of these materials face significant challenges, such as non-biodegradability, high production costs, complex synthesis methods, and difficult separation processes [2]. Lignin, a complex aromatic macromolecule, is recovered from papermaking and polysaccharide-based biorefinery processes. Modifying lignin transforms waste into valuable materials with enhanced utilization potential [3]. Beta-cyclodextrin (β-CD), a macrocyclic oligosaccharide, has a truncated cone-like structure with a hydrophobic inner cavity and a hydrophilic outer surface [4]. The synthesis and characterization of β-CD@lignin/Fe_3O_4 form this study's foundational stage and primary focus. This adsorbent was prepared using a simple and eco-friendly method involving the modification of magnetic lignin (lignin/Fe_3O_4) with β-CD as a non-toxic modifying agent and citric acid as a cross-linker. Subsequently, β-CD@lignin/Fe_3O_4 was employed as a novel and highly efficient adsorbent for removing cationic dye.

METHODOLOGY

The suggested method for preparing β-CD@lignin/Fe_3O_4 as a green adsorbent involves two distinct steps, detailed as follows: First, lignin/Fe_3O_4 was synthesized using a modified technique by Han et al. [5]. In the second step, to synthesize β-CD@lignin/Fe_3O_4, 0.1 g of lignin/Fe_3O_4, 0.4 g of β-CD, 0.4 g of citric acid, and 0.24 g of KH_2PO_4 catalyst were combined in a particular volume of water. Then, the solution was heated at 140 °C for 2 h. Finally, the synthesized magnetic adsorbent was dried overnight.

RESULTS & DISCUSSION

In the FTIR spectrum of β-CD@lignin/Fe_3O_4 (Fig. 1(b)), the broadband at 3455 cm^{-1} and the band at 2939 cm^{-1} are attributed to O-H bond stretching vibrations and the antisymmetric stretching of -CH_2 groups, respectively [4]. A prominent peak at 1740 cm^{-1} corresponds to the stretching vibration of C=O [1]. The peak at 1635 cm^{-1} is attributed to the stretching vibrations of C-C bonds [4]. The lignin/Fe_3O_4 component is indicated by a distinct peak at 1594 cm^{-1}, corresponding to benzene ring vibrations. This peak overlaps with the peak at 1635 cm^{-1}

in β-CD@lignin/Fe_3O_4. Moreover, the peaks at 1157 cm^{-1} and 1028 cm^{-1} are associated with C-O-C and C-OH vibrations, respectively [4]. A peak at 586 cm^{-1} corresponds to the vibrations of the Fe-O bond in Fe_3O_4 [5].

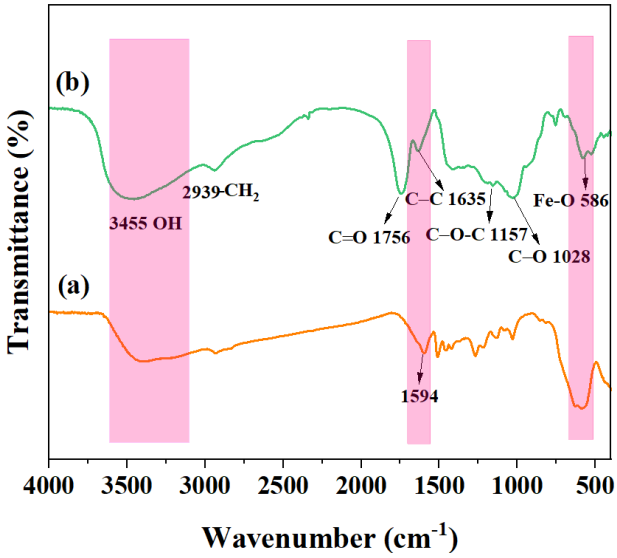

Fig. 1 Fourier transform infrared spectra of (a) lignin/Fe_3O_4 and (b) β-CD@lignin/Fe_3O_4.

To evaluate the effect of β-CD@lignin/Fe_3O_4 dosage on MB adsorption, varying amounts of adsorbent (0.3–1.2 g L^{-1}) were added to 20 mg L^{-1} of MB solution, and the mixture was agitated for 45 min. As adsorbent dosage increases from 0.3 to 0.6 g L^{-1}, the removal efficiency of MB increases (Fig. 2). This trend is attributed to the greater availability of vacant adsorption sites. Therefore, the optimal dosage for the adsorbent is determined to be 0.6 g L^{-1}.

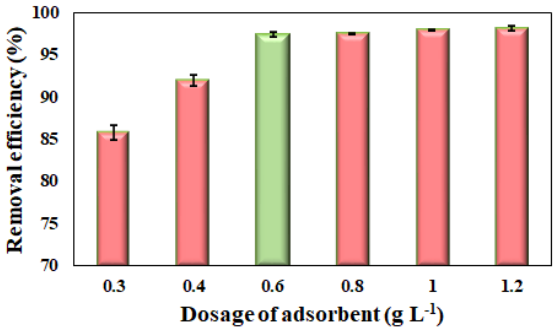

Fig. 2 Effect of β-CD@lignin/Fe_3O_4 dosage on the MB removal (C_0: 20 mg L^{-1}, pH: 7, and contact time: 45 min).

CONCLUSIONS

This research presents a novel method for synthesizing β-CD@lignin/Fe_3O_4 through a simple process utilizing safe and economical materials: lignin, beta-cyclodextrin, and citric acid. Fourier-transform infrared spectroscopy (FTIR) was employed to confirm the successful synthesis of the adsorbent. Subsequently, the performance of the synthesized adsorbent in the removal of methylene blue was investigated. Under optimal conditions, the highest removal efficiency of methylene blue was 97 % within 45 min.

ACKNOWLEDGMENT

The authors appreciate the support of Ferdowsi University of Mashhad, Iran (Grant No. 61254) for this work.

REFERENCES

Sun, Z., Feng, T., Zhou, Z., and Wu, H. (2021). Removal of methylene blue in water by electrospun PAN/β-CD nanofibre membrane. e-Polymers, 21(1), 398-410. https://doi.org/10.1515/epoly-2021-0041

Zong, E., Huang, G., Liu, X., Lei, W., Jiang, S., Ma, Z., Wang, J., and Song, P. (2018). A lignin-based nano-adsorbent for superfast and highly selective removal of phosphate. Journal of Materials Chemistry A, 6(21), 9971-9983. https://doi.org/10.1039/C8TA01449C

Li, T., Tong, Z., Zheng, Q., Bao, H., Partow, A., Meng, S., Li, L., and Li, Y.C. (2021). Fabrication of a lignin-based magnetic nanocomposite adsorbent to recover phosphorus in water for agricultural reuse. ACS Sustainable Chemistry & Engineering, 9(31), 10468-10478.

https://doi.org/10.1021/acssuschemeng.1c01492

Wei, T., Wu, H., and Li., Z. (2023). Lignin immobilized cyclodextrin composite microspheres with multifunctionalized surface chemistry for non-competitive adsorption of co-existing endocrine disruptors in water. Journal of Hazardous Materials, 441, 129969-129980. https://doi.org/10.1016/j.jhazmat.2022.129969

[5] Han, Y., Ma, Z., Cong, H., Wang, Q., and Wang, X. (2022). Surface Chitosan-coated Fe3O4 immobilized lignin for adsorbed phosphate radicals in solution. Biochemical Engineering Journal, 187, 108662-108629. https://doi.org/10.1016/j.bej.2022.108662

Investigating Effects of Sinusoidal leading Edge on a Lambda-wing UAV at pre-stall angles

A. Hosseinikargar[1], M.H. Djavareshkian[1]*, A.H. Gholami[1]

[1]*Ferdowsi University of Mashhad, Mashhad, Iran*

*Corresponding author: javareshkian@um.ac.ir

Abstract— This study examines the aerodynamic benefits of implementing a sinusoidal leading edge on a lambda-shaped, subsonic flying wing with a 56-degree sweep angle and -3-degree twist. Numerical simulations, validated by experimental data over angles of attack from -5° to 20°, focused on optimizing lift, drag, and vortex formation. Results show that the sinusoidal leading edge improves the lift-to-drag ratio by approximately 20% within the 5° to 15° range, enhancing range and reducing fuel consumption. Unlike conventional dual-vortex structures, vortices form at each crest along the sinusoidal edge, potentially delaying flow separation at higher angles of attack by adding turbulent energy and promoting lateral reattachment.

Keywords: Sinusoidal leading edge, Flying wing, Numerical simulation, Lift-to-drag ratio

INTRODUCTION

In recent years, various industries, particularly aviation, have been seeking continuous innovation to enhance performance and efficiency. One prominent advancement is the flying wing design, which integrates the wing and fuselage into a unified structure, improving aerodynamics, reducing fuel consumption, and enhancing stealth capabilities. Originally implemented in the Horten Ho-229 [1] and later advanced in modern designs like the B-2 Spirit by Northrop Grumman, this configuration removes the tail, reducing drag and radar cross-section, which is beneficial for both military and commercial use [2]. The flying wing's optimal design, with high sweep angles and lower wing loading, suits subsonic UAVs. For example, the Flying-V from Delft University could reduce fuel consumption by up to 20% [3]. Recent studies suggest that performance can be further enhanced with modifications such as split-drag systems and geometric twists, improving control surfaces and maneuverability [4].

This research focuses on the Swing UAV, introduced by Stenfelt and Ringertz [5], examining geometric modifications such as adding sinusoidal tubercles to the leading edge. Numerous studies have already explored its stability and lateral control [6]. This concept draws inspiration from the humpback whale's pectoral fin, where unique bumps function similarly to vortex generators, delaying stall and enhancing stability [7]. Building on findings by Chen et al. [8], this study applies the optimal sinusoidal configuration to a delta wing UAV to investigate pre-stall effects, offering insights for optimizing future UAV designs.

TEST CASE

This study examines a lambda-shaped flying wing UAV with a span of one meter, a leading-edge sweep of 56 degrees, and a negative outer twist of 3 degrees. The wing uses a NACA-66009 airfoil and includes a central bulge for system integration, reflecting realistic aircraft conditions. Tests were conducted in the L-2000 wind tunnel at KTH, Stockholm [9]. Chen et al. [8] identified an optimal configuration with four wavelengths and an amplitude of 5% of the root chord, enhancing stall characteristics with minimal drag increase. This sinusoidal wave design maintains constant wing surface area by placing zero amplitude points on the leading edge (Fig. 1), ensuring consistent lift comparison between the baseline and sinusoidal models.

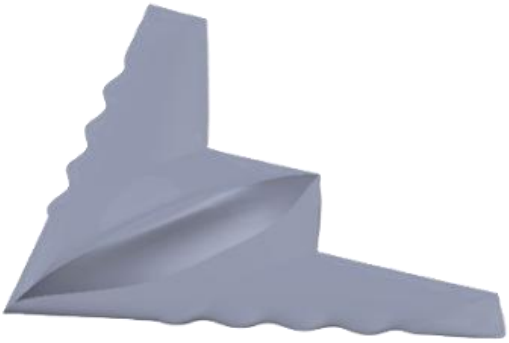

Fig. 1 Swing model with sinusoidal leading edge

SIMULATION METHODOLOGY

In this study, the continuity and momentum equations are solved in a steady-state manner using the finite volume method. A flow speed of 30 m/s with a Reynolds number of 6.9 × 10^5 is used, and the RANS model with "k-ω SST" turbulence modeling is applied for accurate boundary layer prediction. The computational domain is a cylinder (30 m diameter, 45 m height), with refined meshing near the UAV and an unstructured grid of tetrahedral, pyramidal, and prismatic elements. Boundary conditions include velocity at the inlet, ambient pressure at the outlet, and a no-slip condition on the UAV's surface. The mesh is densified in areas with high velocity and pressure gradients, with y+ maintained below 30 to optimize accuracy and computation.

RESULTS

The sinusoidal leading edge generally outperforms the plain edge, providing more stable lift, lower drag, and a higher lift-to-drag (L/D) ratio (Fig. ٢), particularly at optimal angles of attack (5–10 degrees). This shape minimizes flow separation and enhances stability, benefiting UAV efficiency and flight endurance.

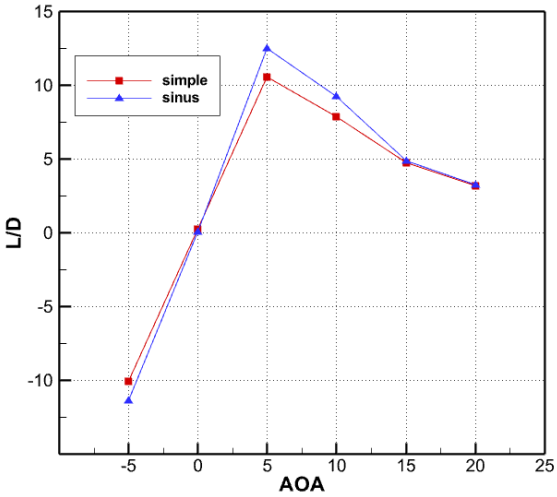

Fig. ٢ Lift-to-drag ratio L/D variation with AoA

Detailed L/D behavior across attack angles is as follows:

-From -5 to 5 degrees angle of attack, there is no significant change between the sinusoidal and simple edge results

-From 5 to 10 degrees: Optimal efficiency is achieved, with the sinusoidal edge providing a higher L/D, suggesting improved flow control.

-From 15 to 20 degrees: L/D decreases for both edges, though it remains slightly higher with the sinusoidal edge due to reduced drag and stable lift.

Further testing at varied speeds and angles would provide additional insight into the aerodynamic benefits of the sinusoidal design for UAV applications.

REFERENCES

Myhra, D. (1998). The Horten brothers and their all-wing aircraft. Schiffer Publishing, Limited.

John D. Anderson. (1998). Aircraft Performance & Design. McGraw-Hill Education; 1st edition.

Oosterom, W.J. (2020), "Flying V Family Design", MSc. thesis, Delft University of Technology.

Madani, A., Djavareshkian, M. H., & KARIMI KELAYEH, R. (2022). Optimization of split drag rudder mechanism at different angles of

attack in a flying wing airplane. Fluid Mechanics & Aerodynamics, 11(1), 1-16.

Stenfelt, G., & Ringertz, U. (2009). Lateral stability and control of a tailless aircraft configuration. Journal of Aircraft, 46(6), 2161-2164.

Stenfelt, G., & Ringertz, U. (2010). Yaw control of a tailless aircraft configuration. Journal of aircraft, 47(5), 1807-1811.

Fish, F. E., & Battle, J. M. (1995). Hydrodynamic design of the humpback whale flipper. Journal of Morphology, 225(1), 51-60.

Chen, H., Pan, C., & Wang, J. (2013). Effects of sinusoidal leading edge on delta wing performance and mechanism. Science China Technological Sciences, 56, 772-779.

Tomac, M., & Stenfelt, G. (2014). Predictions of stability and control for a flying wing. Aerospace Science and Technology, 39, 179-186.

Numerical Study of Aero-Optical Effects at Hypersonic Regime Around the Optical Sensor of a Projectile

Kamyab Karbasishargh[1], Mahmoud Pasandidehfard [1*], Ali Esmaeili[1]

[1] *Department of Mechanical Engineering, Faculty of Engineering, Ferdowsi University of Mashhad, Mashhad, Iran*

**Corresponding author: fard_m@um.ac.ir*

Abstract— This study presents a numerical investigation into the effects of aero-optical phenomena and light refraction caused by variations in the density field and shock waves on optical sensors and seekers of projectiles in the hypersonic flow regime. The focus is on a detailed analysis to better understand these aero-optical phenomena, the factors influencing light refraction, and how aerodynamic parameters affect density field variations due to airflow in the hypersonic regime, ultimately impacting the displacement and deviation of light beams. The research includes Computational Fluid Dynamics (CFD) simulations to model the fluid flow around guided projectiles and to quantitatively assess the impact of aerodynamic parameters on the performance of optical sensors as a result of aero-optical phenomena. A numerical algorithm has been developed to accurately determine the deviation and tracking of light beams as they pass through a fluid medium with variable density fields. Consequently, this research provides a framework for understanding and mitigating aero-optical effects in aerodynamic environments within the hypersonic regime.

Keyword: Aero-Optics, hypersonic, Optic, Computational Fluid Dynamics, Light Refraction

INTRODUCTION

In recent decades, the advancement and development of technology and emerging technologies have significantly transformed various sectors, including the aerospace industry, with wide-ranging applications such as surveillance, remote sensing, imaging, and environmental and territorial monitoring. Optical instruments, including cameras, infrared sensors, and laser rangefinders, play a crucial role in enhancing the capabilities of UAVs and guided projectiles [1]. These tools enable UAVs and projectiles to perform high-resolution imaging, night vision, and precise distance measurement, essential for surveillance and reconnaissance missions, as optical equipment can accurately and quickly examine and monitor environmental conditions and physical phenomena. Integrating advanced optical sensors in UAVs has significantly improved their efficiency and operational effectiveness, making them indispensable tools in modern military tactical operations [2]. Fig. 1. Illustrate a UAV equipped with optical system.

Fig. 1. UAVs equipped with an optical system used for intelligence operation [3]

Similarly, in the field of guided projectiles, optical sensors are vital for identifying, tracking, and intercepting specific target coordinates or dynamic threats. For example, infrared sensors can detect the movement of a projectile or missile by identifying the thermal jet signatures emitted from the projectile's nozzle [4]. These sensors provide real-time data monitoring, which is crucial for the successful interception of projectiles or hitting predetermined targets, thereby enhancing the defensive capabilities of military forces. Therefore, the development and deployment of optical sensors and efforts to improve the performance and efficiency of these new systems have become part of effective and innovative strategies, ensuring a higher level of security and protection against potential threats [5]. Fig. 2.depicts a cruise projectile equipped with an optical sensor and seeker in its dome section for path tracking.

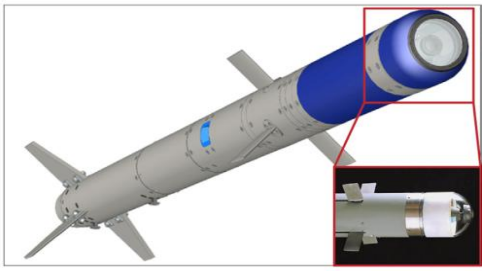

Fig. 2 View of a cruise missile equipped with an optical sensor in the nose [6]

METHODOLOGY

GOVENING EQUATION

The governing equations in this research include the laws of conservation of mass, momentum and energy for a compressible flow with Mach number 9.86.

RAY TRACING METHOD

Ray tracing was done by using the refractive index field based on the obtained density field, then the light deviation was extracted based on the ray equation (1).

$$\frac{d}{ds}(n(r).\frac{dr}{ds}) = \nabla n(r) \qquad (1)$$

In equation (1), r represents the position vector of the unit ray path. n(r) is the refractive index at the location of the ray and ds is the path length. ∇n(r) is the slope of the refractive index at the beam location r.

NUMERICAL METHOD

The turbulence model considered for this simulation was k-ω sst. Table 1. present the input conditions of the problem.

Table 1. input thermodynamic conditions of the problem

Wall temperature ($T_w[K]$)	Free stram static temperature ($T_\infty[K]$)	Free stram static pressure ($P_\infty[Pa]$)	Free stram Mach No. (M_∞)
300	48.88	59.92	9.86

GEOMETRY MODEL

The geometry modeled is shown in Fig. 3.

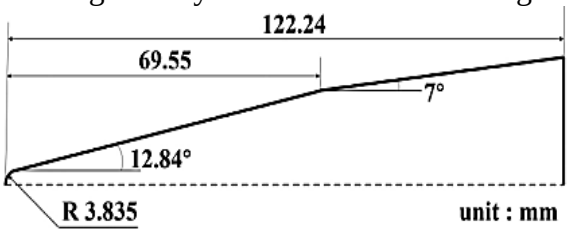

Fig. 3 typical blunt-headed cone of a projectile that include optical window [7]

VALIDATION

In order to validate the simulation, a validation of the wall heat flux ratio distribution at the hypersonic flow regime was performed and compared with experimental data [7] that is shown in Fig. 4.

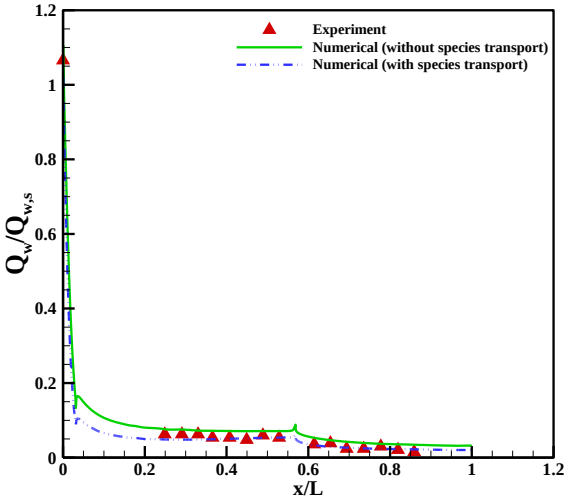

Fig. 4 [7]

RESULTS & DISCUSSION

Figure 5 illustrates the Mach number contour in the hypersonic regime. In this scenario, the shock wave region is thin and adheres closely to the surface, accompanied by heat generated from the chemical reactions of atmospheric elements. This phenomenon results in light deviations.

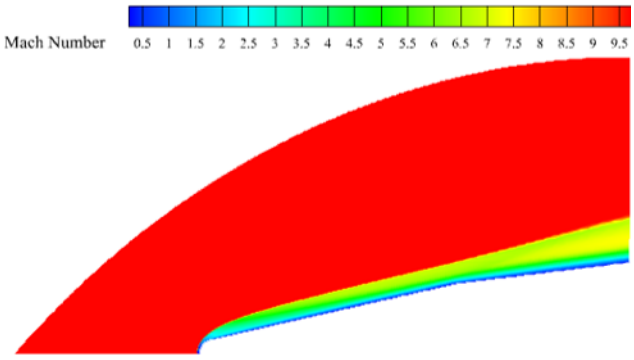

CONCLUSION

this numerical study has provided significant insights into the complex aero-optical effects experienced by optical sensors in the hypersonic flow regime. By meticulously analyzing the interactions between light refraction, density field variations, and shock waves, we have developed a comprehensive understanding of how these factors influence the performance of optical systems on projectiles. The use of CFD simulations has proven invaluable in modeling the fluid dynamics around guided projectiles, allowing for precise quantification of the impact of aerodynamic parameters on sensor functionality.

These investigations are crucial for enhancing the accuracy and reliability of optical sensors in high-speed aerodynamic environments.

REFERENCES

Esfandabadi, M. H. M., Esmaeili, A., & Karbasishargh, K. (2024). Optimizing performance through retrofitting: strategies for effectiveness, defence, and resiliency to enhance safety and reliability. International Journal of Reliability, Risk and Safety: Theory and Application, 7(1), 83-92.

Rumbaugh, W. (2022). Extending the Horizon: Elevated Sensors for Targeting and Missile Defense. Center for Strategic and International Studies (CSIS).

Karbasishargh, K., Moghimi Esfandabadi, M. H., & Esmaeili, A. (2024). Innovative Approaches to UAV Performance: Enhancing Safety, Reliability, and Flexibility. International Journal of Reliability, Risk and Safety: Theory and Application, 7(2), 28-39.

Mills, W., Fox, C., Philips-Levine, D., & Philips-Levine, T. (2021). Use Emerging Technology For ASW. US Naval Institute.

Jayanthi, S., Shaheen, H., Balashivudu, U., & Rani, M. S. (2022). Evolution and significance of unmanned aerial vehicles. In Unmanned Aerial Vehicle Cellular Communications (pp. 287-311). Cham: Springer International Publishing.

Zhao, J., Wang, S., Zhang, C., Wang, J., & Zhao, Q. (2024). Research status and challenges in the manufacturing of IR conformal optics. Defence Technology.

Yang, Z., Wang, S., & Gao, Z. (2022). Studies on effects of wall temperature variation on heat transfer in hypersonic laminar boundary layer. International Journal of Heat and Mass Transfer, 190, 122790.

Compensation of Phase Error Using Efficient Hydrophone Array Arrangement in Synthetic Aperture Sonar

H. Hajirahimi Kashani[1*], H. Afshari Rad, S.A.R. Seyedin

[1]*Faculty of Engineering of Ferdowsi University, Mashhad, Iran*

[2] *Faculty of Engineering of Ferdowsi University, Mashhad, Iran*

[3] *Faculty of Engineering of Ferdowsi University, Mashhad, Iran*

**Corresponding author: hajirahimi.hamid@mail.um.ac.ir*

Abstract— The primary objective of this article is to enhance phase error correction in critical directions. Previous studies indicate that phase correction methods face significant limitations when addressing unwanted platform movements, leading to a degradation in output image quality. This research proposes a novel approach that focuses not solely on improving phase correction techniques but on achieving an efficient geometry for hydrophone array arrangement. The innovative goal is to increase the likelihood of receiver presence and improve the reception of returning signals, which can substantially mitigate the adverse effects of phase error. This issue is addressed by reducing the impact of unwanted impulses in critical degrees of freedom, complementing existing phase error enhancement methods. The findings suggest that optimizing hydrophone array configurations can lead to significant advancements in synthetic aperture sonar (SAS) applications, ultimately improving imaging performance and accuracy.

Keywords —Synthetic Aperture Sonar, Hydrophone Array Arrangement, Efficient Geometry

INTRODUCTION

In Synthetic Aperture Sonar (SAS), phase information is essential for enhancing image quality and accuracy. It refers to the position of a point in time within a waveform cycle, which is crucial for reconstructing images from collected data. Phase information plays a vital role in image reconstruction by allowing for target differentiation and improved resolution. It also aids in compensating for unwanted platform movements, ensuring data integrity and high-quality imagery. Additionally, analysing phase shifts in returned signals is key for detecting and identifying targets. SAS applications include underwater military surveillance, environmental monitoring. Overall, effectively utilizing phase information is fundamental to advancing SAS technologies, leading to enhanced imaging performance and operational effectiveness.

PHASE ERROR SENARIO

Swath refers to the strip or area covered by a sensor during a single pass. It denotes the width of the ground area that is imaged or scanned at one time. The size of the swath is crucial for determining the efficiency of data collection.

As the sonar moves along a defined path with a specific time delay corresponding to the round trip of signals, a chirp signal is generated in the azimuth direction. The compression of this chirp signal results in image formation. However, if unwanted platform movements or disturbances occur, they can induce phase changes in the signal, disrupting the formation of chirps in the azimuth direction.

When isolating a line from the received signal corresponding to a slow time step, the resulting information represents a complex signal that can be mathematically expressed. Each sample represents the sonar return from points within the swath at a corresponding delay. The relationship between distance from the sonar to the swath is given by:

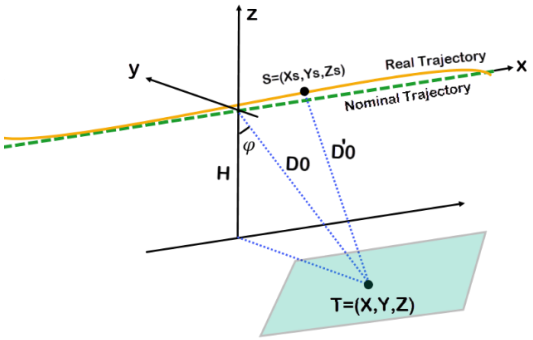

Fig. 1 Effect of translational motion error

where c is the speed of sound in water. The ideal phase from each point within the swath can be determined since both transmitter and receiver positions are known.

PROPOSED METHOD

To address phase errors induced by unwanted impulses, various methods have been proposed, including deploying multiple receivers arranged optimally. In SAS systems, two types of fast time and slow time, are utilized to derive received signals at the end of matrix scanning based on these two timings.

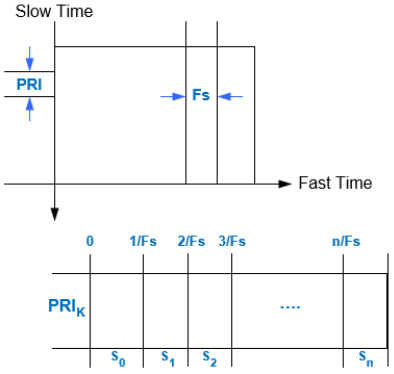

Fig. 2 Steps for Creating a Raw Data Matrix

If disturbances occur without altering the sonar's distance from the swath for each pulse, no phase difference arises. In this geometric scenario centred around a target within a sphere, having multiple receivers increases the probability that at least one receiver will have a phase close to the ideal value. This redundancy allows for effective compensation for any induced phase discrepancies.

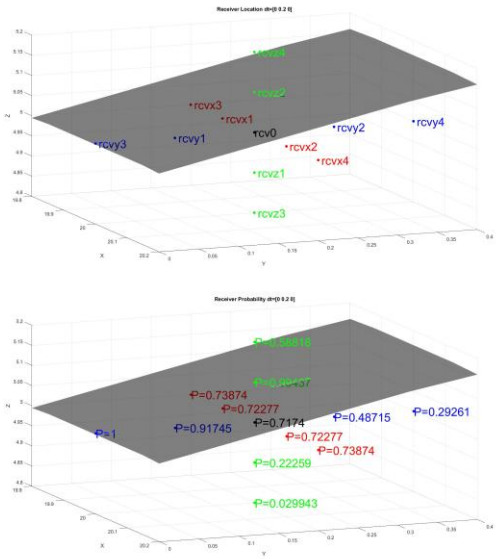

Fig. 3 Efficient correction for any induced phase misalignments

CONCLUSION

The proposed approach suggests that by optimizing hydrophone array configurations and leveraging multiple receivers, it is possible to model and compensate for phase discrepancies effectively. By analysing probabilities associated with each receiver's proximity to ideal phases, we can design efficient decision-making algorithms to correct these errors. This methodology not only enhances imaging performance but also ensures greater operational effectiveness in synthetic aperture sonar applications. In summary, optimizing hydrophone arrangements based on geometric considerations significantly contributes to mitigating phase errors caused by unwanted movements, thereby improving overall imaging quality in SAS systems.

ACKNOWLEDGMENT

The authors gratefully acknowledge the technical support that was provided by Faculty of Engineering - Ferdowsi University.

REFERENCES

X. Sérgio Silva, Interferometric Synthetic

Aperture Sonar: A surface vehicle-based approach, Lamber Academic Publishing, USA-Culumbia-SC, August, 2021.

Zhang, J., & Cheng, G (2023). A Subaperture Motion Compensation Algorithm for Wide-Beam, Multiple-Receiver SAS Systems. J. Mar. Sci. Eng. 11, pp.1-23. https://doi.org/10.3390/jmse11081627

D. Kaliyari, & A. Shukla (2014, March 13-15). Motion Compensation of Airborne Synthetic Aperture Radar. 3rd Int. Conference on Advances in Control and Optimization of Dynamical Systems, Kanpur,India. https://doi.org/10.3182/20140313-3-IN-3024.00065

Development of an Interface for Estimating the GDOP Parameter in the Conceptual Design of Satellite Constellations

M. Haji Jafari[1*], F. Sourani[2], S. Aminabadi[3], Z. Amini[4]

[1]*Associate Professor, Department of Industrial, Mechanical and Aerospace Engineering, Buein Zahra Technical University Qazvin, Iran*

[2]*Bachelor's Degree, Department of Industrial, Mechanical and Aerospace Engineering, Buein Zahra Technical University Qazvin, Iran*

[3]*Master's Degree, School of Interdisciplinary Science and Technology, University of Tehran, Tehran, Iran*

[4]*Master's Student, Faculty of Aerospace Engineering, K.N. Toosi University of Technology, Tehran, Iran*

**Corresponding author: hajijafari@bzte.ac.ir*

Abstract— This study presents the development and evaluation of an automated user interface comprising a MATLAB code and simulations from Systems Tool Kit (STK) (as one of the leading software packages in orbital mechanics). The user interface aims to calculate the GDOP of various orbital scenarios in an iterative and time-saving manner, which is a common feature in the conceptual satellite constellation design step. GDOP, a key metric for positioning accuracy in satellite constellations, plays a vital role in enhancing the reliability of navigation results. in order to attain more explicit and precise results, inverse GDOP (1/GDOP) is utilized here. The research involves simulations of 2100 circular satellite constellations assuming two-body problem conditions in three altitudes—400, 800, and 1400 kilometers—and seven orbital inclinations (0° to 90° at 15° intervals) following the Walker Delta pattern. The results are validated against manually defined STK scenarios, confirming the reliability and efficiency. It can be concluded that results become more accurate versus higher altitudes, while the higher the inclination, the better the outcomes are. The developed tool demonstrates faster performance than manual methods while maintaining satisfactory performance and offers a valuable positioning and satellite navigation research solution, enabling faster and more reliable calculations.

Keyword: Geometric Dilution of Precision (GDOP), Satellite Navigation, User Interface, Systems Tool Kit (STK), Positioning Accuracy.

INTRODUCTION

Dilution of Precision (DOP) parameters are essential indicators used to evaluate the performance of satellite navigation systems, helping to assess the accuracy of position, altitude, and timing provided by these systems. Among these, the Geometric Dilution of Precision (GDOP) is particularly critical, representing the geometric alignment of navigation satellites relative to their ideal positions. A lower GDOP value indicates better satellite geometry, which leads to increased positioning accuracy. This study focuses on GDOP as a primary metric.

Previous studies have addressed GDOP from various perspectives, including tool development for GDOP computation, incorporating GDOP into navigation system analyses, and optimizing its value to improve navigation accuracy. For instance, Yang et al. [1] introduced methods for calculating GDOP with limited visibility constraints, while Morales-Ferre et al. [2] demonstrated the suitability of Low Earth Orbit (LEO) constellations for navigation purposes through GDOP analysis. Furthermore, Xia et al. [3] proposed advanced algorithms, such as the Tabu Search Artificial Bee Colony Algorithm, to enhance satellite selection based on GDOP optimization.

This study aligns with the first category, focusing on developing an automated interface to simplify and accelerate GDOP calculations. Integrating advanced mathematical modeling and automation presents a tool designed to enhance the efficiency and accuracy of GDOP computations, providing a valuable resource for satellite navigation research and applications.

METHODOLOGY

This study develops and evaluates an automated interface integrating the Systems

Tool Kit (STK) and MATLAB software for precise GDOP calculation in satellite constellations. The user interface is designed to calculate the GDOP for various orbital scenarios in an iterative and time-efficient manner, a common feature during the conceptual design phase of satellite constellations. This process allows for accurate GDOP calculations across different satellite configurations.

The interface's mathematical foundation relies on vector relationships between the user and satellite positions. It begins by defining the user's position vector relative to satellites and constructing the geometric matrix representing these relationships. The covariance matrix of positioning errors is then calculated, and GDOP is derived from its diagonal elements, ensuring robust and precise computations. Inverse GDOP (1/GDOP) is used to enhance result interpretation and achieve more straightforward and more accurate results.

The interface was validated by comparing its outputs with results from manually defined STK scenarios, confirming its high reliability. Simulations for satellite constellations in 2100, conducted at three different altitudes and seven orbital inclinations under two-body problem conditions, demonstrated that increasing altitude and inclination significantly enhances GDOP accuracy. This emphasizes the role of constellation geometry in navigation systems.

RESULTS

This study aimed to develop an automated user interface for GDOP calculation in satellite constellations, improving accuracy and efficiency. Simulations of 2100 constellations at altitudes of 400 km, 800 km, and 1400 km, with orbital inclinations from 0° to 90°, revealed that higher altitudes and inclinations resulted in lower GDOP values, indicating better positioning accuracy. The interface's outputs were validated by comparing them to manually GDOP results from STK scenarios, confirming their reliability. The tool enables faster, iterative GDOP calculations. The use of inverse GDOP (1/GDOP) further enhanced result interpretation, making the tool valuable for satellite navigation research.

CHALLENGE

The developed user interface provides faster, ease of use, and adaptability for various satellite constellations. It enables precise and reliable data generation while reducing time and complexity, eliminating the need for multi-platform configurations. Particularly valuable for satellite constellation design, navigation optimization, and performance analysis, this tool streamlines functionality, making it an effective resource for advancing research and practical applications in satellite navigation systems.

FUTURE RESEARCH

Future research should focus on optimizing the tool and minimizing GDOP values to enhance performance and accuracy. This includes refining methodologies for challenging orbital configurations and dense constellations and improving precision in positioning. Optimization for LEO conditions, addressing atmospheric effects and dynamic geometries, is another proposal. Finally, advanced algorithms tailored for real-time applications can further boost the tool's adaptability and computational efficiency, ensuring reliable performance in complex scenarios.

REFERENCES

X. Yang, J. Du, and W. Li, “The Minimum of GDOP for Satellite Navigation System,” in Communications and Networking, B. Li, L. Shu, and D. Zeng, Eds., Cham: Springer

International Publishing, 2018, pp. 443–447. doi: 10.1007/978-3-319-78130-3_46.

R. Morales-Ferre, E. S. Lohan, G. Falco, and E. Falletti, "GDOP-based analysis of suitability of LEO constellations for future satellite-based positioning," in 2020 IEEE International Conference on Wireless for Space and Extreme Environments (WiSEE), Oct. 2020, pp. 147–152. doi: 10.1109/WiSEE44079.2020.9262624.

J. Xia, Y. Wang, and Y. Li, "A Navigation Satellite Selection Method Based on Tabu Search Artificial Bee Colony Algorithm," in 2020 IEEE 3rd International Conference on Electronic Information and Communication Technology (ICEICT), Nov. 2020, pp. 421–425. doi: 10.1109/ICEICT51264.2020.933430.

Comparison of Motion Errors of Surge, Sway and Heave Directions in Synthetic Aperture Sonar Imaging

H. Hajirahimi Kashani[1*], H. Afshari Rad, S.A.R. Seyedin

[1]*Faculty of Engineering of Ferdowsi University, Mashhad, Iran*

[2] *Faculty of Engineering of Ferdowsi University, Mashhad, Iran*

[3] *Faculty of Engineering of Ferdowsi University, Mashhad, Iran*

**Corresponding author: hajirahimi.hamid@mail.um.ac.ir*

Abstract—Synthetic Aperture Sonar (SAS) has become an essential tool in the realm of underwater imaging, paralleling the principles of Synthetic Aperture Radar (SAR). Its ability to produce high-resolution images of the seabed has attracted significant interest, especially in fields such as marine research and offshore operations. The accurate reconstruction of images captured by SAS is critically dependent on the precise control of the sonar platform's movements, which are influenced by various factors, including surge, sway, and heave. This research investigates the complex motion errors associated with these translational movements during INSAS imaging. We analyse how surge, sway, and heave affect the formation and quality of synthetic aperture sonar images, revealing potential artifacts and reductions in image clarity. Furthermore, we evaluate the effectiveness of various motion compensation techniques designed to address these errors. By measuring the impact of each type of motion error, this study provides a foundation for refining motion compensation algorithms, ultimately improving the quality of seabed imagery generated by SAS. The insights gained from this research are vital for advancing underwater imaging technologies and hold promise for diverse applications, including marine biology, underwater archaeology and defence operations. Addressing the challenges posed by motion errors is crucial for enhancing imaging processes and broadening the practical uses of SAS in intricate underwater settings.

Keywords: Surge, Sway, Heave, Synthetic Aperture Sonar, Motion Error

INTRODUCTION

The actual distance $R^*$and the ideal distance R from the target to the transmitter are defined, with H_M representing the difference between the actual distance and the vertical slant range, which indicates the target's azimuth angle. A rectangular coordinate system $o_a x_a y_a z_a$ is established on the sonar array, as illustrated in Figure 1. The center of rotation o_a of the array aligns with the center of the transmitter [1].

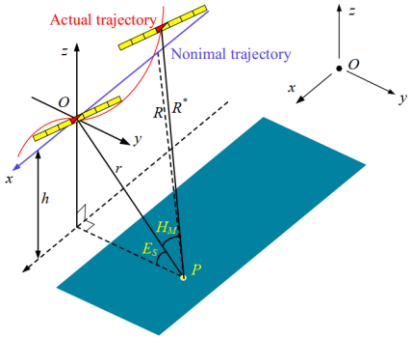

Fig. 1 Motion geometry of multiple-receiver SAS [1].

RANGE HISTORY ERROR

We consider t as the azimuth slow time, while $D_y D_z$ represent the sway and heave, respectively. When the transmitter shifts to the position $(V_A t, \Delta y, \Delta z)$, the distance between the transmitter and the point target P(0, rcosE_s,−h) can be expressed as follows [2]:

$$R_T^*(t, r, \Delta y, \Delta z) = \sqrt{(V_A t)^2 + (\Delta y - r\, cos E_s)^2 + (\Delta z + \mathrm{h})^2} \quad (1)$$

And the distance between the receiver *i* and the point target *P*(0, *r* cos *Es*, -*h*) is [1]:

$$R_{R,i}^*(t, r, \Delta y, \Delta z, \theta, \psi) = \quad (2)$$

$$\sqrt{\begin{matrix}\left(V_A t + V_A\, \tau_i^* + d_i \cos\theta \cos\psi\right)^2 + \\ (\Delta y + d_i \cos\theta \sin\psi - r\, cos E_s)^2 + \\ (\Delta z + d_i \sin\theta + \mathrm{h})^2\end{matrix}}$$

The range history with motion errors is the sum of (1) and (2), and it can also be expressed as the product of sound velocity c and the signal propagation time $\tau_i{}^*$:

$$R_T^*(t,r,\Delta y,\Delta z) + R_{R,i}^*(t,r,\Delta y,\Delta z,\theta,\psi) = c\,\tau_i^* \quad (3)$$

The range history without motion errors given in is [1]:

$$R_i(t,r) = \frac{V_A d_i + V_A^2 t + c\sqrt{V_A^2 t^2 + r^2}}{c^2 - V_A^2} + \frac{\left(\sqrt{(V_A d_i + V_A^2 t + c\sqrt{V_A^2 t^2 + r^2}}\right)^2}{c^2 - V_A^2} c + \frac{(c^2 - V_A^2).(2V_A t d_i + d_i^2)}{c^2 - V_A^2} c$$

the range history error is:

$$\Delta R_i(t,r,e_t) = R_i^*(t,r,e_t) - R_i(t,r) \quad (4)$$

SIMULATION FOR MOTION ERROR

In this scenario simulate the effects of translational motion of the platform about the Surge, Sway and Heave parameter with 5 and 15 meters respectively and image of point target results can be compared.

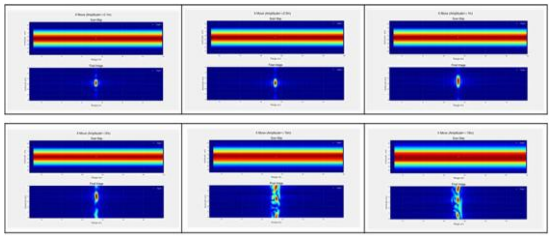

Fig. 2 Effect of surge direction with 0.1m, 0.5m, 1m, 5m,10m and 15m respectively

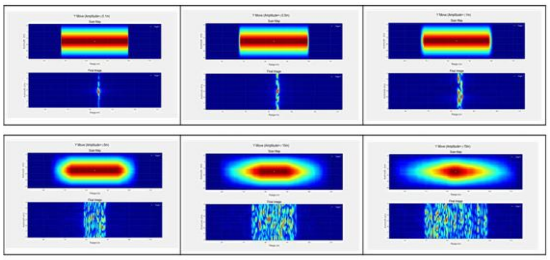

Fig. 3 Effect of sway direction with 0.1m, 0.5m, 1m, 5m,10m and 15m respectively

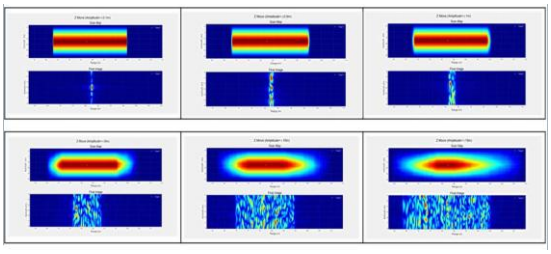

Fig. 4 Effect of heave direction with 0.1m, 0.5m, 1m, 5m,10m and 15m respectively

CONCLUSION

The effects of motion error in three-axis translation worsen with an increase in its magnitude. Additionally, the Surge translation error exhibits the least amount of degradation among the studied errors. Hence, it is possible to neglect this error for SAS imaging purposes. Moreover, the Heave translation error is more critical than the other two errors and must be compensated.

ACKNOWLEDGMENT

The authors gratefully acknowledge the technical support that was provided by Faculty of Engineering - Ferdowsi University.

REFERENCES

Zhang, J., & Cheng, G (2023). A Subaperture Motion Compensation Algorithm for Wide-Beam, Multiple-Receiver SAS Systems. J. Mar. Sci. Eng. 11, pp.1-23. https://doi.org/10.3390/jmse11081627

Zhang, Xuebo & Yang, P. & Huang, Pan & Sun, Haixin & Ying, Wenwei. (2021). Wide-bandwidth signal-based

multireceiver SAS imagery using extended chirp scaling algorithm. IET Radar, Sonar & Navigation. 16. 531–541. 10.1049/rsn2.12200.

Permits for Development and Operation of Unmanned and Autonomous Equipment

Kamyab Karbasishargh[1], Mohammad Hossein Moghimi Esfandabadi[1], Ali Esmaeili[1*]

[1] *Department of Mechanical Engineering, Faculty of Engineering, Ferdowsi University of Mashhad, Mashhad, Iran*

**Corresponding author: aliesmaeili@ferdowsi.um.ac.ir*

Abstract— In recent decades, the aerospace and defense industries, along with unmanned and autonomous systems, have become pivotal to the development and advancement of nations, particularly the Islamic Republic of Iran. These industries play a critical role in enhancing military capabilities, regional and international influence, and mitigating the impact of international sanctions. Given their significance to national security, scientific progress, and economic growth, understanding the opportunities and challenges within these sectors is imperative. This research aims to conduct a thorough examination of these industries, identifying existing opportunities and challenges, and exploring the necessary steps to optimize the development and utilization of aerospace and defense technologies, as well as unmanned and autonomous systems. Through in-depth analysis, the research will provide recommendations and strategies for maximizing the potential of these industries.

Keyword: Unmanned and Automatic Equipment, Cyber Threats, Technological, Economic Challenges

INTRODUCTION

The role of aerospace and military industries, as well as unmanned and automated equipment, is prominent as a fundamental factor in the security and global progress of countries. These industries not only play a crucial role in strengthening the military power and security of countries but also have a significant impact on the technology, economy, and scientific advancement of nations. This research examines the opportunities and challenges in these industries and equipment and provides solutions for improvement and development in this field. The use of new technologies in the aerospace and military industries, as well as unmanned and automated equipment, has become one of the main topics that engage various sectors of industry, research institutes, and research centers. With the expansion of artificial intelligence technology with multiple capabilities, the Internet of Things, and process automation (using robotics and intelligent industrial equipment), more opportunities have been created to improve performance and increase efficiency [1]. Some of the strengths of using these technologies include increased accuracy in monitoring and controlling operations and processes, improving predictions based on data analysis, and enhancing security and reliability. Some of these capabilities include accelerating the process of automation, improving the performance of drone systems, and reducing the risk of casualties caused by military operations [2]. These advancements clearly show that the potential for optimization in the aerospace and military fields through the application of new technologies will improve. In addition, process automation and the use of artificial intelligence-based technologies reduce costs in the production of unmanned and automated equipment. By utilizing these technologies, it is also possible to impact the quality of products and, as a result, increase a country's global power in terms of the balance of power and exports to allied countries. Ultimately, the capabilities provided by new technologies such as artificial intelligence, the Internet of Things, and process automation, bring about a comprehensive upgrade in the technologies and systems used in the aerospace and military fields [4]. For example, using artificial intelligence to improve predictive systems and enhance monitoring of aerospace projects, the Internet of Things for communication between devices and improving the efficiency of automated systems, and process automation for optimizing performance and reducing human error. These technologies increase speed, accuracy, and efficiency in the

aerospace industry and unmanned and automated equipment and are used very effectively in production, maintenance, and improvement of various processes [5].

OPPORTUNITIES AND CHALLENGES IN THE MILITARY AEROSPACE AND UNMANNED SYSTEMS INDUSTRIES

- Security Challenges Associated with the Use of Advanced Technologies in Aerospace, Military, and Automated Equipment, and Countermeasures to Cyber Threats

In the field of aerospace, military, and automation equipment, the use of advanced technologies often comes with security challenges. One of the most significant security challenges in this area is cyber threats, including hacking and intrusion related to military systems and equipment, especially automated and autonomous systems. Cyberattacks can penetrate various types of aerospace and automated equipment, affecting their performance. To combat these threats, innovative and effective solutions are required. One of the most important solutions to counter cyber threats is the use of advanced intrusion detection systems [6].

- The pgrading the necessary infrastructure for the production, implementation, and deployment of unmanned, automated, and intelligent equipment

With the increasing demand for unmanned, autonomous, and intelligent equipment in various industries such as automotive, transportation, medicine, military, and security, upgrading the necessary infrastructure has become crucial. To achieve this goal, the infrastructure related to these devices, including advanced communication networks, sensor systems, cloud technologies, and high-speed processing and artificial intelligence, needs to be developed [7].

Since unmanned equipment requires dynamic communication with the environment and other devices, upgrading communication network infrastructure to ensure fast and reliable data transfer is also vital. Moreover, the development of advanced sensor systems, including infrared sensors, lidar, radar, and high-resolution digital cameras for unmanned equipment, is of great importance. These systems enable the equipment to detect obstacles, identify location, and navigate accurately. Additionally, the use of cloud technologies to store and process the vast amount of data collected and processed by unmanned equipment is essential [8].

- Evaluation of the impact of new technological developments in the aerospace and military industries on economic opportunities and challenges

It is essential to examine the impact of new technological advancements in the aerospace and defense industries on economic opportunities and challenges. With the advancement of technologies such as artificial intelligence, the Internet of Things, augmented reality, and other emerging technologies, significant transformations have occurred in the aerospace and defense sectors. Economic opportunities include increased efficiency in developing high-quality products while reducing costs, creating innovative products, and establishing export markets to regional and global countries. Given these developments, the aerospace and defense industries need to rapidly adapt to new technologies and develop appropriate strategies to optimize the utilization of these technologies [9,10].

CONCLUSION

According to recent research, one of the innovative solutions to advance the goals of developing and utilizing unmanned and intelligent military equipment is the use of blockchain technology. As a decentralized and secure system, blockchain can be used to increase trust and confidence in communications and data transfer. This technology can facilitate the optimization of

data transfer processes and communications in military systems and prevent data fraud and manipulation. In addition, the migration of military systems to cloud environments is also an innovative approach that can help improve the efficiency and flexibility of systems. Using cloud resources for data processing and storage can help reduce costs and increase the scalability of military systems and enable the provision of improved services. Moreover, the integration of augmented reality technologies in unmanned and intelligent military systems can lead to increased training and readiness of military forces. These technologies can enhance simulated training environments and improve the training and readiness process of forces [11,12].

REFERENCES

Esfandabadi, M. H. M., Esmaeili, A., & Karbasishargh, K. (2024). Optimizing performance through retrofitting: strategies for effectiveness, defence, and resiliency to enhance safety and reliability. International Journal of Reliability, Risk and Safety: Theory and Application, 7(1), 83-92.

Karbasishargh, K., Moghimi Esfandabadi, M. H., & Esmaeili, A. (2024). Innovative Approaches to UAV Performance: Enhancing Safety, Reliability, and Flexibility. International Journal of Reliability, Risk and Safety: Theory and Application, 7(2), 28-39.

Burt, Richard R. "The Benefits of Diversification in the Defense Industry. " RAND Corporation, 2017.

Gourley, James H. "The Future of the Defense Industry: Trends and Challenges. " Center for Strategic and International Studies, 2020.

Mahnken, Thomas G. "The Defense Industry and the Future of Warfare. " Johns Hopkins University Press, 2018

Friedman, G. , 2010. The next 100 years: a forecast for the 21st century. Anchor.

Strachan, H. and Scheipers, S. eds. , 2011. The changing character of war. OUP Oxford.

Singer, P. W. , 2009. Military robots and the laws of war. The New Atlantis, (23), pp. 25-45.

Sokolović, V. S. and Marković, G. B. , 2023. Internet of Things in military applications. Vojnotehnički glasnik, 71(4), pp. 1148-1171.

Ahmad, I. , Shah, K. and Ullah, S. , 2016. Military applications using wireless sensor networks: A survey. Int. J. Eng. Sci, 6(6), p. 7039.

McAulay, A. D. , 2011. Military laser technology for defense: Technology for revolutionizing 21st century warfare. John Wiley & Sons.

Whyte, C. and Mazanec, B. , 2023. Understanding cyber-warfare: Politics, policy and strategy. Routledge.

2.3. WATER AND ENVIRONMENTAL SCIENCE

Investigating the Cell Structure and Histology of Scarus Fishes Eyes in the Persian Gulf

Faezeh Akhgarandouz[1], Majid Askari-Hesni[1], Mehdi Abbasnejad[1], Mina Motamedi [1]

[1] *Department of Biology, Faculty of Sciences, Shahid Bahonar University of Kerman, Kerman, Iran*

**Corresponding author: mahesni@gmail.com*

Abstract— In recent years, studies of the nervous and sensory systems have been placed in the research priorities of many researchers, and in this direction, numerous animal models have been used. One of the desired characteristics of researchers in animal models is the longevity of the sample, the possibility of examining different generations in a short period, the simplicity of the cell structure and the similarity of the cell structures to human cells. Therefore, one of the main goals of this project is to use and introduce fish as a model for neuroscience studies. Fish share many common physiological and molecular characteristics with mammals, and this has made it possible to use it as a model to study mammalian diseases and identify the molecular mechanisms of disorders. The purpose of this study is to use different fishes as a model for studies of sensory and nervous systems, so in this project, the effect of changing depth or habitat on the structural changes of nasal and nerve color cells and eye structure of parrot fish was investigated.

Keyword: Eye, Scarus persicus, Scarus ghobban, Rod cells, Con cells

INTRODUCTION

As a vertebrate, fish has many physiological and molecular features in common with mammals. This feature makes fish an excellent model for reviewing existing mammalian disease models and for comparative analysis to identify molecular mechanisms of disorders [1].In recent years, the use of fish as a model to investigate human disorders due to their small size, optical transparency of the embryo, rapid growth, and suitability for large-scale therapeutic screening has received much attention. Due to their relatively small size and short lifespan, they require less space and are more economical to maintain in the laboratory than other models, such as mice. In addition, they have very high fecundity, and their embryos are transparent during development, facilitating non-invasive examination of their development. The complex mechanisms of neurodegeneration can be studied more rapidly than in mice and other animal models. Vertebrates analyzed in fishes [1,2]. Vision is an important sensory system for most fish species. The fish eye is similar to the eyes of terrestrial vertebrates, such as birds and mammals, but has a more spherical lens. Birds and mammals (including humans) usually adjust by changing the shape of their lens, but fish usually adjust by moving the lens closer or further away from the retina [3,4]. Fish retinas generally have cylindrical and cone cells (for scotopic and photopic vision), and most species have color vision. Some fish can see ultraviolet rays, and some are sensitive to polarized light. Within the retina, rod cells provide high visual sensitivity, which is used in low-light conditions. Cone cells provide higher spatial and temporal resolution than rods and allow for colour vision by comparing the absorption in different types of cones, which are more sensitive to different wavelengths. [5]

The ratio of rods to cones depends on the fish species' ecology; for example, fish mainly active during the day in clear waters have more cones than fish living in dimly lit environments. [6] Fish that live in surface waters down to 200 meters, epipelagic fish, live in a region where visual predators use visual systems designed almost as expected [7]. Mesopelagic fish live in deeper waters, in the disphotic zone down to 1000 meters, where the amount of sunlight available is insufficient to support photosynthesis but does stimulate visual cells [8]. Deep in the

water column, below 1000 meters, are bathypelagic fish. At this depth, the ocean is dark, and the fish are sedentary and adapted to produce minimal energy in a habitat with very little food and no sunlight [9].

Deep-sea fish have more enormous eyes, and it has been shown that larger eyes are generally associated with better vision in fish, which is suitable for seeing in low light. It has also been shown that higher visual acuity is associated with brain size [10].

In the past decades, due to the genetic and structural similarities between the eyes of fish and humans, as well as the easy access and proper control of the fish's living environment, some human eye diseases such as cataracts, glaucoma, diabetic retinopathy, and macular degeneration have been modeled in fish [11].

In light of the above, our goal in this study is to investigate changes in nerve cells, vision, and histology of fish eyes according to their habitat type and the effects of habitat on eye structure in terms of depth, substrate change, and environmental turbidity. Given that currently, in new studies, the study of the nervous system of fish (such as Zebrafish) is of interest about nervous system disorders, the results of this study can also be an introduction to studies in mammals.

METHODS

This study collected 6 scarus persicus and scarus ghobban from the country's south.

Fish were collected from waters adjacent to coral reefs (Scarus). This type of sampling is because light changes with increasing water depth. Therefore, this change in light intensity can affect the condition of the visual cells and, subsequently, the condition of the fish's brain. After photographing and identifying the samples, the samples were biopsied, and traits such as total length, standard length, body weight, snout length, eye socket diameter, head height, etc., were measured. After dissecting the fish and extracting the brain and eyes, the samples were immediately fixed in Bowen's solution or formaldehyde. After 12-24 hours, depending on the size of the sample, they were placed in a series of alcohols and finally stored in 70% alcohol for a more extended period to carry out the remaining process.

After catching, the fish are placed in ice water and transported from Bandar Abbas to Kerman. After being transported to Kerman and before sampling, 0.5 grams per liter of cloves was added to the fish water. Cloves cause the fish to become unconscious in the water. The unconscious fish is taken out of the water, its head is cut off, and its eyes and brain are separated. Therefore, there is no problem with the samples. The fish carcasses were transported outside the university and burned.

The fish eyes were stained with H&E stain, and the cellular and histological characteristics of the different layers of the eye were examined.

RESULTS

Our results showed no significant differences between the two species of scarus persicus and scarus ghobban about the rod and cone cells of the eye.

The number of cone cells in the eyes of Persian Gulf scarus is lower than in the eyes of surface-dwelling fish such as the coot. However, according to evidence, the number of rod cells in the eyes of these fish is higher than in surface-dwelling fish, such as the coot, and lower than in bottom-dwelling fish, such as the shoefish.

A. Abbreviations:
N/A
B. Units:
N/A
C. Equations:
N/A

D. Figures and Tables

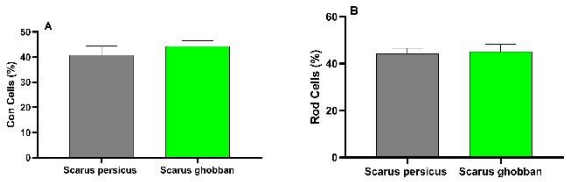

Figure 1. Percentage of rod and cone neurons in the scarus fish eye.

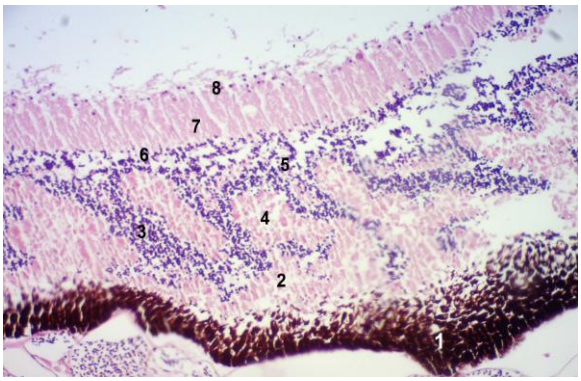

Figure 2. Photo of the eye of a green parrot fish

1-PRE: Primary photoreceptor layer2-OS: Outer segment of cone cell3-ONL: Outer nuclear layer4-IS: Inner segment of cone cell5-INL: Inner nuclear layer6-OPL: Outer reticular layer7-IPL: Inner reticular layer8-GCL: Ganglion cell layer

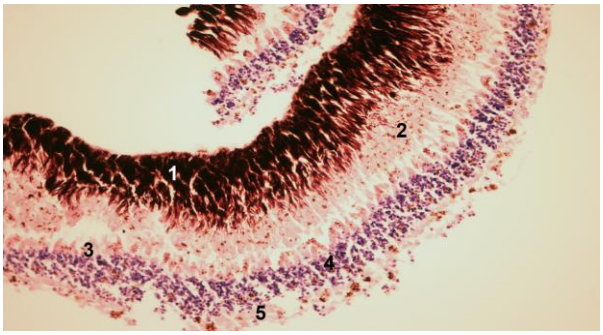

Figure3. Photograph of the eye of the Arabian parrotfish.

1-PRE: Primary photoreceptor layer2-OS: Outer cone segment3-IS: Inner cone segment4-ONL: Outer nuclear layer5-OPL: Outer reticular layer

ACKNOWLEDGMENT

we want to acknowledge the biology department of the Shahid Bahinar University of Kerman.

REFERENCES

[1] Malhotra D, Sebat J: Fish heads and human disease. Nature 2012, 485(7398):318-319.

[2]. Wang J, Cao H: Zebrafish and medaka: Important animal models for human neurodegenerative diseases. International journal of molecular sciences 2021, 22(19):10766

[3] Guthrie D: Role of vision in fish behaviour. In: The behaviour of Teleost fishes. edn.: Springer; 1986: 75-113.

[4] An D, Hao J, Wei Y, Wang Y, Yu X: Application of computer vision in fish intelligent feeding system—A review. Aquaculture Research 2021, 52(2):423-437.

[5] Facey DE, Bowen BW, Collette BB, Helfman GS: The Diversity of Fishes: Biology, Evolution and Ecology: John Wiley & Sons; 2022.

[6] De Busserolles F, Cortesi F, Fogg L, Stieb SM, Luehrmann M, Marshall NJ: The visual ecology of Holocentridae, a nocturnal coral reef fish family with a deep-sea-like multibank retina. Journal of Experimental Biology 2021, 224(1):jeb233098

[7] Caves EM, Sutton TT, Warrant EJ, Johnsen S: Measures and models of visual acuity in epipelagic and mesopelagic teleosts and elasmobranchs. Journal of Comparative Physiology A 2023:1-20.

[8] Salvanes A, Kristoffersen J: Mesopelagic fishes: Academic Press: Cambridge, MA, USA; 2001.

[9] Warrant EJ, Collin SP, Locket NA: Eye design and vision in deep-sea fishes. Sensory processing in aquatic environments 2003:303-322.

[10] Corral-López A, Garate-Olaizola M, Buechel SD, Kolm N, Kotrschal A: On the role of body size, brain size, and eye size in visual acuity. Behavioral Ecology and Sociobiology 2017, 71:1-10.

[11] Hong Y, Luo Y: Zebrafish Model in Ophthalmology to Study Disease Mechanism and Drug Discovery. Pharmaceuticals (Basel, Switzerland) 2021, 14(8).

Hydrogeochemistry Evolution of Water Resources in Dargaz Plain

H. Mohammadzadeh[1,2*], F. Fanoodi[2]

[1]*Groundwater and Geothermal Research Center (GRC), Water and Environment Research Institute, Ferdowsi University of Mashhad, Mashhad, Iran.*

[2]*Department of Geology, Faculty of Science, Ferdowsi University of Mashhad, Mashhad, Iran*

**Corresponding author: mohammadzadeh@um.ac.ir*

Abstract— One of the fundamental problems of sustanable development in a country is the lack of water resources in terms of quantity and quality. The Dargaz aquifer (DA) is located in the north of Khorasan Razavi province near the border of Iran and Turkmenistan. In this paper, an attempt has been made to investigate the hydrogeochemical evolution of water resources in the Dargaz plain using hydrogeochemical techniques. The results show that the the quality of groundwater decreases in flow direction from west to east. In addition to natural factors (dissolution of Tirgan and Sarcheshmeh formations), human factors are also involved in the water quality of the studied area. According to the Piper diagram, the dominant type of water in the region is sodium-calcium sulfate. The groundwater quality is acceptable for drinking and agricultural purposes, and it is hard to completely hard water for industrial purposes.

Keyword: Groundwater, Dargaz Plain, Hydrogeochemical Evolution, Water-Rock Intraction.

INTRODUCTION

Today, the water crisis is one of the country's major challenges, and the lack of rainfall due to drought and excessive exploitation of aquifers has reduced the quality and quantity of groundwater resources (GWR) in alluvial aquifers. GWR are an important component of freshwater resources and the main source of water supply in many parts of the world, and the water quality of these resources is more stable and reliable than surface water against climate change. Groundwater quality is one of the hydrogeochemical aspects that deals with the spatial distribution of various water chemical types, describing the chemical evolution of water, and its usability for drinking, industry, and agriculture purposes [2]. Therefore, understanding hydrogeochemical evolution is vital for the development, protection, and exploitation of GWR. In recent years, extensive research has been conducted in the world [e.g., 3, 6, 7] and in Iran [e.g., 1 ,5] on the mechanism of hydrogeochemical evolution of groundwater and the factors affecting its quality. In order to develop sustainable water in the region, the main objective of this paper is to evaluate the processes affecting hydrogeochemical evolution of GWR in Dargaz plain (DP).

MATERIALS & METHODES

Hydrogeochemical Techniques

To achieve the objectives, sampling were done in two dry and wet seasons, and all samples were analyzed for the concentration of major ions, and total dissolved solids (TDS). In order to investigate the water - rock intractions and hydrogeochemical evolution, different techniques (including Piper, Pie, Gibbs, and combination diagrams, and saturation index -SI) were applied using related softwairs (PHREEQC-2.15, Water Chemistry, ArcGIS -10.8.1).

B. Study Area:

The DP, with a geographical range of 38°58' to 11°59' east longitude and 11°37' to 43°37' north latitude, is located in northeastern of Iran, 220 km northwest of Mashhad. Considering the rainfall (277.7 mm) and average temperature (13.1 °C), the climate of the Dargaz plain region is considered semi-arid.

DISCUSSION

The TDS and the distribution of ion concentrations in DP’s water resources "Fig.

1", indicate that the hydrogeochemical evolution of GWR occurs in the flow direction from the west to the east. In general, the amount of bicarbonate ions decreases, however, the amount of sulfate, chlorine, and sodium ions gradually increases. This has occurred under the influence of both natural (dissolution of gypsum and marl minerals of Sarcheshmeh formation, especially in the eastern parts, low rainfall, evaporation, and high retention time) and antropogenic (agricultural runoff) factors.

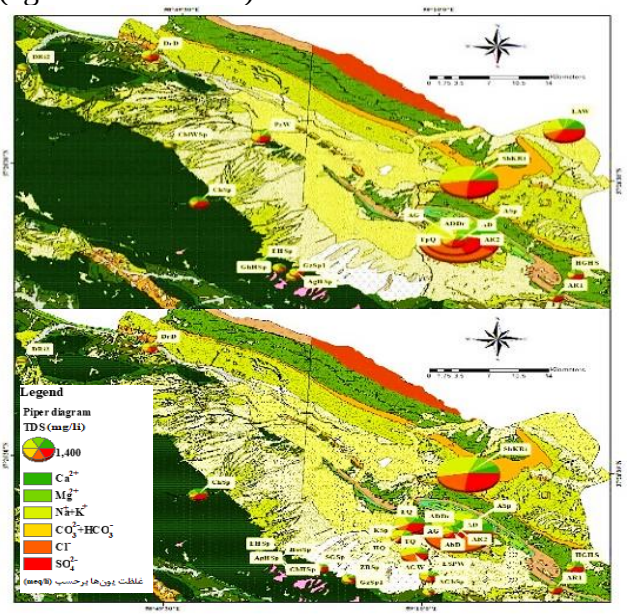

Fig. 1 Distribution of ion concentration in Dargaz plain's water reservoir and their Pie diagrams for Dry (up) and Wet (down) periods in 2023.

The Gibbs diagram, indicate that the water-rock interaction is the mane process effect on water quality. As indicated on Piper diagram, most of the samples have sodium-calcium sulfate type. On Na^+/Cl^- diagram, most samples are located on the 1:1 line (indicating halite dissolution) and above it (indicating direct ion exchange and weathering of silicate minerals). The Ca^{2+}/SO_4^{2-} diagram, indicates that in addition to the dissolution of gypsum, sulfate ions have increased under further processes. Also the $Ca^{2+}+Mg^{2+}/HCO_3^-+SO_4^{2-}$ diagram, show that the dominant process is the dissolution of anhydrite and gypsum in the area. However, some samples were plotted below 10 milliequivalents, indicating the dissolution of calcite and dolomite. The calculated saturation index show that all samples are supersaturated with respect to the calcite, dolomite and aragonite, which tend to settle, however, the saturation index values for the minerals anhydrite, gypsum and halite were negative, which means that these minerals can dissolve in water. The calculated idexecs show that the groundwater quality in DP is acceptable for drinking, agricultural and industrial.

CONCLUSION

The results indicate that the hydrogeochemical evolution in the study area is in line with the flow direction, from west to east. This is consistent with the results of the composite diagrams, saturation index and changing in ion concemtration. The Tirgan limestone formation, due to its high water discharge volume, and the Sarcheshmeh and Sanganeh formations (which containing evaporate minerals and have a negative role in the quality of water resources) have the most effect on GW quqlity. Of course, the agricultural activities are also involved as human factors in water quality. Most of the water samples are acceptable for drinking and agricultural uses and have a sodium-calcium sulfate water type.

REFERENCES

Ahankoub, M., Ayati, F., & Bagheri, H. (2022). Study of hydrogeochemical properties of graoundwater in Lordegan plain aquifer, Chaharmahal and Bakhtiari province, folded Zagros zone. Journal of Environmental Science Studies, 7(4), 5530-5540.

Alley, W.M. (1993). Regional groundwater quality. NewYork, Van Nostrand Reinhold, p.634.

Khong, L.X., Nizar, N.H.A., Ismail, S., Saad, N.A., Kamaruddin, M.A., , & Zabidi, H. (March 2024) Assessing the Groundwater Quality and

Hydrogeochemical Characteristics of Karst Aquifers in Kinta Valley, Perak.. 219-225.

Mohammadzadeh, H., Hussainzadeh, J. & Samani, S. (April 2022). Evaluation of charasteristics and hydrogeochemical evolution of Mashhad-Chenaran by inverse geochemical modeling in Phreeqc. Iranian Journal of Soil and Water Research, 53(4), https://civilica.com/doc/1658551.

Sanz, E., Bezares, C., Pascual, C., Menendez Pidal, I., & Fonolla, C. (2021). Hydrogeochemical Evolution of an Aquifer Regulated by Pyrite Oxidation and Organic Sediments. Water. 13, 2444. DOI: 10.3390/w13172444.

Sun, H., Bian, K., Wang, T., Jin, Z., & Niu, Z. (2023). Hydrogeochemical Characteristics and Genetic Analysis of Karst groundwater in the Fengfeng Mining Area. DOI: 10.3390/w15234049.

Engineering Geology of Holy Karbala City

N.Hafezi Moghaddas[1*], H. Ghorbanpour[2],

[1]*Ferdowsi University of Mashhad, Mashhad, Iran*

[2]*East oil and gas production company*

**Corresponding author: nhafezi@um.ac.ir*

Abstract— In this study, general geology, hydrology and engineering geology of Karbala city is presented. Karbala is one of the holy cities of Shia Muslims. City of Karbala was born simultaneous with martyrdom of Imam Hossein and his companions. But the name of Karbala such as Baghdad and Babylon are an ancient name with several thousand years old. In general, the area of Karbala or Nineveh was known as a holy area and a place of worship since the time of the Babylonians, Chaldeans, Assyrians and Sasanians. Geologically, Karbala located between the Mesopotamia plain and Arabian shield. The Euphrates or Abu-Jir fault system separates these two units. The Mesopotamia region is the continuation of the Zagros foredeep which includes Mesopotamia, Kuwait, the coast of Iran and the Persian Gulf and the northeast of Syria. Rock outcrops in the Karbala area from the past to the recent are included Euphrates Nafil, Injana, Dibdiba, Zahra formations and Quaternary sediments. Quaternary deposits comprise of aeoline, floodplain, channel river, levees, marsh deposits and recent alluvial fans. The area has two shallow and main aquifers. The groundwater table of the shallow aquifer is about 3 meters and water table in the main aquifer decrease from 32 meters from southwest to 22 meters in Northeast which completely follows the topography.

Keyword: Karbala city, Engineering geology, Euphrates, Mesopotamia

INTRODUCTION

The Karbala holy city located in the 32^0 degree and 36` latitude and $44^0$ and 3` longitude, 105 kilometres from the Baghdad, 80 kilometres from the Najaf and 30 kilometres from the Euphrates River. The city of Karbala was born with the martyrdom of Imam Hussein and his companions in the year 61 Hijri, but Karbala is an ancient name similar to Baghdad and Babylon that is several thousand years old [1]. According to the Louis Massignon, the Kufa-Karbala plain was used as a place of worship during the Chaldean period [2]. In general, the area of Karbala or Nineveh was known as a holy area and a place of worship since the time of the Babylonians, Chaldeans, Assyrians and Sasanians [3].

The area has a hot and dry climate. The average annual temperature is 22 degrees Celsius; the average annual rainfall is 80 mm and the dryness index is 30. At present, three sides of the city of Karbala are surrounded by trees and gardens, and on the west side is the Arabian desert.

GEOLOGY OF THE AREA

Karbala is located on the border between the Arabian Shield and the Mesopotamia plain. Mesopotamia is a relatively flat plain, after the last ice age, when the water level of the Persian Gulf was higher, Mesopotamia was a part of the Persian Gulf, which, with regression the sea the lowering of the water level it reached to the present conditions. Rock outcrops in the Karbala region from old to recent include the Euphrates, Nafil, Injana, Dibdiba, Zahra formations and the Quaternary deposits [4]. The Euphrates formation of early Miocene age includes gray to yellow limestone with a thickness of less than 20 meters, the Nefil formation of Middle Miocene age consists of marl and limestone with a thickness of up to 12 meters. The Injana formation is of Upper Miocene age, including mudstone, sandstone, silt with a maximum thickness of 25 meters, and the Dibdiba formation is of Pliocene-Pleistocene age includes of sand with weak cement less than 18 meters and Zahra formation includes conglomerate less than 6 meters. Quaternary deposits include wind, floodplain, river channels, levee, swamp deposits and recent alluvial fans. The thickness of Quaternary

deposits increases from northwest toward the southeast as we get closer to the Persian Gulf and from the northeast and southwest toward the center of area. Figure 1 shows geology map of area.

HYDROLOGY AND HYDROGEOLOGY

The most important source of water in the holy city of Karbala is the Euphrates River, which passes 30 kilometers west of the city. In the past centuries, several canals have been built to irrigate the groves and agriculture of the Karbala land, which during the years and centuries, only some of them have left traces. Alqamah (Al-'alqami) river, due to its attribution to the Ashura event, has always been of interest and has been modified and repaired many times by the people or the rulers.

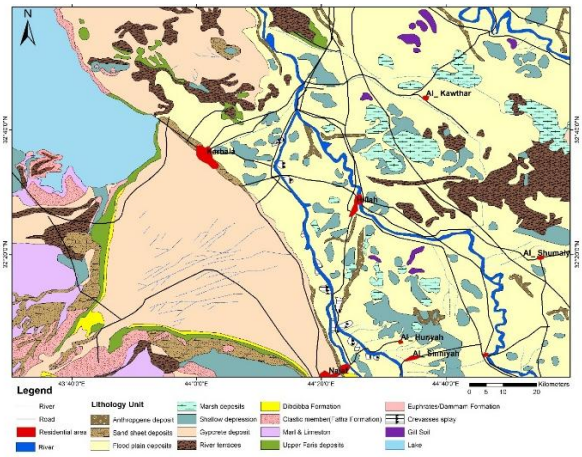

Fig. 1 Geology map of the area [4]

Karbala area is included a surface and a deeper unconfined aquifer. The first aquifer has been expanded in the Quaternary sediments; the thickness of these sediments increases from about 1 meter in the west of Karbala city to about tens of meters on the Euphrates River side. These sediments include sand, silt and clay. This aquifer is recharge through rainfall, irrigation waste water, leakage from the municipal water system and sewage. Water table of the first aquifer in the most of the city is about 3 meters and it has a lot of gypsum and salt and cannot be used for agriculture and drinking. In the central part of the city and holy shrine of Imam Hossein, the water level of the shallow aquifer is higher and the direction of water movement is from this area to the surrounding area [5, 6].

The second aquifer is located under the Quaternary sediments and in the Dibdiba Formation and includes clay, silty layers, fine- to medium-grained yellowish sand with local lenticular structures consisting of coarse-grained cemented sand and gravel. This aquifer is not independent from the upper aquifer and there is a hydraulic connection between them. The water table of the main aquifer changes from 32 meters in the southwest to the 22 meters in the northeast.

SOIL TEXTURE

The city of Karbala is located in the northern corner of Al-Khor alluvial fan. As can be seen in the geological map, there is a gypcrete unit on the surface, wind sand sheets in the end of fan and flood plain deposits after that. The soil texture in the area comprises of silt, sand and clay with significant amount of gypsum sometimes up to 20 percent. Due to the presence of chalk and salt in the dry state, the soil is hard and resistant [6].

CONCLUSION

Holy city of Karbala is located in the edge of an ancient alluvial fan which originate from the western desert. The bedrock of area is Dibdiba formation which also form the main aquifer of the area. The surface soil with different thickness from less than 1 meter in the west up to more than 30 meters includes of silty clay sand with high amount of gypsum up to 20 percent.

REFERENCES

[1] AL-Sharristani, M. A., and Nahdhat al-Hussain H. D, The Uprising of imam

Hussain, Dar al-Kitab al-Arabi, Lebanon.

[2] AL-Ansari, PL, Majalat al-Noor, Issue No. 61, Arabic Text p. 2, London, 1966

[3] wa-'l-Iʿlām, I. W. a-T̲ (1970). Archaeological sites in Iraq: Directorate General of Antiquities.

[4] Barwari, A. M., & Slewa, N. A. (1995). Geological Map of Karbala quadrangle, scale 1: 250000. Iraq Geological Survey Publications, Baghdad, Iraq.

[5]-Al-khalidy, Amer & Mahmood, Ahmed. (2019). An Engineering Study of a Soil for residential Project in Karbala Province. Journal of Engineering and Applied Sciences.

[6] Ketabchi H., Mahmodzadeh D., and Elahi H.R., Investigation on Urban Groundwater Flow and Construction of Subsurface Concrete Cutoff Walls Interaction Using a Numerical Modeling Approach (Case Study: Karbala City, Iraq), Journal of Iran Water Resources Research, 2020, Volume 16, Issue 2

Karst Groundwater Potential Mapping Using Machine Learning Model

H. Mohammadzadeh[1,2*], J. Hashemi[2], H. Ghalibaf Mohammadabadi [2]

[1]*Groundwater and Geothermal Research Group (GRC), Water and Environment Research Institute, Ferdowsi University of Mashhad, Mashhad, Iran*

[2]*Department of Geology, Faculty of Science, Ferdowsi University of Mashhad, Mashhad, Iran*

**Corresponding author: mohammadzadeh@um.ac.ir*

Abstract—The objective of this paper is to present a groundwater potential zoning map for the Hezar Masjid highlands, located northeast of Mashhad, using the Random Forest (RF) machine learning model. The zoning map was developed based on the locations of 1,438 springs in the area and 16 factors influencing groundwater potential. The model's performance was assessed using various statistical criteria, including the area under the receiver operating characteristic (ROC) curve (AUC = 0.93), indicating excellent accuracy.

Keyword: Machine learning, groundwater Potential, Hezar Masjed, Karst, Random Forest

INTRODUCTION

With the decline in alluvial groundwater resources, attention has increasingly turned to karst groundwater. Approximately 7 to 12 percent of the Earth's surface crust consists of karst formations [2], and karst watersheds contribute significantly to drinking and agricultural water supplies. Therefore, identifying areas with high karst groundwater potential is both important and necessary.

The findings of Nugroho et al. (2024) on groundwater potential demonstrated that the Random Forest (RF) machine learning model outperforms artificial neural networks and support vector machines [4]. Similarly, in 2024, Ragragui et al. investigated groundwater potential using machine learning and deep learning models, concluding that hybrid models deliver the best performance [5].

geographical location and springs

The study area is located in the northeastern part of Mashhad city in Khorasan Razavi province, spanning a geographical range of 36°07'35" to 37°37'30" north latitude and 58°05'00" to 61°15'35" east longitude. Springs are indicative of locations with maximum groundwater potential in a given area. Therefore, all 1,438 existing springs in the region, along with three times as many non-spring points randomly selected within the area, were used in the model.

MATERIALS & METHODS

A. Selection and analysis of factors affecting groundwater potential:

Due to the complexity of groundwater dynamics, selecting the factors influencing groundwater potential is highly challenging. However, based on the conditions of the study area and findings from previous research, 16 factors were considered Table 1.

Table 2. Groundwater Influencing Factors

Data Layers
Aspect
Slope
Convergence Index
Sediment Power Index (SPI)
Melton Ruggedness Number (MeRugNu)
Multi-Resolution Ridge Top Flatness (MRRTF)
Multi-Resolution Valley Bottom Flatness (MRVBF)
Slope Length (LS)
Lithology
Distance to Faults
Faults Density
Distance to lineaments
Lineaments density
Distance to Streams
Streams density
Normalized Difference Vegetation Index (NDVI)

In factor analysis, multicollinearity refers to the lack of independence among dependent variables in the dataset. The variance inflation factor (VIF) is used to analyse

multicollinearity in the dependent variable data "Eq. (1) ".

$$\text{VIF} = \frac{1}{1 - R_k^2} \quad (1)$$

Where: R_k^2 is the squared error rate for each regression run.

B. Algorithm:

The Random Forest (RF) algorithm, which is based on a collection of Classification and Regression Trees (CART) [1], serves as a powerful tool for analyzing complex relationships between various variables in hydrogeological studies. This algorithm operates by creating multiple decision trees, each trained on a random sample of the data and a random subset of features [3].

A decision tree is an effective machine learning tool used to classify data. It employs a tree structure to break down complex decisions into a series of simpler ones. Each node in the tree poses a question, and each branch represents a possible answer to that question. Ultimately, the leaves of the tree correspond to different classes into which the data is categorized.

The RF model is trained using 75% of the data, and its performance and accuracy are evaluated with the remaining 25%.

C. Model evaluation:

The validation approach is based on calculating four parameters: true positive, true negative, false positive, and false negative. These parameters are determined by evaluating how accurately spring pixels are classified as springs or non-springs in the training and test datasets.

Statistical metrics for model comparison include accuracy, precision, false positive rate (FP-Rate), Matthews correlation coefficient (MCC), root mean square error (RMSE), mean absolute error (MAE), and the Kappa index. Higher values of sensitivity, specificity, accuracy, precision, FP-Rate, and MCC indicate better model performance, especially when RMSE and MAE values are close to zero.

A Kappa index value of 1 indicates a perfect model, whereas a value of -1 signifies an unreliable model. All equations used to calculate these parameters are provided in "Eq. (2)-(11) ".

$$\text{Accuracy} = \frac{\text{TN} + \text{TP}}{\text{TP} + \text{FPx} + \text{TN} + \text{TP}} \quad (2)$$

$$\text{Specificity} = \frac{\text{TN}}{\text{FP} + \text{TN}} \quad (3)$$

$$\text{Sensitivity} = \frac{\text{TP}}{\text{TP} + \text{FN}} \quad (4)$$

$$\text{FPRate} = \frac{\text{FP}}{\text{FP} + \text{TN}} \quad (5)$$

$$\text{Precision} = \frac{\text{TP}}{\text{TP} + \text{FP}} \quad (6)$$

$$\text{MCC} = \frac{\text{TP} \times \text{TN} - \text{FP} \times \text{FN}}{\sqrt{(\text{TP} + \text{FP})(\text{TP} + \text{FN})(\text{TN} + \text{FP})(\text{TN} + \text{FN})}} \quad (7)$$

$$\text{Kappa} = \frac{\text{Accuracy} - \text{B}}{1 - \text{B}} \quad (8)$$

$$\text{B} = \frac{(\text{TP} + \text{FN})(\text{TP} + \text{FP}) + (\text{FP} + \text{TN})(\text{FN} + \text{TN})}{\sqrt{\text{TP} + \text{TN} + \text{FN} + \text{FP}}} \quad (9)$$

$$\text{RMSE} = \sqrt{\frac{1}{\text{n}}\sum_{\text{i}=1}^{\text{n}}(\text{X}_\text{P} - \text{X}_\text{A})^2} \quad (10)$$

$$\text{MAE} = \frac{1}{\text{n}}\sum_{\text{i}=1}^{\text{n}}|(\text{X}_\text{P} - \text{X}_\text{A})| \quad (11)$$

RESULTS

Based on the calculations, all 16 selected factors have a variance inflation factor (VIF) below 10, indicating no significant multicollinearity. Therefore, all factors were retained and used for modelling. The resulting map was categorized into five classes "Fig. 1".

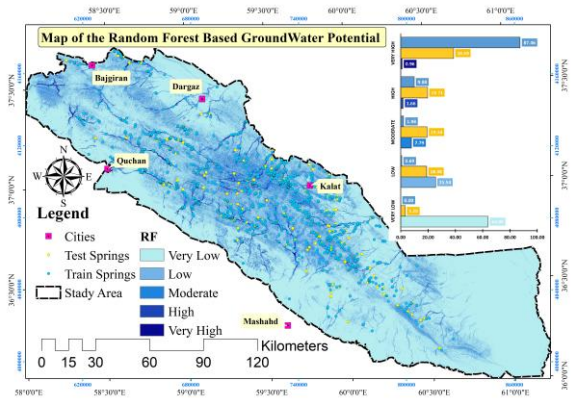

Fig. 1 Groundwater Potential Zoning Map using RF model

As shown, most of the content from the validation and training datasets falls into the high and very high classes. The validation results indicate that the model has achieved an acceptable score in the statistical parameters Table 2. Finally, in terms of the area under the curve, the RF model performed well (AUC = 0.93).

Table 3 Model Metric of RF Model

Model Metrics	RF Model
Accuracy	0.8908
Precision	0.8456
Specificity	0.9616
Sensitivity	0.6667
False Positive rate (FP-Rate)	0.0384
Matthews correlation coefficient (MCC)	0.6850
Root Mean Square Error (RMSE)	0.3304
Mean Absolute Error (MAE)	0.1092
Kappa	0.6773
Area Under Curve (AUC)	0.9300

CONCLUSION

In this study, GIS, remote sensing, and machine learning algorithms have been used to assess groundwater potential. Additionally, the novel aspect of this study is its attempt to integrate as many variables as possible that influence groundwater potential, including geological, topographic, hydrological, climatic, and land cover factors. Sixteen factors were considered, confirming the multicollinearity analysis of their influence and the applicability of these layers for potential detection. The Random Forest model was selected due to its satisfactory results in other regions worldwide. The performance and stability of the model were evaluated using several statistical criteria, which provided very good results for its application in this area. Finally, the developed methodology in this study may be useful for identifying potential groundwater areas, especially in mountainous regions with difficult access and areas where expensive exploration geophysical methods are challenging to apply over large extents.

REFERENCES

Breiman, L. (2001). Random forests. Mach. Learn, 45, 5–32.

Chen, W., Pourghasemi, H.R., & Naghibi, S.A. (2008). A Comparative Study of Landslide Susceptibility Maps Produced Using Support Vector Machine with Different Kernel Functions and Entropy Data Mining Models in China. Bull. Eng. Geol. Environ., 77, 647–664.

Knoll, L., Breuer, L., & Bach, M. (2019). Large scale prediction of groundwater nitrate concentrations from spatial data using machine learning. Sci. Total Environ. 668, 1317–1327

Nugroho, J.T., Lestari, A.I., Gustiandi, B., Sofan, P., Prasasti, I., Rahmi, K.I.N., Noviar, H., Sari, N.M., Manalu, R.J., Arifin, S. & Taufiq, A. (2024). Groundwater Potential Mapping using Machine Learning Approach in West Java, Indonesia. Groundwater for Sustainable Development, 101382.

Ragragui, H., Aouragh, M.H., El-Hmaidi, A., Ouali, L., Saouita, J., Iallamen, Z., Ousmana, H., Jaddi, H. & El Ouali, A. (2024). Mapping and modeling groundwater potential using machine learning, deep learning and ensemble learning models in the Saiss basin (Fez-Meknes region, Morocco). Groundwater for Sustainable Development, 26, 101281

Effect of Smart Water Meters (SWM)' Installation on Water Table Fluctuations in the Roshtkhar Plain

H. Mohammadzadeh[1,2*], M. Torshizi[2]

[1]Groundwater and Geothermal Research Center (GRC), Water and Environment Research Institute, Ferdowsi University of Mashhad, Mashhad, Iran.

[2]Department of Geology, Faculty of Science, Ferdowsi University of Mashhad, Mashhad, Iran

*Corresponding author: mohammadzadeh@um.ac.ir

Abstract— Changing in climat and decreasing in rainfall, and also increasing in population have caused the indiscriminate extraction from deep wells, as the main source of water supply in Rashtkhar plain. The result of which was a severe drop in the groundwater level and a critical situation in the Roshtkhar aquifer. In order to reduce the crisis, several management activities have been carried out, including the project of installing smart water meters (SWMs) on the wells of the plain, as a subset of the rehabilitation and balancing plan. Investigating the trend of changes in the water level of observation wells in 20 years' hydrographs, as well as calculated hours of operation and energy consumption of their corresponding selected agricultural wells shows considerable decreasing in the slope of the water level changes trend line of the observation wells after installing the SWMs compared to before installation. So that, in 9 observation wells, which have continuous and correct statistics, there was an average decrease of 46.4% in the drop of water level after SWMs installation.

Keywords: Smart meter, hydrograph, Roshtkhar plain, water table fluctuations

INTRODUCTION

Numerous natural and human factors have caused excessive withdrawal from aquifers and reduced water table levels. As a result, the drop in water table levels causes severe crises such as water shortage and drying up of water resources, reduced water quality, land subsidence, and increased costs of water extraction and pumping. Given that natural factors are beyond human control, reducing the adverse effects of groundwater level decline and the aforementioned crises requires controlling excessive withdrawal from aquifers as the most important unnatural (human) factors. By now, numerous studies have been conducted in the field of installing smart water meters (SWM) [e.g., 1, 2, 3, 4]. Installing SWM, as a tool to control and manage groundwater withdrawal and prevent unauthorized withdrawal from water wells for various purposes, is one of the 15 important projects of the restoration and balancing plan in Iran [5]. The perpouse of this paper is investigating the effect of SWM' installation on groundwater table fluctuations in the Roshtkhar plain.

MATERIALS & METODES

*A. Smart water meter (*SWM*) and data collection:*

A SWM is a device used to continuously measure, store information, and display the volume of water passing through a transducer, and is the most important tool for demand management and consumption control in the agricultural water sector. Number of 303 smart meters were installed on wells in the Rashtkhar plain include 266 SWM and electricity (more than 87 percent of the meters), and 37 electromagnetic meters. In order to investigate the effect of installing SWMs on groundwater level fluctuations, 20-year monthly statistical data of water level (before and after installing SWMs) in 12 observation wells were used.

B. Study Area:

The Rashtkhar plain, with an area about 2,409 km^2, is located in Khorasan Razavi province at the geographical coordinates of 59-2 to 55-59 East and 34-45 to 35-17 North. The Rashtkhar unconfined aquifer, is located

in the central part of the area, and it covers about 813 km^2.

DESCUSSION

According to the available statistics and data, the hydrograph of 12 piezometers was drawn for a 20-year period (2003-2023) "Fig. 1". As the slope of the water table change trend line with time in Table 1. shows, the overall trend of water table changes in piezometers is decreasing, and this decreasing slope was steeper and the water table drop was greater in the period before the SWM installation (2015). However, with the installation of meters, the decreasing trend has improved in Table 1. The results shows that the improvement in the decreasing trend of water table drop is affected by the installation of meters on agricultural wells.

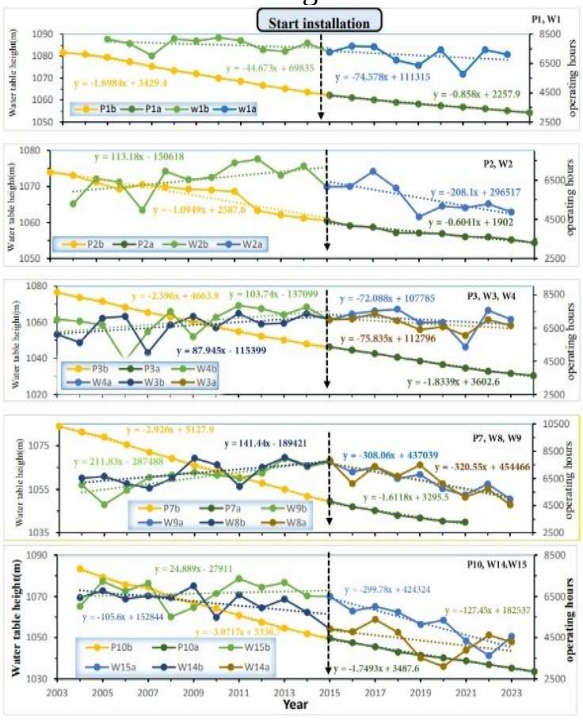

Fig. 1 Trend of changes in groundwater level in observation wells before and after SWM installation

Table 1. Changes in groundwater level in observation wells before and after SWM installation

Observation well specifications			Water Table Slope		Water Table Drop (m)	
symbol	XUTM	YUTM	BI	AI	BI	AI
P1	734125	3878114	-1.70	-0.86	-15.89	-7.98
P2	731131	3875155	-1.09	-0.60	-9.99	-6.14
P3	729831	3883012	-2.60	-1.83	-23.70	-15.88
P4	727704	3885151	-2.80	-1.16	-23.51	-10.99
P5	724760	3878177	-0.08	0.59	-2.90	3.13
P6	721424	3882602	-2.80	Dry	27.10	Dry
P7	720742	3888313	-2.9 3	-1.61	-17.40	-9.48
P8	718485	3885507	-2.75	-1.68	-21.45	-13.79
P9	717300	3892300	-2.94	-2.09	-26.66	-17.20
P10	714593	3888771	-3.07	-1.75	-27.36	-16.14
P11	711915	3893774	-0.33	0.11	-5.12	-0.73
P12	707557	3890201	-1.57	Dry	-13.79	Dry

CONCLUSION

The results of this study show that the water table in the plain continues to decline, but after the SWMs' installation on agricultural wells in 2015, the trend of groundwater level was declined in the critical prohibited Rashtkhar aquifer. The water table of 9 observation wells have had an average decrease of 46% after 2015 compared to before SWMs' installation. This confirmed by decreasing about 12% in the operating hours of the selected wells corresponding to the observation wells.

REFERENCES

Havangi, M., & Khozeymehnezhad, H. (2023). Evaluation of the implementation of the groundwater resources restoration and balancing plan with emphasis on the installation of smart meters (case study: Boshroyeh Plain, South Khorasan), Journal of Soil and Water Conservation Research, 30(2), 161-171. doi: 10.22069/jwsc.2023.21147.3631

Asadi, A., Sadeghzadeh, P., Majnouni, A., & Samadian, M. (2022). Investigating the effectiveness of the groundwater resources restoration and balancing plan based on the fuzzy-TOPSIS method (Case study: Urmia Plain), Water and Irrigation Management, 12(3), 483-496. doi: 10.22059/jwim.2022.337823.960Nugroho,

J.T., Lestari, A.I., Gustiandi, B., Sofan, P.,

Prasasti, I., Rahmi, K.I.N., Noviar, H., Sari, N.M., Manalu, R.J., Arifin, S. & Taufiq, A. (2024). Groundwater Potential Mapping using Machine Learning Approach in West Java, Indonesia. Groundwater for Sustainable Development, 101382.

Daneshpajouh, A., & Bagheri, R. (2019). The effect of the balancing scheme on the hydrogeological behavior of Dasht-e Rukh, Khorasan Razavi, Second International Conference on Biology and Earth Sciences, Hamedan, https://civilica.com/doc/1002002

Abdelhosseinzadeh, F. (2021). The effect of installing smart meters in groundwater wells on changing farmers' behavior in Torbat Heydariyeh County, Master's thesis, Faculty of Agriculture, Ferdowsi University of Mashhad, Iran.

Bio-recycling of Agricultural and Food Waste for Protein Production Using Black Soldier Fly (*Hermetia illucens*) Farming

A. Mohammad Saaid Day Torshizier[1*], B. Alireza Lashgary[2]

[1]*Department of Parasitology and Medical Entomology, Tarbiat Modares University, Tehran, Iran*

[2]*Aria Idea Pazhooh, Razdane Lashgary, Aria Idea Group, Ghazvin, Iran*

**Corresponding author: dayer@modares.ac.ir*

Abstract— This paper examines the feasibility of investing in a pilot bio-recycling plant using bio-convertor edible insects for protein production which can serve as a roadmap to build a full-scale production unit. This paper summarizes the outcome of 4-year experimental study undertaken to evaluate 5 insects registered by FAO as edible species for their capability in recycling biowaste to produce protein direly needed by animal feed industry. These are *Tenebrio molitar*, *Musca domestica*, *Lucilia sericata*, *Gryllus* sp. and *Hermetia illucens*, the black soldier fly (BSF). BSF was found particularly *Hermetia illucens*, was found not only farmable and useful at larval stage as an efficient waste bio-convertor but also harmless through all its developmental stages. BSF larvae can biologically break down organic wastes generated by households, restaurants, food processing industries as well as agro-waste and convert them to protein that can added to animal feed. The dried larvae are rich source of digestible proteins (, essential fatty acids and minerals increasingly required for animal, poultry and fish farming. BSF, therefore, provide an environmentally friendly solution to the serious problem of biowaste disposal and recycling. As an alternative protein source for animal feed, BSF farming can diminish the pressure on agricultural products such as soybeans direly needed to respond to increasing food demands of global population.

Keyword: bio-recycling, biowastes, *Hermetia illucens*, Black Soldier Fly, Animal feed, bioconversion

INTRODUCTION

The predicted high global population by 2050 requires an increase in food production by 70 to 100 %. Therefore, improving efficiency of agricultural inputs, reducing the cost of production and slowing down the negative environmental impacts are imperatives in the coming decades. Entomophagy can provide an urgent solution for global food security. Many countries are using insects as alternative protein sources [1]. Insect protein has many beneficial effects on the production and health of livestock and poultry [2]. Insect meal contains comparable protein and fat contents to beef and chicken and has more unsaturated fatty acids and minerals such as iron and zinc [3]. However, when used for animal feed, insects must be produced in large volumes and with high quality and sustainability. This can only be achieved through a large-scale automated plant with optimized production processes [4]. Although some edible insects, as human food and animal feed have now been marketed in many countries, but safety and health standards must be carefully observed [5]. On average, the protein content of edible insects is between 35 and 60% of the dry weight and 10 to 25% of the fresh weight [6]. This is higher than protein contents of cereals, soybeans and lentils [7]. Studies have shown that the protein digestibility of insects without cuticles is 77–98% [8]. Insects are extremely efficient bio-converts. They are almost twice as efficient as chickens and more than 5 times as efficient as cattle. Insects can feed on low quality bioproducts, require much less space and create less pollution than livestock [9]. The CO2 emission per 1 kg of insect weight gain is 2 g, while that for livestock is between 122 and 2850 g. On average, one kg of insect biomass can be produced from 2-5 kg of food waste [12]. Insect farming consume much less water than plant cultivation.

OBJECIVE

a) Assessing optimal conditions for biomass production per unit area
b) Determining the rearing substrate composition for maximum growth
c) Optimizing conditions for high adult density and fecundity per cubic meter
d) Mapping out requirements for production unit installation

METHODLOGY

The insects were reared in the Insectarium of Tarbiat Modares University under 25±2 ºC, 60% RH and 12h light to 12 h dark photoperiod. Household, restaurant, fruit waste and Agro-waste were used to formulate the test diets of insects. Wheat bran and cattle manure were used to provide a basic substrates for rearing cages. The effects of various diet compositions were examined on insects growth rate, longevity and fecundity as well as other biological indices important for life table.

RESULT & DISCUSSION

The composition of BSF meal is presented in Table 1. The protein comprises 44.5% of BSF meal which is higher than the content of other protein sources supplemented to livestock and poultry feed. It is rich in fibre (10.92 %) and useful fatty acids and hydrocarbons. It has significant amount of calcium, magnesium, sodium and phosphorus salts and the essential amino acids lysine and methionine.

The calcium content of BSF is very high (21.6 g/kg), with 88% higher digestibility than fish meal, and therefore with a better biological value (Gunawan et al., 2018). Our study showed that BSF is a rich source of essential amino acids for human and livestock nutrition.

In general, the black soldier fly can be bred on various waste substrates, and its nutritional quality is suitable for use in feeding livestock, poultry, and aquatic animals.

The weight of consumed food (bran and fruit waste containing 80% water in a ratio of 1 to 2) for a period of larval rearing for the population resulting from one gram of eggs (average 4.5 kg) was 5 to 5.5 times the weight of the larval mass, i.e. rearing 4.5 kg of larvae needs 22 to 25 kg of waste. The percentage of fertilizer obtained from rearing larvae will be 34% of waste and 48% of other waste.

Table 1. Nutritional components of the dried BSF larvae

Minerals	Amounts	Organic matter	Amounts
N	7.13 %	lysine	0.242 ug/g
P	0.73%	Methionine	0.038 (ug/g)
Cl	142.0 (mg/kg)	Protein	44.56 %
Na	2046.6 (mg/kg)	Carbohydrates	21.40 (ug/g)
Ca	21.6 (g/kg)	Fiber	10.92 %
Mg	10.56 (g/kg)	Fat*	27%
Ash	8%	Polysaccharide*	8%

*, Calculated ratio

CONCLUSION

In conclusion, each of the insects studied has specific capabilities in using various types of organic wastes, and their nutritional values can complement each other to convert them into suitable diets for poultry. Therefore, managing their breeding at pilot scale or full-scale production units can lead to increased efficiency in nutritional properties of feed additives, waste valorisation and enhances environmental sustainability.

ACKNOWLEDGMENT

The authors would like to thank the colleagues in Tarbiat Modares University.

REFERENCES

Kim T.K., Yong H.I. Kim Y-B., at al (2019). Edible Insects as a Protein Source, Trends. Food Sci. Anim. Resour. 39(4):521~540.

Driemeyer H. (2016). Evaluation of black soldier fly (Hermetia illucens) larvae as an alternative protein source in pig creep diets in relation to production, blood and manure microbiology parameters. http://hdl.handle.net/10019.1/100283

van Huis, A., Dicke, M. van Loon, J. (2015), Insects to feed the world. Journal of Insects as Food and Feed. 1. 3-5. http://doi.org/10.3920/JIFF2015.x002.

Stoops J., Crauwels S., Waud M., et al. (2016). Microbial community assessment of mealworm larvae (Tenebrio molitor) and grasshoppers

(Locusta migratoria migratorioides) sold for human consumption. Food Microbiology 53 122e127.

Schluter O, Rumpold B, Holzhauser T, et al. (2017). Safety aspects of the production of foods and food ingredients from insects. Mol Nutr Food Res 61:1600520.

Bukkens SG. 1997. The nutritional value of edible insects. Ecol Food Nutr 36:287-319.

Muzzarelli RAA, Boudrant J, Meyer D, et al. (2012). Current views on fungal chitin/chitosan, human chitinases, food preservation, glucans, pectins and inulin: A tribute to Henri Braconnot, precursor of the carbohydrate polymers science, on the chitin bicentennial. Carbohydr Polym 87:995-1012.

Alexander, P.; Brown, C., Arneth, A. et al. (2017). "Could consumption of insects, cultured meat or imitation meat reduce global

FAO, 2010. Forest insects as food: humans bite back .Proceedings of a workshop on Asia-Pacific resources and their potential for development, 19-21 February 2008, Chiang Mai, Thailand, Ed. Patrick B. Durst, Dennis V. Johnson, Robin N. Leslie and Kenichi Shono

2.4. BIOTECHNOLOGIES

Phage Display Technology As a Tool For Vaccine Development

G. Hashemi Tabar[1*], P. Carnegie[2]

[1] *Pathobiology Department, Faculty of Veterinary Medicine, Ferdowsi University of Mashhad, Mashhad, Iran.*

[2] *Murdoch University, Biotechnology Research Group, Murdoch, Western Australia, 6150.*

**Corresponding author: hashemit@um.ac.ir*

Abstract- Vaccines are considered one of the most important bioproducts in medicine. Since the development of the smallpox vaccine in 1796, several types of vaccines for many diseases have been created. However, some vaccines have shown limitations as high cost and low immune responses. Bacteriophages (phages) are playing important roles in vaccine design, particularly in peptide selection and antibody development. Immunoglobulin G (IgG) from sheep which were protected from dermatophilosis with an enzyme preparation from *Dermatophilus congolensis* (*D. congolensis)*, were used to select peptides displayed on phage in the Ph.D.-7 random peptide library which contains 10^9 peptides. Phage displaying peptides which were unrelated to the mimotopes associated with protection to dermatophilosis were removed with IgG from sheep which were vaccinated with the enzyme preparation but were not protected. The IgG from the protected sheep before vaccination was also used for negative selection. From the selected mimotopes those with clearly repeating motifs were chosen and used to vaccinate sheep. A mixture of four phage mimotopes induced antibody to a recombinant protease from *D. congolensis*. The vaccinated sheep, when challenged with two strains of *D. congolensis*, recovered more rapidly from the lesions caused by the strains.

Key words: Vaccine, Phage display, Bacteriophage, sheep.

INTRODUCTION

Vaccination of sheep is a desirable method for control of the disease but until now has only been partially successful and antigens are difficult to produce in sufficient quantity from *D. congolensis*. The goal of vaccine development is to safely induce long-lasting, selective immunity to a targeted antigen. Increasingly, bacteriophages are playing important roles in vaccine design, particularly in peptide selection and antibody development.

MATERIALS & METHODS

IgG for the three positive selections to isolate peptides associated with protection was obtain from 11 sheep protected by vaccination with a preparation of heamolysin and other enzymes from *Dermatophilus congolensis (D. congolensis).* IgG for negative selection to remove peptides binding to unrelated antibodies was obtained from the same sheep prior to vaccination. 12 Merino hogget ewes evidence of dermatophilosis and originating from a flock with no history of dermatophilosis were randomly allocated to 2 groups. Phage group received 10^{14} particle forming unit of each peptide chosen in 1 ml PBS per vaccination of each sheep. Montanide ISA206 was mixed with an equal volume of antigen to form a water-in-oil emulsion giving a dose of 2 ml which was inoculated subcutaneously into one site in the neck region of each sheep. Twenty-eight days after the first injection the sheep were revaccinated as described above. Twenty-one days after the second vaccination each sheep was challenged with zoospore suspension of *D. congolensis*. On the challenge day 4 skin patches (4 cm x 4 cm) were washed with ether. The sites were wet with a light spray of water and then 400 ul of the *D. congolensis* zoospore suspension (2.5×10^7 zoospores/ml) applied to the each site with a syringe without a needle. Two sites each were used for W14 strain. After challenge, lesions were scored 7, 14 and 21 days later using the scoring system.

RESULTS

The results in this experiment provide the first demonstration of induction of a specific immune responses and at least some beneficial effect from vaccination of large animals with mimotopes selected from a phage random peptide library. Vaccination with phage mimotopes resembling recombinant serine protease caused an

improved rate of recovery in lesions with one strain of *D. congolensis*. There was no correlation between the decrease in lesion score and the level of antibody to recombinant serine protease in any of the sheep.

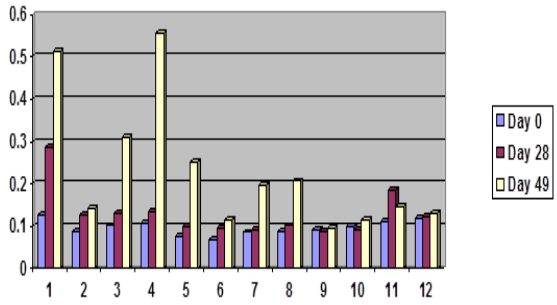

Fig. 1 Serine protease from *D. congolensis* was recognized by antibodies present in sera from some sheep which had been immunized with flagella mimotopes and challenged at day 49 with strain of *D. congolensis.*

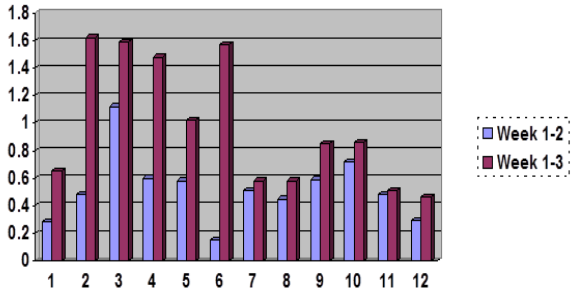

Fig. 2 Sheep numbers 1- 6 which were immunized with flagella mimotopes were challenged with W14 strain of *D. congolensis* and sheep numbers 7-12 were used as control. There was a significant difference at 21 days between the groups (P<0.001).

CONCLUSION

The results reported in this project provide the first demonstration of induction of a specific immune response against natural proteins and at least some beneficial effect after vaccination of large animals with mimotopes selected from phage random peptide library. As mimotopes can be selected, analysed and prepared in quantity much more quickly than the production of recombinant antigens, this technology should have considerable potential for preparing novel vaccines for other diseases.

ACKNOWLEDGMENT

Many thanks to Ministry of Science, Research and Technology of Iran and Murdoch University in Western Australia.

REFERENCES

Andrzej Piekarowicz, Aneta Kłyz˙ and Daniel C. Stein (2022). A New Vaccination Method Based on Phage Ngo86 and Its Phagemid Derivatives. Frontiers in Microbiology. 8, 1-8.

Panel Christiaan R de Vries, Qingquan Chen, Sally Demirdjian, Gernot Kaber, Arya Khosravi, Dan Liu, Jonas D Van Belleghem, Paul L Bollyky (2021). Phages in vaccine design and immunity; mechanisms and mysteries Current Opinion in Biotechnology. 68, 160-165.

Scott J.K and G.P Smith (1990). Searching for peptide ligands with an epitope library. Science. 249, 386-390.

Sharareh Mohammad Hasani , Elham Ghafouri , Shirin Kouhpayeh , Forouzan Amerizadeh , Ilnaz Rahimmanesh , Zohre Amirkhani , Hossein Khanahmad (2023). Phage based vaccine: A novel strategy in prevention and treatment. Heliyon. 9, 1-17.

Sutherland S.S, Ellis T.M & Edwards J.R (1991) Evaluation of vaccines against ovine dermatophilosis. Veterinary Microbiology 27, 91-99

Relation Between *Staphylococcus* Isolated from Domestic Cats and its Owner

A. Nooralhuda Aljawhar[*1]

[1] *microbiology department, vet medicine ,university of diyala , diyala, Iraq*

**Corresponding author: nooralhuda.m.a@uodiyala.edu.iq*

Abstract- Recently, pets animals become closest friends to human because they share an emotional conjunctive with their owners. Pets' animals: Cats and dogs are the most animal breeding by human. Highly closet habit with animal leads them to expose the potential risk to infected and spread zoonotic infections such as *S. aureus*. Staphylococcus is one of the most frequently isolated genera of opportunistic bacteria in animals and human in the skin and mucous membranes. This research aimed to investigate whether staphylococcus transmitted from cats to their owner. Samples were obtained from the saliva of thirty cats and their owner each sample was cultured by mannitol salt agar and blood agar. Oxidase, catalase, coagulase, and gram stain were performed to diagnosis the Staphylococcus spp. And used VITEC method for identified Staphylococcus species. The result was shown proportion of cat samples that showed a growth of gram-positive Staphylococci was 70% (21 out of 30), 52.4% of these 21 samples showed growth of gram-positive Staphylococci in cat owners (11 out of 21). VITEC result confirmed the isolate was *Staphylococcus sciuri*. Conclusion: The result was concluded highly possibility transmitted normal flora *Staphylococcus sciuri* from cat to owner.

Keyword: *Staphylococcus sciuri,* pets animals, cat

INTRODUCTION

Staphylococci are Gram - positive cocci, approximately 1 μ m in diameter, that tend to occur in irregular clusters resembling bunches of grapes. The name derives from the Greek words staphyle and kokkos for a ' bunch of grapes ' and a ' berry ' , respectively. Staphylococcus species occur as commensals on skin and mucous membranes; some may act as opportunistic pathogens causing pyogenic infections. Most staphylococci are facultative anaerobes and catalase - positive. They are non - motile and oxidase - negative and do not form spores. Two species, *S. aureus* subsp. *anaerobius* and *S. saccharolyticus,* are anaerobic and catalase – negative [1].

A total of 43 species of *Staphylococcus* have been described to date, seven of which are coagulase - positive or coagulase - variable species. The coagulase - positive *S. aureus* subsp. *aureus* (referred to as *S. aureus*) , *S. pseudintermedius*, and the coagulase - variable *S. hyicus* are important pathogens of domestic animals[2]. *Staphylococcus intermedius* was previously thought to be the major staphylococcal pathogen of dogs and cats but it is now considered that *S. intermedius* strains isolated from these hosts belong to the species *S. pseudintermedius*[3].

Staphylococcal species occur worldwide as commensals on the skin of animals and humans. They are also found on mucous membranes of the upper respiratory tract and lower urogenital tract and as transients in the digestive tract. The carriage sites of the pathogenic staphylococci are usually the mucous membranes and moist areas of the skin such as the axillae or perineal area. The nares are a major site of carriage of *S. aureus* in animals and humans, and approximately 20% of humans are permanent nasal carriers of this organism [4]. In this study will isolated and identification of *Staphylococcus* spp. from domestic cats and their owners.

METHODOLOGY

Specimen from the saliva (mouth) of thirty cats and their owners (mouth) was collected by using a gel swab. Then cultured in the mannitol salt agar (MSA) plate and incubated at 37o C for 24 h. After that, a single colony was taken and cultured on a blood and nutrient agar plate and incubated at 37o C for 24 h, and oxidase, catalase coagulase, and gram stain were performed on each sample.

The isolated bacteria were identified as Staphylococcus by VITEK test.

RESULT

Isolate growing on mannitol agar was appear yellow with golden colony as presented in Fig (3-1) and all isolate have oxidase negative, catalase and coagulase positive.

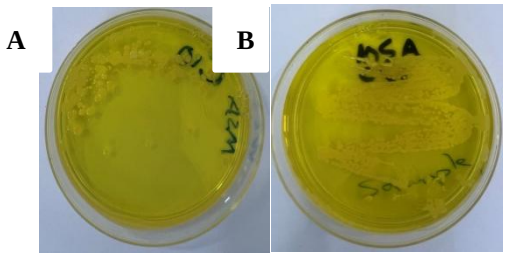

Fig (3-1): Staphylococcus spp. Isolate on Mannitol Salt Agar. (A) from Cat Sample (B) From The Owners

VITEK test was identified that Staphylococcus spp. isolate from cats and theirs owner was Staphylococcus sciuri as shown in Fig (3-2).

Comments:

Identification Information	Analysis Time:	4.35 hours	Status:	Final
Selected Organism	98% Probability	Staphylococcus sciuri		
	Bionumber:	1506000037736 31		
ID Analysis Messages				

Biochemical Details

2	AMY	-	4	PIPLC	-	5	dXYL	-	8	ADH1	+	9	BGAL	-	11	AGLU	+
13	APPA	-	14	CDEX	-	15	AspA	-	16	BGAR	-	17	AMAN	+	19	PHOS	+
20	LeuA	-	23	ProA	-	24	BGURr	-	25	AGAL	-	26	PyrA	-	27	BGUR	-
28	AlaA	-	29	TyrA	-	30	dSOR	-	31	URE	-	32	POLYB	-	37	dGAL	-
38	dRIB	+	39	ILATk	+	42	LAC	-	44	NAG	+	45	dMAL	+	46	BACI	+
47	NOVO	+	50	NC6.5	+	52	dMAN	+	53	dMNE	+	54	MBdG	+	56	PUL	-
57	dRAF	-	58	O129R	+	59	SAL	+	60	SAC	+	62	dTRE	+	63	ADH2s	-
64	OPTO	+															

Fig (3-2) : VITEK test report was identified isolate is *Staphylococcus sciuri*

DISCUSSION

The composition of normal flora on an organism depends on the species, feed and environment, including population density. Nevertheless, S. aureus is the most frequently isolated coagulase positive Staphylococcus (CPS) from the anterior nares and temporarily from the skin of humans, whereas coagulase negative staphylococci (CNS), mainly Staphylococcus epidermidis, are dominant on the skin [5]

The finding of this study is compatible with the finding of Cox HU et al. [6] who isolated S. sciuri from clinically healthy cats.

The organism is considered a principally animal bacterial species and is commonly present on skin and mucosal surfaces of a wide range of pets and farm and wild animals [7,8], and since this strain appears in owners sample so it's probable that strain is transmitted from the cats to their owners.

CONCLUSIONS

The result was concluded highly possibility transmitted normal flora *Staphylococcus sciuri* from cat to owner

REFERENCES

Zaatout, N., A. Ayachi, and M. Kecha, Staphylococcus aureus persistence properties associated with bovine mastitis and alternative therapeutic modalities. Journal of applied microbiology, 2020. 129(5): p. 1102-1119.

Becker K, Heilmann C, Peters G. Coagulase-negative staphylococci. Clin Microbiol Rev. 2014 Oct;27(4):870-926. doi: 10.1128/CMR.00109-13. PMID: 25278577; PMCID: PMC4187637.

Wang N, Neilan AM, Klompas M. Staphylococcus intermedius infections: case report and literature review. Infect Dis Rep. 2013 Jan 22;5(1):e3. doi: 10.4081/idr.2013.e3. PMID: 24470954; PMCID: PMC3892614.

Archer, N.K., et al., Staphylococcus aureus biofilms: properties, regulation, and roles in human disease. Virulence, 2011. 2(5): p. 445-459.

Otto, M., Staphylococcus colonization of the skin and antimicrobial peptides. Expert Rev Dermatol, 2010. 5(2): p. 183-195.

Cox, H.U., et al., Distribution of staphylococcal species on clinically healthy cats. Am J Vet Res, 1985. 46(9): p. 1824-8.

Hauschild, T. and S. Schwarz, Differentiation of Staphylococcus sciuri strains isolated from free-living rodents and insectivores. J Vet Med B Infect Dis Vet Public Health, 2003. 50(5): p. 241-6.

Dakić, I., et al., Isolation and Molecular Characterization of Staphylococcus sciuri in the Hospital Environment. Journal of Clinical Microbiology, 2005. 43(6): p. 2782-2785.

Assessment of the Therapeutic Efficacy of Nano-capsules of Albendazole and Mebendazole Against Hydatidosis in BALB/c Mice

Nooshinmehr Soleymani[1], Hassan Borji[1], Abbas Rahdar[2]

1. Department of Pathobiology, Faculty of Veterinary Medicine, Ferdowsi University of Mashhad, Mashhad, Iran

2. Department of Physics, School of Basic Sciences, University of Zabol, Zabol, Iran

**Corresponding author: nooshinmehrsoleymani@gmail.com*

***Abstract*—**Using nanotechnology, medicine can effectively be made stronger, lighter, more durable, more reactive. In this study, a highly safe emulsion nano-capsule was tested for its superior efficacy, the ability to overcome drug resistance, and the least possible amount of side effects and complications associated with the treatment of hydatidosis. Nano-capsules are synthesized using a micro-emulsion of oil in water. formulations were tested via droplet size, zeta potential and SEM. Following seven months after infection, hydatidosis-infected 30 mice were divided into three groups. Groups 1 was treated daily with Albendazole plus Mebendazole Polymer Nano-capsules (Nano-ABZ+MBZ), group 2 was treated with Albendazole plus Mebendazole (ABZ+MBZ) as a positive control group, and Albendazole as a control group, group 3 was the negative control group without treatments (only received PBS). According to the results of the study, the total cyst numbers, total cyst size and weight of Nano-ABZ+MBZ had significantly lower total cyst numbers than the ABZ+MBZ. As well as the cyst with the maximum size and highest weight of Nano-capsule group had significantly lower than control groups. In conclusion.ABZ+MBZ-Nano-capsule can serve as suitable alternatives to chemical drugs. With the right application of nanotechnology, it is possible to possess the potential to produce safe and effective drugs, which has promising implications.

Keyword: Nanotechnology, Nano capsule, Hydatidosis, Albendazole, Mebendazole

INTRODUCTION

Hydatid cyst is a larval stage of *Echinococcus granulosus*. Hydatidosis is described as a zoonotic. It is still remaining a serious health and economic problem worldwide. The life cycle includes the final hosts, dog and canids, where parasite eggs are released in the environment by faeces, and the intermediate hosts, sheep or other ruminants, as well as humans with Eating fodder, vegetables and fruits infected with parasite eggs will cause hydatidosis [1].

The chemotherapeutic drugs that can treat hydatiosis is benzimidazole, including albendazole (ABZ) and mebendazole (MBZ). It is known that ABZ and MBZ have side effects at high doses over long periods of treatment for human patients. During the last few years, it has become indicated that in addition to the side effects of chemical drugs, drug resistance has also been observed, which made the treatment of hydatidosis complicated [1,2].

Designing and manufacturing newer drugs involves lots of time and cost. Therefore, it is better to Equipping medicines with advanced weapons such as using nanotechnology of nanomedicines [2].

Recently, Nanomedicines are introduced as an emerging drug carrier, a promising way to effectively treat parasitic diseases by overcoming the disadvantages of low bioavailability, non-specific distribution and rapid elimination of anti-parasitic drugs from the body of animals and humans. Nanomedicines are attended to have high drug encapsulation capacity, high stability and good drug holding [2,3].

MATERIALS & METHODS

Nano-capsule was prepared at room temperature using a micro-emulsion of oil in water (pH 7.4). The zeta potential spectrum of the ABZ+MBZ was shown in the range of 0 to -52 millivolts, And the particle size analyser showed, the mean size of ABZ+MBZ nano-capsules was 183.01 nm.

30 BALB/c mice aged up to 2 months were used in this study. A total of 2000 protoscoleces 90% survival (eosin stain 0.01%), were injected intraperitoneally into each mouse to induce infection. Following seven months after infection, 30 mice were

divided into three groups. Eevery other day, Groups 1 was treated with Albendazole plus Mebendazole Polymer Nano-capsules (Nano-ABZ+MBZ), group 2 was treated with Albendazole plus Mebendazole (ABZ+MBZ) as a positive control group, group 3 was the negative control group without treatments (only received PBS). After the treatment period, mice were euthanized painlessly. hydatid cysts were found in the internal organs were carefully removed and the physical properties of the cysts were measured in terms of number, size and weight.

RESULT

According to the results of the study, the total cyst numbers, total cyst size and weight of Nano-ABZ+MBZ had significantly lower total cyst numbers than the ABZ+MBZ. As well as the cyst with the maximum size and highest weight of Nano-capsule group had significantly lower than control groups.

In conclusion, ABZ+MBZ-Nano-capsule can serve as suitable alternatives to chemical drugs. With the right application of nanotechnology, it is possible to possess the potential to produce safe and effective drugs, which has promising implications.

ACKNOWLEDGMENT

We thank the research deputy of the Ferdowsi University of Mashhad for supporting us.

.

REFERENCES

Nooshinmehr Soleymani, Soheil Sadr, Cinzia Santucciu*, Abbas Rahdar*, Giovanna Masala and Hassan Borji*. (2024). Evaluation of the In-Vitro Effects of Albendazole, Mebendazole, and Praziquantel Nanocapsules against Protoscolices of Hydatid Cyst. Pathogens. 13,790. https://doi.org/10.3390/pathogens13090790.

Soheil Sadr, Narges Lotfalizadeh, Amir Mohammad Abbasi, Nooshinmehr Soleymani, Ashkan Hajjafari, Elahe Roohbaksh Amooli Moghadam and Hassan Borji*. (2023). Review-Challenges and Prospective of Enhancing Hydatid Cyst Chemotherapy by Nanotechnology and the Future of Nanobiosensors for Diagnosis. Tropical Medicine and Infectious Disease. 8(11),494. https://doi.org/10.3390/tropicalmed8110494.

Negar Sorouri, Nooshinmehr Soleymani, Soheil Sadr, Abbas Rahdar, Elahe Ebrahimzadeh, Hassan Borji*. (2024). Investigating the therapeutic effects of curcumin nanocapsules in hydatid cyst-infected mice. Experimental Parasitology. 9:267:108860. https://doi.org/10.1016/j.exppara.2024.108860

Investigating the Application of Nanomedicines in Improving the Hydatid Cysts Treatment

Hassan Borji[1*], Soheil Sadr[1], Shakiba Nazemian[1], Cinzia Santucciu[2], Abbas Rahdar[3], Sadanand Pandey[4]

[1]*Department of Pathobiology, Faculty of Veterinary Medicine, Ferdowsi University of Mashhad, Mashhad, Iran.*

[2]*WOAH and NRL for Echinococcosis, Animal Health, Istituto Zooprofilattico Sperimentale della Sardegna, Sassari, Italy*

[3]*Department of Physics, University of Zabol, Zabol, Iran.*

[4]*Department of Chemistry, College of Natural Science, Yeungnam University, 280 Daehak-Ro, Gyeongsan 38541, Korea*

**Corresponding author: hborji@um.ac.ir*

Abstract- Hydatid cyst is a serious zoonotic disease caused by the larval stage of the parasite *Echinococcus granulosus sensu lato* and is particularly prevalent in rural areas and communities where sheep and dogs are raised together. Current treatments include surgery, used only as save-live option, and less invasive techniques, such as watch and wait or cystic liquid aspiration. All cures are used along with drug therapy, and often this is the only option, but significant limitations such as side effects, insufficient drug penetration into the cyst, and drug resistance are often observed. Hence, the current review aims to investigate the application of nanoparticles and nanocoatings in treating hydatid cysts. Moreover, the role of nanotechnology tools in enhancing the effectiveness of conventional and herbal medicines is discussed, and the advantages, challenges, and future of these methods are analyzed. In this regard, nanotechnology has been introduced as a new approach to improve the effectiveness of treatments. Nanodrugs have been widely used to treat hydatid cysts due to their properties, such as increased solubility, stability, and bioavailability of drugs, the ability to target the cyst site, and reduced side effects. Nanocapsules have been investigated for enhancing drugs such as albendazole as a standard treatment to increase the penetration of the drug into the cyst wall. Additionally, nanoformulations based on plant compounds such as curcumin and flavonoids have shown significant antiparasitic and anti-inflammatory effects. In conclusion, nanotechnology has opened up new hopes for increasing efficacy and reducing the side effects of existing methods for hydatid cyst treatment.

Keywords: Nanotechnology, Hydatid Cyst, Nanoparticles, Nanocoatings

INTRODUCTION

Cystic echinococcosis (CE) is a parasitic disease caused by the infection of the larval stage of the parasite *Echinococcus* granulosus *sensu lato (s.l.)*. CE is a significant public health concern, especially in rural areas and communities where the biological cycle is perpetuated by sheep (intermediate host) and dogs (definitive host) raised together [1]. Humans are accidental intermediate hosts of the parasite through the consumption of contaminated food or contact with infected dogs. Once the parasite enters the body, the larvae settle mainly in the liver and lungs, forming fluid-filled cysts that can cause complications such as mechanical obstruction, secondary infections, and even death [2].

Nanotechnology has emerged as a novel approach to treating hydatid cysts by providing targeted drug delivery, increased efficacy, and reduced side effects [3]. Nanotools have improved the ability of drugs to penetrate the cyst wall and achieve long-term therapeutic effects by providing advanced drug delivery systems. Hence, the current review aims to investigate the application of nanoparticles and nanocoatings in treating hydatid cysts.

NANOTECHNOLOGY

In recent decades, nanotechnology has emerged as a powerful tool for treating several diseases, comprehensive of chronic and infectious diseases [4]. In particular, Nanotechnology has significantly benefited CE therapy by providing advanced drug delivery systems. One of the main challenges in the treatment of hydatid cysts is the lacking in penetration of drugs into the cyst wall and the low bioavailability of antiparasitic drugs. Due to their small size and high active surface

area, nanoparticles can penetrate deeper tissues and cyst walls [5].

Another advantage of nanotechnology is the possibility of designing targeted drug delivery systems. These systems deliver drugs directly to the cyst site and prevent non-specific distribution of the drug in the body [6]. This feature increases the effectiveness of the treatment and reduces the risk of systemic side effects [7].

Nanoformulations can also increase the solubility and stability of antiparasitic drugs. Using nanocapsules with herbal compounds such as curcumin enhances anti-inflammatory and antiparasitic effects. As a transformative approach, nanotechnology can help overcome the challenges in treating hydatid cysts [8].

CHEMICAL AND HERBAL MEDICINES

Albendazole is known as one of the primary drugs in treating CE, but its low bioavailability and the need for high doses are its main limitations [9]. Lipid and polymer nanoparticles have been developed to enhance the efficacy of this drug. Albendazole-based nanoformulations and nanocapsules have increased the drug's absorption into the cyst wall and enhanced its antiparasitic effects [10]. These nanoparticles can also increase the drug's half-life and reduce the need for repeated administration.

Regarding herbal compounds, curcumin, as a natural anti-inflammatory and antiparasitic compound, has attracted much attention. However, limitations such as its low solubility and rapid metabolism in the body have led to the development of curcumin-based nanoformulations and nanocapsules. These nanoparticles have enhanced curcumin's therapeutic effects and enabled its targeted delivery to the cyst site [5].

Moreover, nanocoatings for other plant compounds, such as flavonoids and essential oils, can help improve their efficacy and reduce their side effects. Nanotechnology can be combined with existing therapeutic methods and is an effective supplement in treating hydatid cysts [11].

CONCLUSION

As a novel approach to treating CE, nanotechnology has opened up new hopes for increasing efficacy and reducing the side effects of existing methods. Nanoparticles and nanocoatings have provided effective solutions to overcome existing limitations by improving the properties of conventional drugs.

ACKNOWLEDGMENT

Conceptualization: Abbas Rahdar, Hassan Borji; Methodology: All Authors; Writing - original draft preparation: All Authors; Writing - review and editing: Soheil Sadr; Supervision: Hassan Borji. We thank the Ferdowsi University of Mashhad Research Deputy for their support.

REFERENCES

1. Shnawa BH, Al-Ali SJ, Swar SO. Nanoparticles as a new approach for treating hydatid cyst disease. Veterinary Pathobiology and Public Health. 2021;1:180-9.
2. Cheraghipour K, Rouzbahani AK, Fallahi S, Taherpour F, Moradifard F, Shakib P, et al. Recent advances in therapeutic strategies against hydatid cysts using nanomaterials: A systematic review. Letters in Drug Design & Discovery. 2023;20:000-.
3. Sadr S, Lotfalizadeh N, Abbasi AM, Soleymani N, Hajjafari A, Roohbaksh Amooli Moghadam E, et al. Challenges and prospective of enhancing hydatid cyst chemotherapy by nanotechnology and the future of nanobiosensors for diagnosis. Tropical medicine and infectious disease.

2023;8(11):494.
4. Dhahi TS, Dafhalla AKY, Saad SA, Zayan DMI, Ahmed AET, Elobaid ME, et al. The importance, benefits, and future of nanobiosensors for infectious diseases. Biotechnology and Applied Biochemistry. 2024;71(2):429-45.
5. Sorouri N, Soleymani N, Sadr S, Rahdar A, Ebrahimzadeh E, Borji H. Investigating the Therapeutic Effects of Curcumin Nanocapsules in Hydatid Cyst-Infected mice. Experimental Parasitology. 2024:108860.
6. Mahmoudvand H, Harandi MF, Shakibaie M, Aflatoonian MR, ZiaAli N, Makki MS, et al. Scolicidal effects of biogenic selenium nanoparticles against protoscolices of hydatid cysts. International journal of surgery. 2014;12(5):399-403.
7. Soleymani N, Sadr S, Santucciu C, Rahdar A, Masala G, Borji H. Evaluation of the In-Vitro Effects of Albendazole, Mebendazole, and Praziquantel Nanocapsules against Protoscolices of Hydatid Cyst. Pathogens. 2024;13(9):790.
8. Shnawa BH. Advances in the use of nanoparticles as anti-cystic echinococcosis agents: A review article. Journal of Pharmaceutical Research International. 2018;24(1):1-14.
9. Bakhtiar NM, Akbarzadeh A, Casulli A, Mahami-Oskouei M, Ahmadpour E, Nami S, et al. Therapeutic efficacy of nanocompounds in the treatment of cystic and alveolar echinococcoses: challenges and future prospects. Parasitology Research. 2019;118:2455-66.
10. Norouzi R, Ataei A, Hejazy M, Noreddin A, El Zowalaty ME. Scolicidal effects of nanoparticles against hydatid cyst protoscolices in vitro. International journal of nanomedicine. 2020:1095-100.
11. Raziani Y, Shakib P, Rashidipour M, Cheraghipour K, Ghasemian Yadegari J, Mahmoudvand H. Green synthesis, characterization, and Antiparasitic Effects of Gold nanoparticles against Echinococcus granulosus Protoscoleces. Tropical medicine and infectious disease. 2023;8(6):313.

2.5. QUANTUM TECHNOLOGY

Types Of Lasers And Their Applications In Burn Patients

Mahsa Goharara[1*]

Imam Musa Kazem Hospital, Isfahan, Iran

**Corresponding author: Mahsa.goharara2017@gmail.com*

***Abstract*—** Lasers have wide applications in medicine, especially in the treatment of burn patients. They help heal tissue, reduce pain, and speed up the healing process. The use of lasers in the treatment of burns helps to improve the quality of life of patients and reduce the complications caused by burns. The right laser, depending on the type and severity of the injury, requires expert advice. Laser therapy in burn patients is one of the effective methods to heal wounds and reduce side effects caused by burns. Special lasers, such as non-destructive lasers and diode lasers, penetrate deep into the skin and by stimulating fibroblast and collagen cells, they accelerate the process of tissue repair and thus stimulate tissue repair. Also, by reducing inflammation and relieving pain, lasers help patients experience a more comfortable recovery period. Laser therapy can help improve the appearance of wounds and reduce scar tissue. Special lasers such as CO2 lasers can help reduce the thickness and color of scars. By increasing the blood flow in the damaged area, lasers deliver nutrients and oxygen to the cells and help the healing process. With the help of their light waves, lasers generate energy. They transfer to the cells and this energy causes biochemical changes in the cells, which also helps to repair and regenerate the tissue.

Keyword: Lasers, burns, types of lasers, lasers in the operating room

INTRODUCTION

Medical lasers, especially CO_2 and Erbium lasers, can help stimulate the production of collagen and fibroblasts. This accelerates the repair of damaged tissues and improves the condition of the wound. Also, by penetrating deep into the tissue, lasers can reduce inflammation and help relieve the pain of patients. These anti-inflammatory effects improve the quality of life of patients and facilitate the healing process. The use of laser in the treatment of burn wounds can help reduce scars and skin discoloration. With the use of special lasers, the scar tissue becomes softer and less visible. Lasers help to restore the surface of the skin and improve its appearance.

This feature is especially important in patients with deep or extensive burns who may have permanent scars. Lasers are known as a minimally invasive method that does not require large incisions and reduces recovery time. This feature allows patients to quickly return to their daily activities. The use of medical lasers in the treatment of burns is known as an effective and safe method. These techniques are a significant improvement

In the process of wound healing, they reduce side effects and increase patient satisfaction. Lasers play an important role in burn and plastic surgery operating rooms. Their functions include the following:

Precision surgery: lasers cut tissues with high precision and allow surgeons to operate without damaging adjacent tissues.

Bleeding control: Lasers can close blood vessels, thus reducing bleeding and reducing the need for stitches.

Wound healing: In the treatment of burns, lasers can help heal the tissue and repair the wound and help reduce scars and side effects.

Pigment changes: Lasers can be used to improve skin color and reduce pigment changes caused by burns or surgery.

Fat breakdown: In plastic surgery, lasers are used as a tool for lipolysis (fat reduction). The use of lasers in these areas helps to increase accuracy, reduce recovery time and improve final results.

Lasers can be added to several types of surgical devices in the burn and plastic surgery operating room. Some of these devices are:

General surgery devices: Lasers can be added as accessories to general surgery devices to provide more precision and control in cutting tissues.

Tissue destruction devices: lasers can be added to specialized devices such as tissue destruction devices (such as RF devices) to be more effective in destroying damaged tissues.

Liposuction devices: Special lasers can be added to liposuction devices to help break down fat and reduce surgical invasiveness.

Wound healing devices: Lasers can be added to wound healing devices to help improve tissue quality and reduce scarring.

Cosmetic surgery devices: In cosmetic surgery, lasers can be used as a tool to cut and repair the skin. Adding lasers to these devices can help improve accuracy, reduce complications, and increase patient satisfaction.

TYPES OF LASERS AND THEIR APPLICATIONS

In the field of medical lasers, a few types are particularly popular. The following are the most popular lasers and the advantages and disadvantages of each:

CO_2 laser[6]:

The advantages of this laser are that it is very effective in skin surgeries and tissue removal, the ability to regenerate tissue and reduce scars, and it will have lasting results in skin rejuvenation. The disadvantages of this laser are that it has a longer recovery time, may cause side effects such as redness and swelling, and requires post-operative care.

Nd laser[7]:

The advantages of this laser include the ability to penetrate deep into the tissue, suitable for the treatment of blood vessels and tumors, minimal damage to surrounding tissues, and a shorter recovery time than the CO_2 laser. The disadvantages of this laser are that it may not be effective for some skins and there is a possibility of side effects such as skin color change.

Erbium laser[8]:

The advantages of this laser are that it is suitable for superficial skin treatments and rejuvenation, it has a shorter recovery time than the CO_2 laser, and it will have fewer side effects, such as redness and swelling. The disadvantages of this laser are that it may not be as effective as the CO_2 laser in removing deep wrinkles and requires more treatment sessions for better results.

Diode laser[9]:

The advantages of this laser are effective in treating excess hair and low back, less pain and faster treatment time and compatibility with all skin types. The disadvantages of this laser are that it may be less effective for light or thin hair and requires several treatment sessions for optimal results.

Color pulse laser[10]:

The advantages of this laser are that it is multi-purpose and effective in treating various skin problems such as acne and discoloration, and it is painless and does not require anesthesia. The disadvantages of this laser are that the results may vary depending on the type of skin and the side effects are few, but it may cause skin irritation in some people.

LASER DEVICE ACCESSORIES

Medical laser devices have various accessories and components, each of which plays a special role in the performance and efficiency of these devices. The most important accessories include the following:

Laser source: This part produces the laser beam and can be of different types such as diode lasers, CO_2 lasers or Nd lasers.

Optics: include lenses and mirrors that focus the laser beam and direct it to the target point.

Cooling system: To prevent overheating of the device and damage to the surrounding tissues, there are cooling systems (for example, water or cool air) in laser devices.

Pedal or controller: These tools allow the doctor to manually control the laser settings and start or stop the treatment.

Status bar: These displays show information such as laser power, treatment duration and device status.

Bands and Filters: Some devices may have filters that allow only certain wavelengths to reach the target tissue.

Accessory parts: Includes various handles and probes for specific treatments such as dermatological or surgical treatments.

Safety systems: include sensors used to prevent unwanted operation and greater safety during treatment. These accessories help doctors to use laser technology in the best way to treat patients.

CONCLUSION

The use of lasers in burn surgery is an effective and innovative approach with numerous advantages. This technology enables precise cutting, enhances bleeding control, and minimizes side effects, which ultimately improves both the quality of treatment and the recovery speed of patients. Additionally, lasers play a crucial role in reducing and improving the appearance of scars resulting from burns. However, to fully leverage this technology, proper training and specialized infrastructure are essential. Finally, combining lasers with other treatment methods can further optimize surgical outcomes and enhance patient care.

Lasers are an integral tool in the operating room, widely used in various surgeries and medical treatments. These advanced devices offer numerous benefits that contribute to better surgical results and the reduction of side effects.

REFERENCES

EZZATI, Kamran, et al. The beneficial effects of high-intensity laser therapy and cointerventions on musculoskeletal pain management: a systematic review. Journal of lasers in medical sciences, 2020, 11.1: 81.

DOMPE, Claudia, et al. Photo biomodulation underlying mechanism and clinical applications. Journal of clinical medicine, 2020, 9.6: 1724.

CHOI, Katherine J., et al. Fractional CO2 laser treatment for burn scar improvement: a systematic review and meta-analysis. Burns, 2021, 47.2: 259-269.

PENG, Weihai, et al. The efficacy and safety of fractional CO2 laser therapy in the treatment of burn scars: A meta-analysis. Burns, 2021, 47.7: 1469-1477.

KLIFTO, Kevin M.; ASIF, Mohammed; HULTMAN, C. Scott. Laser management of hypertrophic burn scars: a comprehensive review. Burns & Trauma, 2020, 8: tkz002.

DOUGLAS, Helen, et al. Carbon dioxide laser treatment in burn-related scarring: a prospective randomised controlled trial. Journal of Plastic, Reconstructive & Aesthetic Surgery, 2019, 72.6: 863-870.

ROMANOS, George E.; PELEKANOS, Stavros; STRUB, Jörg‐Rudolf. Effects of Nd: YAG laser on wound healing processes: clinical and immunohistochemical findings in rat skin. Lasers in surgery and medicine, 1995, 16.4: 368-379.

KIM, Jin Cheol, et al. Efficacy of combined treatment with intense pulsed light and fractional erbium: YAG laser in scar prevention: a randomized split wound trial. Dermatologic Therapy, 2021, 34.5: e15061.

TANG, Di, et al. The associations between diode laser (810 nm) therapy and chronic wound healing and pain relief: Light into the chronic wound patient's life. Wound Repair and Regeneration, 2023, 31.2: 227-232.

MATUSZCZAK, Ewa, et al. Effects of combined Pulsed Dye Laser and Fractional CO2 Laser treatment of burn scars and correlation with plasma levels of collagen type I, MMP-2 and TIMP-1. Burns, 2021, 47.6: 1342-1351.

Scalability and Performance of Dual Wire Gate All Around Nanosheet FETs in Next-Generation Electronics

Reza Abbasnezhad[1], Hassan Rasooli Saghai[2]*, Reza Hosseini[3], Aliasghar Sedghi[4], Ali Vahedi [5]

[1] *Department of Electrical Engineering, Shabestar Branch, Islamic Azad University, Shabestar, Iran.*

[2]*Department of Electrical Engineering, Tabriz Branch, Islamic Azad University, Tabriz, Iran.*

[3*]*Department of Electrical Engineering, Khoy Branch, Islamic Azad University, Khoy, Iran.*

[4]*Department of Physics, Shabestar Branch, Islamic Azad University, Shabestar, Iran.*

[5]*Department of Physics, Tabriz Branch, Islamic Azad University, Tabriz, Iran.*

**Corresponding author: H_Rasooli@iaut.ac.ir*

Abstract— In this paper, we propose a new variation of the Gate All Around Nanosheet Field Effect Transistor (GAA NS FET), incorporating Dual Wire (DW) strained channels. We examine its electrical performance at a temperature of 300K and compare it with the Conventional DW GAA NS FET and the Conventional GAA FET. Our study investigates the impact of electrostatic control on DC and analog parameters, such as gate capacitance and transconductance, for all three device types. The channel regions of the proposed structures are composed of Silicon Germanium (Si/Ge/Si), and the combination of strain and the heterojunction design leads to significant enhancements in device performance. To accurately model the semiconductor device, we solve the Density Gradient (DG) equation self-consistently, applying the Shockley-Read-Hall (SRH) equation to estimate carrier generation, while also considering the effects of bandgap narrowing on transport behavior and accounting for Auger recombination. Notably, at 300K, the Conventional DW GAA NS FET demonstrates a substantial improvement in both Ion and Ioff compared to the Conventional GAA FET.

Keyword: Conventional GAA FET, Naonosheet-Dual wire, Density Gradient (DG)

INTRODUCTION

In recent decades, the semiconductor industry has advanced significantly by shrinking device sizes, allowing more transistors on a single chip and improving performance, as predicted by Moore's Law. This miniaturization aims to increase density, speed, and cost-efficiency in integrated circuits but also introduces challenges like short-channel effects. Multi-gate transistors and alternative structures like FinFET and GAA transistors help address these issues. Additionally, techniques like strain engineering and new materials, including high-k dielectrics and metal gate electrodes, are enhancing CMOS technology [1-5]. The semiconductor industry has been a crucial foundation for modern communication technologies, including wireless networks, cellular systems, military applications, navigation, identification, and radio broadcasting [6]. The consistent miniaturization of metal-oxide-semiconductor field-effect transistors (MOSFETs) has been largely enabled by advancements in fabrication technology and device engineering, aiming to achieve greater packaging density and enhanced performance [7–9]. As outlined in the International Technology Roadmap for Semiconductors (ITRS), CMOS scaling into the sub-nanometer range necessitates advanced channel engineering methods. Therefore, to address the limitations of traditional bulk MOSFETs, the development of new architectures and devices is essential to drive further improvements in sub-nanometer scaling [10]. Researchers have explored various architectures, including double gate, gate-all-around, quadruple gate, dual-material double gate, triple-material double gate, and junctionless double-gate MOSFETs, achieving enhancements in electrostatic control, analog, and RF performance [11]. As integrated circuits continue to increase in density, exploring nanoscale devices has become essential. However, as devices shrink to nanoscales, they encounter unwanted effects, including hot carrier effects (HCE), elevated off-state currents, and higher gate currents. Silicon-on-

insulator (SOI) technology presents a promising solution for nanoscale applications, offering advantages such as minimized short channel effects (SCEs), enhanced drive currents, and reduced junction capacitances [12]. Due to its ability to suppress SCEs, Nanosheet transistors have been extensively studied and shown to outperform conventional MOSFETs. To further address SCEs, a new device Nanosheet FET with dual wire in gates has been proposed.

Nanosheet field-effect transistors (NS FETs) are a promising technology for future analog and RF System-on-Chip (SoC) applications at the 3 nm scale. They enable shorter gate lengths, improving performance at lower voltages and boosting chip density [13-15]. The gate-all-around (GAA) design helps control nanosheet channels, reducing short-channel effects. Additionally, NHJS technology supports digital CMOS scaling through FinFET and multi-gate designs, enhancing analog and RF integration [16]. This study conducted simulations on existing structures, comparing them with heterojunction structures. Enhanced carrier mobility was mainly attributed to strain from lattice mismatch. To incorporate heterojunction structure and strain engineering, we used multilayered Si/Ge/Si materials. The paper is organized as follows:

Section 2 details the design, geometry, and simulation methods for both Heterojunction GAA NS FET and Conventional GAA NS FET, with brief insights on their potential applications. Section 3 examines the impact of strain engineering and heterojunction structure on the devices' electrical properties. Section 4 summarizes the key findings.

DEVICE STRUCTURE AND SIMULATION METHOD

Figure 1 illustrates 3D schematic views of the Conventional DW GAA NS FET, characterized by a rectangular cross-section. This structure uses silicon in the source and drain regions, with SiGe forming the channels. The tensile-strained SiGe significantly impacts energy levels within these structures. For our simulations, we applied a set of parameters for the Conventional DW GAA NS FET, outlined in Table 1. Aluminum, with a work function of 4.7 eV, was used as the gate material, producing an internal electric field that repels electrons from the channel in the OFF state. Key parameters include t_{si} (silicon body thickness), W (channel width), and L (channel length). We assumed a gate oxide thickness of 0.5 nm for SiO_2 and 1.5 nm for HfO_2. Figure 2 shows the comparison of the transfer characteristics of the primary structure with a reference transfer curve, used to calibrate simulation parameters.

To improve the accuracy of our simulations, we employed an effective quantum-corrected potential as the basis for a Scharfetter-Gummel discretization scheme. These equations were then solved using the 3D ATLAS simulator. To achieve reliable predictions of subthreshold behavior and Auger recombination effects, the bandgap narrowing (BGN) model was integrated into our simulations. We also applied the Shockley-Read-Hall (SRH) model to assess carrier generation and recombination, allowing us to evaluate the influence of doping on device performance. Additionally, Fermi-Dirac (F-D) statistics were used to describe the likelihood of electron or hole occupancy in specific energy states under equilibrium conditions [17].

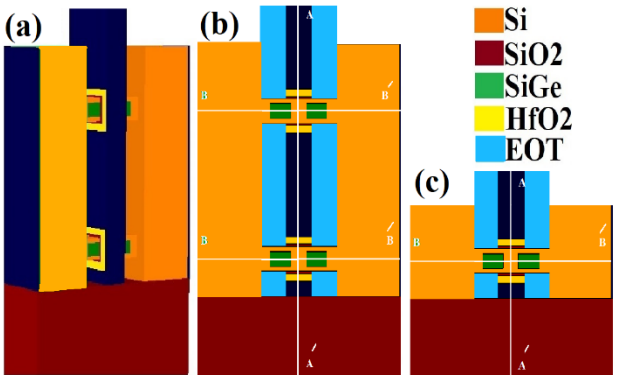

Figure.1: (a)3D schematic view of Conventional DW GAA NS FET with nitride spacer (b) 2D view and cross section of

Conventional DW GAA NS FET (c) 2D view and cross section of Conventional DW GAA FET

RESULTS AND DISCUSSIONS

Figure 2 presents the $I_D\_V_G$ characteristics under varying temperature conditions. Notably, as the temperature decreases, the drain current I_D increases. This increase in I_D can be attributed to the enhanced mobility of charge carriers at the source-channel interface, as shown in Fig. 2. Electron mobility can be determined using a linear regression technique, as outlined in references. The mobility is inferred from the relationship between drain current and electron mobility in the transfer characteristics [18]. Specifically, electron mobility can be calculated by differentiating I_D with respect to drain voltage. Equations (1) to (4) demonstrate that electron mobility is directly linked to changes in drain current, indicating its sensitivity to the electric field.

Table 1: Parameters used for devices modeled in this work

Parameters	Conventional DW GAA NS FET	Conventional DW GAA FET
Height of the devices (nm)	60	25
Height of the substrate (nm)	30	30
Nanosheet width (nm)	15	15
Gate length(nm)	5	5
Source/Drain length (nm)	12	12
Channel doping	Without doping	Without doping
Source/Drain doping	n.type 10^{20}	n.type 10^{20}
Dual wire doping	p.type 10^{16}	p.type 10^{16}
Spacer dielectric/Underlap (nm)	Nitride\5	Nitride\5

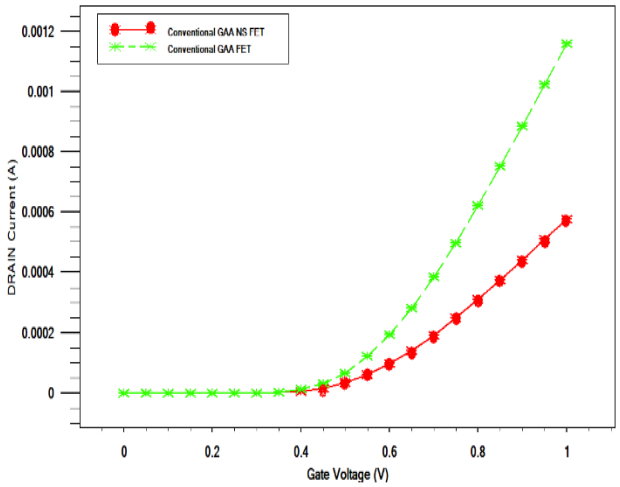

Figure.2 : Drain current of the Conventionakl DW GAA NS FET and Conventional DW GAA FET under versus gate voltage at $V_{DS} = 0 \cdot 6V$

$$I_D = \frac{\mu_{eff} C_{ox}}{2}\left(\frac{W}{L}\right)\left(2(V_{GS} - V_T)V_{DS} - V_{DS}^2\right) \quad (1)$$

If V_{DS} is low, then

$$I_D \cong \mu_{eff} C_{ox}\left(\frac{W}{L}\right)\left((V_{GS} - V_T)V_{DS}\right) \quad (2)$$

$$\left.\frac{\partial I_D}{\partial V_{DS}}\right|_{smallV_{DS}} = \mu_{eff} C_{ox}\left(\frac{W}{L}\right)(V_{GS} - V_T)(3) \quad (3)$$

$$\mu_{eff} = \frac{\left(\partial I_D / \partial V_{DS}\right)\Big| V_{DS}}{C_{OX}\left(\frac{W}{L}\right)(V_{GS} - V_T)} \quad (4)$$

In relation to points (1) to (4), it is important to emphasize that electron mobility is closely linked to changes in drain current, indicating that it is also affected by the electric field. The dual wire (DW) channels in the device increase the electric field strength beneath the gate region. However, the "effective" electron mobility is primarily governed by the source and drain regions. These regions typically exhibit lower electron

mobility due to their high doping concentrations. Additionally, the heterojunction structure at the interface between the source and the channel plays a key role in enhancing mobility.

Figure 3 shows the variations in drain current for both the Conventional DW GAA FET and the Conventional DW GAA NS FET at a temperature of 300K. These are depicted as functions of drain voltage under different V_{GS} conditions. When a drain voltage is applied, it drives charge carriers through the transistor's channel region. As the temperature exceeds room temperature, the diffused drain current increases, resulting in reduced mobility and further degradation of the drift current. As the drain voltage V_{DS} increases, more charge carriers attempt to pass through the narrow channel. However, beyond a certain threshold, the drain current reaches saturation, even as the drain voltage continues to rise. This saturation is due to strain engineering and the heterojunction structure, both of which improve carrier transport efficiency by aiding the movement of additional carriers toward the drain side. Furthermore, the heterojunction structure offers several advantages over homojunctions, such as improved carrier mobility, better bandgap alignment, lower leakage currents, and more effective carrier confinement. The curve clearly shows that the drain current is notably higher for the Conventional DW GAA NS FET compared to the Conventional DW GAA FET, highlighting the advantages of using a heterojunction structure in semiconductor devices.

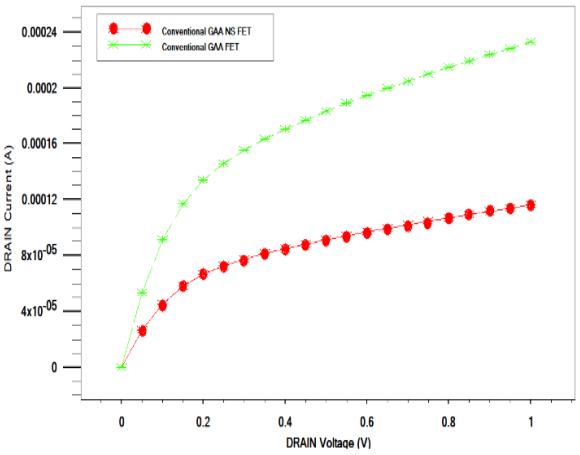

Figure.3: Drain current of the Conventionakl DW GAA NS FET and Conventional DW GAA FET under versus Drain voltage

It is clear that the Conventional DW GAA NS FET delivers a higher ON current and a lower OFF current. The currents in both the ON and OFF states for these structures are shown in Fig. 4. The ratio of $I_{ON}$to $I_{Off}$is an important factor for integrated circuits (ICs) and CMOS technology, particularly for low-power applications that require high-speed performance. The Conventional DW GAA NS FET provides more space at the source-channel interface for carriers to drift when the transistor is in the ON state. This increased carrier velocity in the source region, along with the effective channel width, results in a larger ON current. Additionally, the conduction band offset energy enables electrons to acquire more kinetic energy, further contributing to the higher I_{ON} values.

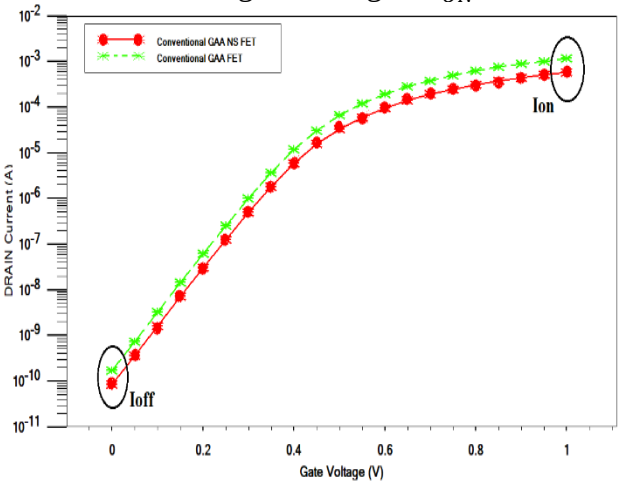

Figure. 4 : Drain current of the Conventional DW GAA NS FET and Conventional DW GAA FET under versus different temperatures on $V_{DS} = 0 \cdot 6V$ in logarithmic scale

Transconductance, denoted as g_m and calculated using the formula $g_m = \partial I_{DS}/\partial V_{GS}$, is directly derived from Fig. 5. We analyze the transconductance $g_m$characteristics of both the Heterojunction DW GAA NS FET and Conventional DW GAA NS FET at varying ∂V_{GS} values, with ∂V_{GS}=0. , taking into account the source-relaxed SiGe/channel-strained Si heterointerface.

As the gate overdrive voltage exceeds 0.25V, a continuous increase in transconductance is observed for both devices, due to the corresponding rise in drain currents. A higher ∂V_{GS} in a device signifies improved transport efficiency within the channel, increased voltage gain for analog applications, and better overall device performance. As shown in Fig. 5, the transconductance of the Conventional DW GAA NS FET structures exceeds that of the conventional devices.

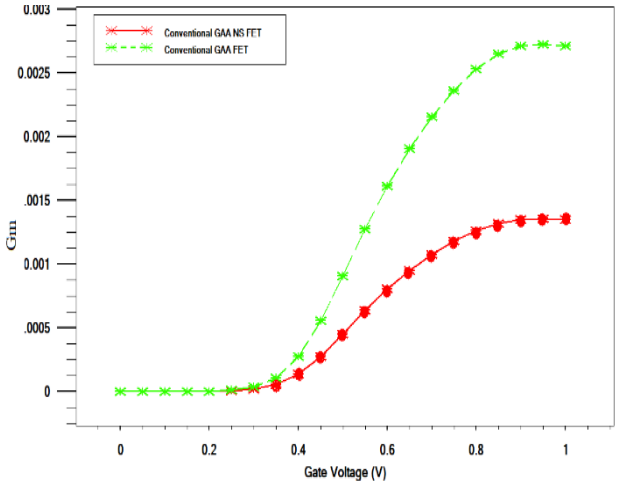

Figure.5: Transconductance (gm) characteristics of the Conventional GAA NS FET and Conventional GAA FET under under versus different temperatures on V_{GS} and $V_{DS} = 0 \cdot 6V$

In Figure 10, both the total gate capacitance (C_{GG}) and gate-source capacitance (C_{GS}) are shown as functions of the gate voltage (V_G). The performance of these devices is significantly influenced by both capacitances, which can be optimized by reducing C_{GG} and C_{GS}. In heterojunction-strained structures, C_{GG} is primarily affected by two factors: lowering the barrier between the source and the channel, and the accumulation of charges at the hetero-interface. As the gate-source voltage (V_{GS}) increases, both C_{GG} and C_{GS} increase, leading to extended propagation delays and reduced circuit performance. Specifically, C_{GS} plays a crucial role in the device's switching characteristics, as it directly influences the speed at which the transistor charges and discharges. This increase in capacitance results in slower switching speeds and higher energy consumption, thus reducing overall performance. Therefore, minimizing both C_{GG} and C_{GS} is key to enhancing device performance, reducing energy loss, and achieving faster switching times.

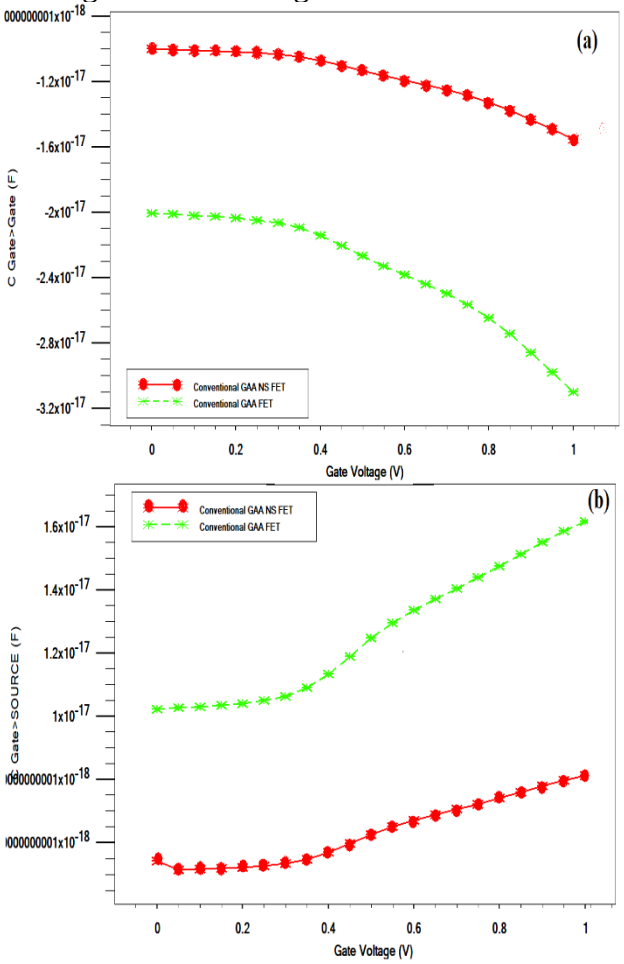

Figure.6: The (a) C_{GS} with ac frequency=1MHz under various V_{GS} and $V_{DS} = 0 \cdot 6V$ (b) The C_{GS} with ac frequency=1MHz under various V_{GS} and $V_{DS} = 0 \cdot 6V$

CONCLUSION

We conducted a comprehensive analysis of various performance parameters for both the Conventional GAA NS FET and the

Conventional GAA FET devices. The study compared the behavior of the Conventional GAA Nanosheet FET with the Conventional GAA FET in both DC and AC modes. By simulating a 3D Gate-All-Around transistor and incorporating dual wires (DW) at the leftmost and rightmost ends of the main channel, we observed enhanced electron depletion in the OFF state. In partial depletion mode, the influence of the electric field from the drain voltage on the electrons was notably reduced. Our findings showed significant improvements in key parameters in the Conventional GAA Nanosheet FET compared to the Conventional GAA FET. Specifically, the ON-state current in the Heterojunction structures was approximately 15% higher than that in the Conventional GAA FET across a range of 300K temperatures. In conclusion, our analysis demonstrated superior performance characteristics of the Conventional GAA NS FET over the Conventional GAA FET.

REFERENCES

Sreenivasulu VB, Narendar V (2021) Performance improvement of spacer engineered n-type SOI FinFET at 3-nm gate length. AEU - International Journal of Electronics and Communications 137:153803

K. Baral, P.K. Singh, S. Kumar, S. Chander, S. Jit, Ultrathin body nanowire hetero dielectric stacked asymmetric halo doped junctionless accumulation mode MOSFET for enhanced electrical characteristics and negative bias stability, Superlattice. Microst. 138 (2019), doi: https:// doi. org/ 10. 1016/j. spmi. 2019. 106364

Kumar B, Chaujar R (2021) Numerical Study of JAM-GS-GAA FinFET: A Fin Aspect Ratio Optimization for Upgraded Analog and Intermodulation Distortion Performance. Silicon. https:// doi. org/ 10. 1007/ s12633-021- 01395-8

Sreenivasulu V. B, Narendar V. Design and Temperature Assessment of Junctionless Nanosheet FET for Nanoscale Applications. Springer Nature B.V. 2021. https://doi.org/10.1007/s12633-021-01145-w

Roy Barman K, Baishya S (2019) Performance analysis of vertical super-thin body (VSTB) FET and its characteristics in presence of noise. Appl. Phys. A 125:401. https:// doi. org/ 10. 1007/s00339- 019- 2682-x

Yogesh Pratap, Subhasis Haldar, R.S. Gupta, Mridula Gupta, Performance evaluation and reliability issues of junctionless CSG MOSFET for RFIC design, IEEE Trans. Electron Devices 60 (2013) 418–425.

R.K. Sharma, R. Gupta, R.S. Gupta, M. Gupta, Dual-material double-gate SOI n-MOSFET: gate misalignment analysis, IEEE Trans. Electron Devices 56 (2009) 1284–1291.

R.Y. Yan, A. Ourmazd, K.F. Lee, Scaling the Si MOSFET: from bulk to SOI to bulk, IEEE Trans. Electron Devices 39 (1992) 1704–1710.

K. Shzuki, T. Tanaka, Y. Tosaka, H. Horie, Y. Arimoto, Scaling theory for doublegate SOI MOSFETs, IEEE Trans. Electron Devices 40 (1993) 2326–2329.

Santosh Kumar Gupta, Threshold voltage model of junctionless cylindrical surrounding gate MOSFET including fringing field effect, Superlattices Microstruct. 88 (2015) 188–197.

Abbasnezhad R, et al. (2023). Electrical performance estimation and comparative study of heterojunction strained and conventional gate all around nanosheet field effect transistors. Journal of Electrical Engineering. 74. 503-512. 10.2478/jee-2023-0058.

T. Ohno, Y. Kado, M. Harada, T. Tsuchiya, IEEE Transaction on Electron Devices 42 (1995) 1481–1486.

Bhol K, Nanda U (2021) Nanowire Array-based MOSFET for Future CMOS Technology to Attain the Ultimate Scaling Limit. Silicon. https://doi.org/10.1007/s12633-020-00909-0

Ryu D, Kim M, Kim S, Choi Y, Yu J, Lee J-H, Parket B-G (2020) Design and optimization of triple-k spacer structure in two-stack Nanosheet FET from OFF-state leakage perspective. IEEE Trans Electron Devices. 67:1317–1322. https://doi.org/10.1109/TED.2020.2969445

Shukla AK, Nandi A, Dasgupta S (2020) Modeling source/drain lateral Gaussian doping profile of DG-MOSFET using green's function approach. Solid State Electron 171:107866. https://doi.org/10.1016/j.sse.2020.107866.

A. Chaudhry, M.J. Kumar, Controlling short-channel effects in deep-submicron SOI MOSFETs for improved reliability: a review, IEEE Trans. Device Mater. Reliab. 4 (1) (2004) 99–109. DOI: 10.1109/TDMR.2004.824359

Atlas User Manual, Device Simulation Software; 2011

Richter A, Glunz S W, Werner F, Schmidt J, Cuevas A (2012) Improved quantitative description of Auger Recombination in crystalline silicon. Physical Review B. 86, 165202.

Dynamic Longitudinal Conductivity of a Magnetic Two-Dimensional Electron with Rashba Spin-orbit coupling in the Presence of Electron-Electron Interaction

M. Mir[1]*

[1]*Department of Physics, University of Zabol (UOZ), Zabol 98615-538, Iran*

**Corresponding author: moslem.mir@uoz.ac.ir*

Abstract— We investigate the effects of the electron-electron interaction on the intrinsic longitudinal conductivity in a magnetic two-dimensional electron gas with Rashba spin-orbit coupling. The breakdown of Galilean invariance in this system enhances the effects of electron-electron interaction. In the clean system or high-frequency limit, the longitudinal conductivity is obtained in terms of the spin-spin response functions. Here, we considered the electron-electron interaction effects within the Hubbard approximation for the local field factor, which is beyond the random phase approximation, then obtained the intrinsic longitudinal conductivity. We show that the intrinsic longitudinal conductivity increases with increasing interaction strength in two-band regimes.

Keyword: Longitudinal Conductivity, linear response theory, random phase approximation, Hubbard approximation

INTRODUCTION

In this article, our aim is to examine the effects of electron-electron interaction on the intrinsic longitudinal dynamic conductivity in a two-dimensional magnetic electron gas with Rashba spin-orbit interaction. The electron-electron interaction is considered beyond the random phase approximation, within the Hubbard approximation for the local field factor. In the clean limit or at high frequencies, the intrinsic longitudinal conductivity, as well as the intrinsic anomalous Hall and spin Hall conductivities, are expressed in terms of interacting spin-spin response functions[1,2].

Hamiltonian and the linear spin-density response functions of a two-dimensional magnetic electron gas with Rashba spin-orbit coupling

Consider a two-dimensional electron gas with Rashba spin-orbit coupling in the presence of a perpendicular exchange field. Additionally, assume that the electrons interact with each other via Coulomb interaction. The Hamiltonian for this system is provided in reference [1]. The effective interaction in the Hubbard approximation for systems with spin-orbit interaction is given by [1].

$$W_{\alpha\beta}(q) = v(q)\delta_{\alpha,0}\delta_{\beta,0} - \frac{1}{2}v_H(q)\delta_{\alpha,\beta} \quad (1)$$

The screened Coulomb potential in the long-wavelength limit is considered as $v_H(q) = v(\sqrt{k_F^2 + q^2}) \approx U$. In the Hubbard approximation, the non-zero elements of the spin-density response function matrix associated with the longitudinal conductivity are given by [1,2].

$$\chi_{xx}(\omega) = \frac{\left[1 + \frac{U}{2}\chi^0_{yy}(\omega)\right]\chi^0_{yy}(\omega) + \frac{U}{2}\left[\chi^0_{yy}(\omega)\right]^2}{\Gamma(U,\omega)} \quad (2)$$

Where

$$\Gamma(U,\omega) = \left[1 + \frac{U}{2}\chi^0_{yy}(\omega)\right]^2 + \left[\frac{U}{2}\chi^0_{xy}(\omega)\right]^2$$

Where χ_{AB} are obtained from the linear retarded response function relation [1,2]. The non-interacting spin-spin response function in the two-band regime has been derived in reference [1].

LONGITUDINAL CONDUCTIVITY

Longitudinal conductivity refers to the electric current generated in response to a homogeneous electric field. Consider a two-dimensional system in the xy-plane. If an electric field E is applied along the x-axis, the x-component of the particle current (j_x) can be obtained from the following relations.

$$j_x(\omega) = \sigma_{xx}(\omega)E_x(\omega) \quad (3)$$

In the above equation, $\sigma_{xx}(\omega)$ is the dynamic longitudinal Hall conductivity, and its value is obtained from the following relation [1].

$$\sigma_{xx}(\omega) = \frac{i\, e^2 \alpha_R^2}{\omega}\, \chi_{\mathrm{xx}}(\omega) \qquad (4)$$

$\chi_{\mathrm{xx}}(\omega)$ is, in general, the interacting spin-spin response function with the, as given in Eq. (2). To obtain the non-interacting longitudinal conductivity, we substitute the non-interacting spin-spin response functions into Eq. (4).

RESULTS

In this section, we calculate the intrinsic dynamic longitudinal conductivity in the two-band regime. By substituting the interacting response function $\chi_{xx}(\omega)$ into equation (4), the intrinsic dynamic longitudinal conductivity is given by:

$$\sigma_{xx}(\omega)\left[\frac{e^2}{2\,\pi}\right] = \frac{i}{\bar{\omega}} \frac{\left[-1+u\left(1+\frac{\bar{\omega}^2+4}{8\omega\bar{\alpha}}\mathrm{L}(\bar{\omega})\right)\right]\left(1+\frac{\bar{\omega}^2+4}{8\omega\bar{\alpha}}\mathrm{L}(\bar{\omega})\right)}{\left[1-\frac{u}{2}\left(1+\frac{\bar{\omega}^2+4}{8\omega\bar{\alpha}}\mathrm{L}(\bar{\omega})\right)\right]^2 - \frac{u^2}{4\bar{\alpha}^2}[\mathrm{L}(\bar{\omega})]^2} \qquad (5)$$

Where the real part of the intrinsic dynamic longitudinal conductivity is plotted in Figure 1.

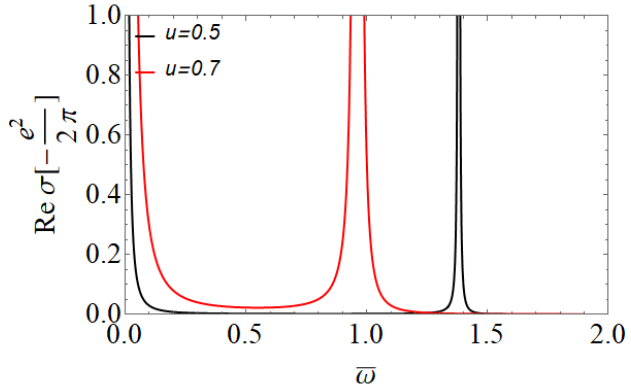

Fig. 1 Intrinsic dynamic longitudinal conductivity for the dimensionless spin-orbit interaction $\bar{\alpha} = (m\alpha_R^2/\Delta) = 0.4$ and dimensionless Fermi energy $\bar{\varepsilon}_F$ (two-band regime) for different values of u.

CONCLUSION

In this article, we studied the intrinsic dynamic longitudinal conductivity in a two-dimensional magnetic electron gas with Rashba spin-orbit coupling. We showed that an increase in electron-electron interaction leads to an increase in the real part of the intrinsic dynamic longitudinal conductivity in the two-band regime. Additionally, we demonstrated that the real part of the intrinsic dynamic longitudinal conductivity at non-zero frequencies exhibits a peak, and this peak shifts towards lower frequencies for stronger electron-electron interactions

REFERENCES

Mir, M., & Abedinpour, S. H. (2022). Many-body correction to the intrinsic anomalous and spin Hall conductivities. Phys. Rev. B 106, L2011021-5. https://doi.org/10.1103/PhysRevB.106.L201102

Mir, M., & Abedinpour, S. H. (2017). Coupled spin-charge dynamics in helical Fermi liquids beyond the random phase approximation.Phys. Rev. B 96, 245110. https://doi.org/10.1103/PhysRevB.96.245110

Revolutionizing Biological Network Modeling: Quantum Computing Applications in Metabolic Pathways, Genetic Mutations, and Molecular Interactions

Mohammadalizadeh rami.S[1]

[1]*Animal Biology Faculty, Tabriz University, Tabriz,Iran*

**Corresponding author: sanaalizadehrami@gmail.com*

Abstract- Biological networks, such as complex metabolic and cellular signaling pathways, are fundamental for understanding molecular interactions and advancing fields like personalized medicine, biotechnology, and drug discovery. However, the dynamic and nonlinear nature of these networks presents significant challenges for conventional modeling techniques. Quantum computing, leveraging principles like superposition and entanglement, offers a transformative approach to overcoming these limitations. By employing quantum algorithms such as Hamiltonian simulation and Grover's search, quantum tools facilitate precise modeling of molecular interactions, metabolic pathways, and genetic mutation effects. This study explores quantum platforms, including Qiskit and D-Wave Ocean SDK, alongside a comprehensive review of research spanning 1995 to 2020 and data from the Protein Data Bank (PDB). Applications investigated encompass mutation impact prediction, protein-ligand interaction studies, and optimization of metabolic pathways. These quantum-based methods hold promise for deeper insights into cellular processes, accelerated drug development, and enhanced efficiency of biological systems. Despite challenges such as algorithmic complexity, computational demands, and hardware limitations, advances in hybrid quantum-classical frameworks and emerging technologies offer a path forward. With its capacity for high-precision simulations and groundbreaking insights, quantum computing is poised to redefine the fields of biology and biochemistry, paving the way for novel scientific breakthroughs.

Keywords: Quantum computing, Quantum methods, Biology networks

INTRODUCTION

Biological networks comprise a complex set of metabolic and cellular signaling pathways regulating molecular interactions at various biological levels. In fundamental biological research, a thorough grasp of these networks is necessary for applied domains including drug development, biotechnology, and personalized medicine [1**]**. Although these systems are complex in terms of their time-dependent dynamic behaviors and the abundance of variables and nonlinear interactions, they have become powerful computational tools today due to their speed of operation. Quantum computing, which takes advantage of quantum mechanical concepts like superposition and entanglement. This technology could simulate molecular interactions at the atomic level and analyze the dynamic behaviors of biological pathways with unprecedented precision [2, 3]. It is based on quantum algorithms such as Hamiltonian simulation and quantum Graver's algorithm is used to solve optimization problems and analyze complex biological networks.

Quantum computer modeling of biological networks can be used to optimize biological pathways for creating biological products, identify important locations in molecular interactions, and predict the impact of mutations [4, 5]. This article examines the perspective of that subject and evaluates the challenges and potential applications of quantum techniques in biological network modeling.

METHODOLOGY

TOOLS AND DATA SOURCES

- Research papers published between 1995 and 2020 in reputable journals.
- Quantum simulation platforms, such as Qiskit and D-Wave Ocean SDK.
- Structural data from databases, such as the Protein Data Bank (PDB), for analyzing biological interactions.

This study is designed as an analytical-conceptual investigation into the role of quantum tools in modeling biological networks. The methodology includes the following steps:

A Comprehensive Analysis of Scientific Research

A review was conducted of several research works and articles about quantum tools in biology and biochemistry networks. This review used scholarly databases like PubMed, Web of Science, and Google Scholar:

Biological systems are simulated in quantum mechanics.

The application of quantum algorithms to the resolution of intricate biological issues.

Using quantum computers to examine genetic mutations' consequences and molecular interactions.

The chosen articles were assessed according to their impact on biological modeling, inventiveness, and relevance.

Quantum Algorithm Conceptual Analysis

At this point, a conceptual examination of important quantum algorithms was conducted. Among these were:

Hamiltonian simulation, which models biological systems' atomic-level behavior.

Grover's algorithm: Solving optimization problems in biological networks.

Quantum-classical hybrid algorithms: Combining quantum and classical computing for modeling.

Each algorithm's advantages and disadvantages in examining molecular interactions, biological processes, and the consequences of genetic mutations were analyzed.

INVESTIGATION OF CURRENT QUANTUM TOOLS AND SIMULATIONS

Practical examples of quantum technologies used in previous investigations were studied, including:

a. IBM Quantum Experience.
b. Google Sycamore.
c. D-Wave systems.

These studies demonstrated how quantum tools are currently applied in analyzing biological networks.

Applied Analysis in Biological Networks

To gain a deeper understanding of quantum computing applications, several applied examples in metabolic pathways and cell signaling were selected and analyzed:

Analysis of the glycolysis pathway as a complex metabolic pathway.

Investigation of protein-ligand interactions in signaling pathways.

For these analyses, quantum modeling methods were reviewed, and their advantages and disadvantages were noted.

Analysis of Challenges and Opportunities

Challenges in using quantum tools for modeling biological networks were identified, including hardware limitations, computational costs, and algorithm complexity. Simultaneously, potential improvements in these areas were explored.

Updated Tools and Data Sources

Scientific articles published in reputable journals between 2015 and 2024.

Quantum simulation platforms, such as Qiskit and D-Wave Ocean SDK.

Structural data from databases, such as the Protein Data Bank (PDB), for analyzing biological interactions.

RESULTS

This approach has made it possible to thoroughly and methodically investigate the potential and constraints of quantum tools for biological network modeling. It has also made it possible to determine potential avenues for future study in this field.

1. Highly accurate simulation of biological processes

Although it can be challenging to study complex biological reactions with conventional methods, quantum technologies have made it possible to simulate them. Simulations on metabolic pathways such as glycolysis demonstrate that these methods can identify the smallest changes in system properties. This capacity can be used to improve metabolic pathways for the synthesis of biological substances and predict cellular responses to environmental alterations [2, 3].

2. Accurate modeling of molecular interactions

Using quantum algorithms, the structure and stability of biological complexes such as protein-ligand have been analyzed with atomic precision. These modelings have increased the ability to identify key interaction sites and critical points in cell signaling networks, enabling targeted drug development [6].

3. Estimating the consequences of genetic alterations

The potential of quantum techniques to accurately forecast mutation-induced alterations has been demonstrated through modeling genetic mutations and their effects on protein structure and metabolic pathway activity. Finding mutations linked to disease and creating efficient treatments are two areas in which this skill is especially helpful [1, 5].

4. Optimizing mechanisms in biology

Quantum simulations of constructed biological pathways, including those that produce ethanol or particular amino acids, have demonstrated that by carefully adjusting the system parameters, the efficiency of these routes may be greatly boosted. These accomplishments have a direct bearing on the biotechnology sector [7, 8].

CHALLENGES

Despite significant advances, there are limitations such as the small number of qubits available in current hardware and the high complexity of the algorithms. However, the development of hybrid methods and hardware improvements can overcome these challenges [8].

DISCUSSION

Quantum Tools' Significance in Biochemistry Because of their special ability to mimic complex systems, quantum computers have completely changed our understanding of biological systems. It enables a more thorough and accurate examination of systems than classical computing techniques, which necessitate large approximations for modeling [9] . The drug development process can be accelerated by employing these technologies to anticipate molecular interactions and model biological pathways. Also, the simulation of genetic mutations has a special application for identifying genetic diseases and targeted therapies. These tools also enable the design of more efficient biological pathways for the production of valuable compounds in bioengineering [10] .

CHALLENGES AND LIMITAIONS

Quantum technologies are still in their early stages of development, and hardware limitations, such as the need for very low temperatures for operation and the limited number of qubits, prevent the simulation of very large biological systems. Also, the development of suitable algorithms for modeling these systems requires further research. However, recent advances in the development of quantum computers are

promising and could reduce these limitations [11, 12].

Prospects In the future, the use of hybrid quantum-classical methods and improved hardware could expand the applications of quantum tools in biochemistry. Also, combining machine learning with quantum computing could help discover new relationships in biological networks.

CONCLUSION

Biological networks can be accurately and thoroughly modeled thanks to the special opportunities presented by quantum technology. Significant developments in biology and biochemistry may result from these tools' exceptional accuracy in modeling biological events, forecasting molecular interactions, evaluating the consequences of genetic mutations, and streamlining biological pathways. Notwithstanding the current obstacles, advancements in hardware and algorithms will clear the way for the wide-ranging use of these tools in the biological sciences in the future. Leveraging these technologies can help design more efficient biological processes, discover new medications, and get a deeper understanding of biological systems.

REFERENCES

1. Barabasi AL, Oltvai ZN. Network biology: understanding the cell's functional organization. Nat Rev Genet. 2004;5(2):101-13.
2. Aspuru-Guzik A, Dutoi AD, Love PJ, Head-Gordon M. Simulated quantum computation of molecular energies. Science. 2005;309(5741):1704-7.
3. Cao Y, Romero J, Olson JP, Degroote M, Johnson PD, Kieferova M, et al. Quantum Chemistry in the Age of Quantum Computing. Chem Rev. 2019;119(19):10856-915.
4. Grover LK. A fast quantum mechanical algorithm for database search. Computer Science. 1996.
5. Perdomo-Ortiz A, Benedetti M, Realpe-Gómez J, Biswas R. Opportunities and challenges for quantum-assisted machine learning in near-term quantum computers. Quantum Science and Technology. 2018;3(3):030502.
6. Kandala A, Mezzacapo A, Temme K, Takita M, Brink M, Chow JM, Gambetta JM. Hardware-efficient variational quantum eigensolver for small molecules and quantum magnets. Nature. 2017;549(7671):242-6.
7. J. Romero JO, Alán Aspuru-Guzik. Quantum autoencoders for efficient compression of quantum data. Quantum Science and Technology, 2016.
8. Preskill J. Quantum Computing in the NISQ era and beyond. Quantum. 2018.
9. Arute F, Arya K, Babbush R, Bacon D, Bardin JC, Barends R, et al. Quantum supremacy using a programmable superconducting processor. Nature. 2019;574(7779):505-10.
10. Nielsen MA CI. Quantum Computation and Quantum Information. Cambridge University Press. 2010.
11. Zurek WH. Decoherence, einselection, and the quantum origins of the classical. REVIEWS OF MODERN PHYSICS. 2003;75.
12. Biamonte J, Wittek P, Pancotti N, Rebentrost P, Wiebe N, Lloyd S. Quantum machine learning. Nature. 2017;549(7671):195-202.

2.6. MEDICAL ENGINEERING

Nanobiosensors as a Revolutionizing Technique for Diagnosing Parasitic Infection Diseases

Soheil Sadr[1], Shakiba Nazemian[1], Alireza Sazmand[2], Cinzia Santucciu[3], Abbas Rahdar[4], Sadanand Pandey[5] and Hassan Borji[1*]

[1]*Department of Pathobiology, Faculty of Veterinary Medicine, Ferdowsi University of Mashhad, Mashhad, Iran.*

[2]*Department of Pathobiology, Faculty of Veterinary Medicine, Bu-Ali Sina University, Hamedan 6517658978, Iran*

[3]*WOAH and NRL for Echinococcosis, Animal Health, Istituto Zooprofilattico Sperimentale della Sardegna, Sassari, Italy*

[4]*Department of Physics, University of Zabol, Zabol, Iran.*

[5]*Department of Chemistry, College of Natural Science, Yeungnam University, 280 Daehak-Ro, Gyeongsan 38541,*

**Corresponding author: hborji@um.ac.ir*

Abstract- Parasitic infections, including malaria, hydatid cysts, leishmaniasis, and schistosomiasis, remain a significant cause of mortality and morbidity worldwide. In addition to their severe public health impacts, parasitic diseases impose a heavy economic burden on health systems. Control and treatment of zoonotic parasitic infections depend mainly on early and accurate diagnosis. Traditional diagnostic techniques, such as microscopic examinations, immunological methods, such as enzyme-linked immunosorbent assay (ELISA), and molecular tests, such as polymerase chain reaction (PCR), are standard tools for parasite identification. However, these methods are time-consuming and expensive and rely on sophisticated equipment; however, their application has many challenges. Nanobiosensors are novel devices that use nanotechnology and biology to provide new approaches for rapid and accurate diagnosing techniques, and they can detect many biomarkers. Hence, the current review aims to introduce nanobiosensors and their types and review their specific applications in diagnosing parasitic diseases. These sensors use the unique properties of nanomaterials to detect parasite biomarkers with high sensitivity and accuracy. Nanobiosensors can directly detect parasites or their metabolic products, enabling early disease detection. In conclusion, nanobiosensors could be essential in controlling and eradicating parasitic diseases.

Keywords: Nanotechnology, Nanobiosensors, Parasites, Helminth, Protozoa

INTRODUCTION

Parasitic diseases, such as malaria, cystic echinococcosis (CE), leishmaniasis, and schistosomiasis, remain a significant cause of mortality and morbidity worldwide. In addition to their severe public health impacts, parasitic diseases impose a heavy economic burden on health systems. Control and treatment of parasitic diseases depend mainly on early and accurate diagnosis [1].

Traditional diagnostic techniques, such as microscopic examinations, immunological methods, such as enzyme-linked immunosorbent assay (ELISA), and molecular tests, such as polymerase chain reaction (PCR), are standard diagnostic tools for parasite identification. However, these methods are time-consuming, expensive, and require sophisticated equipment. Furthermore, in many resource-limited settings, such tools are difficult to access [2].

Nanobiosensors are novel devices that combine nanotechnology and biology to provide new approaches for rapid and accurate disease diagnosis. They use the unique properties of nanomaterials to detect parasite biomarkers with high diagnostic and analytical performances, such as sensitivity, specificity, and accuracy [3]. Nanobiosensors can also be used to detect parasites or their metabolic products directly. Hence, the current review aims to introduce nanobiosensors and their tools and review their specific applications in diagnosing parasitic diseases [4].

NANOBIOSENSORS

Nanobiosensors are advanced devices that combine nanomaterials and biological elements such as antibodies, DNA, and enzymes to detect specific molecules such as proteins, parasite DNA, and other biomarkers [5]. Nanobiosensors operate in three main

steps: first, the target molecule is recognized by the biological element, then the signal produced is amplified using nanomaterials, and finally, the signal is converted into a measurable output.

The most important types of nanobiosensors include electrochemical, optical, and magnetic sensors [6]. Electrochemical nanobiosensors measure electrical changes resulting from the interaction of the target molecule with the biological element and use gold nanoparticles and carbon nanotubes to increase sensitivity [7]. In contrast, optical nanobiosensors take advantage of changes in optical properties such as absorption and fluorescence, and quantum dots and metal nanoparticles play a crucial role in this technology [8]. Magnetic nanobiosensors are also designed based on the magnetic properties of nanomaterials and are used to detect molecules at very low concentrations.

APPLICATION

Nanobiosensors have provided new opportunities for the early detection of parasitic diseases. Nanobiosensors have numerous applications in diagnosing parasitic diseases and can provide a novel and accurate solution for rapidly identifying parasites. For example, in malaria, researchers developed gold nanobiosensors and specific antibodies to detect surface proteins of *Plasmodium falciparum* accurately [9]. Regarding CE, electrochemical nanobiosensors sensitive to the parasite's DNA have detected the genetic material of *Echinococcus granulosus* in body fluids [10]. Moreover, optical nanobiosensors using quantum dots detect *Leishmania*-specific antigens with high sensitivity in leishmaniasis [11]. In schistosomiasis, magnetic nanobiosensors have also been successfully used to detect *Schistosoma* antigens in blood and urine samples, improving the accuracy and speed of diagnosis [12].

CONCLUSION

Nanobiosensors are revolutionary tools for rapid and accurate detection of parasitic diseases. Nanobiosensors, using advanced nanomaterials and biological elements, have increased the sensitivity and accuracy of diagnostic methods. Although nanobiosensors are promising, further research on cost, safety, and feasibility for widespread use in global health systems is needed. In the future, nanobiosensors could be an essential support in controlling and eradicating parasitic diseases.

ACKNOWLEDGMENT

Conceptualization: Abbas Rahdar, Sadanand Pandey, Hassan Borji; Methodology: All Authors; Writing - original draft preparation: All Authors; Writing - review and editing: Soheil Sadr, Alireza Sazmand, Cinzia Santucciu; Supervision: Hassan Borji. We thank the Ferdowsi University of Mashhad Research Deputy for their support.

REFERENCES

Dhahi TS, Dafhalla AKY, Saad SA, Zayan DMI, Ahmed AET, Elobaid ME, et al. The importance, benefits, and future of nanobiosensors for infectious diseases. Biotechnology and Applied Biochemistry. 2024;71(2):429-45.

El-Abeid SE, Mosa MA, Boudaden J, Ibrahim DS, Attia EM, Shaban WM, et al. Nanobiosensors: A powerful Technology for Early Detection of Plant Parasitic Nematodes. Sensing and Imaging. 2024;25(1):23.

Sadr S, Lotfalizadeh N, Abbasi AM, Soleymani N, Hajjafari A, Roohbaksh Amooli Moghadam E, et al. Challenges and prospective of enhancing hydatid cyst chemotherapy by nanotechnology and the future of nanobiosensors for diagnosis. Tropical

medicine and infectious disease. 2023;8(11):494.

Anand A, Sharma A. Potential applications of nanotechnology in management of parasitic diseases. Nanosensors in Healthcare Diagnostics: Elsevier; 2025. p. 321-54.

Kerry RG, Ukhurebor KE, Kumari S, Maurya GK, Patra S, Panigrahi B, et al. A comprehensive review on the applications of nano-biosensor-based approaches for non-communicable and communicable disease detection. Biomaterials Science. 2021;9(10):3576-602.

Noah NM, Ndangili PM. Current trends of nanobiosensors for point‐of‐care diagnostics. Journal of Analytical Methods in Chemistry. 2019;2019(1):2179718.

Huang X, Zhu Y, Kianfar E. Nano biosensors: properties, applications and electrochemical techniques. Journal of Materials Research and Technology. 2021;12:1649-72.

Rather SA, Mustafa RA, Ashraf MV, Hannan Khan M, Ahmad S, Wani ZA. Implications of Nano-Biosensors in the Early Detection of Neuroparasitic Diseases. Theranostic Applications of Nanotechnology in Neurological Disorders: Springer; 2024. p. 43-83.

Krampa FD, Aniweh Y, Kanyong P, Awandare GA. Recent advances in the development of biosensors for malaria diagnosis. Sensors. 2020;20(3):799.

Hajjafari A, Sadr S, Santucciu C, Masala G, Bayat M, Lotfalizadeh N, et al. Advances in Detecting Cystic Echinococcosis in Intermediate Hosts and New Diagnostic Tools: A Literature Review. Veterinary Sciences. 2024;11(6):227.

Jain S, Santana W, Dolabella SS, Santos AL, Souto EB, Severino P. Are Nanobiosensors an improved solution for diagnosis of leishmania? Pharmaceutics. 2021;13(4):491.

Qadeer A, Ullah H, Sohail M, Safi SZ, Rahim A, Saleh TA, et al. Potential application of nanotechnology in the treatment, diagnosis, and prevention of schistosomiasis. Frontiers in Bioengineering and Biotechnology. 2022;10:1013354.

2.7. CLEAN AND RENEWABLE ENERGIES

Construction of Flexible Supercapacitors from Metal Organic Framework Composite Electrode

S. Ramandi[1*], M.H. Entezari2

[1,2] *Sonochemical Research Center, Department of Chemistry, Faculty of Science, Ferdowsi University of Mashhad, 91779 Mashhad, Iran*

**Corresponding author: s_ramandi_01@yahoo.com*

Abstract— Nowadays, constructing hetero-structure materials is an efficacious procedure to uplift the electrochemical performance of layered double hydroxide (LDH) materials. The logical design of such elegant nanostructures is still challenging. Herein, NiCo-LDH nanosheets derived from Co-ZIF grown on graphene/polyaniline (G/PANI)@cotton cloth (CC) was synthesized by a facile and novel two-step strategy for supercapacitors. The electrode material exhibited areal specific capacitance of 88.15 mF cm^{-2} at a current of 0.3 mA. Long-term stability test demonstrates that 84.05 % of the original capacitance remains after 10,000 cycles at the current density of 0.2 mA cm^{-2}. The results indicate that NiCo-LDH/G/PANI@CC will be an appropriate candidate for high-performance supercapacitors. The NiCo-LDH/G/PANI@CC//NiCo-LDH/G/PANI@CC flexible solid-state supercapacitor was assembled with the PVA/KOH gel electrolyte.

Keyword: Cotton cloth, NiCo-LDH, supercapacitor, specific capacitance

INTRODUCTION

In recent years, flexible and wearable electronic devices such as electronic sensors, health monitors, flexible displays, and portable, wearable energy storage devices have become a remarkable technological procedure and proliferated. To achieve quite flexible and wear able electronics, suitable flexible devices are required with features including tiny volume, lightweight, and good electrochemical performances, such as flexible supercapacitors (SCs) [1-3].

EXPERIMENTAL & RESULTS

Herein, the superiorities of G, PANI, and NiCo-LDH were used for synthesizing composite containing proper electrochemical properties. Firstly, G and PANI were loaded on cotton fabric using a simple chemical bath deposition (CBD) method. As PANI and G deposited on CC, a better compound formed between them, which assist the electron transportation during the charge/discharge process. The NiCo-LDH nanosheets improve the stableness of the structure and further enhance electrochemical active sites. Besides, this approach is low-cost, simple, and environmentally friendly.

To investigate the structural properties of the samples, the CC, G/ PANI@CC, and NiCo-LDH/G/PANI@CC were first analyzed by FESEM. Fig. 1a displays that the pristine CC has a 3D fibrous configuration with relatively smooth surface. After deposition of G/PANI on CC, the fiber surface became rough due to the presence of G sheets and PANI, as shown in Fig. 1b. It found out that PANI was pasted entirely to G, when the CC was immersed into the polymerization reaction solution of aniline in an ice bath. In the second step, the NiCo-LDH nanosheets were grown on the surface of the as-prepared G/PANI@CC hybrid in which dense NiCo-LDH nanosheets self-assemble on G and PANI from a top view (Fig. 1c, d). Such heterostructure could increase ions/ electrons transportation.

Fig. 2 exhibits the calculated specific capacitances (C_s) versus different current of the G/PANI@CC and NiCo-LDH/G/PANI@CC electrodes. The NiCo-LDH/G/PANI@CC electrode has the highest C_s of 88.15 mF cm^{-2} at 0.075 mA cm^{-2} current density, which is more than that of G/PANI@CC (38.70 mF cm^{-2} at 0.075 mA cm^{-2} current density).

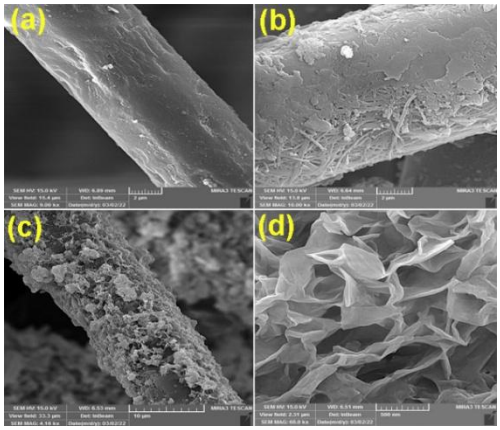

Fig. 4 FESEM images of the (a) CC, (b) G/PANI@CC, (c, d) NiCo-LDH/G/PANI@CC

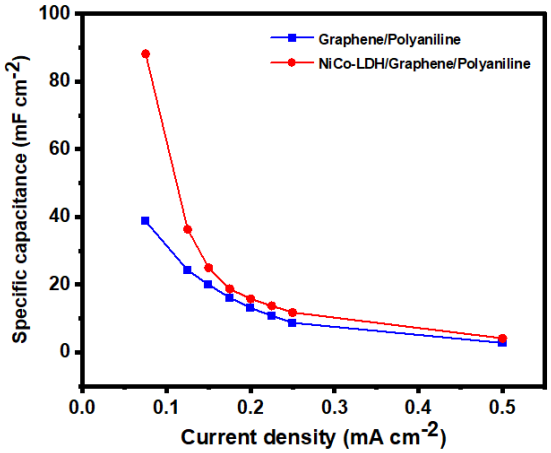

Fig. 5 Specific capacitance of the G/PANI and NiCo-LDH/G/PANI at different current densities

The energy density and power density of the SC were computed and plotted on the Ragone plot (Fig. 3). The as-manufactured device can render a maximum energy density of 0.082 mWh cm^{-3} at a power density of 11.35 mW cm^{-3}, and still retains 0.050 mWh cm^{-3} at a high power density of 18 mW cm^{3}.

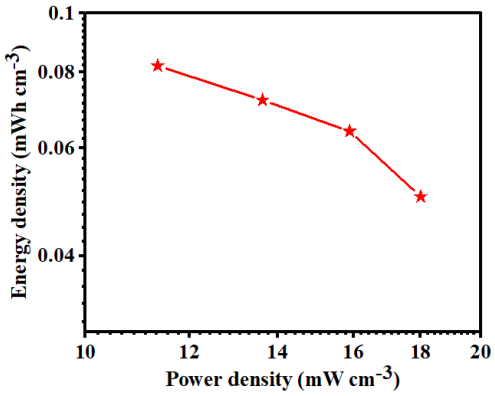

Fig. ۳ Ragone plot of flexible solid-state supercapacitors

ACKNOWLEDGEMENTS

This work was supported by Ferdowsi University of Mashhad (Code No. 3/52786) and Iran National Science Foundation: INSF (Code No. 99022290).

REFERENCES

Huang, Q., Wang, D., & Zheng, Z. (2016). Textile-based electrochemical energy storage devices. Advanced Energy Materials. 6, 1600783. https://doi.org/10.1002/aenm.201600813

Tang, J., Yuan, P., Cai, C., Fu, Y., & Ma, X. (2016). Combining nature-inspired, graphene-wrapped flexible electrodes with nanocomposite polymer electrolyte for asymmetric capacitive energy storage, Advanced Energy Materials. 6, 1600813. https://doi.org/10.1002/aenm.201600813

Yun, T.G., Park, M., Kim, D.-H., Kim, D., Cheong, J.Y., Bae, J.G., Han, S.M., & Kim, I.-D. (2019). All-transparent stretchable electrochromic supercapacitor wearable patch device. ACS Nano. 13, 3141–3150. https://doi.org/10.1021/acsnano.8b08560

Control Strategy Based on a Maximum Power Point Tracking Control or a Constant Power Generation Control

Mohammadreza Mohammadiyan Asiabar[1*]

[1]*Department of Electrical Engineering, Islamic Azad University, Karaj Branch*

**Corresponding author: mohammadrezamohammadiyan28@yahoo.com*

Abstract— In this paper, a hybrid power control concept for grid-connected photovoltaic (PV) inverters is proposed. The control strategy is based on a maximum power point tracking control or a constant power generation (CPG) control depending on the instantaneous power available from the PV panels. A case study on a single-phase PV inverter under annual operation is presented by analyzing thermal load, lifetime, and annual energy efficiency. and also confirmed the feasibility and effectiveness of the proposed control concept.

Keyword: maximum power point tracking, reliability, photovoltaic.

INTRODUCTION

Maximum power point tracking (MPPT) is effective for photovoltaic (PV) inverters to maximize the energy harvested from PV panels [1]. However, with increasing installations of PV systems into the grid, the following issues appear if the inverters keep operation at MPPT mode even within the rated power range: 1) overloading of the grid at peak power generation [2] which may induce system level over voltage and line frequency instability [3]; The proposed Maximum power point tracking-constant power generation control concept allows a reduction of required power ratings of PV inverters and also a reduction of junction temperature peaks and variations on the power devices (i.e., an extended lifetime [4], [5], [6]). Meanwhile, it could contribute to the system level power management to some extent, due to its role in smoothing and limiting the power fed into the grid. The concept, implementation, feasibility and effectiveness of the control strategy are discussed below.

PROPOSED HYBRID POWER CONTROL CONCEPT

The single-phase two-stage configuration is preferable for residential PV applications [1]. The control structure of a two-stage single-phase PV system with the proposed control concept is shown in Fig. 1, which indicates that the hybrid control strategy is implemented in the control of the boost stage. As the available PV power is weather-dependent, the operation modes will alter accordingly with the solar irradiance and ambient temperature. Fig. 2 exemplifies different operation regions for a single-phase PV system during a day with the proposed control strategy. According to Figs. 1 and 2, and (1), the operation principle of the proposed hybrid MPPT-CPG control can be described as follows.

When PPV(t) ⩽ Plimit, the system enters into CPG operation mode and the MPPT control is deactivated. Perturb and Observe (P&O) and incremental conductance methods [7], [8]. The third one is applied in this study by using Plimit as a power reference since it is relatively simple. It is worthwhile investigating the dynamic performance of different implementation methods, which is beyond the scope of this letter and is considered as a further in-depth study.

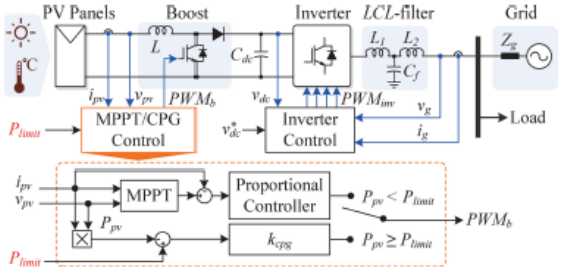

Fig. 1. Schematic and control diagram of a two-stage single-phase PV system with the proposed hybrid control concept.

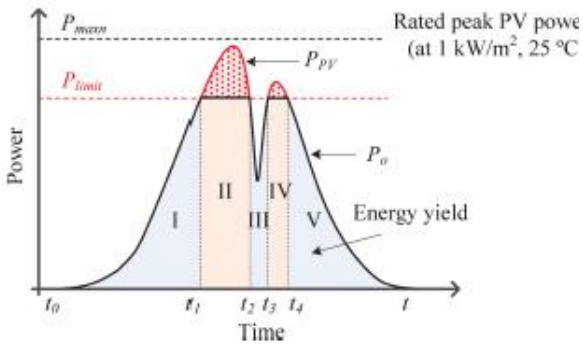

Fig. 2. Operation regions (I, III, V - MPPT; II, IV - CPG) for a single phase PV system during a day with the proposed control concept, where Plim it is determined by the tradeoffs among the device thermal performance, the inverter utilization factor, and the annual energy yield [13].

OPERATION EXAMPLES

To illustrate the effectiveness of the proposed hybrid control concept, simulations of a 3-kW two-stage single-phase PV system are carried out referring to Fig. 1. The system consists of three PV strings (15 panels of each). The parameters of the system are listed in Table 1. The P&O MPPT control method is adopted in the MPPT operation mode [12]. In both operation modes, the dc-link voltage is regulated within 400 ± 5 V to ensure the power injection, and the proposed power control is adopted according to Figs. The benefit of lifetime extension by the proposed control concept has been demonstrated in Fig. 3, where the energy yield and reliability improvement under different power limitations Plimit are presented. The power limit Plimit can be selected according to Fig. 3 when considering the energy yield and lifetime extension. Fig. 4 shows the experimental results of the efficiency of a single-phase PV inverter and the case temperature of the power devices under different power levels. It can be observed in Fig. 4 that the efficiency of the PV inverter varies with the dc input power (i.e. the PV output power) and also the case temperature of the power devices. When the input power is kept constant (e.g., 2.4 kW of Point A and Point B), the case temperature is increased from 51 ◦C to 52 ◦C, while the efficiency is also increased from 93.20 % to 94.19 %.

TABLE 1: PARAMETERS OF THE 3 KWTWO-STAGE SINGLE-PHASE PV SYSTEM

Parameter	Value
PV panels rated power	Pn = 2925 W
Boost converter inductor	L = 5 mH
DC-link capacitor	Cd c = 2200 μF
LCL-filter	L1 = 2 mH, L2 = 3 mH, Cf = 4.7 μF
Switching frequencies for boost stage and inverter	fboost = finv = 10 kHz
Grid nominal voltage (RMS)	Vg = 230 V
Grid nominal frequency	ω0 = 2π × 50 rad/s

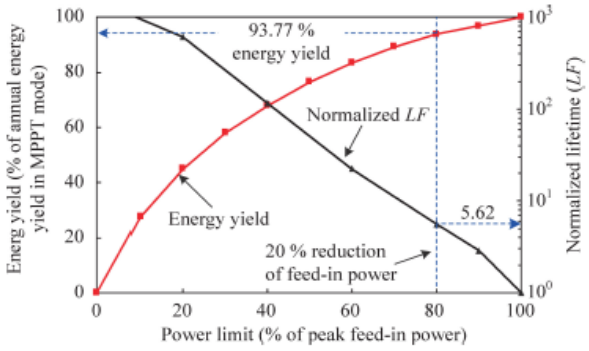

Fig. 3. Energy yield of the PV inverter and normalized lifetime of the power device in the PV inverter with the proposed control concept.

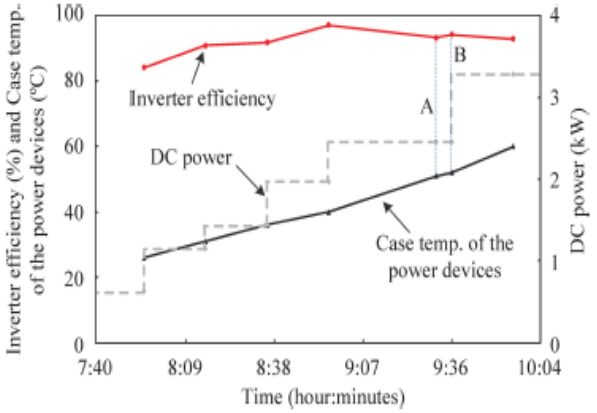

Fig. 4. Experimental results (inverter conversion efficiency and case temperature of the power devices) of a grid-connected single-phase PV inverter under different input power levels.

CONCLUSION

The proposed control strategy allows for increasing the utilization factor of PV inverters and reducing temperature variations in power devices. This advantage is particularly important for increasing PV installations with existing grid infrastructure under high PV penetration rates in the future. The mentioned advantages are not compromised by the energy losses due to the proposed control and allow for the optimal selection of the power control limit

depending on specific mission profiles. In the case of the study of a single-phase PV inverter, the power limit is chosen as 80% of the maximum feed power of the PV panels, which corresponds to a reduction in energy efficiency of 6.23% under a specific annual mission profile.

REFERENCES

F. Blaabjerg, R. Teodorescu, M. Liserre, and A. V. Timbus, "Overview of control and grid synchronization for distributed power generation systems," IEEE Trans. Ind. Electron., vol. 53, no. 5, pp. 1398–1409, Oct. 2019.

D. Maxwell. (2019, Nov. 13). Parts of northern Ireland's electricity grid overloaded. BBC News. [Online]. Available: http://www.bbc.co.uk/

A. Ahmed, L. Ran, S. Moon, and J.-H. Park, "A fast PV power tracking control algorithm with reduced power mode," IEEE Trans. Energy Convers., vol. 28, no. 3, pp. 565–575, Sep. 2020.

H. Wang, M. Liserre, F. Blaabjerg, P. de Place Rimmen, J.B. Jacobsen, T. Kvisgaard, and J. Landkildehus, "Transitioning to physics-of-failure as a reliability driver in power electronics," IEEE J. Emerging Sel. Topics Power Electron., vol. 2, no. 1, pp. 97–114, Mar. 2020.

U. Scheuermann, "Pragmatic bond wire model," Presentation at ECPE Workshop Lifetime Modeling Simulation, Jul. 3–4, 2020.

Y. Yang, H. Wang, and F. Blaabjerg, "Reduced junction temperature control during low-voltage ride-through for single-phase photovoltaic inverters," IET Power Electron., pp. 1–10, in press, 2018. DOI: 10.1049/ietpel. 2019.0734.

D. Sera, L. Mathe, T. Kerekes, S. V. Spataru, and R. Teodorescu, "On the perturb-and-observe and incremental conductance MPPT methods for PV systems," IEEE J. Photovoltaics, vol. 3, no. 3, pp. 1070–1078, Jul. 2021.

L. Nousiainen, J. Puukko, A. Maki, T. Messo, J. Huusari, J. Jokipii, J. Viinamaki, D.T. Lobera, S. Valkealahti, and T. Suntio, "Photovoltaic generator as an input source for power electronic converters," IEEE Trans. Power Electron., vol. 28, no. 6, pp. 3028–3038, Jun. 2022.

Providing an Optimization Scheme for Energy Planning in a Micro Grid Connected to the Residential Grid

Mohammadreza Mohammadiyan Asiabar[1]

[1]*Department of Electrical Engineering, Islamic Azad University, Karaj Branch*

**Corresponding author: mohammadrezamohammadiyan28@yahoo.com*

Abstract— This paper proposes a control scheme to estimate the operating cost of a grid-connected micro grid supplemented by a battery energy storage system. By modelling battery degradation as a function of discharge depth and discharge rate and converting the incremental capacity loss per cycle into the associated cost, the objective function is defined and solved using GAMS. Simulation results are presented to verify the proposed approach. that the proposed optimization scheme can easily manage the DG units in a way that reduces the operation cost and meets the constraints and objectives of the existing system.

Keyword: energy storage system, photovoltaic, renewable energy sources.

INTRODUCTION

With technological improvements in battery energy storage systems and proliferation of renewable energy sources such as photovoltaic panels and wind turbines, concept of micro grid began to be conceived as a kind of energy hub which can efficiently aggregate these units and show itself as a unitary whole [1]- [2]. The optimization problem presented in next section is solved in centralized fashion. One option is to apply this optimal strategy to tertiary layer of a classical MG hierarchical control system and interface to lower layers via low bandwidth digital communication technology [3].

SYSTEM DESCRIPTION

Block diagram of a DC micro-grid that is operated in grid connected mode is shown in Fig. 1. It is comprised of RESs such as PV panels, WTs, battery ESS and grid connection. Power flows between the MG and each of the respective components is regulated via power electronics interface. RESs are operated in Maximum Power Point Tracking (MPPT) mode and loads are considered to be uncontrollable. In this paper, higher level control of a grid-connected DC MG with aforementioned architecture is proposed. For that matter, issues such as primary voltage and current control, as well as stability are not taken into account and system is assumed to be well tuned. Incorporation of strategy developed here into a complete solution that considers both local and coordinated control functionalities is a subject of present investigation.

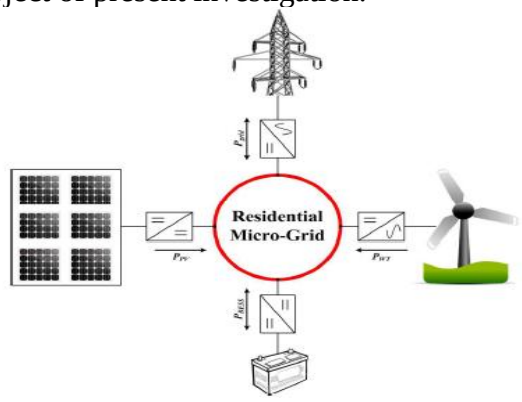

Fig. 1. Schematic layout of a generic DC micro grid.

COMPUTER SIMULATIONS

In this section, the simulation results are presented to show the performance of the proposed scheme in operation management of a typical DC micro-grid. In this regard, a residential MG with a given load profile, as shown in Fig. 2, is considered as the case study. In the same figure the real time utility electricity prices (RTP) are plotted for the examined period. To simulate DGs in the analysis, a Morphic SWT20 type with 20 kW rated power at a wind speed of 9 m/s is used as a WT model in the proposed residential MG. The mentioned system is a direct driven, variable speed, pitch controlled WT whose

related parameters are adopted from [4]. Likewise, Hyundai mono-crystalline solar module with a rated power of 0.25 kW is applied as the building block of the PV system [5]. In the computer simulation, the storage device is also modelled based on NiCd battery pack considering the specifications expressed in Table 1. Other environmental conditions such as hourly temperature, wind speed and solar radiation at the studied place are tabulated in Table 2. It should be mentioned that all of the algorithms and simulations are carried out on a PC with an Intel i5-2430M chip running Windows 7(64 bit) with GAMS and Cplex/Dicopt solvers. The simulation results for the MG operation management and BESS optimal performance are shown in Fig. 3 and Fig. 4, respectively. As it can be seen in Fig. 3, during some periods of time when the real time electricity prices and the amount of power from renewable energy sources (RESs) are relatively low, most of the residential load is supplied by the utility; and the charging process of the battery is done with lower costs. With the growth of demand and bids of the utility during the other hours of the day, the BESS, not only generate electricity in a cost effective way to meet the load, but also sell the surplus of energy to the utility and make profits. Moreover, as observed from Fig. 4 with high penetration of renewables into the MG environment during the midday and in the afternoon, the discharge of BESS is stopped due to the degradation cost of batteries and the load is supplied by RESs.

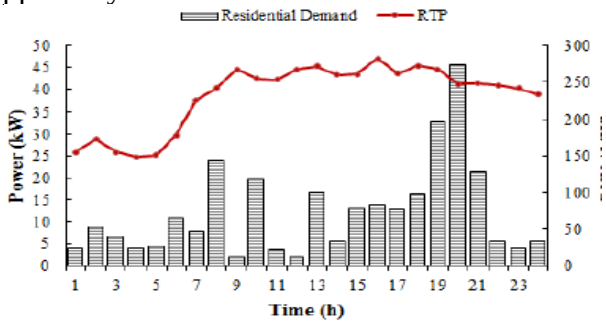

Fig. 2. Residential demand and RTP profiles

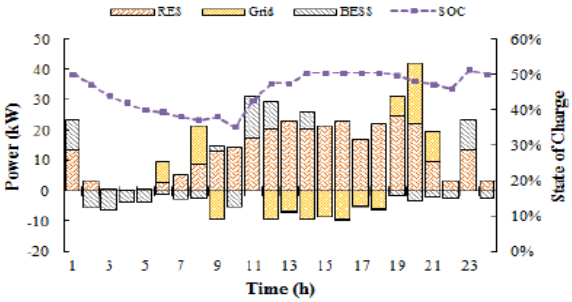

Fig. 3. Optimal operation of micro gird

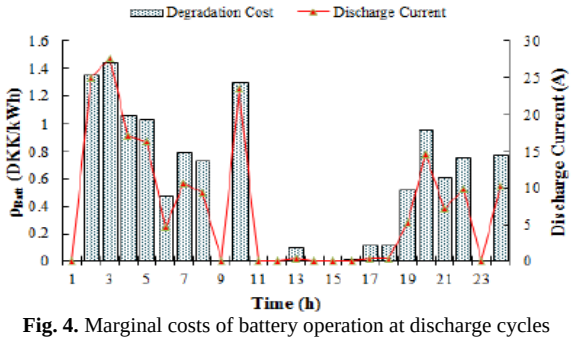

Fig. 4. Marginal costs of battery operation at discharge cycles

TABLE 1. BESS SPECIFICATIONS [14]

Parameters	Value	Unit
Battery Pack Data		
PBatt,ch, PBatt,dch	33,33	kW
SOCmin,SOCmax	20,80	%
ηch, ηdch	87,90	%
Cell Information		
Nominal capacity (CR)	85	Ah
Nominal charge life (ΓR)	175000	Ah
Rated voltage	230	V

TABLE 2. METEOROLOGICAL DATA

Hour	Irradiation (W/m2)	Temp (oC)	Wind (m/s)	Hour	Irradiation (W/m2)	Temp (oC)	Wind (m/s)
1	0.0	13	4.12	13	857.2	18	3.09
2	0.0	12	2.57	14	836.2	18	2.57
3	0.0	10	1.54	15	772.9	19	3.09
4	0.0	10	0.51	16	672.3	19	3.60
5	34.4	10	0.00	17	543.1	18	3.09
6	115.4	12	0.51	18	396.8	19	4.12
7	242.7	12	0.51	19	248.9	17	4.63
8	390.1	13	1.03	20	12.3	15	4.63
9	536.9	16	2.06	21	36.8	14	3.60
10	667.2	17	1.54	22	0.0	12	2.57
11	769.2	17	2.06	23	0.0	12	4.12
12	834.3	18	2.57	24	0.0	12	2.57

CONCLUSION

In this paper, an optimization scheme has been proposed for energy scheduling in a residential grid-connected micro-grid (MG) supplemented by battery energy storage system. cycle life and capacity data commonly available from battery manufacturers. It has been also demonstrated through computer simulations that the proposed optimization scheme could easily manage DG units in a way to reduce the cost of operation and meet available system constraints and objectives.

REFERENCES

R. H. Lasseter, "MicroGrids," in 2019 IEEE Power Engineering Society Winter Meeting. Conference Proceedings (Cat. No.02CH37309), vol. 1, pp. 305–308.

N. Hatziargyriou, H. Asano, R. Iravani, and C. Marnay, "Microgrids," Power Energy Mag., IEEE, vol. 5, no. 4, pp. 78–94, Jul. 2020.

T. Dragicevic, Hierarchical Control of a Direct Current Microgrid with Energy Storage Systems in a Distributed Topology. PhD Thesis, 2020, p. 183.

A. Anvari-Moghaddam, H. Monsef and A. Rahimi-Kian, "Cost- Effective and Comfort Aware Residential Energy Management under Different Pricing Schemes and Weather Conditions", Energy and Buildings, vol. 86, pp. 782-793, 2021.

A. Anvari-Moghaddam, H. Monsef, and A. Rahimi-Kian, "Optimal Smart Home Energy Management Considering Energy Saving and a Comfortable Lifestyle", IEEE Trans. on Smart Grid, vol.6, no.1, pp. 324-332, 2022Artificial Intelligence and Cloud Computing

Hardware Implementation of the DVI Protocol for Displaying Neural Network and Image Processing Outputs on FPGA ML605

Saeed Yazdani[1], Danial Bayati[2], Sara Ershadi-Nasab[3]

[1,2,3] *Ferdowsi University of Mashhad, Mashhad, Iran*

**Corresponding author: ershadinasab@um.ac.ir*

Abstract— This paper presents the implementation and testing of the Digital Visual Interface (DVI) protocol on the ML605 FPGA hardware. The goal was to create a DVI transmitter capable of converting VGA output to DVI pinouts while adhering to protocol standards. Using VHDL and the Xilinx Virtex-6 architecture, the system successfully met DVI specifications and demonstrated its applicability in displaying outputs from neural networks and image processing tasks.

Keyword: ML605 Field-Programmable Gate Array, Digital Visual Interface, Neural networks, Image Processing

INTRODUCTION

The Digital Visual Interface (DVI) protocol is widely used for transmitting digital video signals. FPGAs, like the ML605 with the Xilinx Virtex-6 architecture, offer a versatile platform for implementing such protocols. Displaying neural network and image processing outputs on monitors requires precise synchronization of pixel data and clock signals, a task well-suited for FPGA-based systems.

In recent years, FPGAs have gained attention for their ability to implement deep learning algorithms efficiently, combining low power consumption with real-time processing capabilities. This paper addresses the challenge of integrating a DVI transmitter to display neural network outputs accurately.

The structure of this paper is organized as follows: Section 2 introduces relevant studies addressing the topic. The proposed method architecture is presented in Section 3. The experimental results are provided in Section 4. Finally, the conclusions are presented in Section 5.

RELATED WORK

The development of hardware implementations of neural networks and image processing systems on FPGA platforms has significantly advanced, particularly with the integration of DVI protocols for efficient output display.

Paper [1] demonstrated the effective use of FPGAs for neural network deployment, specifically YOLO-tiny, using the DVI protocol for video output. The work highlighted the advantages of hardware-software codesign in achieving real-time video processing. Similarly, paper [2] employed lightweight neural networks on FPGAs for citrus fruit sorting, showcasing the com- bination of neural network inference and DVI-based display mechanisms. These approaches align with the broader design principles for embedded image processing on FPGA platforms discussed in [3], which emphasizes efficient interfacing for real-time applications.

The DVI protocol's utility in healthcare monitoring systems was explored in [4]. This work implemented convolutional neural network (CNN) architectures for contactless epidemic prevention, leveraging FPGA-embedded DVI Transmitter IP cores for efficient image processing and recognition. Comparable results were achieved in [5], which developed memory-efficient FPGA designs for real-time motion detection using a similar DVI interface for video output. Such advancements are consistent with the signal integrity optimization techniques reviewed in [6], where high- speed interconnect protocols like DVI were analysed for efficient data transmission in FPGA systems.

In the field of video analytics, paper [7] proposed an FPGA-based system for smart sports monitoring. Their integration of CNNs with DVI-supported output significantly

improved object recognition and real-time analytics for hockey games. Meanwhile, [8] investigated edge artificial intelligence, employing FPGA implementations of oscillatory neural networks with DVI support for displaying AI-powered edge analytics. These studies resonate with [3], which covers advanced FPGA design techniques for real-time multimedia applications.

The application of neural networks in industrial automation has also been well-documented. Paper [9] implemented image processing blocks on FPGA platforms, integrating feedforward neural networks for real-time bottle classification. This work aligns with [10], which utilized memristor-induced fractional-order neural networks on FPGAs for image encryption, combining high-speed processing with secure output via the DVI interface.

Additionally, [11] examined the integration of DVI and VGA interfaces with FPGA systems for video enhancement. Their work employed convolutional neural networks for multimedia processing, underlining the versatility of FPGAs in handling various output standards. Further advancements in multimedia applications were demonstrated in [12], which utilized feedforward neural networks for image processing and efficient DVI display. These findings complement the statistical methodologies discussed in [6], particularly in terms of improving signal integrity for multimedia outputs.

PROPOSED METHOD

The implementation of the DVI protocol involved the following key aspects:

- Clock Domain Crossing (CDC): Synchronizing multiple clock frequencies (pixel, character, and timing signals).
- Timing Signal Generation: Producing pixel clock, horizontal/vertical sync, and data enable signals to meet DVI specifications.
- Neural Network Output Display: Visualizing processed neural network outputs, such as class probabilities or heatmaps, on a monitor using the DVI interface.

DVI SIGMAL CONVERSION

Pixel data (RGB values), synchronization signals (HSYNC, VSYNC), and a clock signal (DVI_CLK) ensure accurate rendering of images on an LCD. The FPGA-generated signals align pixel data with the display's grid structure.

VERILOG IMPLEMENTATION

The system comprises modules for clock generation, display timing, and neural network output visualization:

- Clock Module: Generates pixel clock signals for synchronization.
- Timing Module: Produces sync signals and pixel positions (sx, sy) for rendering.
- AI Model Module: Maps neural network out- puts to RGB pixel values for display.

A User Constraints File (UCF) was used to assign FPGA pins to DVI signals, ensuring correct routing and functionality.

EXPERIMENTAL RESULT

The implementation successfully met DVI protocol standards, supporting resolutions up to 1920x1080 at 60 Hz. Key findings include:

- Precise synchronization with no visible distortion.
- High-resolution video output, capable of rendering neural network results in real time.
- Efficient resource utilization, allowing additional FPGA tasks.

The results validated the feasibility of using the ML605 FPGA for real-time visualization of neural network and image processing outputs has been shown in Fig. 1.

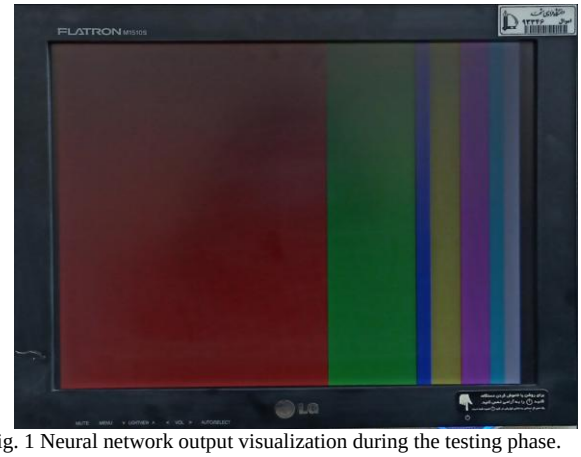

Fig. 1 Neural network output visualization during the testing phase. The width of the colour bar represents the probability of the most likely class.

CONCLUSION

This work demonstrates the ML605 FPGA's capability to implement the DVI protocol for displaying neural network outputs and image processing tasks. The system provides real-time feedback, enabling better validation and interaction in embedded applications.

Future work includes optimizing for higher resolutions, exploring additional video protocols, and integrating more complex neural networks. The results validate FPGAs as powerful platforms for intelligent, real-time systems in embedded applications.

REFERENCES

H. Al-Qaysi. Solent university school of media art and technology, 2022.

M.A. Nuño-Maganda et al. Real-time embedded vision system for online monitoring and sorting of citrus fruits. Electronics, 12(18), 2023.

Donald G Bailey. Design for embedded image processing on FPGAs. John Wiley & Sons, 2023.

W. Lingzhi et al. Design of contactless intelligent epidemic prevention system based on pynq. Engineering Letters, 2022.

S. Singh et al. Memory efficient vlsi implementation of real-time motion detection system using fpga. MDPI, 2023.

Junyong Park and Donghyun Kim. Statistical eye diagrams for high-speed interconnects of pack- ages: A review. IEEE Access, 2024.

V.V. Thyagarajan et al. Video analytics with fpga-based smart cameras for object recognition in hockey games. IEEE, 2023.

M. Abernot. Digital oscillatory neural network implementation on fpga for edge artificial intelligence applications, 2023.

M.A. Nuño-Maganda et al. Implementation and integration of image processing blocks in a real- time bottle classification system. Scientific Re- ports, 2022.

H. Lin et al. Memristor-induced fractional-order neural networks and fpga implementation. Neural Networks, 2024.

J. Müller et al. A low-cost fpga implementation for real-time video enhancement. Journal of Real-Time Image Processing, 2020.

S. Navaneethan et al. Image display using fpga with bram and vga interface for multimedia ap- plications. IEEE, 2023.

Securing Healthcare Data with Blockchain and AES Encryption: A High-Performance Approach to Data Integrity, Confidentiality, and Availability

Zainab A. Abdlhasan[1,2], Maalim A. Aljabery[1,3]

[1]*Faculty of Computer Science and Information Technology, Computer Science Dept., University of Basrah, Basrah, Iraq*

[2]*https://orcid.org/0009-0009-0001-6911, 3https://orcid.org/0000-0002-6133-494X*

Emails: zainab.abdalwahid@uobasrah.edu.iq, maalim.aljabery@uobasrah.edu.iq

**Corresponding author email: maalim.aljabery@uobasrah.edu.iq*

*Abstrac*t - Blockchain's decentralization, security, and transparency make it capable of revolutionizing many industries, particularly in healthcare. Our proposed system leverages the inherent features of blockchain to establish a tamper-resistant and transparent framework for storing medical records. We uniquely identify each patient and assign them an individualized ID number, which serves as a secure password for accessing and managing their medical records. The topic delves into an effective method of safeguarding a patient's information using blockchain technology and AES encryption. The used strategy involves acquiring data in the form of CSV, encrypting it using AES, and then storing it on the blockchain.

Keywords: Blockchain, Security, AES encryption.

INTRODUCTION

Health data is one of the most important and sensitive types of data, making it a prime target for cyber-attacks. Given the importance of this data, the need for a multi-dimensional approach that combines strong encryption, and secure storage has become essential [1].

By combining blockchain technology and encryption, we can achieve high security and trust in health data management. This research aims to discover the balance of encrypting and securely storing medical data, both visual and textual, in a blockchain network.

PROPOSED METHODOLOGY

The given methodology starts with the data collection which includes the data in the CSV format and the image data. These datasets contain different patient information, such as SOL, sensors, medical images, and patient history. To improve the security of this type of information, the data is encrypted using AES before it is added to the blockchain. This encryption step is applied to ensure that only allowed users can access the data and therefore keep it secret[2].

The encrypted data is then integrated into the blockchain and becomes part of a block. Each block in the blockchain contains a set of encrypted patient records, leveraging the blockchain's characteristics of immutability and distributed data storage[3]. This integration ensures that the data remains tamper-proof and that the database securely stores patients' records.

There is a way that only authorized users can access the data stored in the blockchain. The encrypted data is decrypted through the AES decryption process to retrieve the original patient records but in a highly secure manner. This retrieval and decryption process helps to maintain the data in the database accessible to authorized users but at the same time protects it from people who have no permission to access the information.

The entire process starting from collection, going through the encryption, blockchain, and finally, retrieval and decryption is depicted in Fig. 1.

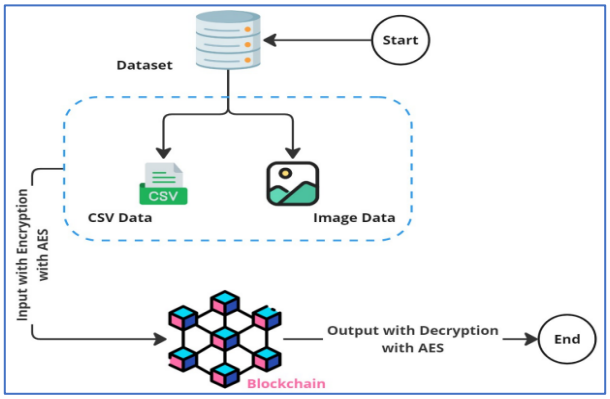

Fig. 1: Proposed Scheme

Blockchain Structure

This methodology's blockchain framework is designed for the secure storage and sharing of patient data. The blockchain commences with a genesis block, which serves as the foundational block in the chain; no other block can precede it. In the blockchain framework, a block consists of a collection of transactions; here, we encrypt the patient's records. From end to end, these blocks sequentially connect and remain immutable.

Each block generates a distinct hash value, serving as its fingerprint. We apply a hash function to this block to ensure that any alterations will be visible in the hash value. The hash is the SHA-256 of a string representation of all block data, omitting the prior block's hash; hence, to obtain a block's hash, one converts all block data into a string and applies the SHA-256 hashing method. Similarly, the sequence preserves the hash of the previous block, giving the blocks a chain-like appearance.

The distributed ledger employs proof of work to ensure its high security. This entails locating a nonce that, when combined with the block's data, generates a hash that satisfies a specific condition, such as commencing with zeros. The complexity of this condition closely correlates with the level of security and computational intensity.

$$\text{Hash (Block)} = \text{SHA} - 256(\text{Block Data} + \text{Nonce}) \quad (2).$$

FLASK FRAMEWORK AND TOOLS

To meet the needs of a web interface, we used Flask, a lightweight Python web application framework, for the core backend, which includes web requests, HTML template generation, and routes for a blockchain-based healthcare management system.

Flask offers two primary tools for web development, one of which is the app. At its core, the `route()` function maps specific URLs of tasks that serve as responses to web page requests[4]. This function allows the creation of routes that interact with the blockchain, enabling the addition of new patient data, viewing current records, and navigation through the relevant

sections of the blockchain structure. The `render template () ` function is also employed to dynamically display HTML pages, passing patient records or blockchain data to the front end, where this information is presented in a readable format.

This framework facilitates the management of data files and image uploads. For instance, the web interface allows users to upload patient images upon request. The secure filename function in the file's utility guarantees the safe storage of uploaded files, filtering their names to avert security risks. Thus, you can send images to a website that links with patient data in a blockchain, securely storing and retrieving text- and image-based medical records.

The handy feature Flask gives us is jsonify(), which transforms Python dictionaries into the JavaScript Object Notation format[5]. This is useful when developing APIs for blockchain data, as it allows users to access a single endpoint, such as the JSON endpoint, for comprehensive information about the blockchain.

Downstream systems or frontend applications can then ingest JSON in a structured, human-readable manner for the blockchain's records.

The system incorporates Jinja2, a renowned templating engine, to create responsive pages with a straightforward syntax that prevents code duplication[4]. This feature allows the direct injection of patient data and other blockchain-specific information into the webpage in real time.

During development, we used debug mode to provide real-time error messages and enable live application reloading. This feature is crucial for identifying issues promptly and supports rapid iterations in web application development. Flask's robust debugging capabilities facilitated efficient application iterations.

Fig. indicates 5 layouts of the home page of a “Patient Blockchain Interface” web application. This creates numerous ways to input or access patient data safely through a Blockchain space whilst using the interface. It is subdivided into five main buttons, each providing the user with certain features.

Fig. 2: home interface

Fig. is a form from a web application for managing patient information.

Fig. 3 shows the web page for patient details and blockchain-related patient data is displayed and recorded securely.

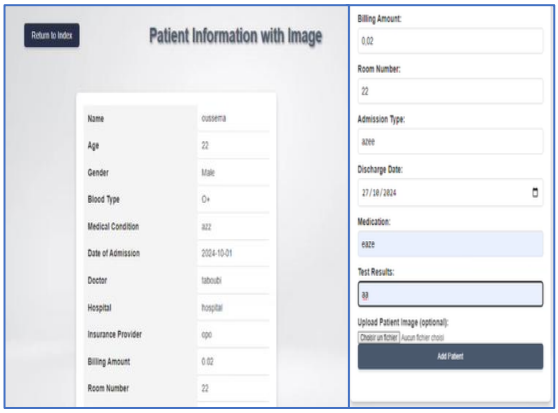

Fig. 3: Patient information

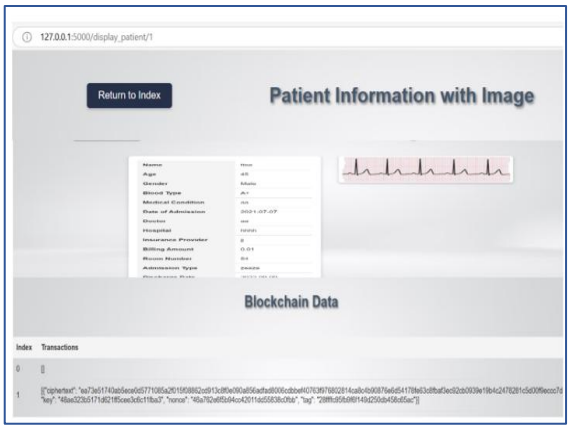

Fig. 4: Adding patient to blockchain according to his ID

COMPARISON WITH RELATED WORKS

Previous studies, such as those employing RSA encryption or hybrid schemes like Elliptic Curve Cryptography (ECC), have reported significant increases in execution time and computational overhead by as much as 75% in the case of RSA and 55% with ECC, as noted in [6]. In contrast, adopting AES encryption achieves markedly faster execution times while maintaining robust security standards.

Furthermore, whereas prior research has focused on securing textual or image data, our method provides comprehensive protection across both data types through a unified encryption framework.

In summary, our system enhances data confidentiality and integrity while providing a more efficient solution that balances security with processing speed and is well-

suited for deployment in large-scale healthcare environments.

CONCLUSION

To that end, its methodology regarding data acquisition and general workflow comprises the following steps: Gather text data in CSV format and image data, then encrypt them using AES and store them on the blockchain, by pursuing this methodology, and using a clear and easy-to-use framework like Flask the safety of the patient's data is achieved while at the same time ensuring the performance of this application at various levels. The features of AES are optimal for serving as the encryption method while providing maximal data protection without severely conflicting with the processing speed.

REFERENCES

[1] B. H, R. N, S. S, and V. Pious, "Patient Data Management Using Blockchain," International Journal of Scientific and Research Publications (IJSRP), vol. 10, no. 7, pp. 310–316, Jul. 2020, doi: 10.29322/IJSRP.10.07.2020.p10339.

[2] M. A. Aljabery, "Enhancing Steganography with Blockchain: A Novel Approach for Secure Text Hiding in Encrypted Images," Informatica, vol. 48, no. 21, Nov. 2024, doi: 10.31449/inf.v48i21.6689.

[3] S. Fatima et al., "A Secure BlockChain Framework for IoT Healthcare," in 2022 International Conference on Emerging Trends in Electrical, Control, and Telecommunication Engineering (ETECTE), IEEE, Dec. 2022, pp. 1–6. doi: 10.1109/ETECTE55893.2022.10007122.

[4] K. Y. Yang, "A full-stack news intelligence web platform with text mining and NLP techniques," 2022.

[5] P. I. Ritharson, D. S. Juliet, J. Anitha, and S. I. A. Pandian, "Multi-Document Summarization Made Easy: An Abstractive Query-Focused System Using Web Scraping and Transformer Models," in 2023 3rd International Conference on Intelligent Technologies (CONIT), IEEE, 2023, pp. 1–6.

[6] A. G. de Moraes Rossetto, C. Sega, and V. R. Q. Leithardt, "An Architecture for Managing Data Privacy in Healthcare with Blockchain," Sensors, vol. 22, no. 21, p. 8292, Oct. 2022, doi: 10.3390/s22218292.

Challenges and Security Threats in Lithium-Ion Batteries and Countermeasures (The Role of Lithium-Ion Batteries in the Explosion of Pagers in Lebanon)

Abbas Ghaemi Bafghi[1*], Bibi Marzieh Rezvan Panah[2]

[1]*Data and Communication Security Research Laboratory, Department of Computer Engineering, Ferdowsi University of Mashhad*

[2]*Data and Communication Security Research Laboratory, Department of Computer Engineering, Ferdowsi University of Mashhad*

**Corresponding author: ghaemib@um.ac.ir*

*Abstract_* One of the most important factors in pager explosions in Lebanon is lithium-ion batteries. Due to their high energy density, light weight, and long durability, these batteries are used as one of the most advanced energy storage technologies in various industries such as electronics, electric vehicles, and aviation. Although these batteries play a key role in the development of sustainable technologies, they face safety challenges, particularly thermal runaway. This article discusses vulnerabilities, threats, and cyberattacks on battery management systems and countermeasures.

Keywords: Lithium-ion battery, Lebanon explosion, thermal runaway, malicious code

INTRODUCTION

Lithium-ion batteries used in pagers typically have capacities ranging from 300 to 1000 milliampere-hours, physical dimensions of approximately 30 to 50 millimeters in length and 5 to 15 millimeters in thickness, and a voltage of around 3.7 volts. These batteries, due to their high energy density and advanced performance, have become one of the most widely used energy storage technologies. However, these advantages are accompanied by serious safety challenges.

Thermal runaway, as one of the main causes of fires and explosions, occurs when a battery is subjected to factors such as overcharging, excessive heat, or a short circuit. Additionally, structural failure or improper management can trigger dangerous chain reactions that lead to the complete destruction of the battery and cause damage. The increasing complexity of battery management systems and remote data communications has increased the level of vulnerability of these systems.

Figure 1 illustrates the cyber-physical battery system and its potential cybersecurity vulnerabilities [1].

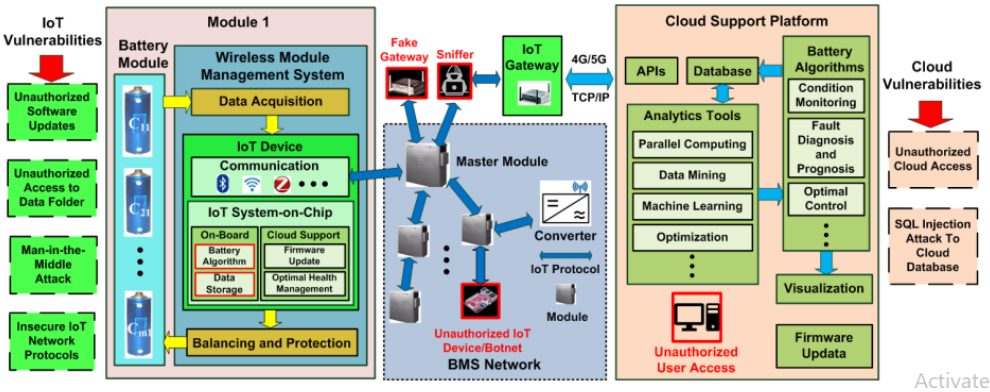

Fig. 1 Overall system architecture of a cyber-physical battery system and demonstration of potential cybersecurity vulnerabilities [1]

A short circuit in the battery causes a very high current, which can lead to rapid heating of the battery and a fire or explosion. Possible causes of a short circuit include physical damage, internal circuit failure, changes in external circuitry, and RF software attacks, where the attacker sends specific signals containing malicious commands to the pagers. Voltage Spike Attacks occur when an attacker uses malicious code to force a device to receive a voltage higher than normal.

Overload Attacks, in which an attacker forces the system to perform tasks beyond its capabilities through software, are two types of technical attacks that can cause lithium-ion batteries to overheat or even explode.

The paper [2] examines the technological aspects of pager explosions in Lebanon from various perspectives, discussing cyber-physical attacks and the role of explosives in the same paper, as well as the security challenges and threats faced by the targeted pagers in Lebanon. Countermeasures to these threats are explored in [3].

Other parts of the article are included in sections ٢. Lithium-ion battery vulnerabilities, ٣. Cybersecurity threats and attacks in lithium-ion battery systems, and ٤. Solutions to counter security threats to lithium-ion batteries.

LITHIUM-ION BATTERY VULNERABILITIES

Thermal management and controlling the thermal behavior of batteries are critical factors in their safety and performance. Thermal management and controlling the thermal behavior of batteries are crucial aspects of their safety and performance.

In the paper [4], issues such as overload, excessive discharge, and overheating are identified as the causes of "thermal runaway," which can lead to fires or explosions.

The paper [5] discusses thermal runaway, where the temperature rises rapidly and uncontrollably, causing the degradation of internal materials, short circuits, fires, and explosions. It emphasizes the importance of thermal management.

Papers [6, 7] points out the explosion risks caused by gases released due to thermal runaway in these batteries, where even small amounts of these gases can create serious explosion hazards, especially in confined spaces.

In [8], potential explosion risks are discussed considering arc faults and thermal runaway behaviour in batteries.

CYBERSECURITY THREATS AND ATTACKS IN LITHIUM-ION BATTERY SYSTEMS

The vulnerabilities and threats to lithium-ion batteries have been analyzed in numerous studies. In paper [1], data manipulation attacks on the battery management system and SQL Injection attacks, which can lead to battery overheating or even explosions, are discussed. In the article [9], it describes methods such as network intrusion, unauthorized access attacks, virus and malware-based attacks, data modification attacks, remote attacks, attacks using malicious software updates, Command Injection Attack, attacks based on hardware flaws that lead to the injection of malicious commands and cause batteries to be damaged or explode.

[10] Refers to cyberattacks such as Command Injection Attack, MITM Attacks, DOS Attacks, and unauthorized hardware access attacks that can lead to manipulation of algorithms, control signals, or battery sensor data, resulting in battery destruction or even fire.

In [11], the vulnerabilities of lithium-ion batteries to Deception Attacks are examined. These attacks can easily manipulate measured data, leading to significant errors in estimating the battery's state of charge. Papers [12, 13] address the vulnerabilities that allow cyberattacks to infiltrate the management systems of these batteries.

In paper [14], the vulnerabilities of Digital Twin-based lithium-ion battery monitoring systems are discussed, where timestamp attacks can disrupt the temporal order of battery data and damage the accuracy of state-of-charge predictions.

In [15], attacks such as MITM (Man-in-the-Middle) and techniques like Spoofing are discussed, which aim to access information during transmission. In [16, 17], attacks that can lead to service disruption such as DDoS and other attacks are discussed.

COUNTERMEASURES TO SECURITY THREATS IN LITHIUM-ION BATTERIES

To counter cybersecurity and security threats related to lithium-ion batteries, it is essential to adopt appropriate solutions to maintain the security of these systems.

In the paper [1], to prevent unauthorized access, data encryption, the use of secure SQL parameters, user accounts with limited access, and non-disclosure of database errors are examined.

In the paper [10], machine learning and artificial intelligence algorithms for identifying anomalies in battery data, encryption of wireless communications, use of firewalls, use of standard security protocols such as TLS for secure communications, use of strong encryption algorithms, and multi-factor authentication for access to battery control systems are considered as solutions to prevent cyber threats. It also states that monitoring and alert systems should continuously track the performance of batteries so that corrective actions can be taken promptly in the event of any abnormal activity or cyberattack. Furthermore, battery management software should be regularly updated to prevent new vulnerabilities.

In paper [9], intrusion detection systems, multi-factor authentication, data encryption, and security models such as Chain-of-Trust are introduced as key solutions to strengthen protection against attacks. It also highlights the use of hardware encryption functions to prevent unauthorized access to encryption keys and sensitive information, particularly at the software level. Additionally, the inclusion of a secure recovery mode to handle attacks and security failures during issues, as well as the use of security standards like MACsec for network communications, are recommended as essential measures to maintain the security of lithium-ion battery systems against cybersecurity threats.

In paper [11], the ARFOEKF method is proposed to counter Deception Attacks. This method can minimize estimation errors against such attacks and maintain the accuracy of SOC (State of Charge) estimation under attack conditions.

COCLUSION

Despite their unparalleled advantages, lithium-ion batteries face significant challenges such as thermal runaway, short circuits, excessive heat, structural failures, vulnerabilities to safety threats, and cyberattacks, including remote malicious commands, which can lead to overheating or explosions. The use of solutions such as strong encryption, multi-factor authentication, regular software updates, and intelligent monitoring systems can be effective in mitigating these threats. Finally, the security of lithium-ion batteries must be strengthened through a comprehensive approach, covering hardware, software, and communication networks, to prevent the risks associated with explosions.

ACKNOWLEDGMENT

We extend our gratitude and appreciation to the esteemed members of the Data and Information Security Laboratory, especially Fatemeh charlank Bakhtiari, for assisting us in compiling this collection.

REFERENCES

[1] Kumbhar, Sourabh, et al. "Cybersecurity for battery management systems in cyber-physical environments." 2018 IEEE Transportation Electrification Conference and Expo (ITEC). IEEE, 2018.

[2] Abbas Qaemi Bafghi, Bi Bi Marzieh Rezvan, "Technological Examination of Pager Explosions in Lebanon from Various Perspectives," submitted to https://resist.um.ac.ir/2025, 1403.

[3] Abbas Qaemi Bafghi, Bi Bi Marzieh Rezvan, "Challenges and Security Threats in the Pagers Targeted in Lebanon and Countermeasures," submitted to https://resist.um.ac.ir/2025, 1403.

[4] Yin, Sumiao, Jianghong Liu, and Beihua Cong. "Review of thermal runaway monitoring, warning and protection technologies for lithium-ion batteries." Processes 11.8 (2023): 2345.

[5] Abraham, K. M. "How Safe Are Li-ion Batteries?" Journal of the Electrochemical Society 170.11 (2023): 110508.

[6] Explosion-venting overpressure structures and hazards of lithium-ion batteries thermal runaway gas induced by multiple vents of energy storage system container" (2024 - Elsevier)

[7] Sauer, Nathaniel G., Benjamin Gaudet, and Adam Barowy. "Experimental investigation of explosion hazard from lithium-ion battery thermal runaway effluent gas." Fuel 378 (2024): 132818.

[8] "Failure mechanism and thermal runaway behavior of lithium-ion battery induced by arc faults" (2025 - Elsevier).

[9] Crocetti, Luca, et al. "A novel and robust security approach for authentication, integrity, and confidentiality of Lithium-ion Battery Management Systems." 2023 IEEE 3rd International Conference on Industrial Electronics for Sustainable Energy Systems (IESES). IEEE, 2023.

[10] Naseri, Farshid, et al. "Cyber-physical cloud battery management systems: review of security aspects." Batteries 9.7 (2023): 382.

[11] Yang, Tong, Yan Li, and Yi Zeng. "Secure state of charge estimation for lithium-ion batteries under deception attacks based on attack-resilient fractional-order extended Kalman filter."Journal of Energy Storage 95 (2024): 112438.

[12] Akhil, S. Sai, et al. "A Brief Review of Cyber Attacks on Electric Vehicle Battery Management System." International Conference on Innovation in Energy Management and Renewable Resources. Singapore: Springer Nature Singapore, 2023.

[13] Kumari, Shreya, et al. "Lithium-ion (li-ion) battery with smart cars and hijacking preventions." 2024 15th International Conference on Computing Communication and Networking Technologies (ICCCNT). IEEE, 2024.

[14] Pooyandeh, Mitra, and Insoo Sohn. "A Time-Stamp Attack on Digital Twin-Based Lithium-ion Battery Monitoring for Electric Vehicles." 2024 International Conference on Artificial Intelligence in Information and Communication (ICAIIC). IEEE, 2024.

[15] Redonet Klip, T. H. Monitoring crowd dynamics by passively sniffing cellular traffic. MS thesis. University of Twente, 2020.

[16]Molcut, Alex-Ionut, Septimiu Lica, and Ioan Lie. "Cybersecurity for embedded systems: a review."2022 International Symposium on Electronics and Telecommunications (ISETC). IEEE, 2022.

[17] Sanchez, Donald. Assessing Bear: Tool Usability for Wireless CTF. MS thesis. California Polytechnic State University, 2021.

Machine learning based Prediction of Habitat Suitability of *Prosopis juliflora* under present and future climatic scenarios in arid coastal region of Pakistan

Saima Shaikh[1], Sana Arshad*[3], Jamil Hasan Kazmi[1,2],

1 Department of Geography, University of Karachi, Karachi 75270, Pakistan

2 FatimyiahHigher Education System (FHES), 173 Britto Road, Soldier Bazar, Karachi, Pakistan

3 Department of Geography, The Islamia University of Bahawalpur, Bahawalpur, 63100, Pakistan

**Corresponding author: sana.arshad@iub.edu.pk*

Abstract -The invasion of alien plant species poses a significant global threat to biodiversity, exacerbated by climate change. Pakistan is particularly vulnerable to the rapid spread of *Prosopis juliflora*, introduced in 1857 during the unpartitioned Indian subcontinent. This species thrives in harsh environmental conditions without ecological competition, making Pakistan's coastal regions, especially Karachi, highly susceptible to its invasion. Climate change has further accelerated this process. Despite its ecological and environmental impact, limited studies have assessed its invasion or predicted its future spread under changing climatic conditions. This research evaluates *Prosopis juliflora's* habitat suitability in Karachi using three pseudo-absence methods (Random, Buffer, and Cluster) within the Google Earth Engine's machine learning framework. It integrates multisource environmental data, including bioclimatic, Terra Climate, topographical, and vegetation indices. Results indicate that the clustering approach, based on environmental profiling, yields the most accurate predictions, with high AUC-ROC (0.942), AUC-PR (0.871), sensitivity (0.887), specificity (0.992), and Kappa (0.80). Future climate scenarios reveal ssp245 predicts the highest distribution probability (49%), followed by ssp585 (47.7%). The findings highlight the urgency of managing *Prosopis juliflora's* spread in coastal Pakistan to mitigate its impact under present and future climate conditions.

Keywords: Species Distribution Modelling, invasive plants, Google Earth Engine, Gradient Boosting Regression

INTRODUCTION

Climate change along with human caused activities have brought significant changes in ecological perspectives [1]. One of the most important effects of anthropogenic activities is assessed through the diffusion of invasive species in the environment. Investigating the niche or habitat suitability of invasive species is substantial to understand the ecosystem response towards climate [2].

The main objectives of the research include 1) to predict the habitat suitability of P. juliflora employing and testing machine learning algorithms in open-source geospatial cloud computing platform of Google Earth Engine (GEE). 2) to test the predictive performance of three pseudoabsence methods (random, cluster, and buffer) for the habitat suitability of P.
juliflora in present and future (ssp245 and ssp 585) climatic scenarios.

METHODOLOGY

Currently, the incidence points of the *P. juliflora* were collected from the densely populated metropolitan Coastal Division of Pakistan, *i.e.*, Karachi. As our survey data was comprised of only presence points of P. juliflora along the coastal region of Pakistan. Therefore, we aimed to model the climatic suitability of P. juliflora occurrence using three different methods of pseudoabsence generation as suggested by Crego, Stabach and Connette [53]. These include a) Random method of pseudoabsence generation across the whole study area, b) Buffering method with limiting random pseudoabsence at a specified distance (3000 metres currently) around presence point, c) clustering on selected predictors method deals with identifying the environmentally dissimilar areas of the presence points.

RESULT

The selected variables for distribution modelling of *P. juliflora* were based on the local environmental traits and different trials of best performance and less correlation among them. A threshold of (r <0.75) was selected to avoid the collinearity among variables. The Spearman's correlation test was implemented before the running the models revealing a low to moderate correlation among bioclimate, environmental, and other remote sensing variables. The selected bioclimate variables such as annual mean temperature (bio01), temperature seasonality (bio04), and precipitation seasonality (bio15), exhibited a low spearman correlation of -0.3 and 0.04 among them. However, bio01 showed a high negative correlation with elevation (r = -0.8), which exceeded the threshold (**Figure**). Despite this, both variables were considered in the modelling due to their significant impact on the distribution probability of *P. juliflora* in the study area. Furthermore, real time climatic variables, including Tmax, Tmin, and def also revealed a low to moderate correlation below threshold among them and other variables (**Figure**).

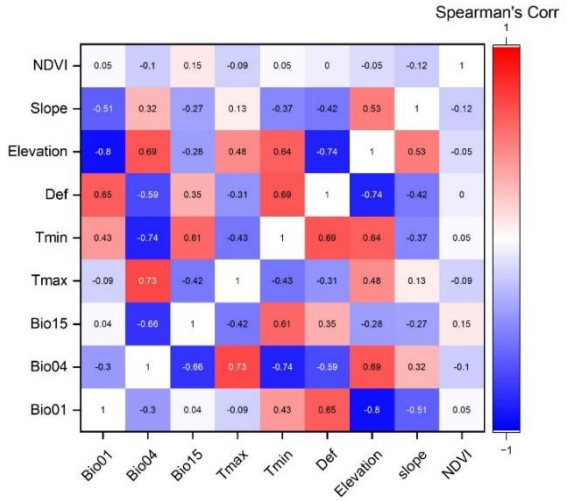

Figure. Heat map of Spearman's correlation between all selected predictors

REFERENCES

Fussmann, K.E.; Schwarzmüller, F.; Brose, U.; Jousset, A.; Rall, B.C. Ecological stability in response to warming. Nature Climate Change 2014, 4, 206-210, doi:10.1038/nclimate2134.

Singh, M.; Arunachalam, R.; Kumar, L. Modeling potential hotspots of invasive Prosopis juliflora (Swartz) DC in India. Ecological Informatics 2021, 64, 101386, doi:https://doi.org/10.1016/j.ecoinf.2021.101386.

Ab Lah, N.Z.; Yusop, Z.; Hashim, M.; Mohd Salim, J.; Numata, S. Predicting the Habitat Suitability of Melaleuca cajuputi Based on the MaxEnt Species Distribution Model. Forests 2021, 12, 1449.

Improving the Accuracy of Intrusion Detection Systems by Optimizing Random Forest Algorithm Parameters Using Genetic Algorithm

M. Karimi[1*], MM. Shirmohammadi [2], S. Alikhani [3]

[1]*Department of Knowledge and Information Science, Islamic Azad University, Hamedan, Iran*

[2] *Computer Engineering Department, Hamedan Branch, Islamic Azad University, Hamedan, Iran*

[3] *Department of Knowledge and Information Science, Islamic Azad University, Hamedan, Iran*

**Corresponding author: mahdi-karimi@farabi.tums.ac.ir*

Abstract— In the field of cyber security, intrusion detection is one of the vital issues that requires high accuracy and efficiency. However, traditional models usually face challenges such as high false alarm rate and inability to identify new attacks. In this article, an improvement model based on genetic algorithms and random forest is presented, which aims to improve the accuracy and efficiency of intrusion detection systems. The proposed method includes the use of the genetic algorithm to optimize the parameters of the random forest model, which is the optimal setting for the intrusion detection model. The results show that the proposed model has been able to diagnose with 99.96 % accuracy. Precision 99.96%, Recall 99.96% and the F1-Score equal to 99.95%, has a much better performance than other existing models. These results show the high power and efficiency of the model in real environments and provide new directions for researchers in this field to further improve intrusion detection systems.

Keyword: Intrusion detection, genetic algorithm, random forest algorithm, information technology, security, cyber attacks.

INTRODUCTION

In the current digital age, information security and protection of computer systems against intruder attacks is one of the most important challenges for organizations and institutions. Every day, the number and complexity of cyber-attacks are increasing forever, and the need for intrusion detection systems that can be able to effectively identify and stop these attacks is needed more than ever. One of the most famous and widely used datasets for the evaluation and development of intrusion detection systems is the NSL-KDD dataset.

In this research, our goal is to investigate the use of the genetic algorithm to improve the random forest model in intrusion detection using the NSL-KDD dataset. First, we will review the literature and previous research in this field, and then we will present a new model based on the combination of the two methods. The results of this research can help to develop more efficient and accurate intrusion detection systems and play an important role in the protection of information systems.

RESEARCH BACKGROUND

In this section, we examine a number of articles and researches related to the use of the genetic algorithm to improve the random forest model in intrusion detection and compare their results.

Breiman has shown that the random forest makes a decision by leaving a few trees. Its result is the introduction and explanation of the random forest algorithm and its high performance in classification and prediction, which is the basis of many other researches. [3]

Azad and Jha examined the use of the genetic algorithm to estimate the parameters of the random forest model in case intrusion detection, and the researchers use genetic algorithm to optimize random forest model parameters and evaluate its performance [4].

Ahmim and Harous present a hybrid framework for intrusion detection that uses a random forest model and a genetic algorithm. Its results include providing a hybrid framework for intrusion detection, improving the detection accuracy and reducing the rate of false positive errors, and optimizing the

features and parameters of the random forest model [5].

Almseidin et al. have compared the performance of different machine learning algorithms in intrusion detection systems, and random forest is one of the algorithms investigated in this study and its results have been compared with other algorithms [6].

Idris and Selamat present a hybrid intrusion detection system that uses a combination of genetic algorithm and particle swarm optimization (PSO) algorithm. Its results include increasing accuracy and reducing the rate of false positive errors in intrusion detection and taking advantage of the advantages of both algorithms for better optimization [8].

Govindarajan and Chandrasekaran It has investigated the use of the genetic algorithm and data mining techniques for the diagnosis of intrusion. The genetic algorithm was used to select the important features and to optimize the penetration diagnosis models [9].

A comprehensive review of various machine learning techniques for intrusion detection is provided by Tsai et al. In this review, the random forest model and its applications in intrusion detection are also discussed [10].

Folino et al. have investigated the use of genetic programming and decision trees for the development of intrusion detection systems [11].

Various studies have shown that the combination of genetic algorithm with random forest model and other optimization and data mining techniques can lead to a significant improvement in the accuracy and performance of intrusion detection systems. These results indicate the high potential of using optimization algorithms in improving machine learning models for intrusion detection.

METHOD

The purpose of this research is to use the genetic algorithm to improve the random forest model in intrusion detection using the NSL- KDD dataset. This research is carried out in order to increase accuracy, reduce the rate of false positive and negative errors and predict.

The techniques used for the proposed model include the genetic algorithm to optimize the model parameters and the random forest is the basic model for intrusion detection, which is used for the modelling of Python software.

THE PROPOSED SYSTEM

In this model, random forest is used as part of the evaluation function for the genetic algorithm, then this function is used as the evaluation function in the genetic algorithm. In this way, the parameters optimized by the genetic algorithm are given to the random forest model to find the best settings for the model. In other words, random forest is combined with genetic algorithm to find the best parameters.

Outputs and its analysis

In general, the results show that the model optimized by combining the random forest and the genetic algorithm has a very good performance in intrusion detection and has been able to achieve very high evaluation criteria.

Genetic Algorithm Convergence Chart: As seen in Figure 6, both in accuracy and criteria recall and F1-score is a fast convergence algorithm.

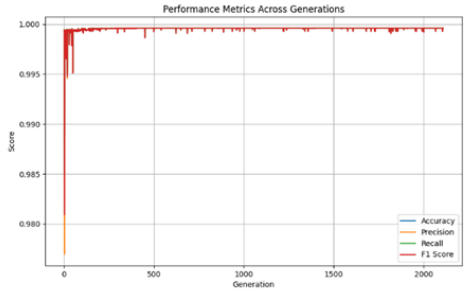

Figure 6 Convergence diagram of the proposed model

Confusion Matrix

In this research, the confusion matrix is as described in **Table 4**:

Table 4: Confusion matrix of the proposed model

	DoS	**Probe**	**R2L**	**U2R**	**normal**
DoS	9224	0	0	0	0
Probe	0	2371	0	0	2
R2L	0	0	196	0	3
U2R	0	0	3	9	1
normal	0	1	0	0	13382

Classification Report

The classification report for each category includes measures of precision, recall and F1-score. These criteria are described in **Table 5**

Table 5.Classification report of the proposed model

	precision	recall	f1-score	support
DoS	1.00	1.00	1.00	9224
Probe	1.00	1.00	1.00	2373
R2L	0.98	0.98	0.98	199
U2R	1.00	0.69	0.82	13
Normal	1.00	1.00	1.00	13386
accuracy			1.00	25195
macro avg	1.00	0.94	0.96	25195
weighted avg	1.00	1.00	1.00	25195

Comparison of the results with the results of other case studies

In table 6 a comparison of the three results obtained with other studies is given. As it can be seen, the results of this model show the improvement of the performance of this model in all criteria. Accuracy, precision, and Recall in the diagnosis of the disease are compared to other methods that have been done previously in other ways.

Table 6. Comparison of the intrution detection results of the proposed method with other studies [15]

Algorithm	Accuracy	Precision	Recall
PSO-RNN [12]	96.08%	85.63%	85.63%
RF-SMOTE [13]	98.31%	98.61%	98.41%
PSO-KNN [12]	98.9%	98.89%	92.33%
EGA-PSO [14]	98.97%	99.84%	96.12%
PSO-RF [12]	99.76%	99.75	96.45
Proposed model	99.96%	99.96%	99.96%

In this regard, comparing the proposed model conducted in this research with the results of the model presented by Jafari and Hosseini shown in **Table 7** shows that the proposed model in all evaluation criteria including Accuracy, Precision, Recall and F1-Score in intrusion detection has performed better.[17].

Table 7. Comparison of the intrution detection results of the proposed method with other studies [6]

Algorithm	Accuracy	Precision	Recall	F1-Score
DNN-12L [6]	99.49%	99.39	96.39	99.41
Proposed model	99.96%	99.96%	99.96%	99.95

CONCLUSION

In this project, the main goal was to detect network intrusion using the NSL-KDD dataset and combining machine learning models and optimization algorithms. First, the data were modeled using random forest. Then, to improve the performance of the model, the genetic algorithm was used to optimize the random forest parameters, which increased the accuracy of the model.

The confusion matrix and classification report showed that the optimized model performed very well in identifying different categories of attacks, especially in DoS, Probe and normal categories whose accuracy, recall and F1 score were almost perfect.

However, the performance of the model in the U2R category was slightly lower than other categories due to the lack of samples.

The random forest model optimized using the genetic algorithm has a very good performance in intrusion detection. The evaluation criteria show that the model has been able to identify almost all attacks with a very high accuracy. However, the small number of samples of the R2L and U2R categories could be a weakness and more data is needed for these categories. In general, this method, a combination of random forest and genetic algorithm, provides an effective solution for intrusion detection. The results show that the optimized model with the combination of random forest and genetic algorithm has a very good performance in intrusion detection and has been able to achieve very high evaluation criteria. This shows the power and high efficiency of this model in real environments.

As a result, using the genetic algorithm to optimize the random forest model significantly improved the performance of the model. This research shows that by combining machine learning models and optimization algorithms, high accuracy can be achieved in network intrusion detection.

REFERENCES

Disha, RA, Waheed, S. Performance analysis of machine learning models for intrusion detection system using Gini Impurity-based Weighted Random Forest (GIWRF) feature selection technique. Cybersecurity 5, 1 (2022).

Tavallaee, M., Bagheri, E., Lu, W., & Ghorbani, AA (2009). A detailed analysis of the KDD CUP 99 data set. In IEEE Symposium on Computational Intelligence for Security and Defense Applications (CISDA) (pp. 1-6). IEEE.

Breiman, L. (2001). Random forests. Machine learning, 45(1), 5-32.

Azad, MS, & Jha, DN (2019). An improved intrusion detection system using genetic algorithm and random forest classifier. Journal of King Saud University-Computer and Information Sciences.

Ahmim, A., & Harous, S. (2018). Hybrid intrusion detection framework based on random forests and genetic algorithms. Proceedings of Computer Science, 138, 189-196.

Almseidin, M., Alzubi, S., Kovacs, S., & Alkasasbeh, M. (2017). Evaluation of machine learning algorithms for intrusion detection system. In 2017 IEEE 15th International Symposium on Intelligent Systems and Informatics (SISY) (pp. 000277-000282). IEEE.

Dhanasekar, R., Palaniammal, S., & Rajagopalan, SP (2019). Hybrid model for intrusion detection using genetic algorithm and random forest. Proceedings of Computer Science, 165, 596-602.

Idris, IB, & Selamat, A. (2013). Improved intrusion detection system using hybrid GA-PSO. International Journal of Simulation--Systems, Science & Technology, 14(3), 60-64.

Govindarajan, M., & Chandrasekaran, RM (2013). Intrusion detection using genetic algorithm and data mining techniques. Proceedings of the International Conference on Advances in Computing, Communications and Informatics (ICACCI), 1376-1381.

Tsai, CF, Hsu, YF, Lin, CY, & Lin, WY (2009). Intrusion detection by machine learning: A review. Expert Systems with Applications, 36(10), 11994-12000.

Folino, F., Pizzuti, C., & Spezzano, G. (2016). GPDT: Genetic programming and decision trees for evolving intrusion detection systems. Proceedings of the Genetic and Evolutionary Computation Conference 2016, 1013-1020.

Saheed, YK; Arowolo, MO Efficient cyber attack detection on the internet of

medical things-smart environment based on deep recurrent neural network and machine learning algorithms. IEEE Access 2021, 9, 161546–161554

Karthik, MG; Krishnan, MBM Hybrid random forest and synthetic minority over sampling technique for detecting internet of things attacks. In Journal of Ambient Intelligence and Humanized Computing; Springer: Berlin/Heidelberg, Germany, 2021; pp. 1–11.

Balyan, AK; Ahuja, S.; Lilhore, UK; Sharma, SK; Manoharan, P.; Algarni, AD; Elmannai, H.; Raahemifar, K. A Hybrid Intrusion Detection Model Using EGA-PSO and Improved Random Forest Method. Sensors 2022, 22, 5986.

Norouzi, M.; Gürka¸s-Aydın, Z.; Turna, Ö.C.; Ya˘ gci, MY; Aydin, MA; Souri, A. A Hybrid Genetic Algorithm-Based Random Forest Model for Intrusion Detection Approach in Internet of Medical Things. Appl. Sci. 2023, 13, 11145.

Holland, JH (1992). Adaptation in natural and artificial systems: An introductory analysis with applications to biology, control, and artificial intelligence. MIT press.

Jafar Harestan , S. and Q. The feeling of old age (2020). Intrusion detection system in software - based networks using deep neural networks . Fourth International Conference on Smart Cities , Internet of Things and Applications (SCIoT2020) , 2020-09-16 .

Neural Network-Based Inverse Model for Non-Invasive Estimation of Corneal Mechanical Properties

S. S. Abedi-Shahri[1*], M. Baradari[2], and I. Z. Oskui[2]

[1]*Department of Biomedical Engineering, Isfahan University, Isfahan, Iran*

[2]*Department of Biomedical Engineering, Sahand University of Technology, Tabriz, Iran*

**Corresponding author: abedisadjad@gmail.com*

Abstract— This study presents a novel approach to estimate corneal mechanical properties using non-contact tonometry data and machine learning techniques. A neural network-based inverse model was developed to predict Ogden material parameters from corneal apex displacement data. The model was trained on simulated data generated via finite element analysis. Rather than employing standard evaluation metrics, the mechanical behavior of the material model was integrated into the model as the loss function, which minimizes the difference in stress fields between predicted and reference data. The method demonstrated strong performance in accurately predicting the mechanical response of the cornea. This approach offers a promising non-invasive diagnostic tool, bridging the gap between clinical measurements and complex biomechanical properties.

Keyword: Cornea, Inverse Problem, Machine Learning, Neural Networks, Ogden Material Model

INTRODUCTION

Non-invasive assessment of corneal mechanical properties plays a critical role in diagnosing and monitoring various ocular conditions, such as keratoconus and glaucoma. While non-contact tonometry is widely used in clinical practice to estimate intraocular pressure and corneal stiffness, it does not directly yield accurate mechanical properties. Existing methods often rely on computationally expensive inverse FEM procedures [1], which limit their practicality in clinical settings. This study aims to overcome these limitations by developing a neural network-based inverse model to estimate corneal mechanical properties from non-contact tonometry data, offering a more efficient and accurate alternative.

METHODOLOGY

A. Finite Element Simulation:

Finite element modeling and simulation of the cornea under non-contact tonometry test conditions were performed using Abaqus software. Corneal geometry was extracted from healthy corneas using the Pentacam device (Oculus, Germany). The cornea was modeled as a hyperelastic material using the Ogden constitutive model to capture its nonlinear mechanical behavior [2]. Simulations were conducted to replicate the Corvis-ST test, where air pressure was applied to simulate real-world tonometry conditions. The corneal apex displacement data for various Ogden material parameters were recorded as the primary output. In total, approximately 1700 simulations were performed [3].

B. Neural Network Model Development:

An inverse model using feedforward neural network with four hidden layers was developed to predict Ogden material parameters from corneal apex displacement data. The input layer consists of 16 neurons representing corneal displacements over time steps during simulation. The hidden layers consist of 64, 32, 16, and 8 neurons, respectively, each using ReLU activation. The output layer consists of 3 neurons, corresponding to the Ogden material parameters μ_i in Eq. (1), with ReLU activation ensuring that all predicted parameters remain positive, as required by the model.

$$W = \sum_{i=1}^{3} \frac{2\mu_i}{{\alpha_i}^2} \left({\lambda_1}^{\alpha_i} + {\lambda_2}^{\alpha_i} + {\lambda_3}^{\alpha_i} - 3\right) \quad (1)$$

where $\alpha_i = 1,2,3$.

C. Custom Loss Function:

To ensure accurate prediction of the Ogden material parameters, a custom loss function was implemented. Instead of directly comparing the predicted and target parameter values, the loss function compares the stress-strain curves generated by these parameters. Specifically, the error is defined as the norm of the difference between the predicted and true uniaxial nominal stresses (Eq. (2)) over a range of feasible stretches [0.5,1.5] for corneal tissue.

$$P_1 = \frac{\partial W}{\partial \lambda_1} \qquad (2)$$

RESULTS

The model demonstrated strong performance in predicting corneal material behavior, with an average error of 0.1932 across the test set. While a few outlier cases were observed (Fig. 1), the predicted stress-stretch curves closely matched the target behavior in most cases.

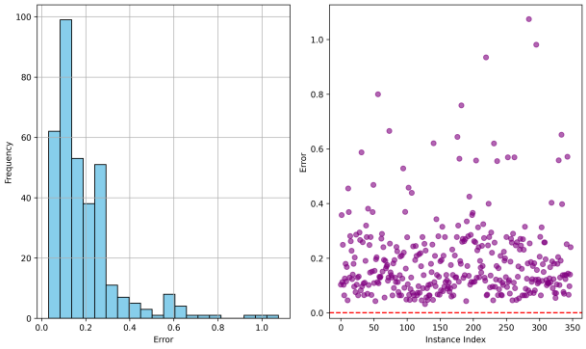

Fig. 2 Error distribution across test samples

The largest error was 1.075, yet even in this case, the predicted mechanical behavior was still very similar to the true behavior (Fig. 2). For the vast majority of samples, the differences between the predicted and true stress-stretch curves were barely distinguishable.

DISCUSSION

The results demonstrate that the neural network-based inverse model can effectively predict Ogden material parameters from corneal apex displacement data. This method offers several advantages: it is non-invasive, relying on readily available non-contact tonometry data, and provides an efficient, rapid estimation of mechanical properties. Moreover, the model's accuracy suggests potential for clinical application, where it could assist in the diagnosis and monitoring of ocular conditions such as keratoconus and glaucoma, offering a practical tool for assessing corneal biomechanics in routine practice.

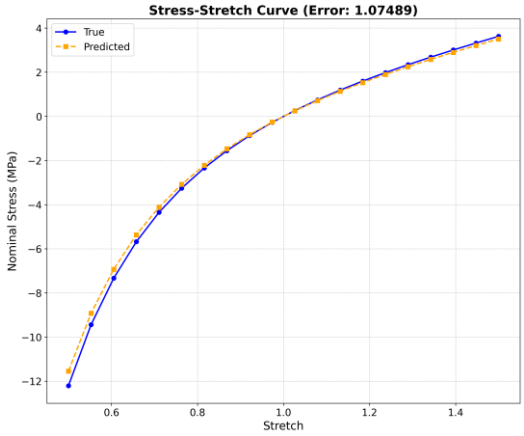

Fig. 3 Comparison of true and predicted stress-stretch curves for the worst-performing sample

CONCLUSION

This study presents a novel neural network-based approach for estimating corneal mechanical properties using non-contact tonometry data. The model demonstrated strong accuracy in predicting Ogden material parameters, offering a promising non-invasive and efficient tool for clinical applications. Future work could focus on integrating the model into clinical workflows for diagnosing and monitoring ocular conditions along with investigation into more advanced neural network architectures and the incorporation of additional input features, such as individual corneal geometric measures, to further improve the model's accuracy and generalizability.

REFERENCES

Huang, L., Shen, M., Liu, T., Zhang, Y., & Wang, Y. (2020). Inverse solution of corneal material parameters based on non-contact tonometry: A comparative study of different constitutive models. Journal of biomechanics, 112, 110055.

Elsheikh, A., Wang, D., Kotecha, A., Brown, M., & Garway-Heath, D. (2006). Evaluation of Goldmann applanation tonometry using a nonlinear finite element ocular model. Annals of biomedical engineering, 34, 1628-1640.

Baradari, M. (2023). The Determination of Mechanical Properties of Cornea Using Inverse Finite Element, Master's thesis, Sahand University of Technology

.

Application of Enhanced Raman Scattering (SERS) and Advanced Statistical Methods in Veterinary Diagnostics

T. Yaghoopour[1*], H. Sharifiyazdi[1], E. Rakhshandehroo[2], A.Safaie [3]

[1]*Department of Clinical Sciences, Faculty of Veterinary Medicine, Shiraz University, Shiraz, Iran*

[2]*Department of Clinical Sciences, Faculty of Veterinary Medicine, Shiraz University, Shiraz, Iran*

[3]*Faculty of Science, Department of Physics, Shiraz University, Shiraz 71454, Iran*

**Corresponding author: Tinayaghoobpour75@gmail.com*

Abstract— Raman spectroscopy is a non-destructive analytical technique that reveals a substance's molecular interactions, chemical structure, phase, polymorphism, and crystallinity. It operates on the principle of atomic vibrations interacting with the inelastic scattering of monochromatic light, typically generated by a laser. Although conventional Raman spectroscopy encounters challenges in detecting biological molecules such as DNA, RNA, and organisms—or even in tumor identification—Surface Enhanced Raman Scattering (SERS) has been developed to overcome these issues. SERS-based biosensors significantly enhance sensitivity and accuracy, allowing rapid analysis of complex biological samples.Advanced statistical techniques like Support Vector Machines (SVM), Linear Discriminant Analysis (LDA), and Principal Component Analysis (PCA) are essential for analyzing SERS data in biomolecular studies. The integration of these techniques with SERS can significantly improve the detection and identification capabilities in various fields, such as parasitology and veterinary diagnostics.

Keyword: Application ,enhanced Raman scattering, veterinary diagnostics, statistical methods

INTRODUCTION

Raman spectroscopy provides insights into a material's chemical structure and molecular interactions through vibrational analysis. It uses the inelastic scattering of laser-produced monochromatic light, revealing a unique spectral fingerprint associated with molecular vibrational modes. Micro-Raman spectrometers enhance spatial resolution by focusing laser light on small sample areas and collecting scattered light via microscopy.

Conventional Raman spectroscopy is limited by weak scattering signals and potential fluorescence interference when used with biological molecules like DNA and RNA. SERS effectively addresses these challenges by providing substantial electromagnetic enhancement, enabling the detection of low concentrations of biomolecules, including Leishmania DNA.

For thorough biomolecular analysis, advanced statistical methods such as SVM, LDA, and PCA are crucial. These methods enhance detection sensitivity and accuracy, enabling precise identification, classification, and discrimination of biomolecules.

APPLICATIONS OF SERS IN BIOLOGICAL STUDIES

Raman spectroscopy has been shown to accurately analyze hemozoin, a byproduct of hemoglobin breakdown by the malaria parasite, as demonstrated in a 2006 study by Wood et al. Hemozoin is a critical marker for malaria presence and a target for antimalarial drugs. Similarly, Rule et al. in 2009 employed the SERRS technique to detect waterborne pathogens Giardia lambia and Cryptosporidium parvum, using gold nanoparticles conjugated with specific antibodies as Raman markers[1,3].

In a 2022 study, Giuseppe et al. utilized Raman spectroscopy to detect structural alterations in canine blood serum proteins for identifying Leishmania infantum. This approach highlights the method's ability to discern subtle changes in serum proteins due to parasitic infections.[2,5,6]

ADVANCEMENTS IN CANCER DIAGNOSTICS AND OTHER APPLICATIONS

Recent research has focused on using Raman spectroscopy for intraoperative assessments, particularly in diagnosing margins during breast cancer surgery—an essential factor in local recurrence for both human and veterinary patients. Non-invasive optical spectral/imaging methods, enhanced by SERS, have shown significant promise for real-time, precise diagnostic applications[10].

Eady et al. demonstrated that integrating SERS with support vector machines enhances detection and classification accuracy, notably in identifying Salmonella typhimurium in chicken rinse samples. Moreover, Zheng and colleagues utilized Python-assisted SERS chips for photothermal inactivation of pathogens like Salmonella typhimurium and Staphylococcus aureus in blood samples, thus minimizing secondary contamination during detection[11].

CONCLUSION

The integration of SERS, PCA-LDA, and SVM represents a powerful approach for the precise identification and differentiation of organisms, crucial for parasitology and veterinary diagnostics. The ability of SVM classifiers to establish clear boundaries between species, alongside the visualization of species separation via PCA-LDA, underscores the technique's reliability in capturing distinct molecular signatures [4,7].

In summary, combining SERS with PCA-LDA and SVM offers a robust tool for diagnostic and species differentiation applications, with broader implications for clinical diagnostics and scientific research. This integrated strategy enhances accuracy and efficiency, representing a valuable advancement in species identification methodologies and offering reliable tools for improved diagnostic and disease management practices[8,9].

REFERENCES

Wood, B. R. & D. McNaughton (2006). Resonance Raman spectroscopy in malaria research. Expert review of proteomics, 3 (5), 525-544.

Giuseppe, A., Annastella, F., Giannetto, C., Elisabetta, G., Giuseppe, P., Barbara, T., Cicero, L., Cassata, G., & Simona, D. P. (2022). Preliminary study for the application of Raman spectroscopy for the identification of Leishmania infected dogs. Scientific Reports, 12(1), 7489 .

Malyshev, D., Dahlberg, T., Öberg, R., Landström, L., & Andersson, M. (2022). Reference Raman spectrum and mapping of Cryptosporidium parvum oocysts. Journal of Raman Spectroscopy, 53(7), 1293-1301.

Birtoiu, I. A., Rizea, C., Togoe, D., Munteanu, R. M., Micsa, C., Rusu, M. I., & Grigorescu, C. E. A. (2016). Diagnosing clean margins through Raman spectroscopy in human and animal mammary tumour surgery: A short review. Interface Focus, 6(6), 20160067.

F. Farshchi, G. Dias-Lopes, L. M. Castro-Côrtes, C. R. Alves, & F. Souza-Silva (2023). Recent advances in surface plasmon resonance as a powerful approach for studying Leishmania spp. and Trypanosoma cruzi parasites. Talanta Open, 08.10.2023.

G. Acri, A. Falcone, C. Giannetto, E. Giudice, G. Piccione, B. Testagrossa, L. Cicero, G. Cassata, and S. Di Pietro (2022). Preliminary study for the application of Raman spectroscopy for the identification of Leishmania infected dogs. Sci. Rep, 12(1), 1–10.

H. Zhao, Y. Zhan, Z. Xu, J. John Nduwamungu, Y. Zhou, R. & Powers, C. (2022). The application of machine-

learning and Raman spectroscopy for the rapid detection of edible oils type and adulteration. Food Chem, 373(PB), 131471.

Mandrell, C. T., Holland, T. E., Wheeler, J. F., Esmaeili, S. M. A., Amar, K., Chowdhury, F. & Sivakumar, P. (2020). Machine Learning Approach to Raman Spectrum Analysis of MIA PaCa-2 Pancreatic Cancer Tumor Repopulating Cells for Classification and Feature Analysis.

Liu, R., Tan, F., Wang, Y., Ma, B., Yuan, M., Wang, L. & Zhao, X. (2022). Machine Learning Identification of Saline-Alkali-Tolerant Japonica Rice Varieties Based on Raman Spectroscopy and Python Visual Analysis. Agric., 12(7).

Wu, M., & He, H. (2024). Recent advances on surface enhanced raman spectroscopy in safety assessment and quality control of meat and meat products. Food Materials Research, 4(1).

Zhang, P., Wu, X. H., Su, L., Wang, H. Q., Lin, T. F., Fang, Y. P., ... & Zheng, D. W. (2022). Rapid, Label-free prediction of antibiotic resistance in Salmonella typhimurium by surface-enhanced Raman spectroscopy. International Journal of Molecular Sciences, 23(3), 1356.

Combining Machine Learning and Nanobiosensors for Improving Lung Cancer Detection

Shakiba Nazemian[1], Soheil Sadr[1], Ashkan Hajjafari[2], Khashayar Hajjafari[3], Abbas Rahdar[4*],Mahdis Khajehmohammadi[5], Hassan Borji[1]

[1]*Department of Pathobiology, Faculty of Veterinary Medicine, Ferdowsi University of Mashhad, Mashhad, Iran.*

[2]*Department of Pathobiology, Faculty of Veterinary Specialized Science, Science, and Research Branch, Islamic Azad University, Tehran, Iran*

[3]*Medical Doctor, Shahid Bahonar University of Kerman, Kerman, Iran*

[4]*Department of Physics, University of Zabol, Zabol, Iran.*

[5]*Department of Basic Sciences, Faculty of Veterinary Medicine, Baft branch, Islamic Azad University, Baft, Iran*

**Corresponding author: a.rahdar@uoz.ac.ir*

Abstract- Lung cancer is one of the most prevalent types of cancer in the world, and its clinical prognosis and early detection are of great importance. With recent advances in artificial intelligence and nanotechnology, combining machine learning (ML) and nanobiosensors has been considered a novel approach for diagnosing and monitoring lung cancer. Hence, the current review aims to examine the combination of these two technologies for lung cancer diagnosis and explores its potential and challenges. ML can identify patterns associated with lung cancer with its capabilities in processing complex data and simulating predictive models. Nanobiosensors, on the other hand, can detect biological changes at the molecular and cellular levels with high sensitivity. These two technologies allow for more accurate, faster, and non-invasive lung cancer diagnosis. In addition, using these two technologies simultaneously could help identify more advanced changes in the disease, even before clinical symptoms become apparent. In conclusion, combining machine learning and nanobiosensors offers a novel and efficient approach to lung cancer diagnosis that can significantly increase the accuracy of diagnosis and prognosis.

Keywords: Lung cancer, Nanotechnology, Nanobiosensors, Artificial intelligence

INTRODUCTION

The early detection of lung cancer is vital to ensuring effective treatment for this disease, as it is one of the leading causes of cancer deaths worldwide. Data science and artificial intelligence are two rapidly growing areas in the fields of data science and nanotechnology. In particular, the combination of machine learning (ML) and nanobiosensors has created new possibilities for rapid and more accurate diagnosis of lung cancer [1]. It has been shown that machine learning can help identify hidden patterns in biological and medical data, thus providing a more accurate prediction of lung cancer through the study of complex data [2]. Furthermore, nanobiosensors are highly sensitive biological tools that can be used to detect molecular and biochemical changes within the human body, which may serve as a sign of cancer [3, 4]. It is believed that combining these two technologies will result in a substantial improvement in the diagnosis of lung cancer and other chronic diseases soon. Accordingly, this review examines how these two technologies can detect lung cancer.

ARTIFICIAL INTELLIGENCE

Artificial intelligence (AI), ML, is progressively used to diagnose many types of cancers, especially lung cancer [5]. ML algorithms can use complex medical data such as medical images (computed tomography scans, magnetic resonance imaging, and radiographs) to identify early signs of cancer. AI is capable of processing and analyzing huge amounts of data in a very short time and can predict treatment outcomes and identify risk patterns [6]. In addition, using deep learning techniques such as neural networks can significantly increase the accuracy of diagnosis.

NANOBIOSENSORS

There is growing evidence that nanobiosensors are effective tools for diagnosing a variety of cancers, including lung cancer [7]. Gold, silver, or metal oxide nanoparticles are useful nanomaterials for nanobiosensors that accurately detect molecular and cellular biological changes [8, 9]. Nanobiosensors in blood and lung secretions can detect lung cancer biomarkers to diagnose early signs of the disease [10]. Moreover, nanobiosensors can monitor the patient's condition and assess their response to treatment continuously in addition to rapid detection. Patients with lung cancer can benefit from non-invasive, more accurate diagnoses through nanobiosensors [11].

COMBINING ARTIFICIAL INTELLIGENCE AND NANOBIOSENSORS

Combining machine learning and nanobiosensors could provide an innovative and comprehensive approach to lung cancer diagnosis [12]. Nanobiosensors collect biological information from patients, and machine learning analyzes this information to detect cancer patterns [13]. For instance, nanobiosensors detect specific molecules altered in cancerous tissues, which can be used to infer the cancer stage from this information and categorize lung cancer patients according to these indicators [14]. Furthermore, it could also be possible to use these two technologies concurrently to detect more advanced changes in a disease, even before clinical symptoms are evident, thereby reducing the risk of fatal disease [15].

CONCLUSION

In the future, it is anticipated that machine learning combined with nanobiosensors will offer a novel and efficient approach to the diagnosis of lung cancer that will contribute greatly to enhancing the accuracy of diagnosis as well as prognosis. The combination of these two technologies can be vital in achieving advanced precision medicine for lung cancer.

ACKNOWLEDGMENT

Conceptualization: Abbas Rahdar; Methodology: All Authors; Writing - original draft preparation: All Authors; Writing - review and editing: Soheil Sadr; Supervision: Abbas Rahdar. We thank the Ferdowsi University of Mashhad Research Deputy for their support.

REFERENCES

1. Wang S, Yang DM, Rong R, Zhan X, Fujimoto J, Liu H, et al. Artificial intelligence in lung cancer pathology image analysis. Cancers. 2019;11(11):1673.
2. Chassagnon G, De Margerie-Mellon C, Vakalopoulou M, Marini R, Hoang-Thi T-N, Revel M-P, et al. Artificial intelligence in lung cancer: current applications and perspectives. Japanese journal of radiology. 2023;41(3):235-44.
3. Hajjafari A, Sadr S, Rahdar A, Bayat M, Lotfalizadeh N, Dianaty S, et al. Exploring the integration of nanotechnology in the development and application of biosensors for enhanced detection and monitoring of colorectal cancer. Inorganic Chemistry Communications. 2024:112409.
4. Sadr S, Hajjafari A, Rahdar A, Pandey S, Jafroodi PP, Lotfalizadeh N, et al. Gold Nanobiosensors: Pioneering Breakthroughs in Precision Breast Cancer Detection. European Journal of Medicinal Chemistry Reports. 2024:100238.
5. Chiu H-Y, Chao H-S, Chen Y-M. Application of artificial intelligence in lung cancer. Cancers. 2022;14(6):1370.

6. Svoboda E. Artificial intelligence is improving the detection of lung cancer. Nature. 2020;587(7834):S20-S.
7. Sheervalilou R, Shahraki O, Hasanifard L, Shirvaliloo M, Mehranfar S, Lotfi H, et al. Electrochemical nano-biosensors as novel approach for the detection of lung cancer-related MicroRNAs. Current molecular medicine. 2020;20(1):13-35.
8. Hao Z, Pan Y, Huang C, Wang Z, Zhao X. Sensitive detection of lung cancer biomarkers using an aptameric graphene-based nanosensor with enhanced stability. Biomedical Microdevices. 2019;21:1-9.
9. Chen S, Li M, Weng T, Wang D, Geng J. Recent progress of biosensors for the detection of lung cancer markers. Journal of Materials Chemistry B. 2023;11(25):5715-47.
10. Preetam S, Dash L, Sarangi SS, Sahoo MM, Pradhan AK. Application of nanobiosensor in health care sector. Bio-Nano Interface: Applications in Food, Healthcare and Sustainability. 2022:251-70.
11. Eftekhari-Sis B, Aliabad MA, Karimi F. Graphene oxide based nano-biosensor for the detection of deletion mutation in exon 19 of EGFR gene, leading to lung cancer. Materials Letters. 2016;183:441-3.
12. Chaudhary V, Taha BA, Lucky, Rustagi S, Khosla A, Papakonstantinou P, et al. Nose-on-Chip Nanobiosensors for Early Detection of Lung Cancer Breath Biomarkers. ACS sensors. 2024;9(9):4469-94.
13. Kokabi M, Tahir MN, Singh D, Javanmard M. Advancing healthcare: synergizing biosensors and machine learning for early cancer diagnosis. Biosensors. 2023;13(9):884.
14. Banerjee A, Maity S, Mastrangelo CH. Nanostructures for biosensing, with a brief overview on cancer detection, IoT, and the role of machine learning in smart biosensors. Sensors. 2021;21(4):1253.
15. Ganesh S, Dharmalingam P, Das S, Venkatakrishnan K, Tan B. Mapping Immune–Tumor Bidirectional Dialogue Using Ultrasensitive Nanosensors for Accurate Diagnosis of Lung Cancer. ACS nano. 2023;17(9):8026-40.

2.8. COGNITIVE SCIENCES AND TECHNOLOGIES

Patching Methods of Cardiac Patches for Treatment of Myocardial Infarction

A. Elham Sadat Rahimi[1], B. Zeinab Neshati[2*]

[1,2]*Department of Biology, Faculty of Science, Ferdowsi University of Mashhad, Mashhad, Iran*

**Corresponding author: neshati@um.ac.ir*

Abstract— Considering the high mortality rate of cardiovascular diseases (CVDs), especially myocardial infarction (MI), and the deficiency of current treatments for proper recovery after the occurrence of MI, scientists started to develop cardiac patches that after implantation on the surface of the failing heart can improve cardiac function. However, one of the major obstacles is how to implant the cardiac patch firmly on the surface of a beating heart without causing further damage. To achieve this purpose many methods have been suggested. Among these methods using sutures and glues, producing a cardiac patch with photocurable adhesives, and applying microneedle patches are noteworthy.

Keywords: myocardial infarction, cardiac patches, transplantation, heart attack

CARDIOVASCULAR DISEASES

Cardiovascular diseases, mainly myocardial infarction, are the leading cause of death worldwide. In 2020, CVDs caused 19.05 million deaths which shows an 18.71% increase from that of 2010 [1].

Myocardial Infarction, commonly known as heart attack, happens when the blood is prevented partially or completely from reaching a part of the myocardium, leading to necrosis of heart muscle cells [2]. The death of cardiac cells finally results in the formation of an unfunctional scar tissue which impairs the heart's ability to pump blood properly, ultimately causing heart failure [3].

Although common methods for the treatment of CVDs, such as utilization of medications and medical devices can improve the quality of patients' lives, they are unable to stop the progression of the disease [3].

CARDIAC PATCHES

Cardiac patches are biomaterials that can be used for transplantation and repair of the damaged myocardium. These biomaterials utilize diverse scaffolds and are often accompanied by seeded cells with the ability to differentiate into cardiomyocytes [4]. These patches offer temporary support for the infarct region and also repair the damaged myocardium through cells and bioactive materials that are able to integrate with the host [4]. One of the determining factors in their effectiveness is their implantation method to the surface of the beating heart so they can play their role fully with strong adhesion and without any disruption in patch function or damage to the cardiac tissue [5].

PATCHING METHODS

A. Sutures

Suturing cardiac patches to the heart surface is a widely used method to achieve firm adherence but its various drawbacks such as disrupting blood supply to the patch, bleeding, damage to the healthy tissue and infection create many problems that can endanger the functionality of the infarcted heart further or decreases the effect of the patch [5,6]. Such traumas can even lead to the escalation of LV dysfunction and therefore extend the scope of the damage [5].

B. Glues

Patches can also be glued to the surface of the heart. Nowadays the standard glue for this purpose is fibrin glue which is commonly added as an adjuvant for the attachment of cell sheets or dECM scaffolds to the epicardium [5]. Although fibrin glue can help with the attachment of the cardiac patch on the epicardium without causing any chronic inflammation [5] and in a less invasive way,

it has a weak attachment ability that can hinder the attachment of larger patches on the surface of the beating heart [6]. The other drawbacks affiliated with fibrin glue are the inhibition of cell migration [6] and infiltration of cell secretions from the patch to the damaged tissue following the creation of an unwanted gap between the two [5], improper stiffness, and the potential presence of viruses in the fibrin glue [6]. Reports show that suturing does not have any negative effects on the cardiac patch in comparison with those of fibrin glue [5].

C. Photocurable adhesives

Using materials with photocurable characteristics like gold nanorods when producing a cardiac patch is another way to achieve strong and direct attachment of the patch to the heart surface [5]. These materials usually absorb light in special wavelengths, heat up, and melt the tissue locally which results in patch attachment [7].

D. Microneedle patches

Considering the need for a method to adhere cardiac patches to the heart surface in a less damaging manner which can also be strong enough, scientists have suggested the use of microneedle patches [6]. In 2018, Tang et al. developed a microneedle patch integrated with stromal cells which by creating "channels", as the authors name it, between the damaged myocardium and the therapeutic cardiac stromal cells, the direct secretion of regenerative factors into the infarcted myocardium and therefore amelioration of heart is possible [8].

CONCLUSION

Patches produced for improving the function of a damaged heart after MI should be implanted on the epicardium using the most efficient method which can provide firm adherence with minimal damage. Although different methods have been used in experiments, further studies are required to find the best patching method to heal an infarcted heart with minimal side effects.

REFERENCES

Tsao, CW., Aday, AW., Almarzooq, ZI., Anderson, CAM., Arora, P., Avery, CL., et al. (2023). Heart Disease and Stroke Statistics—2023 Update: A Report From the American Heart Association. Circulation, 147(8), 93-621. https://www.ahajournals.org/doi/10.1161/CIR.0000000000001123

Saleh, M., & Ambrose, J. A. (2018). Understanding myocardial infarction. F1000Research, 7(1), 1378. https://doi.org/10.12688/f1000research.15096.1

Hasan, A., Khattab, A., Islam, M. A., Hweij, K. A., Zeitouny, J., Waters, R., Sayegh, M., Hossain, M. M., & Paul, A. (2015). Injectable Hydrogels for Cardiac Tissue Repair after Myocardial Infarction. Advanced Science, 2(11), 1500122. https://doi.org/10.1002/advs.201500122

Zhang, Y., Mu, W., Zhang, Y., He, X., Wang, Y., Ma, H., Zhu, T., Li, A., Hou, Q., Yang, W., Ding, Y., Ramakrishna, S., & Li, H. (2022). Recent Advances in Cardiac Patches: Materials, Preparations, and Properties. ACS Biomaterials Science and Engineering, 8(9), 3659–3675. https://doi.org/10.1021/acsbiomaterials.2c00348

Li, M., Wu, H., Yuan, Y., Hu, B., & Gu, N. (2022). Recent fabrications and applications of cardiac patch in myocardial infarction treatment. VIEW, 3(2), 20200153. https://doi.org/10.1002/VIW.20200153

Ghofrani, A., Taghavi, L., Khalilivavdareh, B., Rohani Shirvan, A., & Nouri, A. (2022). Additive manufacturing and

advanced functionalities of cardiac patches: A review. European Polymer Journal, 174, 111332. https://doi.org/10.1016/j.eurpolymj.2022.111332

Malki, M., Fleischer, S., Shapira, A., & Dvir, T. (2018). Gold Nanorod-Based Engineered Cardiac Patch for Suture-Free Engraftment by Near IR. Nano Letters, 18(7), 4069–4073. https://doi.org/10.1021/acs.nanolett.7b04924

Tang, J., Wang, J., Huang, K., Ye, Y., Su, T., Qiao, L., Hensley, M. T., Caranasos, T. G., Zhang, J., Gu, Z., & Cheng, K. (2018). Cardiac cell-integrated microneedle patch for treating myocardial infarction. Science Advances, 4(11), 9365. https://doi.org/10.1126/sciadv.aat9365

2.9. ENVIRONMENTS AND MICROBIOLOGY

Rapid Detection of Standard Strains of Enterococcus Faecalis Using Extrinsic Fluorescence

Abolfazl Zanghaei[1,2*], Ali Ameri[3*], Vahid Soheili[4], Ali Hashemi[5], Saeed Karima[6], Hossein Ghanbarian[7], Kiarash Ghazvini[8]

[1] *Department of Biomedical Engineering and Biophysics, School of Medicine, Shahid Beheshti University of Medical Sciences, Tehran, Iran*

[2] *Sinus and Surgical Endoscopic Research Center, Mashhad University of Medical Sciences, Mashhad, Iran*

[3] *Department of Biomedical Engineering and Biophysics, School of Medicine, Shahid Beheshti University of Medical Sciences, Tehran, Iran*

[4] *Department of Pharmaceutical Control, School of Pharmacy, Mashhad University of Medical Sciences, Mashhad, Iran*

[5] *Department of Microbiology, School of Medicine, Shahid Beheshti University of Medical Sciences, Tehran, Iran*

[6] *Department of Clinical Biochemistry, School of Medicine, Shahid Beheshti University of Medical Sciences, Tehran, Iran*

[7] *Department of Medical Biotechnology, School of Advanced Technologies in Medicine, Shahid Beheshti University of Medical Sciences, Tehran, Iran*

[8] *Department of Microbiology and Virology, School of Medicine, Mashhad University of Medical Sciences, Mashhad, Iran*

**Corresponding author: ZanghaeiA4031@mums.ac.ir*

Abstract—Enterococcus faecalis (E. faecalis) is a gram-positive bacterium associated with humans as a member of gut microflora. The approaches based on the intracellular and extracellular metabolites are of major interest. Four strains of bacteria, including standard samples of *E. faecalis*, *Staphylococcus aureus*, *Escherichia coli*, and *Shigella flexneri*, with seven levels of concentrations, were included in this study. After 30 minutes of incubation, the bacteria were treated with ROS indicator, and subsequently, after 30 minutes, the samples were scanned by a fluorescence spectrometer. The intensity greater than a threshold, indicates the detection of *E. faecalis* with a concentration of 10^5 CFU/mL or higher. Regarding the specific enzymes of *E. faecalis* and its high level of redox reactions, a fast, a low-cost method, using ROS indicator, is presented. The fluorescence emission after 60 minutes and greater than a threshold indicates the detection of *E. faecalis*.

Keyword: ROS indicator, Fluorescence spectroscopy, Rapid detection, Enterococcus faecalis

INTRODUCTION

Enterococcus faecalis (*E. faecalis*) is a gram-positive bacterium that can survive extreme challenges, due to its diverse metabolic capabilities.

In general, *Enterococcus* strains produce antioxidative enzymes against ROS stress, but *E. faecalis* is unusual among prokaryotic organisms, because it produces significant extracellular ROS such as superoxide, hydroxyl radical, hydrogen peroxide, and a variety of antioxidative enzymes in stress conditions [1]. The ability to cope with endogenous or host-generated ROS, and direct production of oxygen-derived free radicals seems to be related to its pathogenesis [1], as well as inducing damage to the DNA of surrounding eukaryotic cells [1].

The ROS in this bacterium are by-products of aerobic glycerol metabolism and the interaction of respiratory chain semiquinone radicals with oxygen. This bacterium produces NADH, which is responsible for producing ROS [2]. Metal ions affecting ROS production are crucial for the survival of this bacterium [3].

MATERIALS AND METHODS

First, using the serial dilution method, 7 different concentrations of 10^8 CFU, 10^7 CFU, 10^6 CFU, 10^5 CFU, 10^4 CFU, 10^3 CFU, and 10^2 CFU of each bacterium were prepared. Then, using a 96-well black ELISA plate, the wells were filled with twice of 100

µL of each concentration. Subsequently, the wells were separately treated with 2.5 µL of fluorophore, including Fluorophore Molarity (FM) concentrations of 250 µmole/L and 25 µmole/L. The viability of bacteria in this DMSO concentration (2.5 µL per 100 µL) was proved by the tetrazolium assay (for brevity, these results are not presented).

The scanned emission data made raw data of this study. Finally, by plotting the Fluorescence Intensity versus Logarithmic Concentration (FILC) spectra of bacteria, the patterns of fluorescence intensity were obtained. There were two FILC patterns, one pattern was obtained by staining the sample with FM of 250 µmole/L, and the other is obtained by staining the sample with FM of 25 µmole/L. It worth mentioning that the experiment was repeated for multiple samples to ensure the validity of the method.

RESULT

As shown in Fig.7.a, the emission spectrum of standard *E. faecalis* stained with FM of 250 µmole/L is higher than other bacteria for concentrations greater than or equal to 10^4 CFU/mL. The FILC spectra of bacteria concentrations less than 10^4 CFU/mL overlap. As shown in Fig.7.b, the maximum fluorescence intensity of *E. faecalis* is greater than 100,000 AU (Arbitrary Unit) for the bacteria concentrations of 10^7 CFU/mL and 10^8 CFU/mL, because the detector is saturated. It means the maximum value or saturation limit of the detector is 100,000 AU. The embedded detector is a high-sensitivity Photon Multiplier Tube (PMT).

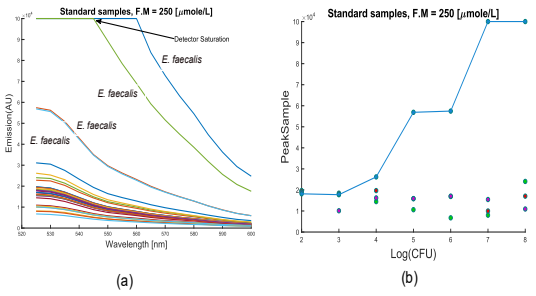

Fig.7 (a) Fluorescence spectra of standard samples at 522 nm. The FM is 250 µmole/L. The maximum fluorescence intensity is related to the bacteria concentration of 108 CFU. (b): FILC of standard bacteria with FM of 250 µmole/L.

DISCUSSIONS AND CONCLUSIONS

Briefly, in this study, a rapid detection method based on the redox reactions and ROS activity of E. faecalis within 30 minutes after staining is presented.

REFERENCES

Szemes, T., et al., On the origin of reactive oxygen species and antioxidative mechanisms in Enterococcus faecalis. Redox Report, 2010. 15(5): p. 202-206.

Uribe-Querol, E. and C. Rosales, Phagocytosis: Our Current Understanding of a Universal Biological Process. Front Immunol, 2020. 11: p. 1066.

Abrantes, M.C., F. Lopes Mde, and J. Kok, Impact of manganese, copper and zinc ions on the transcriptome of the nosocomial pathogen Enterococcus faecalis V583. PLoS One, 2011. 6(10): p. e26519.

Gene Detection of Some Virulence Factors In *Klebsiella Pneumoniae* Isolated From UTI

Sara Hadi Jassim

Microbiology Department, College of Veterinary Medicine, University of Diyala, Diyala, Iraq

**Corresponding author: sara.h.j@uodiyala.edu.iq*

Abstract- Klebsiella spp. is one of the most common causes of nosocomial infections in the United States, causing 8% of all nosocomial infections Out of 160; 24 sample shows the infection of *KlebsiellaI* identified on the basis of DNA isolation and checking with PCR using identified maker like rmpA and iroN markers. The infection was observed more predominant in female and immunodeficient persons. The organism were identified by the. Antibiotic susceptibility was checked for the different group of antibiotic like Cell Wall synthesis inhibitors - Ampicilln-sulbactam, Impenem, Cefotaxime, Piperacillin. Protein synthesis inhibitors included – Tobromycin, Nitrofurantion, Tetracycilln, Chloramphenicol and Nalidixic acid, Ciprofloxacin will be used as DNA synthesis inhibitors. The antibiotic resistance was seen to different antibiotics at their specified concentration.The above obtained data will suggest us that the microorganism like *Klebsiella pneumonia* are the deadly pathogens and become more deadly with their capacity of drug resistant so there is need to find out alternate therapy to eradicate the infection of sush organism.

Keyword: *Klebsiella pneumoniae, UTI, antibiotic resistance*

INTRODUCTION

Klebsiella pneumoniae is a Gram-negative rod in the Enterobacteriaceae family. The bacterium is found indigenously in soil and waters, but also on mucosal surfaces in mammals, including humans [1]. This organism is liable for epidemic nosocomial infections and its increasingly high level. World wild Due to drug resistance this organism is resulting in high mortality and morbidity. The dominant antibiotics used for treating infections today are the β-lactam antibiotics, which inhibit trans peptidases participating in bacterial cell wall synthesis. Beta-lactam antibiotics are often deactivated by β-lactamase enzymes [2].

The World Health Organization classified K. pneumoniae as a critical priority and established the need to promote the search for new antimicrobial agents [3]. Next to it the resistance is depends on microbial characteristics, selective pressure and technological and societal changes and this could affect very seveiourly for different types of patients especially with renal dialysis, cancer patients with chemotherapy, and organ transplantation surgery [4]. The World Health Organization classified K. pneumoniae as a critical priority and established the need to promote the search for new antimicrobial agents [5].

Therefore, in this study the essential focus was given to study the relationship between antibiotic resistance and biofilm formation in k. pneumoniae and there infection

METHODOLOGY

Collection of urine samples

A total of 160 urine sample were collected from patients suffering from Urinary Tract Infection from both sexes (males and females), during the study period from (September / 2019 –December / 2019) from patients attendinggeneral Baladruz hospital and Al- Batool Teaching hospital., A positive urine culture is based on the growth of bacteria at high number of colony forming uniits (CFU). Urine culture results should be interpreted in conjugation with clinical symptoms of UTI ;Out of 160 ,24 samples of klebsiella isolated, .Pure colonies of isolated microorganisms were identified using morphological, biochemical tests including API (analytical profile index) system. [6].

Antimicrobial Susceptibility Testing:

All 24 strains of K. pneumonia isolates were screened for their antibiotics susceptibility by using Disc diffusion method, also known as the Kirby- Bauer

method. Experiment was performed according to the Clinical and Laboratory Standard Institute guidelines (CLSI), formerly the National Committee for Clinical Laboratory Standards (NCCLS).

Detection of rmpA gene and iroN gene of klebsiella pneumoniae

PCR assay was performed in a monoplex pattern in order to amplify ifferent fragments of genes under study in a single tube. The primers listed as below were selected for this study;

Primer Name	Vol. of nuclease free water (µl)	Concentration (pmol/µl)
27F	300	100
1492R	300	100

PCR reaction tubes were placed into thermocycler PCR instrument where DNA was amplified as indicating in the Tables

Table 2: Conditions used to amplify the klebsiella pneumoniae rmp A gene

Steps	Temp °C	Time m:s	No. Of cycle
Initial Denaturation	95	05:00	1
Denaturation	95	00:30	30
Annealing	54	00:30	
Extension	72	00:30	
Final extension	72	07:00	1
Hold	10	10:00	

Agarose Gel Electrophoresis

After PCR amplification, agarose gel electrophoresis was adopted to confirm the presence of amplification. PCR was completely dependable on the extracted DNA. After completion of electrophoresis ethidium bromide stained bands in gel were visualized using Gel imaging system.

RESULT

For study the causative microorganism of illness with the symptoms of UTI amongst 160 patients their urine sample was collected and screened for the isolation.the samples were collected from Baladroz and Al-Batool hospitals in Diyala city . The incidence of *K.pneumoniae* infection in female more than in male as the rate of infection (83.3%) and (16.7%), respectively. The age range of these patients was (10- ≥50) years, the smallest age group (8.3%) were (40-49) and (≥50)years and the largest groups (29.2 %) was (30-99) years old. The individuals divided into different groups according to their smoking, pregnant and chronic disease (diabetes, hypertension,chronic UTI,) , It was noted that the incidence of diabetes in people infected with *K.pneumoniae* was 29.2%, patient suffering from hypertension was 20.8%, patients suffering from chronic UTI was 12.5% and pregnant was 12.5%. as shown in figure1

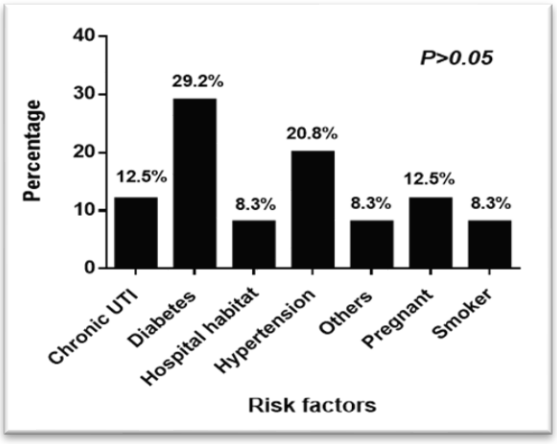

Figure1: frequency and percentage of risk factors are associated with klebsiella pneumonia infected are compared by using X2 test.

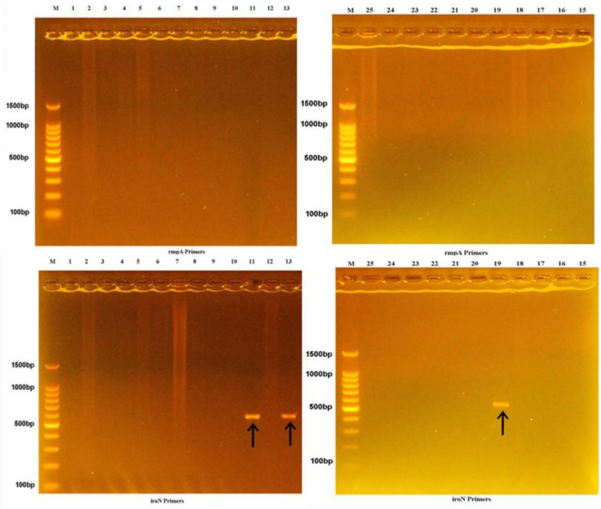

Figure 2: electrophoresis profile of bacterial DNA sample for identification iroN sample rmpA primer markers (arrow shows iroN gene markers).

The DNA sequencing was done to identify the strains of *Klebsiella pneumoniae* that cause UTI in Iraq especially in Diyala city, the results showed that there are two strains responsible to the UTI in this city, *Klebsiella pneumoniae* strains D16KP0042 and KPWIQ25.

DISCUSSION

From another gel electrophoresis results it was observed that, when the bacterial genomic samples were extracted and amplified by using PCR with some of the marker primer. It was observed that the sample no10, 13, 19 were shows iroN gene band from amplified sample which is marker gene used for the identification of *Klebsiella sp.* With iroN sample rmpA marker primer band was also checked but these marker gene was not observed in any of the sample but the identification report shows that amongst screened total sample 24 sample was shown to be *Klebsiella sp.* in this rmpA genes are responsible for the production of capsule polysaccharides [7] but these gene was not amplified in the prier based PCR which interprets that the isolated *Klebsiella sp.* are mostly non capsulated. Some of these species will have the potential of iorn uptake

CONCLUSION

The above obtained data will suggest us that the microorganism like *Klebsiella pneumonia* are the deadly pathogens and become more deadly with their capacity of drug resistant so there is need to find out alternate therapy to eradicate the infection of such microorganism.

REFERENCES

Podschun, R. and Ullmann, U., 1998. Klebsiella spp. as nosocomial pathogens: epidemiology, taxonomy, typing methods, and pathogenicity factors. Clinical microbiology reviews, 11(4), pp.589-603

Byarugaba DK (2005) Antimicrobial resistance and its containment in developing countries. Antibiotic Policies Springer, Boston, MA 617-647

World Health Organization, 2014. Antimicrobial resistance: global report on surveillance. World Health Organization.

Walsh, C., 2000. Molecular mechanisms that confer antibacterial drug resistance. Nature, 406(6797), pp.775-781. Author, A., Author, B., & Author, C. (Year, Month Day–Day). Paper title. Conference Name, City, Country. URL

Centers for Disease Control and Prevention, 2013. Modified Hodge test for carbapenemase detection in Enterobacteriaceae. Atlanta, GA.

Fertas-Aissani, R., Messai, Y., Alouache, S. and Bakour, R., 2013. Virulence profiles and antibiotic susceptibility patterns of Klebsiella pneumoniae strains isolated from different clinical specimens. Pathologie Biologie, 61(5), 209-216.

Yu, W.L., Ko, W.C., Cheng, K.C., Lee, H.C., Ke, D.S., Lee, C.C., Fung, C.P. and Chuang, Y.C., 2006. Association

between rmpA and magA genes and clinical syndromes caused by Klebsiella pneumoniae in Taiwan. Clinical infectious diseases, 42(10), 1351-1358

Serological and Molecular Detection of Highly Pathogenic Avian Influenza of Layan Hens Circulating in Diyala Governorate

Zainab Abd Awan Al-Talabani[1], Amer Khazaal Al-Azzawi[1*]

Department of Microbiology, Collage of Veterinary Medicine, University of Diyal, Iraq

**Corresponding author: zainab.a.a@uodiyala.edu.iq*

Abstract— This study was conducted at the College of Veterinary Medicine, University of Diyala, to evaluate the seroprevalence and molecular detection of avian influenza virus (AIV) H5N8 in layer chickens. Samples were collected from eight commercial flocks displaying severe respiratory symptoms, facial edema, followed by cyanosis in all parts of unfeather skin predominantly the wattles comb. Serological analysis was performed using ELISA on 364 serum samples to detect IgG antibodies specific to AIV H5N8. The results showed a significant increase of IgG antibodies in such serum samples at days 70 and 200 of age. Additionally, 48 postmortem tissue samples from trachea, lung, and liver were collected from birds at 200 days of age for RT-PCR analysis by using specific primers for H5N8 strain. Results indicated that 32 out of 48 samples (66.6%) were positive for H5N8, confirmed by sequencing of the 320 bp amplicon. The local H5N8 strain exhibited 99% sequence identity with reference sequences and was registered in GenBank under accession number (ON247929.1.). Phylogenetic analysis showed that the local sample (ON247929.1) was closely related to reference isolates from the NCBI, including MW961428.1, MW961444.1, MW961476.1, MW961436.1, and MW961484.1, which were deposited from Nigeria.

Keyword: avian influenza virus (AIV), layer chickens, ELISA, RT-PCR, GenBank

INTRODUCTION

Due to viral strain and herd immunity, global avian influenza epidemics have an adverse effect on the chicken sector and increase morbidity and mortality [1]. Negative-sense single-stranded RNA genomes are seen in avian influenza viruses [2]. The genome is divided into 8 segaments, totaling 13.5 kilobases. The disease-causing virus belongs to the Orthomyxoviridae family's genus Alph ainfluenzavirus. This virus's genome is fragmented by 13.5 kb, includes single-stranded RNA, and is negative sense [3] Differences in the matrix (M1) protein and nucleoprotein (NP) lead to classification into four genera: A, B, C, and recently discovered D [3] B, C, and recently discovered D—based on variations in their matrix (M1) protein and nucleoprotein (NP)[4] Two influenza types A virus has been named based on their capacity to significantly infect a host. The mild to subclinical symptoms of low-pathogenicity (LP) avian influenza virus include minimal respiratory and digestive effects as well as a moderate impact on ovarian follicles, which lower egg output and death in hens [5]. Due to its rapid transmission and fatality of domestic poultry, highly PAIV is referred to as the "fowl plague." Due to the Re-assortment of avian and human influenza in the 20th century, epidemics of the H1N1, H2N2, H3N2, H1N1, and H5N1 viruses respectively broke out in Asia, Africa, and [6] First time in 2010 and spread to farmed birds via migrating aquatic birds. [7] that led to a mortality rate of more than 90%. The current study's objectives are to analyze the HPAIV (H5N8) in various flocks of layer chickens in the Diyala Governorate of Iraq by serological, molecular, and phylogenetic methods.

MATERIALS & METHODS

The current study was conducted at the College of Veterinary Medicine, University of Diyala from September 2021 to April 2022, and sought to assess the seroprevalence and molecular of the major and very harmful viral illness of layer hens termed AIV. All of this study's samples processing and testing were done in the virology laboratory. All samples were collected from 8 suspected commercial layer farms suspected to be infected with AIV(H5N8) that were located in four areas of Diyala Governorate.

RESULTS

The results showed a significant increase of IgG antibodies in such serum samples at days 70 and 200 of age. According to the instruction manual of ELISA kit manufacturer and to mean titers of layers of present study, all farms are infected with AIVH5N8 strain. However, at the age of 200 days, 48 postmortem tissue samples. including trachea, lung and liver of affected birds were collected from clinically and sub-clinically infected flocks from all farms. These samples were processed, RNA extracted and submitted to RT-PCR using specific primers for H5N8 strain. The results showed that 32 out of the 48 tissue samples (66.6%) tested positive for H5N8.The resulted Amplicon (320bp) was commercially sequenced and analyzed. The sequencing of the local AIV H5N8 revealed a 99% sequence identity with the reference sequences. The detected strain was registered in GenBank data (NCBI) under acc.number ON247929.1. Phylogenetic tree for locally detected virus in comparison to data from of NCBI was created and showed that the investigated S1(ON247929.1, AIV (A/laying hens/Iraq/(H5N8) segment 4 hemagglutinin (HA) gene, partial cds, local sample is closely related to reference isolates from the NCBI acc. no. of MW961428.1, MW961444.1, MW961476.1, MW961436.,1 and MW961484.1. These strains of the Influenza H5 virus have been deposited from Nigeria.All paragraphs should be justified, both left-justified and right-justified.

DISCUSSION

Worldwide, highly pathogenic avian influenza (HPAI) viruses have emerged in poultry and other animals, causing infrequent but devastating outbreaks. The (AIV) H5N8 subtype among these produces a serious respiratory disease in chicken that has a high morbidity and mortality rate. Most bird species have been affected by highly pathogenic avian influenza (HPAI)(H5N8) epidemics over the past 20 years.

CONCLUSION

It concluded that most layer farms of Diyala Governorate are endemic with HPAIV H5N8 as four locations of layer flocks with wide geographical distributions were infected with this virulent virus.

REFERENCE

Vigeveno, R. M., Poen, M. J., Parker, E., Holwerda, M (2020). Outbreak severity of highly pathogenic avian influenza A (H5N8) viruses is inversely correlated to polymerase complex activity and interferon induction. Journal of Virology, 94(11), e00375-20.

Maclachlan, N. J. and Dubovi, E. J (2010). Fenner's veterinary virology (4th Eds): Coronaviridae, pp: 410-412.

Lamb, R. A (2001). Orthomyxoviridae: the viruses and their replication. Fields virology, 1353-1395.

Capua, I., and Alexander, D. J (2009). Avian influenza and Newcastle disease: a field and laboratory manual. Springer Science and Business Media.

Swayne, D. E., Suarez, D.L., Sims, L.D (2013). Influenza. In: Diseases of Poultry, 13th Ed. J. R. Glisson, D. E. Swayne, L. R. McDougald, V. Nair,L. K. Nolan, and D. L. Suarez, (Ed.) Wiley-Blackwell, Ames, IA, pp.181-218.

Gonzales, J. L. and Elbers, A. R (2018). Effective thresholds for reporting suspicions and improve early detection of avian influenza outbreaks in layer chickens. Scientific Reports, 8(1), 1-9.

Lee, D. H., Torchetti, M. K., Winker, K., Ip, H. S., Song, C. S. and Swayne, D. E (2015). Intercontinental spread of Asian-origin H5N8 to North America through Beringia by migratory birds.

Journal of virology, 89(12), 6521-6524.

2.10. OIL, GAS, PETROCHEMICAL PROCESSES

Feasibility Study of the Effect of Synthesized Egyptian Blue Dye on Pigment-Sensitive Solar Cells

A. Masume Khakshoor se yek ab[1], B. Mohammad Reza Bayati[2*], C. Mahmood Reza Golzarian[3], D. Navid Ramezanian[4]

[1,2 and 3] *Respectively, graduated and members of Biosystems Engineering Department, Faculty of Agriculture, Ferdowsi University of Mashhad, Mashhad, Iran*

[4]*Members of Chemistry Department, Faculty of Science, Ferdowsi University of Mashhad, Mashhad, Iran*

**Corresponding author: bayati@um.ac.ir*

Abstract— This study investigates the synthesis of Egyptian blue pigment and its effect on dye-sensitized solar cells (DSSCs). The synthesis results show that Egyptian blue has high light absorption in the visible range and can be used in DSSCs. Three solar cells were fabricated with different dye sensitizers. Experimental results for open-circuit voltage, short-circuit current density, fill factor, and efficiency were as follows: 0.56 V, 15.6 mA/cm², 62%, and 5.53% for N719; 0.55 V, 2.28 mA/cm², 63%, and 0.79% for Egyptian blue; and 0.57 V, 16.9 mA/cm², 64%, and 6.32% for the blend of Egyptian blue and N719. These results demonstrate the potential of Egyptian blue as a good sensitizer for DSSCs.

Keyword: Dye-sensitized solar cells (DSSCs), Efficiency, Egyptian blue

INTRODUCTION

The rapid growth of the global population and increasing social welfare have significantly boosted the demand for energy. Energy is a pivotal element in modern life, influencing economic stability and development. This rising demand for energy, coupled with the finite nature of fossil fuels and environmental concerns about greenhouse gas emissions, has escalated the need for renewable energy sources [1]. Among these, solar energy stands out as one of the most promising options. The vast energy from sunlight exceeds the global consumption of energy annually [1]. presenting an opportunity for efficient energy conversion. Solar cells, particularly dye-sensitized solar cells (DSSCs), offer a cost-effective and sustainable solution for converting sunlight into electricity, showing great potential for commercialization [2].

The aim of this study was to increase the efficiency of the pigment-sensitive solar cell using the synthesis of Egyptian blue pigment.

COLOR SYNTHESIS METHOD

The method of Poes et al., was used for the synthesis of Egyptian blue dye. Figure 1[3]. In order to investigate the effect of each of the reactants on the optical properties of Egyptian blue, different proportions of each substance in weight percentages of one, three and five percent were placed in the oven according to the determined temperature conditions and Figure 3 shows the results of color synthesis.

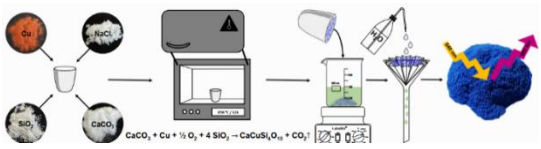

Fig.1 How to synthesize color and medium with HCl solution [3].

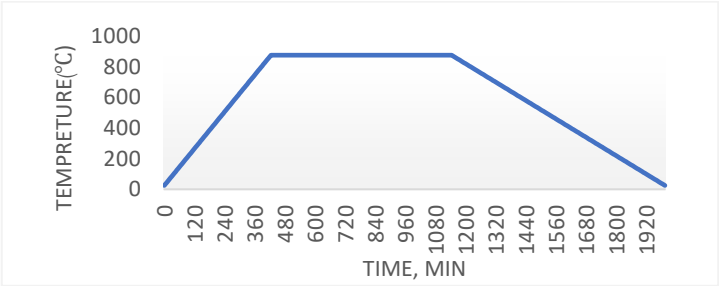

Fig. 2 Temperature conditions - time of synthesis of Egyptian blue dye

Fig. 3 The results of synthesis of samples

EGYPTIAN BLUE

Among the mineral colors, Egyptian blue is an extremely important mineral. This term refers to the complex and porous mixture of $CaCuSi_4O_{10}$ and SiO_2 (glass and quartz), which is distinct from the first artificial pigment produced in human history. Egyptian blue is the mineral cuprorivite. In fact, from the chemical point of view, it is indistinguishable from cuprorivit and is very rare in nature. In its natural form, it is used in a very low concentration to create durable pigments, and in its synthetic form, it is known as Egyptian blue [4].

CONCLUSION

In this research, the synthesis of Egyptian blue mineral dye, which has the ability to absorb light in the visible region and is very long lasting, was carried out. In order to investigate the effect of each of the reactants on the optical properties of Egyptian blue paint, different proportions of the reactants in weight percentages of one, three and five percent were placed in the oven according to the determined temperature conditions. The results of the UV-Visible test for 10 synthesized samples showed that pigment number four can be used as a good sensitizer in solar cells sensitive to the pigment due to having the broadest visible light absorption spectrum. be placed In order to identify the phase and structure of the synthesized pigment, XRD, SEM-EDS and FTIR analyzes were performed for pigment number four, and the results showed that the synthesized substance is Egyptian blue ($CaCuSi_4O_{10}$) with a small amount of impurity.

In this research, to investigate the effect of Egyptian blue pigment on pigment-sensitive solar cells, three solar cells were made, and the difference between these cells is the difference in their sensitizer or pigment. The first cell was made with N719 pigment, the second cell with Egyptian blue pigment and the third cell with a combination of both pigments. After the experimental investigations, the photovoltaic characteristics of the three cells are listed in Table 1.

Table 1. Photovoltaic characteristics of three manufactured cells

Fill factor,%	Short circuit current density, mA/cm^2	Open circuit voltage, V	Solar cell
٦٢	١٥/٦	٠/٥٦	Dye sensitized solar cell N719
٦٣	٢/٢٨	٠/٥٥	Solar cell sensitive to Egyptian blue Dye
٦٤	١٦/٩	٠/٥٧	Solar cell sensitive to Egyptian blue dye and N719

REFERENCES

Lewis, N. S., Crabtree, G., Nozik, A. J., Wasielewski, M. R., Alivisatos, P., Kung, H., ... & Nault, R. M. (2005). Basic research needs for solar energy utilization. report of the basic energy sciences workshop on solar energy utilization, april 18-21, 2005. DOESC (USDOE Office of Science (SC)).

O'regan, B. and M. Grätzel, A low-cost.(1991) high-efficiency solar cell based on dye-sensitized colloidal TiO2

films. nature. 353(6346): p. 737.
Pues, P., Exeler, J., & Jüstel, T (2020). Egyptian Blue–An Efficient Infrared Emitting Blue Pigment.
Scott, D. A. (2016). A review of ancient Egyptian pigments and cosmetics. Studies in Conservation, 61(4), 185-202.

Targeted Identification of Biopolymer Sphingan Producers: RAPD-PCR Analysis and the Development of Degenerate PCR Primers

Monir-sadat Shakeri [1*]

[1]*Department of Food Biotechnology, Research Institute of Food Science and Technology, Mashhad, Iran*

**Corresponding author: m.shakeri@rifst.ac.ir*

Abstract— *Sphingomonas* strains are the main focus for producing various microbial polysaccharides such as welan, gellan, and diutan, all of which are based on sphingan. These substances and their different forms are commonly used in various fields, including medicine, food, and the petroleum industry. It is crucial to identify local strains in order to obtain high-yield strains. In this study, screening of indigenous *Sphingomonas* isolates obtained from environmental sources including soil and water was conducted using degenerate primers designed from the pgmG gene, along with RAPD-PCR technique. The strains were precisely identified by sequence analysis of the 16SrDNA region. The study found 44 bacterial isolates classified as gram-negative bacilli that showed positive results for the catalase test. The isolates were analyzed for RAPD patterns, which led to the identification of 14 subclusters with a similarity of 45%. The identification of ten distinct *Sphingomonas* strains was achieved through sequencing the 16SrDNA within these subclusters. The designed primers were assessed to determine the target band, revealing that all ten strains produced the expected band and have the ability to produce sphingan-based biopolymers. Combining PCR with degenerate primers and RAPD analysis provides a systematic and accurate method for carrying out epidemiological research on *sphingomonas* strains.

Keyword: S*phingomonas* identification, Cluster analysis, RAPD-PCR, MCA.

INTRODUCTION

The term "Sphingan" encompasses a wide range of extracellular polymers that are created by different strains of Sphingomonas. These include welan, gellan, rhamsan, diutan and sanxan. Their superior gelling characteristics make them ideal for applications within the medical, food, and chemical industries. Characterizing strains through advanced typing techniques is essential for accelerating microbial research and can be used to explore the functional metabolites produced by these strains [1]. Random amplified polymorphic DNA (RAPD) is a PCR technique that has been widely employed to differentiate between various strains of bacterial species. The RAPD technique offers a notable benefit in that it enables quick and straightforward identification, even without requiring prior knowledge of the organism's genomic DNA. [2]. Microbial genes that encode enzymes in the biosynthetic pathway of polysaccharides could serve as ideal biomarkers for directly identifying producers of such metabolites [3]. The phosphoglucomutase (PGM; EC 5.4.2.2) is crucial among the gellan biosynthetic enzymes. The work presented here aimed to create new degenerate primer sets for PCR specifically designed to target the pgm gene found in sphingan producers.

METHODS

Nutrient Broth culture medium was used to isolate bacteria from various sources of water and soil. The isolates were first identified according to their colonial appearance, gram staining results, positive catalase test, and negative indole reaction.

Genomic DNA was extracted from cell cultures utilizing a DNA extraction kit (Qiagen, Germany) following the guidelines provided by the manufacturer. Degenerate primers were created from conserved areas of the phosphoglucomutase protein sequences found in databases (*Sphingomonas paucimobilis* ATCC 31461), designed using Primer Primier 5. The synthetic oligonucleotides included F (5`-AGAGTTTGATCCTGGCTCAG -3`) and R (5`- TACGGGTACCTTGTTACGACTT -3`).

The RAPD-PCR analysis employed the M13 primer. A phylogenetic tree was generated through UPGMA average cluster analysis utilizing NTSYS version 2.02. For

the sequencing of 16S rDNA, primers 27f and 1492r were used. The PCR was set up to begin with an initial denaturation step at 94 °C for 5 minutes, followed by 30 cycles of denaturation at 94 °C for 1 minute, annealing at 55 °C for 1 minute.

RESULTS AND DISCUSSION

A substantial level of genetic diversity was achieved from the resulting dendrogram of the various M13 profiles (Fig. 1). A total of fourteen notable groups were identified at the 45% similarity threshold. In addition, multiple correspondence analysis (MCA) illustrated how bacterial isolates were distributed according to colony color, RAPD subclusters, and PCR bands generated by degenerated primers (Fig. 2). The F-test indicated that both the color of the colony and the PCR products obtained whit degenerated primers significantly affect ($p \geq 0.05$) the distribution of the isolated strains.

As shown in the Fig. 2, F1 successfully separated the variables into two distinct clusters. The first cluster (located on the right side) consists of distinct strains identified by a positive degeneracy PCR band and a dark yellow colony. Additionally, it includes RAPD-PCR subclusters 3, 4, 5, and 13, suggesting a possible relationship between colony color and molecular characteristics. The analysis of 16S rDNA sequencing for these strains indicated that 91% of the isolates in this cluster have been identified as Sphingomonas species, known for their ability to produce sphingan biopolymers.

This research aids in recognizing Sphingomonas strains by uncovering possible links between their morphology, genetic diversity, and the developed molecular marker.

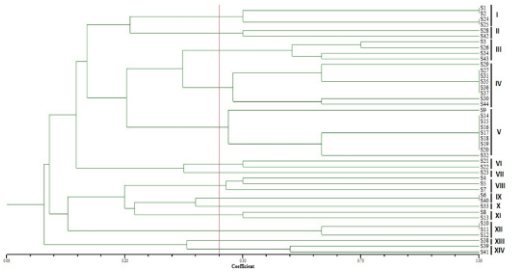

Fig. 1 UPGMA dendrogram generated based on the comparison of RAPD-M13 patterns for the 45 tested bacterial isolates

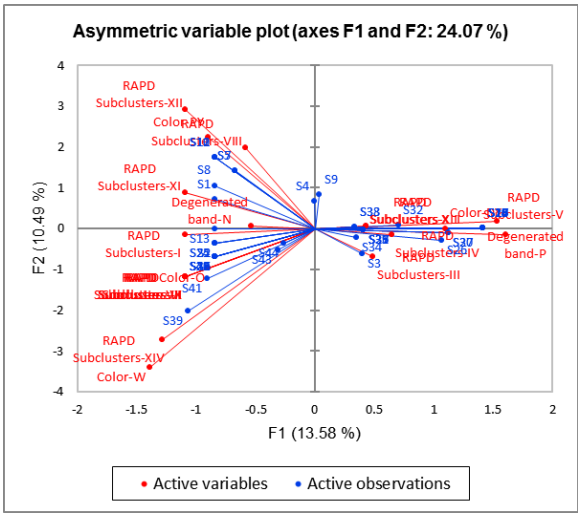

Fig. 2 the Multiple correspondence analysis (MCA) for the studied variables concerning the selected bacterial isolates

ACKNOWLEDGMENT

The author thanks Mohammad Doosti for his assistance in the molecular analysis.

REFERENCES

Huang, H. Lin, J. Wang, W. Li, S. (2022) Biopolymers produced by Sphingomonas strains and their potential applications in petroleum production. Polymers, 2022, 14, 1920.https://doi.org/10.3390/polym14091920

Matsumoto S, Watanabe K, Kiyota H, Tachibana M, Shimizu T, Watarai M (2022). Distinction of Paramecium strains by a combination method of RAPD analysis and multiplex PCR. PLoS ONE 17(3). https://doi.org/10.1371/journal.pone.0265139

Keeley R. F., Rodriguez-Gonzalez L., Class U.S.F. Genomics, Briggs G. E., Frazier V. E., Mancera P. A., Manzer H. S., Ergas S. J., Scott K. M. (2020). Degenerate PCR primers for assays to track steps of nitrogen metabolism by taxonomically diverse microorganisms in a variety of environments. Journal of Microbiological Methods,175,105990. https://doi.org/10.1016/j.mimet.2020.105990.

Synthesis and Characterization of Polyaniline/Graphene Nanocomposite Coating on Copper Condenser Tubes of Ramin Power Plant, Ahvaz

Meysam Bavi[1], Dariush Besharnejad[2]

[1]*Head of Chemistry Department, Ramin Ahvaz Power Plant,Iran*

[2]*Manager of Chemistry Affairs, Ramin Ahvaz Power Plant,Iran*

**Corresponding author: meysambavi.raminpoweplant@gmail.com*

Abstract— One of the common methods used in the field of protection is the application of nano-protective coatings made of paints, organic resins, plastics or noble metal films on equipment. In this research, the polyaniline-graphene nanocomposite coating was electrochemically coated on a copper electrode by cyclic voltammetry, and the corrosion resistance of copper substrates covered with polyaniline-graphene nanocomposite was measured using potentiodynamic polarization and electrochemical impedance spectroscopy methods in 5000 ppm of NaCl aqueous solution at room temperature. The results showed that the corrosion potentials in the presence of polyaniline-graphene nanocomposite were transferred to the anodic regions and electrochemical measurements of this coating protected copper against corrosion and protected up to 98% of copper in the condenser tubes of Ramin Power Plant.

Keywords: Nanographene coating, polyaniline-graphene nanocomposite, Ahvaz Ramin Power Plant

INTRODUCTION

Copper has been one of the important materials in the industry owing to its high electrical and thermal conductivity, mechanical workability, and its relatively noble properties. It is widely used in many applications of electronic industries and communications as a conductor; also, it is used in electrical power lines, pipelines for domestic and industrial water utilities, heat conductors, and heat exchangers. Thus, corrosion of copper and improving the corrosion resistance of this metal in a wide variety of media has attracted the attention of researchers [1–5].In order to protect metal surfaces, use of conducting polymers as advanced coating materials has become one of the most exciting research fields in recent decades [6–8]. Therefore, the goals of synthesizing these coatings as in metals and evaluating their corrosion protection properties have led to growing interest.A common method involves the application of protective coatings made from paints, organic resins, plastics, or films of noble metals on the structure itself (e.g., the coating on tin cans) [9]. These coatings form an impervious barrier between the metal and the oxidant but are only effective when the coating completely covers the structure. Flaws in the coating have been found to produce accelerated corrosion of the metal. Within coatingtechnology, there is increasing interest in the development of an efficient anticorrosive coating that is able to replace the conventional inorganic anticorrosive pigments usually added to paints, which may have detrimental effects on both environment and health. Researchers have invented a revolutionary corrosion control system using conducting polymers in the last two decades [10]. Since DeBerry [11] reported that an electrochemically deposited polyaniline film could provide anodic protection for stainless steel, conductive polymers have been candidates for metal protection against corrosion [12–15]. Polyaniline is one of the most extensively investigated conducting polymers because of its good stability, low cost, low toxicity and valuable electronic properties.Polyaniline exhibit different chemical structures that are both pH and potential dependent [16]: leucoemeraldine base (LB: fully reduced form), leucoemeraldine salt (LS: fully reduced and protonated form), emeraldine base (EB: half-oxidized form), emeraldine salt (ES: half-oxidized and protonated form) and pernigraniline base (PB: fully oxidized form). The emeraldine form has excellent air and

thermal stability [17] and thus has been extensively studied for corrosion control either as a thin primer, pigment or coating on inorganic pigment. Anticorrosive effect of polyaniline has been explored for aluminum and aluminum alloys [18,19], mild steel [20], stainless steel [21,22], iron [23,24], copper[25] and other metals [26,27].Recent investigations have shown that the synthesis of polymers in the presence of nanoparticles can increase thepolymer surface area [28]. Over the last decade, nano-sized fillers have played an important role in improving the corrosion resistance and the thermal and mechanical properties of the coatings. Organic coatings have been employed to protect steel surfaces against mobile corrosion environments for a long time by introducing a barrier to prohibit ionic transport and electrical conduction. There are various reports about the improvement of coatings performance in such environments using nanoparticles as reinforcement such as TiO2 [29,30], SiO2 [31], ZnO [32], Fe2O3 [33],carbon nanotube [34,35] and graphene [36].Graphene, which is a two-dimensional monolayer of sp2 bonded carbon, has been attracting increasing scientific and technological attention due to its outstanding mechanical, optical, thermal and electrical properties [37,38]. Graphene exhibits potential application in many fields such as sensors [39,40], nanoelectronics [41], electrode materials for electrochemical capacitors and lithium ion batteries [42].

RESULTS AND DISCUSSION

3.1. Electrosynthesis of PANI/G nanocomposite

Fig. 1 shows the CV of the 10 cycles in 0.4 M sodium salicylate solution containing 0.2 M aniline and 0.01%w/w dispersed graphene. In the first anodic potential scan, the irreversible oxidation peak starting from about + 0.7 V corresponds to aniline oxidation and this oxidation process gives a start to the formation of the PANI film on the Cu surface [51]. The positive cycle of these voltammograms is characterized by: an anodic peak at the +0.7 V which has been attributed to the transformation of PANI from reduced leucoemeraldine (LE) state to the partially oxidized emeraldine (EM) and the conversion of emeraldine to fully oxidized pernigraniline (PF)form. This behavior can be explained.

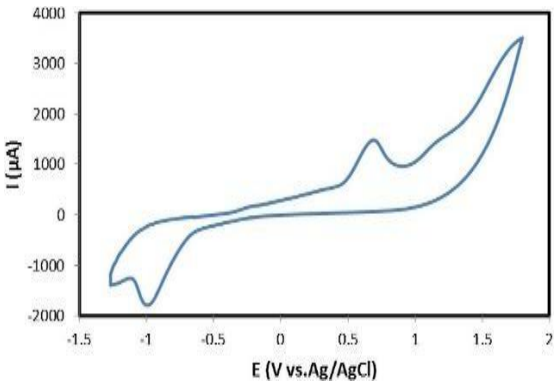

Fig. 2. Image of formation of the black layer PANI/G nanocomposite in the substrate Cu.in the following mode: it is well known that PANI/G nano- composite can exist in three different oxidation states, such as leucoemeraldine (fully reduced form), emeraldine (partially oxidized form) and pernigraniline (fully oxidized form). These forms of PANI/G nanocomposite are dependent on the applied potential. The reduction peak at -0.9 V is due to the transformation of PANI/G from emeraldine to leucoemeraldine state. Increases in the current of peak shows that the deposition thickness increases with cycles [1,52–57].It is clearly seen that the position of peak +0.7 V is shifted in anodic direction and the current density corresponding to this peak decreases gradually with the number of scans. At the

end of10 cycles, a dark green colored, uniform PANI/G film was synthesized on the Cu surface (Fig. 2). In order to examine the adhesion of the PANI/G nanocomposite coating over Cu substrates, the ASTM D 3359 standard tape adhesion test was applied and the adhesion remaining (AR%) values of all the coatings exhibited above 95% without any failed regions, 5B, which implies good adhesive strength of PANI/G nanocomposite coating toward Cu surface [58].

3. 2.Characterization of nanocomposite coating

3.2.1.Electrochemical measurement

Cyclic voltammogram of PANI/G nanocomposite, deposited on a Cu electrode, was recorded in an aqueous solution of 0.5 M sodium salicylate solution has shown in Fig. 3. CV of PANI/G nano- composite exhibit one pairs of redox waves with the first one observed at E = 0.6 V indicating the transformation of leucoemer- aldine from to conducting emeraldine form and the second one at E = 1.2 V which is due to the conversion of emeraldine into the pernigraniline form. A pair of humps in the region of E = -1 V has been assigned to overoxidation products. This indicates that graphene layer influenced the electrochemical properties of polyaniline the intercalation favor a polymer with different properties as could evidence with this electrochemical technique. There is only a minor shift of the reduction peak associated with the pernigraniline-emeraldine transition [59].

3.2.2. Spectroscopic characterization

Fig. 4 shows the UV–vis spectrum of graphene, PANI and PANI/G nanocomposite film. The characteristic peaks of the PANI/G nanocomposite doped by sodium salicylate appeared at 350 and650 nm, which was attributed to polaron-p* and p-polarontransitions, respectively [60]. The spectrum of PANI/G nano- composite film was similar to that of the polyaniline [50], except that the absorbance intensity of the former was lower than that ofthe latter. In addition, the absorption peaks of the ppolarontransition of the two were broader and appeared at the high wavelength. This result indicated that the polyaniline of the two samples with high doping level was delocalized.

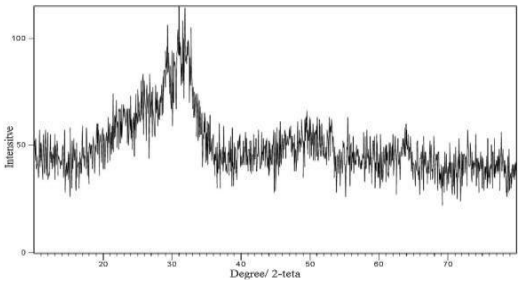

Fig. 5 show the FTIR spectrum of graphene (a), polyaniline (b) and the PANI/G nanocomposite (c) film. The presence of the graphene sheets can be confirmed by the FTIR data, as shown in Fig. 5. The FTIR spectrum of graphene

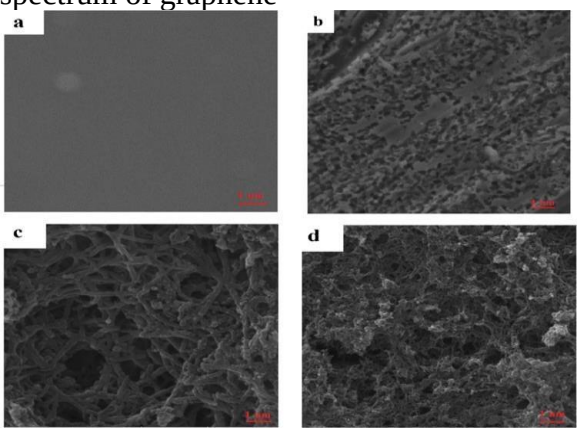

shows a strong absorption.band at 1620 cm-1 due to aromatic C¼C as well as bands due to carboxy C--O 1420 cm-1 groups situate at the edges of the graphene nanosheets while the broadband at ca. 3300 cm-1 can be due to the O--H stretching mode. This is in agreement with the reported data [61,62]. However, these absorption bands are decreased significantly in the FTIR spectrum of the PANI/G nanocomposite film, indicating that most of the functional groups have been essentially removed by electrochemical reduction. As shown in

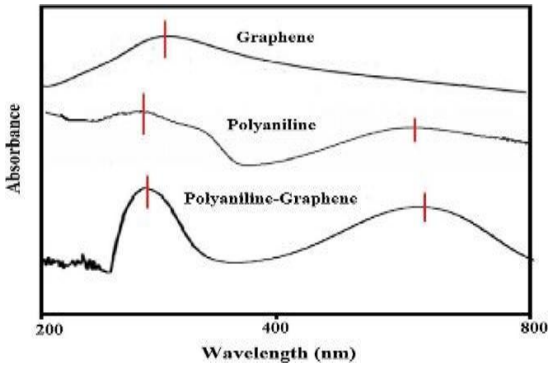

Fig. 5, the main peaks at 1570 and 1460 cm-1 can be assigned to the stretching vibrations of quinoid and benzene rings, respectively. The peaks at 1292 and 1227 cm-1 correspond to the C--N stretching vibration. The in-plane bending of C--H is reflected in the 1111 cm-1 peak. The peak at 790 cm-1 is attributed to the out-ofplane bending of C--H. All of the above peaks can be seen from a spectrum of

PANI/G nanocomposite film, showing graphene is existent in the nanocomposite film [57].

3.2.3.XRD analysis

The crystal structure of PANI/G nanocomposites was character- izeby Xray diffraction (XRD). The XRD pattern of PANI/G nanocomposites is shown in

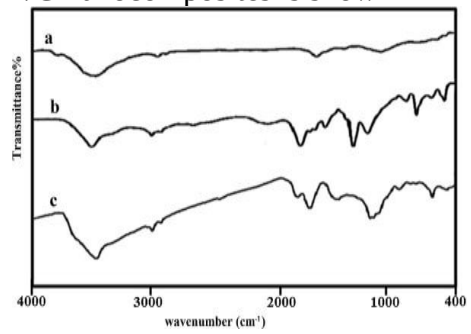

Fig. 6. The XRD patterns of PANI/G nanocomposite coating regarded to in the emeraldine salt form. Polyaniline has basically pseudo-orthorhombic crystal structure with chains parallel to the c-axis where the dopant ions are present at the central of the cell. The XRD pattern of polyaniline shows abroad peak at around

35 u. This reflection is indexed to the (11 0)plane and the ionomer decreases the order of the stacking formed by polyaniline chains and graphene. This could imply that the polyaniline on the surface of graphene sheet maintains a similar crystal structure to pure polyaniline [63].

3.2.4. Thermal gravimetric analysis

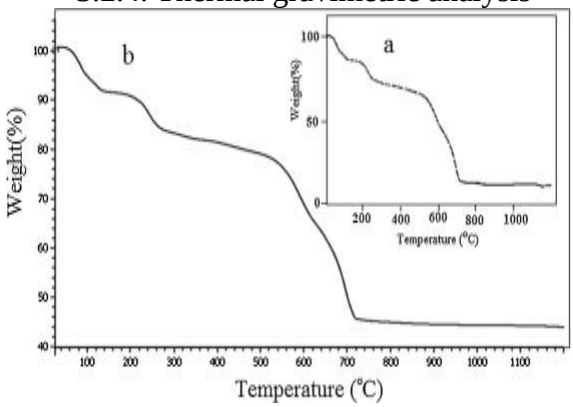

Fig. 7 depicts TGA thermogram in the air of neat polyaniline and PANI/G nanocomposite. The TGA curves show, as expected, that as graphene content adds the thermal stability of the composite is higher since graphene is significantly more stable than polyaniline. Furthermore, the addition of graphene also produces a char barrier effect that prevents oxygen from reaching the material and thus lowering the burning rate and increasing thermal stability [64,65].

3.3. Corrosion tests

3.3.1. Potentiodynamic polarization studies

Fig 8 displays the typical potentiodynamic polarization curves obtained on uncoated and coated Cu substrates in 5000 ppm NaCl

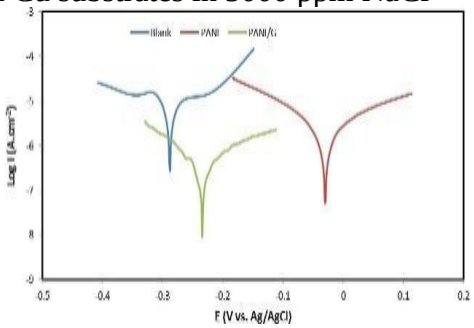

solution. The values of Ecorr, Icorr, corrosion rate (CR) and

REFRENCES:

B. Duran, G.z. Bereket, Cyclic voltammetric

synthesis of poly(N-methyl pyrrole) on copper and effects of polymerization parameters on corrosion performance, Ind. Eng. Chem. Res. 51 (2012) 5246–5255.

L. Nunez, E. Reguera, F. Corvo, E. Gonzalez, C. Vazquez, Corrosion of copper in seawater and its aerosols in a tropical island, Corros. Sci. 47 (2005) 461–484.

B.M. Thethwayo, A.M. Garbers-Craig, Laboratory scale investigation into the corrosion of copper in a sulphurcontaining environment, Corros. Sci. 53 (2011) 3068–3074.

K. Khaled, Corrosion control of copper in nitric acid solutions using some amino acids—a combined experimental and theoretical study, Corros. Sci. 52 (2010) 3225–3234.

K.-C. Chang, S.-T. Chen, H.-F. Lin, C.-Y. Lin, H.-H. Huang, J.-M. Yeh, Y.-H. Yu, Effect of clay on the corrosion protection efficiency of PMMA/Na+MMT clay nanocomposite coatings evaluated by electrochemical measurements, Eur. Polym. J. 44 (2008) 13–23.

V.J. Gelling, M.M. Wiest, D.E. Tallman, G.P. Bierwagen, G.G. Wallace, Electroactive-conducting polymers for corrosion control: 4. Studies of poly(3-octyl pyrrole) and poly(3-octadecyl pyrrole) on aluminum 2024-T3 alloy, Prog. Org. Coat. 43 (2001) 149–157.

H.N.T. Le, B. Garcia, C. Deslouis, Q. Le Xuan, Corrosion protection and conducting polymers.

2.11.MINERALS AND ORE DEPOSITS

Iranian bentonite: characteristics, challenges, and opportunities

Z. Alaminia[1*], H. Sadeghi[2], and M. Vahidinia[3]

[1]*Department of Geology, Faculty of Science, Ferdowsi University of Mashhad, Mashhad, Iran*

[2]*Department of Geology, Faculty of Science, Ferdowsi University of Mashhad, Mashhad, Iran* [3]*Department of Geology, Faculty of Science, Ferdowsi University of Mashhad, Mashhad, Iran*

**Corresponding author: Alaminia_geo@yahoo.com*

Abstract— Bentonite, a versatile clay primarily composed of montmorillonite, beidellite, and cristobalite, has been utilized in Iran for centuries across various industries, including construction, drilling, and agriculture. Despite the country's substantial bentonite reserves, particularly in regions such as southern Khorasan, Yazd, and Ghazvin, the industry faces significant challenges that hinder its development. This paper examines the key issues confronting the Iranian bentonite sector, including quality variability due to inconsistent mineral composition and contamination, extraction inefficiencies stemming from outdated mining techniques, and economic constraints exacerbated by international sanctions. Environmental concerns, such as land degradation and water resource management, further complicate the landscape. Additionally, fluctuating regulations and a lack of standardization create uncertainty for investors. However, opportunities for growth exist through investment in research and development, the implementation of sustainable practices, and the exploration of new markets. By addressing these challenges and leveraging its abundant resources, Iran can enhance its position in the global bentonite market, fostering economic development and innovation in this vital industry.

Keyword: Bentonite, Iran, Challenges, Sustainable practices.

INTRODUCTION

Bentonite is a versatile clay, primarily composed of montmorillonite, beidellite, and cristobalite. It is widely used in various industries, including construction, drilling, and agriculture. Since ancient times, Iranians have known Bentonite by the names of colorremoving soil, mud, sap soil, and soapy clay, and they were familiar with some of its properties, including washing clothes and as a cleaning agent. Ibn Sina (preeminent philosopher) also mentioned this mineral as a brittle substance that dissolves well in water. In the past, in some parts of Iran, this substance was used as food, which is still very rare in some villages. From a medical point of view, these people have a habit of eating flowers due to calcium deficiency.

Iran is endowed with substantial bentonite reserves, yet the sector faces numerous challenges that hinder its development. This paper aims to explore these challenges and propose potential solutions.

IRANIAN BENTONITE

Iran has several regions rich in bentonite deposits, including Yazd, southern Khorasan, and Ghazvin. Ferdows area in south Khorassan is known for high-quality deposits and Tabas in Yazd contains significant reserves but with varying quality.

Bentonite export is considered a profitable business due to the popularity of this product in the world markets. Bentonite is considered a profitable compound for export because it is produced in high volumes in Iran (Figs. 1 and 2).

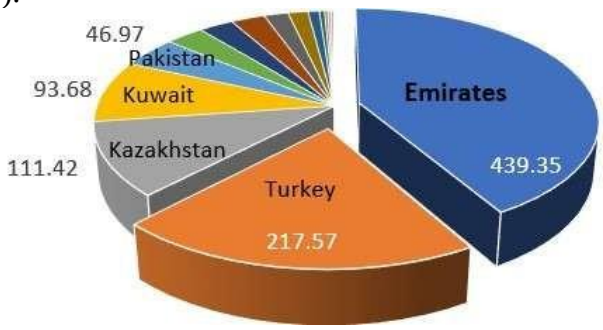

Fig. 1 Trade value of Iranian bentonite exports in 2023 (based on 1000 USD) [1].

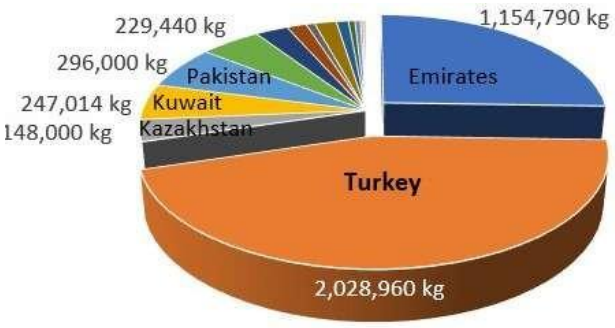

Fig. 2 Quantity of Iranian bentonite exports in 2023 [1].

Iranian bentonite is high absorbency, plasticity, and cation exchange capacity. Iranian bentonite is utilized in various sectors, including oil and gas, foundry, and environmental.

CHALLENGES FACING THE IRANIAN BENTONIT INDUSTRY

- Quality variability

Inconsistent composition: Variations in mineral content across deposits can affect performance.

Contamination: The presence of impurities can limit applications.

- Extraction and mineral processing issues

Mining techniques: inefficient practices lead to quality degradation. Open pit mining and selective mining are the most common method for extracting bentonite.

Processing limitations: lack of advanced technology hampers product refinement.

- Economic and market factors

Composition: Iranian bentonite faces competition from global suppliers.

Sanctions: Economic restrictions limit access to international markets.

- Environmental concerns

Land degradation: mining activities can lead to environmental damage.

Water usage: Processing requires significant water resources, impacting local availability.

- Regulatory and policy issues

Inconsistent regulations: Fluctuating polices create uncertainty for investors.

Lack of standardization: absence of quality assurance protocols affects product consistency.

OPPORTUNITIES FOR GROWTH

-Investment in R&D

Innovative applications: Research can lead to new uses for bentonite in various industries.

Quality improvement: Developing better extraction and processing techniques can enhance product quality.

- Sustainable practices

Environnemental management: implementing satinable mining practices can mitigate environmental impact.

Water conservation: Employing waterefficient processing methods can address resource scarcity.

- Market expansion

Diversification: Exploring new markets and applications can increase demand for Iranian bentonite.

International collaboration: Partnerships with foreign companies can enhance technology transfer and market access.

CONCLUSIONS

Iranian bentonite has significant potential due to its abundant reserves and diverse applications. However, to capitalize on these opportunities, the industry must address the challenges of quality variability, extraction inefficiencies, and market competition. By investing in research, adopting sustainable practices, and enhancing regulatory frameworks, Iran can position itself as a competitive player in the global bentonite market.

REFERENCES

https://wits.worldbank.org/trade/comtrade/en/country/All/year/2023/tradeflow/Imports/partner/IRN/product/250810


الله اكبر